ASSESSMENT OF THE ARTEMIS MALONE ENGINE

Uwe Bernhard Pascal Stein

A Thesis Submitted for the
Degree of Doctor of Philosophy

The University of Edinburgh
2003

Abstract

The work in this thesis presents the results of a theoretical and experimental investigation of a "Stirling Cycle Engine" with water in the dense phase as its working media and a digitally controlled hydraulic power take off system. The engine is based on the Malone engine as developed by J. F. Malone in the 1920s but also incorporates a number of novel alterations to improve performance. The main changes are the replacement of the crank drive with a multi-cylinder digital hydraulic power take-off system, and a regenerator design which differs from Malone's original contraflow method. Further, the proposed engine includes an advanced hot end heat exchanger and an efficient, low pollution combustion system. Professor S. H. Salter first proposed such an engine in the early 1990s. Dr. Md. Ehsan has done a theoretical study on the subject for his PhD. The aim of this study was to validate the existing theoretical models and to prove the concept in an experimental study.

Given the scale and complexity of the complete system and the large number of individual components that had to function together, it was decided to divide the engine into three subsystems. Firstly the combustion system; including the external structure of the hot end heat exchanger. Secondly the "Thermodynamic Pile"; with the regenerator and the hot and cold end heat exchanger. And lastly the hydraulic power take-off system; including the regenerator drive system and the separator unit between the hydraulic oil and the working fluid. The performance of these three systems was then analysed by using individual test rigs where the conditions on the interference between the systems were made to be the same as in the complete engine. These tests were then used to produce a detailed experimental and numerical analysis of the separate systems. Functional designs and material combinations for the individual components could be found in this way.

An efficient, low pollution combustion system, using a burner working on the principal of flameless oxidation, and a vortex flow combustion chamber was made and tested. With a test rig, using air at ambient temperature, it was possible to show how the combustion chamber geometry affects the flow profile inside the chamber. It was possible to optimize these parameters to maximize the heat transfer into the engine.

Experiments were conducted on a number of different hot end heat exchanger designs. The advantages of the different material combinations are discussed.

From the theoretical regenerator study it was found that a careful optimization of the different regenerator parameters is required to achieve acceptable regenerator efficiencies in the Malone engine. It can be shown that the Malone engine requires a more sophisticated regenerator system to achieve high regenerator efficiencies than would typically be the case in Stirling cycle engines. A number of different regenerator systems are described and a numerical analysis was made.

A discussion is made on the power take-off system in engines with supercritical water as the working fluid. The experimental results from the hydraulic power take-off system show that it is possible to create the required piston motions with a digital multi cylinder hydraulic pump. The efficiency of the hydraulic power take-off system was found to be lower than initially predicted. From test results and numerical calculations it was possible to show that offsetting the tank pressure to the lower cycle pressure could increase this efficiency.

The thesis concludes with a discussion on the overall system performance of the engine. Possible areas of improvements and areas for further research are also addressed.

ASSESMENT OF THE ARTEMIS MALONE ENGINE

U.B.P. Stein

A Thesis Submitted for the
Degree of Doctor of Philosophy

University of Edinburgh

2003

Declaration

I certify that the work presented in this thesis,
except where credited to others, is my own.

ACKNOWLEDGEMENTS

I would like to thank the following people for their help throughout this work:

Firstly I would like to take this occasion to thank W.H.S. Rampen, my supervisor, for his guidance and help throughout this project. Without his directions, inspiration and belief in the project, very little of this work would have been possible.

Next I would like to thank Professor S.H. Salter, my other supervisor. Without his fundamental idea and determined motivation this thesis would not have occurred.

My thanks will also go to all members of Artemis Intelligent Power Ltd, MD Ehsan and Kim Almond who offered help and advice at various occasions.

Finally and most importantly, I would like to thank my wonderful wife, Pim for her love that supported me through the work. Without her understanding and patience I would not been able to bring this work to a conclusion.

To all, I offer my sincerest gratitude.

U. Stein

June 2003

Table of Contents

1 INTRODUCTION 1

1.1 Preface 1

1.2 Stirling engine history 2

1.3 Malone engine 8

1.4 The Artemis Malone engine 13

1.5 Overview of thesis structure 17

2 LITERATURE REVIEW 18

2.1 Introduction 18

2.2 Stirling cycle engine 19

2.3 Cycle analysis 19

2.3.1 Stirling engine regenerator analysis 23

2.3.2 Malone engine development 28

2.3.3 Malone engine regenerator 29

2.3.4 Working fluid 30

2.3.5 Hot end heat exchanger 38

2.4 Mechanical configuration 41

2.4.1 Classification of Piston/Displacer arrangement 42

2.4.2 Mechanical drive mechanisms for Malone engines 44

2.5 Combustion system 46

2.5.1 Pollution reduction 47

3 COMBUSTION SYSTEM 50

3.1 Introduction 50

3.2 Experimental study of the combustion system 54

3.2.1 First combustion system 55

3.2.2 Second test rig 58

3.3 Energy flow 61

3.4 Flow test rig 64

3.5 Experimental test results 74

3.6 Discussion of results 77

4 HOT END HEAT EXCHANGER 78

4.1 Introduction 78

4.2 Hot end heat exchanger 81

4.2.1 Heat exchanger materials 83

4.2.2 Initial Copper-Inconel heat exchanger 86

4.2.3 Revised Copper-Inconel heat exchanger 88

4.2.4 Molybdenum washer heat exchanger 90

4.2.5 Heat exchangers for the proposed engine 92

4.3 Test results 97

4.4 Conclusion 101

5 MALONE ENGINE REGENERATOR 102

5.1 Introduction 102

5.2 Regenerator test rig 103

5.3 Regenerator analysis 106

5.3.1 Basic theory in contraflow regenerators 111

5.3.2 Utilization factor 116

5.3.3 Fluid to matrix heat transfer 117

5.3.4 Flush ratio 123

5.3.5 Length over diameter ratio 127

5.3.6 Pumping losses 128

5.4 Theoretical regenerator optimization 134
5.4.1 Fixed parameters 136
5.4.2 Variable Parameters 139
5.4.3 Optimization results 139
5.5 Malone regenerator variants 146
5.5.1 Constant heat transfer regenerator 146
5.5.2 Malone contraflow regenerator 147
5.5.3 Collapsible regenerator 150
5.5.3.1 Mechanically controlled dead volume 153
5.5.3.2 Flow controlled regenerator dead volume 156
5.6 Discussion of results 156

6 HYDRAULIC POWER TAKE-OFF SYSTEMS 159
6.1 Introduction 159
6.2 High bottoming cycle pressure 160
6.3 Piston motion profiles 164
6.4 Digital displacement power-take off system 172
6.1.1 Multi cylinder test machine 175
6.1.2 Digital displacement with elevated tank pressure 180
6.1.3 Test results 181
6.5 Crank drive power take-off system 183
6.1.4 Conventional crank arrangement 184
6.1.5 Partially balanced piston arrangement 185
6.1.6 Fully balanced piston system 188
6.6 Summary and conclusion 190

7 CONCLUSION AND FURTHER RECOMMENDATION 192
7.1 Summary 192

7.2 Conclusion 192

7.3 Recommendation for further work 196

References **ref 1**

Appendices

A. Regenerator optimization

B. System pressure change

C. Combustion chamber energy flow

D. Heat transfer by radiation

E. Data sampling schematics

F. Internal hot end heat transfer calculation

List of Figures

Figure 1.1. The four different phases in the Stirling engine cycle are shown. 1-2 isothermal compression; 2-3 constant volume heating; 3-4 isothermal expansion; 4-1 constant volume cooling and the relating P-V and T-S diagram. 7

Figure 1.2. Malone's original regenerator system is shown. The fluid from the cold blow is channeled with a non-return valve (right) through the regenerator and up into the hot end. In the hot blow the fluid returns through different flow passages (left) downwards into the cold end. It takes a number of engine cycles for the fluid to shift from the hot end to the cold end and back. (Drawing from Malone's report in the "Journal of the Royal Society of Arts", June 1931)..... 9

Figure 1.3. Pressure – Specific Volume diagram for water with indicated operating points of Malone's original engine. Notice the significant change of specific volume per temperature change just above critical temperature and pressure. (Graph from Malone's report in the "Journal of the Royal Society of Arts", June 1931) 10

Figure 1.4. The layout of Malone's original engine is shown. The main components are: top left- working piton crank drive; top- working piston, bottom left- regenerator/displacer crank drive, bottom- T-D Pile with hot end, cold end and regenerator; right- coal fired furnace with exhaust gas heat recovery. (Drawing from Malone's report in the "Journal of the Royal Society of Arts", June 1931) 12

Figure 1.5. The left figure shows Malone's original engine from 1931. The right figure shows the Artemis Malone Engine as analysed in this study. 15

Figure 2.1. PV-diagram of the ideal Stirling cycle. 1-2 isothermal compression, 2-3 isometric heating, 3-4 isothermal expansion, 4-1 isometric cooling 21

Figure 2.2. Energy flow in a typical Stirling cycle engine with inlet air preheater and working regenerator. It can clearly be seen that the regenerator shifts a multiple higher amount of energy around than the total energy supplied to the system 23

Figure 2.3. Inlet and outlet temperature of regenerator and temperature profile in regenerator during the constant volume heating and cooling stroke 25

Figure 2.4. The typical matrix and fluid temperature inside a Stirling engine regenerator working with an ideal gas are shown. An ideal regenerator works with a minimum difference between matrix temperature (dotted line) and fluid temperature (solid line) and a small temperature swing of the matrix material in relation to the total temperature difference between T-hot and T-cold. 36

Figure 2.5. Fluid properties of water as a function of temperature at 300, 400, 500 bar. (Afshin J. Ghajar 1980, "Physical Properties Expressions for some fluids in the supercritical region"..... 37

Figure 2.6. Alpha configuration (source: "Stirling Cycle Engine Analysis", I Urieli, 1984)..... 43

Figure 2.7. Beta configuration (source: "Stirling Cycle Engine Analysis", I Urieli, 1984)..... 43

Figure 2.8. Gamma configuration (source: "Stirling Cycle Engine Analysis", I Urieli, 1984)..... 44

Figure 2.9. Exhaust gas recirculation (EGR) and combustion gas recirculation (CGR) have been used to reduce NO_x development. (source: Hargreaves, "The Philips Stirling Engine" 1991)..... 48

Figure 2.10. Development of NO depending on temperature and time at high temperature level. (A.P.J. Michel 1971)..... 49

Figure 3.1. Layout of the first test rig with the burner to the left the combustion chamber, the hot end heat exchanger in the center, and the pressurizing pump to the right of the drawing..... 56

Figure 3.2. Picture of the fully assembled test rig with two of the test hot end heat exchangers in the front of the picture..... 56

Figure 3.3. The gas passage inside the swirl chamber of the combustion system is shown. The gas swirls for a number of times around the hot end of the engine before is passes through the exit on the bottom of the inner combustion chamber and enters the exhaust gas heat exchanger..... 58

Figure 3.4. Picture of the 15 kW low NOx combustion system with the water cooled dummy hot end.59

Figure 3.5. Comparison of the temperature profiles in conventional combustion and flameless oxidation. The temperature of the combustion gas in flameless oxidation mode is slowly rising to its maximum temperature, whereas in conventional flame mode the combustion gas temperature peeks at the burner nozzle..... 61

Figure 3.6. The results from the Math-Cad model of the combustion system are presented. It is possible to see the combustion gas temperature and mass flow at each point in the system. The line width represents the energy flow rate. The calculations are done on basis of a lambda number of 1.3 and a recirculation factor of two..... 63

Figure 3.7. Room temperature test rig with flow measurement probes to the left of the test chamber the hot end heat exchanger in the center. Two further combustion chamber walls with different diameters are shown on the right..... 64

Figure 3.8. Photograph of three thermal anemometer probes positioned to analyse the flow velocity around the outer fins of the hot end heat exchanger..... 65

Figure 3.9. The left figure shows the measuring planes in relation to the combustion chamber and inlet tube. Plane one is, hereby, 90°, plane two 180° and plan three 270° past the burner inlet. The right figure shows the location of the measuring points in each plane. 66

Figure 3.10. Picture of the dummy hot end as used to simulate the thermal load of the engine. The dummy hot end is internally water-cooled. The wall thickness and material is chosen to create an increased thermal resistance in the wall, resulting in the same fin base temperature as the proposed test engine. 74

Figure 3.11. Temperature profiles at different points in the combustion system during a 500 s long test. 75

Figure 3.12. The main results for the energy flow in the combustion system are illustrated. The different energy flows are calculated from the measured temperatures and mass flow rates. 76

Figure 4.1 Thermodynamic pile of the proposed Artemis Malone engine as used for the experimental study on the hot-end heat exchanger and the regenerator. It was possible to work with internal pressures of up to 400 bar and hot-end fluid temperatures of up to 550 °C. 80

Figure 4.2 First hot-end heat exchanger made from copper and Inconel washers. The washers were laser cut and then vacuum brazed together. 86

Figure 4.3 Creep on electrical grade Copper per 1000h at elevated temperatures. (source for 149°C, 204°C and 260°C : Copper Development Association (1994)) 88

Figure 4.4 Revised copper Inconel hot-end heat exchanger with completely enclosed copper washers. The edges of the Inconel washers were TIG welded. Two copper washers were used for each external fin and spaced apart along the inner radius to increase the surface area of the internal fins. 89

Figure 4.5. First hot-end heat exchanger made from Molybdenum. The washers were machined from Molybdenum grade TZM sheet material of 1 mm thickness. The complete surface was then coated with nickel based compound and vacuum brazed. 90

Figure 4.6 The non return valve on top of the regenerator directs the fluid in the hot blow, through the flow passages in the heat exchanger wall. In the cold blow, the valve opens and most of the fluid bypasses the heat exchanger directly entering the regenerator. 94

Figure 4.7 Shows the solid Monel hot-end heat exchanger during assembly left and fully assembled right. The end caps are vacuum brazed onto the heat exchanger after the twisted wires are inserted into the holes. 95

Figure 4.8 The picture shows the inner fin structure of the hot-end heat exchanger. It is possible to see the fine flow passages that have been milled into the inner copper part. To the right, a section of a complete inner structure can be seen. 97

Figure 4.9. Hot-end heat exchanger prototypes made from copper inner section and washer stack for the external fin structure. Left: heat exchanger made from Monel washers after use in TD-Pile test rig. Right: unused heat exchanger made from molybdenum washers that have been coated with the "Durak B" process. 98

Figure 4.10. Completely assembled TD-Pile with solid Monel hot-end heat exchanger. 99

Figure 4.11 Section view of a Monel K500 part that has been friction welded. No recrystallization in he weld could be observed and initial high-pressure tests at room temperature showed no leaks. . 102

Figure 5.1. Regenerator made from 0.2 mm stainless steel foil. The foil has been dimpled to create constant flow channel width. The entry and exits have been corrugated to avoid blockage..... 104

Figure 5.2. Regenerator matrix and regenerator dead volume for a given swept volume in a Stirling and a Malone engine. The areas represent the volumes for a similar heat capacity ratio of swept fluid to matrix volume and flush ratio. 110

Figure 5.3 shows the reduced regenerator efficiency as a function of the reduced length and reduced period. (source: Hausen 1983) 115

Figure 5.4. Volumetric heat capacity and heat conductivity data for possible regenerator metals at elevated temperatures illustrated (source: Howard and Timothy 1984; Incropera, 1990; Copper Development Association 1994) 120

Figure 5.5. In engines with large regenerator dead volumes, compared to swept volumes, each particle of fluid passes only through a part of the regenerator (top). The exchange can be divided into boxes, whereby, the shifts between the hot space and box (a), and the fluid from (a) shifts between box (a) and (b), and so on. In engines with small swept volumes (bottom), the majority of the fluid shifts between the hot and cold space of the engine. 125

Figure 5.6. The effect of the regenerator dead volume for regenerators with large heat transfer coefficient to the left and with a poor heat transfer coefficient to the right is shown. While for the regenerator with a large heat transfer coefficient the ratio of temperature change in the fluid dT to

length traveled **dX** remains unchanged in the case of poor heat transfer coefficient a reduction in the ratio **dT** to **dX** can be seen..... 127

Figure 5.7. The different parameters that define the geometry, fluid and thermodynamics of the regenerator system are displayed. To simplify the process, about half the parameters have been set to fixed values leaving five variables to be optimised..... 137

Figure 5.8. Section view of the TD-pile as used by Malone. Malone used two, one-way, valves on the cold side of the regenerator to direct the fluid to and from the hot-end into different flow passages. The flow passages were created by coiling steel sheets with cut outs for the different flow channels. (Drawing from Malone's report in the "Journal of the Royal Society of Arts", June 1931)..... 152

Figure 5.9. shows the collapsible regenerator during the stroke from hot to cold-end. The initial regenerator position is at the top dead center with a minimum of dead volume in the compressed regenerator, and the swept volume in the cold-end space. In the first half of the stroke the swept fluid enters the expanding regenerator matrix until, at mid stroke, all the fluid has been absorbed into the matrix. In the second half of the stroke, the regenerator empties the swept fluid into the hot-end space..... 155

Figure 5.10. Proposed technique to minimise dead volume in the regenerator at times of TDC and BDC. The angle of the connecting rod is used to control the dead volume in the regenerator. At times of maximum flow through the regenerator, the connectiong rod angle is at its maximum with a large opening between the matrix layers. At times of minimum flow, around TDC and BDC the connecting rod angle is zero with a minimum space between matrix layers..... 157

Figure 5.11. Springs between the washers cause the regenerator matrix to expand at mid stroke. End stops at the hot and cold-end are used to compress the regenerator at TDC and BDC to minimise dead volume. The flow is channeled in alternating direction over the washers, whereby, a number of washers are connected in parallel. By changing the number of washers used in parallel, it is possible to optimise between pressure drop and heat transfer. It is further possible to vary the numbers of washers connected in parallel, along the regenerator to optimise for different fluid properties between the hot and cold-end..... 158

Figure 6.1. PV-diagram of Malone type engine working with high critical pressure in relation to peak cycle pressure. In such systems small losses in the power take-off system can create significant losses in relation to the output power..... 161

Figure 6.2. Theoretical power take-off system efficiency for system working at 250 bar mean compression stroke pressure. The efficiency is shown as a function of mean expansion stroke pressure for pump/motor efficiencies of 90 %, 95 % and 98 %. 163

Figure 6.3. Compressibility of water as a function of pressure and temperature. It can be seen that the fluid in the cold end and in the cold part of the regenerator is virtually incompressible. 165

Figure 6.4. PV-Diagram of Malone`s engine. Left, predicted PV-Diagram from the AMESim® model. Right, PV-Diagram presented by Malone in 1931..... 166

Figure 6.5. Results from the simulation showing the effect of change in hot end dead volume on the PV-diagram..... 169

Figure 6.6. Results from the simulation showing the effect of change in phase angle on the PV-diagram. 170

Figure 6.7. Results from the simulation showing the effect of change in working piston displacement on the PV-diagram. 171

Figure 6.8. Schematic of the digital displacement pump motor arrangement. The low and high pressure valves are solenoid actuated allowing full control over displacement in each shaft revolution. 173

Figure 6.9. Efficiency from 6-cylinder digital displacement pump/motor. The pump motor has 2 cc displacement per piston and is operated with mineral oil at 1500 rpm. (Results are provided by N. Caldwell, Artemis Intelligent Power Ltd)..... 174

Figure 6.10. Digital displacement power take-off system for Artemis Malone engine. The 12 cylinder Pump/Motor operates at 10 times the shaft speed of the Thermodynamic Pile, allowing up to 120 pump or motor actuations in each thermodynamic cycle..... 176

Figure 6.11. Shows this machine with the control system to the left, and the different oil water separators, and the TD-Pile to the front of the picture..... 177

Figure 6.12. Calculated and measured separator motion profile of intensifier piston. 32 of the 120 cylinders available were pumped and 37 were motored to compensate for the difference in volumetric efficiency. 178

Figure 6.13. Hydraulic circuit and photo of the single cylinder digital displacement Pump/Motor with elevated crankcase pressure. The crankcase pressure could be lifted to a maximum of 200 bar

allowing output pressures of up to 400 bar. The Pump/Motor could supply flow of up to 6 l/min at 300 rpm shaft speed. 181

Figure 6.14. Test results from single cylinder Pump/Motor. The output from the pump motor has been connected to an accumulator and the pressure change was recorded for a flow demand of 1 and 3 Hz. 182

Figure 6.15. The conventional crank arrangement for the working piston, as used by Malone, can be seen to the left of the figure. The force on the working piston and torque on output shaft during the cycle are shown to the right of the figure..... 184

Figure 6.16. The part balanced piston arrangement can be seen to the left of the figure. The force on the working piston and torque on the output shaft during the cycle are shown to the right of the figure..... 186

Figure 6.17. Maintaining a positive force on the working piston during the cycle allows the use of cam type eccentrics to create non-sinusoidal piston motion profiles. 187

Figure 6.18. The fully balanced piston arrangement can be seen to the left of the figure. The force on the working piston and torque on the output shaft during the cycle are shown to the right of the figure..... 189

List of Tables

Table 2.1 Properties of water at low temperature, 0.7 * $T_{critical}$ and in the dense phase. For comparison the properties of He are given..... 34

Table 3-1 shows the air velocity profile in the area between the hot-end heat exchanger fins and the combustion chamber wall, for a hot-end heat exchanger diameter of 80 mm and an inner combustion chamber diameter of 155 mm. The velocity profiles are measured at 30, 150 and 270 degrees past the burner inlet (see drawing 3.9)..... 67

Table 3-2 shows the air velocity profile in the area between the hot-end heat exchanger fins and the combustion chamber wall, for a hot-end heat exchanger diameter of 80 mm and an inner combustion chamber diameter of 210 mm. The velocity profiles are measured at 30, 150 and 270 degrees past the burner inlet (see drawing 3.9)..... 68

Table 3-3 shows the air velocity profile in the area between the hot-end heat exchanger fins and the combustion chamber wall, for a hot-end heat exchanger diameter of 80 mm and an inner combustion chamber diameter of 310 mm. The velocity profiles are measured at 30, 150 and 270 degrees past the burner inlet (see drawing 3.9)..... 69

Table 3-4 Average flow velocity in sector 1 and 3 for three different combustion chamber diameters. 70

Table 3-5 Recirculation factor for 155 mm, 210 mm and 310 mm combustion chamber diameter calculated from volume flow in inlet tube and volume flow in Sector 1..... 70

Table 3-6 Air flow velocity at fin tip and between hot-end fins for 155 mm, 210 mm and 310 mm combustion chamber diameter. The air velocities are measured at the middle fin of the hot-end in sector three..... 71

Table 3-7 Emissivity of combustion chamber and hot end heat exchanger materials at elevated temperatures. (source: Greene and Finfrock (2000) [Inconel 718]; Siegel and Howell (1992) [Monel]; Incropera and Dewitt (1990) [Copper]; Plansee (1992) [Molybdenum])..... 73

Table 3-8 Heat transfer by radiation from the combustion chamber wall to the hot-end. The heat transfer is calculated for 1300, 1400 and 1500 K combustion chamber wall temperature and 900 K hot-end temperature for three different wall diameters..... 73

Table 4.1. The advantages and disadvantages of a number of different possible materials for the use in the hot-end heat exchanger are illustrated (Inco Alloy Intl. 1984, 1985a, 1985b; Howard and Timothy 1984; Plansee 1992, Copper Development Association 1994). 83

Table 4.2 Creep on electrical grade Copper at 550 °C. Tests were carried out on strips of pure copper in a nitrogen atmosphere and with nickel coating to prevent corrosion..... 88

Table 5.1 Input values as used in the final step of regenerator optimisation..... 141

Table 5.2. Values found for geometric regenerator parameters at the different input values. The values used for flow channel width **tf**, shim thickness **ts**, matrix mass **ms** and the regenerator length **rl** are shown in table 5.1 (calculations are shown in appendix A)..... 142

Table 5.3 Reynolds numbers in the regenerator matrix for different regenerator geometries and different temperature sections. The input values for the different parameters are shown in table 5.1 (calculations are shown in appendix A)..... 143

Table 5.4 Reduced periods and reduced lengths for different regenerator geometries and temperature sections. The reduced periods and reduced length are not effected by the length to diameter ratio. The input values for the different parameters are shown in table 5.1 (calculations are shown in appendix A). 144

Table 5.5 Flush ratio for different regenerator geometries and different temperature section. The flush ratio is not affected by the length to diameter ratio. The input values for the different parameters are shown in table 5.1(calculations are shown in appendix A)..... 144

Table 5.6 Losses arising from thermal conductivity in the axial direction for different regenerator geometries. The input values for the different parameters are shown in table 5.1 (calculations are shown in appendix A)..... 145

Table 5.7 Irreversible regenerator losses arising from imperfect heat exchange and matrix temperature swing for the different regenerator geometries. The length to diameter ratio does not affect the heat exchange for the case of laminar flow. The input values for the different parameters are shown in table 5.1 (calculations are shown in appendix A)..... 145

Table 5.8 Shows the losses arising from the pressure drop in the regenerator for the different regenerator geometries. The input values for the different parameters are shown in table 5.1 (calculations are shown in appendix A)..... 146

Table 5.9 Effect on the input power arising from conductivity losses, flow losses and imperfect regeneration in each section of the regenerator. The input values for the different parameters are shown in table 5.1 (calculations are shown in appendix A)..... 147

Table 5.10 Effect on the input power arising from conductivity losses, flow losses and imperfect regeneration. The input values for the different parameters are shown in table 5.1 (calculations are shown in appendix A). 147

Symbols

A	=	surface area [m^2]
Bi	=	Biot number
c	=	specific heat [J/kg*K]
c_v	=	specific heat capacity at constant volume [J/kg*K]
c_p	=	specific heat capacity at constant pressure [J/kg*K]
CV	=	specific heat value of fuel [J/kg]
d	=	hydraulic diameter [m]
h	=	heat-transfer coefficient [$W/m^{2*}K$]
k	=	thermal conductivity [W/m*K]
k_f	=	thermal conductivity of working fluid [W/mK]
k_s	=	thermal conductivity of matrix material [W/mK]
L	=	characteristic length [m]
L_b	=	time of hot or cold blow [s]
L_s	=	length of regenerator shim [m]
m	=	mass [kg]
$\dot{m}$	=	mass flow rate [kg/s]
M	=	molecular weight of fluid [kg/kmol]
Nu	=	Nusselt number
P	=	power [W];
		duration of period [s]
p	=	pressure [bar]
Q	=	energy transfer [J]
Qin	=	energy added to hot end during each cycle [J]
$Qout$	=	energy added to cold end during each cycle [J]
Qr	=	energy released from regenerator during each cycle [J]
Qa	=	energy absorbed by regenerator during each cycle [J]
Q_{ex}	=	exhaust gas losses [J]
Q_{sup}	=	heat energy supplied to TD Pile [J]
q	=	heat flow rate [W]
R	=	cylinder radius [m];
		universal gas constant
Re	=	Reynolds number
Rf	=	recirculation factor
r	=	compression ratio
s	=	reduced dead space V_s/V_0
T	=	temperature [K]
T_{hot}	=	hot end temperature [K]
T_{cold}	=	cold end temperature [K]
T_0	=	ambient temperature [K]

T_{eo}	=	temperature of fluid entering regenerator from hot end
T_{re}	=	temperature of fluid leaving regenerator at hot end
T_{co}	=	temperature of fluid entering regenerator from cold end
T_{rc}	=	temperature of fluid leaving regenerator at cold end
tf	=	gap between regenerator shim [m]
U	=	utilization factor (Λ/Π)
ΔV	=	displaced volume during expansion or compression stroke [m^3]
V_{swept}	=	working fluid volume swept through regenerator [m^3]
V_{dead}	=	working fluid volume inside regenerator [m^3]
V_e	=	volume of expansion space [m^3]
V_0	=	maximum volume of V_e [m^3]
V_s	=	dead space (space not swept by pistons) [m^3]
w	=	semithickness of matrix material [m]
y	=	distance from entrance of regenerator matrix [m]

Greek letters

Λ	=	reduced regenerator length
Π	=	reduced regenerator time
Ω	=	Schalkwijk term
Λ	=	Lambda number (amount of extra air in combustion)
μ	=	dynamic viscosity [Pa*s]
ρ	=	mass density [kg/m^3]
η	=	efficiency
σ	=	Stephan-Bolzmann Constant
θ	=	phase shift of pressure cycle with respect to expansion space volume [deg]
ϕ	=	working piston/regenerator ratio
ν	=	kinematic viscosity [m^2/s]
γ	=	isotropic index cp/cv
τ	=	temperature ratio T_{hot}/T_{cold}

1 Introduction

1.1 Preface

The Malone engine and the Stirling engine may be classified as external combustion engines. In comparison to the Stirling Engine, which uses gas as its working fluid, the Malone engine employs a liquid as the working medium. The working fluid changes from the liquid phase in the cold space, to the supercritical phase in the hot space of the engine. The use of supercritical liquid produces high working pressures for most working fluids. The much higher viscosity of liquids in turn requires the use of a slower cycle frequency. The Malone engine has two fundamental advantages over the Stirling engine. Due to the low compressibility and large thermal expansion of supercritical fluids a large working pressure and volume fluctuation can be achieved. This, together with the high heat conductivity of supercritical water, allows for machines with a high power density. The use of liquid rather than gas means that the seal on the working piston is more readily maintained. The system pressure will return to atmospheric pressure when the engine is cold.

The original Malone engine was developed by John Fox Jennens Malone in Newcastle on Tyne and patented in March 1924 (Malone, 1924; 1931). After the original work by Malone between 1920 and 1932, some additional work has since been done in the field of the Malone Engine with liquids in the supercritical state as the working medium. But almost all of this was with the focus on refrigeration rather than engine cycles (Swift, 1990; 1993).

In the mid 1990s Professor S. H. Salter started to explore the use of Artemis Digital Didisplacement™ hydraulic pump motor, as a power take-off system for Stirling cycle engines (Salter and Rampen, 1993). Dr W. H. S. Rampen recognized that the high cycle pressures and low cycle frequencies of the Malone engine were well matched with the capabilities of the Artemis motor (Rampen et al. 1997). Pioneered by Salter and Rampen, the Artemis Digital Displacement™ pump motor is a multi-

cylinder piston machine with microprocessor-controlled inlet and outlet poppet valves. In this machine each cylinder can be commanded to pump, motor or idle within each shaft revolution. This enables the creation of a controllable bi-directional flow with high efficiency and fast response times. The selection of cylinders allows the output power of the pump/motor to behave like a fluid function generator capable of very high levels of power transmission.

The experimental and analytical study presented in this thesis consists of three parts. The study on a regenerator system for such an engine presents hereby the main part. The design criteria for an efficient regenerator system in a Malone engine differs substantially to that in a Stirling engines. Little work has been done in the past to analyse the regenerator for these engines. A fundamental study to establish the design criteria followed by a more engine specific study is presented in this work. The other two parts present a study on the proposed hydraulic power take-off system and combustion system for the engine.

Taking into account the complexity of this project, it would be impossible to do an in depth analysis of all the parts of the engine, though they may have been built and tested during the study.

1.2 Stirling engine history

The first engine, working on the principle of thermal expansion of the working media, in a thermodynamic cycle can be credited to Denis Papin (Kolin, 1972). Papin's invention from 1690 consisted of a pressurized steam vessel that was heated by an open fire and then cooled with atmospheric air. The vacuum created by the condensation of the steam was applied to a piston which was connected to a load. His engine can be seen as the ancestor to the steam engine.

Glazebrook describes the first engine working on an open hot gas cycle in 1797 (Zarinchang, 1972). His engine consists of a compressor piston and a working piston, which were connected to the ends of a beam. The smaller piston was used to compress

the incoming air, which was then heated and applied to the larger working piston. This engine already utilized the energy from the outgoing air to preheat the cold compressed new air. Glazebrook patented the idea to cool and reuse the outgoing gas in 1801. This can be seen as the first external combustion engine, working on a closed regenerative cycle. Glazebrook mentioned the idea of using a regenerator in his patent from 1801 but dose not appear to have used one in his engine (Zarinchang, 1972).

The Stirling Engine works on the same principal, of cyclic thermal expansion and construction of the working media in a closed regenerative cycle and was invented in 1815 by the Reverend Dr Robert Stirling (1790 – 1878). The original Stirling Engine configuration uses a working piston to expand the working space and a displacer to shift the fluid between the hot and the cold parts of the engine. The key element in Stirling's invention is the idea of having a "regenerator" between the hot and cold space of the engine. Robert Stirling invented this device, which he called an economizer, in 1817 in order to avoid the otherwise large internal losses (Stirling, 1817). His original regenerator system consisted of a thin wire wrapped around the displacer. With the regenerator it is possible to store and reject the bulk of the energy from the fluid when it passes between the hot and cold space and, therefore, substantially improve the engine efficiency. Theoretically, at least, the engines can achieve the Carnot efficiency, which is the highest possible for a heat engine (Senft, 1991). The first commercial use of Stirling's regenerator was by the Siemens brothers in the manufacture of glass, for which Stirling received no payment (Walker, 1980). A complete description of the Stirling cycle is given in chapter 2.2.

Throughout the 19th century these engines, at this time known as hot air engines, were made in relatively large numbers and mainly used for applications such as the pumping of water and the driving of small machinery. Compared with other engines at the time, these engines were reasonably safe and efficient. By the end of the 19th century, the production of Stirling engines had virtually stopped worldwide. Internal combustion engines had become better and cheaper and quickly replaced both Stirling and steam engines.

Driven by the need to power tube radios, in remote places, the Philips research group started work on small Stirling engine generators in 1937 and opened the chapter of the modern Stirling engine. Extensive research on Stirling engines and Stirling refrigerators was done at the Philips Research Laboratories in Eindhoven (Holland) between 1940 and 1979. In 1938, Philips demonstrated its first Stirling engine with 16 W shaft power at 1000 rpm. By 1943, Philips had its first double acting engine running, a 4-cylinder machine with wobble plate and an output power of 5 kW at 3000 rpm. Phillips developed the last Stirling engine in Eindhoven in 1979. This was a 3 kW displacer engine to drive heat pumps for domestic heating and cooling systems (Hargreaves, 1991).

Over the years Philips granted a number of licenses to other companies. The three main licencees were the General Motors Company, the United Stirling AG of Sweden and the German company MAN.

The development program with General motors started in 1958 and included a number of different engines that ranged from small mobile power units, car, bus, and locomotive engines (Walker, 1980). In spite of making good progress, General Motors stopped the development work on Stirling engines in 1970, though primarily due to problems that the company was facing in other areas. The Ford Motor Company took over the General Motors licenses in 1972 and concentrated on the development of engines for the automotive market. Philips and Ford developed a 135 kW double acting Siemens type engine. In 1976 Ford and Philips were able to demonstrate the Ford Torino powered by a Stirling engine system. A number of unsolved technical problems mainly with regards to piston seals, output power control and hot end heat exchanger remained unsolved (Hargreaves, 1991).

United Stirling focused initially on the development of a silent and low emission bus engine. Philips converted an advanced flat four boxer Stirling engine, that had been developed for marine applications, into a four-cylinder in-line bus engine. Later work at United Stirling included research on a double-acting square-four Siemens-type engine and, also, the development of Stirling powered cars. They worked with American Mechanical Technology Inc. and the American Motors Corporation on this

project. The research program eventually resulted in the successful underwater propulsion system for submarines (Neelen et al. 1971).

The work at MAN in Augsburg-Nuerenberg in Germany started off with the development of small single-acting machines and progressed to larger double-acting machines by 1970. The German Ministry of Defense then funded further development at MAN but, unfortunately, little is known about any result (Walker, 1980).

It is difficult to understand why such a promising line of development has not resulted in the widespread use of these engines. The main reason for this might be the combination of high production costs, especially for the hot end heat exchanger, coupled with technical problems which mainly involved sealing. Another difficulty the Stirling engines are facing is the large technical lead that the competing internal combustion engines have due to continuous development over the last 130 years. When the manager of the Phillips program was asked, "What is wrong with the Stirling engine?" His answer was: "The existence of other engines" (Hargreaves, 1991).

Stirling engine principles

In the broadest way the Stirling Engine can be described as a mechanical device that converts thermal energy into mechanical work energy. The thermal energy is, supplied from an external source such as external combustion and mechanical work is extracted with the help of a working piston-crank arrangement. The conversion of thermal energy to mechanical energy is achieved through the regenerative cyclic thermal expansion and contraction of the working fluid between two different temperature levels.

The thermal expansion and contraction is achieved by creating a hot and a cold space in the engine and mechanically displacing the fluid with a displacer between the two spaces (see figure 1.1).

A regenerator is placed in the alternating flow passage so that when the fluid is displaced from the hot to the cold space the bulk of the thermal energy is stored in a matrix of low thermal expansion and returned in the next stroke as fluid moves through it in the opposite direction. The thermal expansion and contraction of the working fluid causes the system pressure to cycle between low and high pressure. The working piston is phased to the thermodynamic cycle in such a way that the compression stroke is done at the time in the cycle when the system pressure is low and the expansion (working) stroke is done at the time when the system pressure is high.

The resulting pressure volume cycle (P-V Diagram) as shown in Figure 1.1 can be divided into four distinct parts. Starting from the time of low system pressure and large system volume (Point 1) the cycle can be described as follows:

In the first part of the cycle, 1-2, the working piston is driven towards the engine and the working fluid undergoes an isothermal compression. It the second part, 2-3, the fluid is displaced through the regenerator from the cold space into the hot space and undergoes constant volume heating, whereby the system pressure rises. In the third part, 3-4, the working piston is driven away from the engine and extracts mechanical work, during which fluid undergoes an isothermal expansion. In the fourth part, 4-1, the fluid is displaced from the hot space into the cold space and undergoes constant volume cooling. The pressure drops and the cycle starts again.

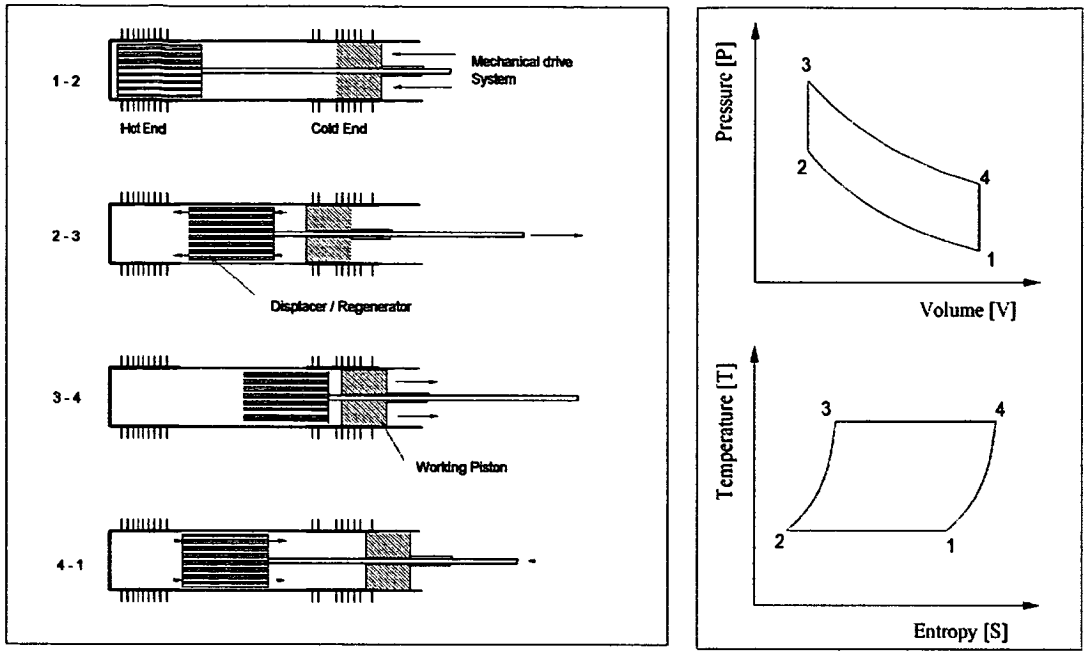


Figure 1.1. The four different phases in the Stirling engine cycle are shown. 1-2 isothermal compression; 2-3 constant volume heating; 3-4 isothermal expansion; 4-1 constant volume cooling and the relating P-V and T-S diagram.

Since the invention of the Stirling engine, a large number of different mechanical arrangements have been described and made. All the systems follow the described cycle as shown in figure 1.1. There are a number of different ways in which these components can be arranged. A detailed description of these is given in 2.4.

In principle the Stirling cycle is equivalent to the Carnot and, therefore, could achieve the highest thermal efficiency possible for a heat engine. However, this is only possible with the assumption of ideal gas behavior of the working fluid and in the absence of any irreversible losses. Practically, it is not possible to achieve the Carnot efficiency, due to internal losses. These losses are mainly due to imperfect heat transfer in the regenerator and due to pumping losses.

To achieve high efficiency it is essential to exchange most of the heat energy from the working fluid into a regenerator matrix during the constant volume cooling stroke and to return this energy into the fluid in the isometric heating stroke.

1.3 Malone engine

The basic principle of the Malone Engine is the same as that of the regenerative hot-air cycle originated by Robert Stirling in 1815. The engine incorporates all the main components found in Stirling engines and follows the same characteristic PV-diagram (Malone, 1924).

There are however a number of fundamental differences between the Stirling and Malone engines. Malone's engine uses fluid in the liquid and supercritical region as the working medium. As a result of this, his engines worked at very high pressures, with small swept volumes and piston displacements. In all of his engines, the quantity of the compressible working fluid inside the regenerator was much larger than the quantity outside of it (Malone, 1924; 1931). This differs from the Stirling engine where only a small portion of the working fluid is, at any one time, contained in the regenerator. Consequently, Malone used a different type of regenerator in his engines.

The regenerator used by Malone in his liquid engines was made from a number of concentric steel tubes with flow passages between them. Malone installed two one-way valves towards the cold end of the regenerator, in order to direct the flow through different channels (see figure 1.2). The valves were arranged, so that liquid coming from the hot end in the isometric compression stroke, and liquid coming from the cold end in the isometric expansion stroke, were forced to pass through the regenerator in different flow passages. This arrangement is different to that of the regenerators used in the Stirling engine, in which the fluid from the hot and cold end alternates in the same flow passages (Malone, 1931).

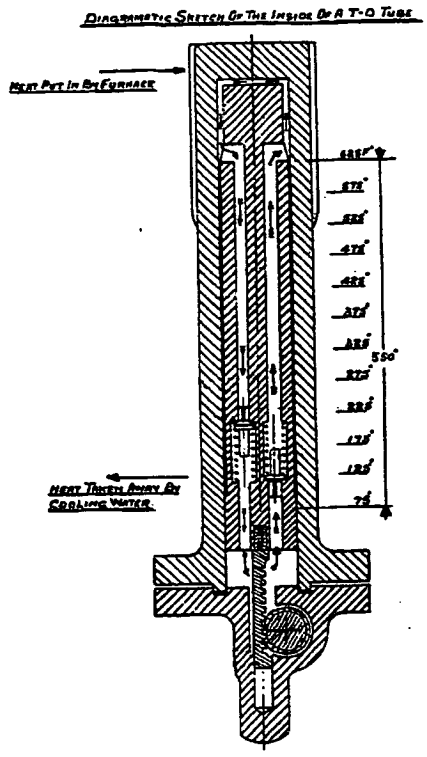


Figure 1.2. The regenerator system of Malone's original engine is shown. The fluid from the cold blow is channeled with a non-return valve (right) through the regenerator and up into the hot end. In the hot blow the fluid returns through different flow passages (left) downwards into the cold end. It takes a number of engine cycles for the fluid to shift from the hot end to the cold end and back. (Drawing from Malone's report in the "Journal of the Royal Society of Arts", June 1931)

In his article for The Journal of Art, Malone (1931) defines the ideal working medium such that: "The liquid needs to be a mobile liquid between atmospheric temperature and the temperature at which steel has its economic strength. Its compressibility should be proportionate to its dilatation, it should be a stable compound not easily disassociated chemically, and it should not be explosive, poisonous, nor too readily burnt."

Malone experimented with a number of different liquids and came to the conclusion that water is the most suitable thermodynamic medium for this new type of engine. Oils fail as a result of their high viscosity at low temperatures or are too unstable at high temperatures. Malone found Sodium, Potassium and their alloys to be too dangerous and Mercury to be too expensive. It is doubtful that any of these liquids

will ever be used in liquid engines, because of the need to work up to the supercritical phase. Leaving aside the viscosity problem of the oils, the thermal stability lies far below the critical temperature.

All of Malone's Engines operated in the supercritical pressure region with working pressures of 220 to 800 bar, see graph 1.3. By working with pressures always above the critical pressure, Malone avoided any evaporation or condensation of the working fluid. There is no liquid or gas phase in the supercritical phase and Malone's description of the liquid and gas phase in the critical area of figure 1.3 has to be treated as incorrect. His engines typically worked at around 50°C in the cold end and 400°C in the hot end (Malone 1931). Given the poor thermal expansion of water at the temperatures towards the cold end, and the high viscosity, it is difficult to understand the effectiveness of such low cold end temperatures. It can be presumed, that the high pumping losses coming from high viscosity of liquid water will use up most of the relatively small amount of work coming from the thermal expansion of the water at these temperatures. This problem will be considered in greater detail in Chapter 5.

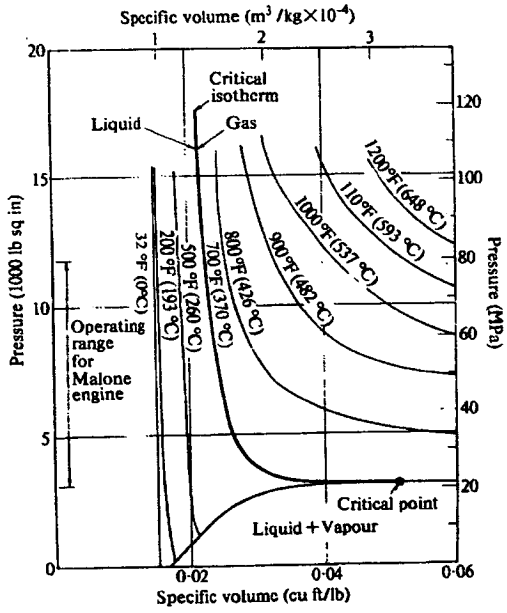


Figure 1.3. Pressure – Specific Volume diagram for water with indicated operating points of Malone's original engine. Notice the significant change of specific volume per temperature change just above critical temperature and pressure. (Graph from Malone's report in the "Journal of the Royal Society of Arts", June 1931)

History

John Fox Jennens Malone, was born in 1880 in northern England. Malone's formal education ended in his 18th year and he spent the next 14 years in the merchant marine working on large steam ship engines. He started his own company "The Fox Instrument Company" and began experimenting with liquid engines in the 1920's (Swift, 1989, 1992). He patented his liquid engine in 1924 and designed and built three different machines working on this principal over the following years. The center of his engine is what Malone called the "Thermodynamic Pile" often referred to as TD-Pile. It incorporates the hot and cold end heat exchangers and the displacer with the regenerator. His first machine was a large vertical engine with 80 TD-Piles and two working pistons and which produced 50 brake horsepower in 1925. Malone conducted a large number of tests with this first machine between 1925 and 1927. He tried a number of different working fluids including oil, petrol, alcohol liquid CO_2 and SO_2 and concluded later that water was the most appropriate fluid. He was also able to gain knowledge of the basic operation of the engine and optimized the displacement ratios and phase angle. Based on the experience that he gained from the first engine, he built a smaller horizontal engine. This more versatile 50 horsepower engine was in constant use as a test and demonstrator engine (Ford, 1983). In the late 1920s liquid fuel became more economical and the internal combustion engine became dominant. This, together with the economic depression at the time, brought Malone's work to a halt. By the end of 1931 Malone had to declare bankruptcy and all his work ceased (Swift, 1992). Unfortunately his engines were all scrapped and documents relating to his work have been closely guarded by his family.

With his second engine Malone was able to prove that his machines could run reliably over long periods of time and also achieve overall efficiencies of 21%, a very high value for the time. Malone had been able to demonstrate a number of advantages of his liquid engines over the Stirling engine. Firstly, working with high-pressure liquid rather than gas, he did not experience the same sealing problems on the working piston. Secondly, there was the advantage that the pressure in his liquid engine returned to atmospheric when the engine was cold, solving the problem of containing the working fluid while the engine is switched off. In his early experiments, he

discovered that water in the dense phase had both larger thermal conductivity and larger thermal expansion compared to gas (Malone, 1931).

In his paper, published in The Royal Journal of the Arts (Malone, 1931), the test results from three independent engineers are described. It was claimed that Malone's engine had an indicated efficiency of 27%. This is about double that achieved by locomotive or marine steam engines of the time. Malone further claimed that one of his smaller engines had run well over 30,000,000 shaft revolutions. This relates to a running time of 2500 hours at the typical low shaft speeds of around 200-rpm.

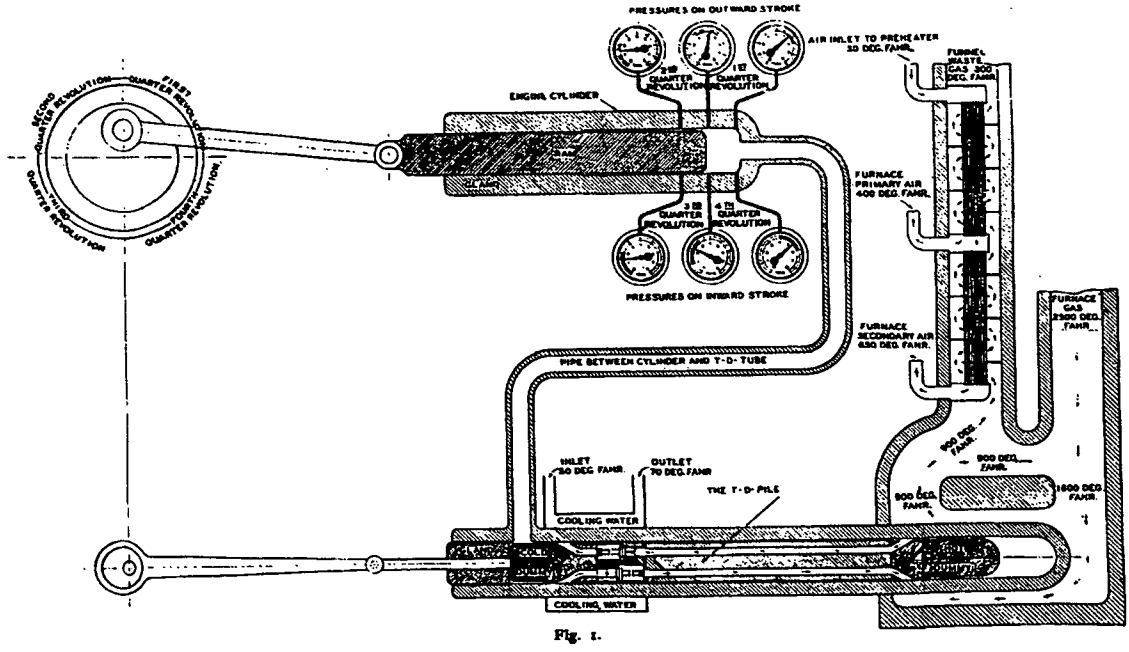


Figure 1.4. The layout of Malone's original engine is shows. The main components are: top left- working piton crank drive; top- working piston, bottom left- regenerator/displacer crank drive, bottom- TD-Pile with hot end, cold end and regenerator; right- coal fired furnace with exhaust gas heat recovery. (Drawing from Malone`s report in the "Journal of the Royal Society of Arts", June 1931)

Malone used a coal-fired furnace as a heat source for the hot end, and a water-cooling jacket to cool the cold end (see figure 1.4). The furnace already incorporated an

exhaust gas recuperator to preheat the combustion gas and to minimize the exhaust gas losses.

Due to the high working pressures and the limited high temperature strength of cast steel at the time, Malone had to work with relatively small diameters for the hot end heat exchanger in order to minimize stress in the TD-Pile wall. For his larger engines, Malone chose to use a number of TD-Piles connected in parallel and working off the same drive shaft and with a common working piston.

1.4 The Artemis Malone engine

The basic principle of the Artemis Malone Engine is based on the Stirling cycle and is the same that Malone used in 1924. The fluid is shifted between the hot and the cold space of the engine and the thermal expansion and contraction of the working fluid is applied to drive the working piston, which is mechanically linked to a crankshaft. In the original Malone engine the working fluid acts directly on the working piston. In contrast, the Artemis Malone Engine uses a separator to transfer the working fluid pressure and displacement into hydraulic oil. A multi-cylinder hydraulic pump/motor is then used to replace the fixed harmonic piston motion. In addition to this the Artemis Malone engine uses a different type of regenerator system, rather than the contraflow system originally used by Malone. Figure 1.5 presents a comparison of Malone's original engine with the proposed Artemis Malone engine.

The Artemis-Malone concept arose from the need to address the three key technical problems experienced with the Stirling engine. These were: controllability of the output power, sealing of the working fluid at the working piston and the high cost of the hot end heat exchanger. To describe the problems and solution more specifically:

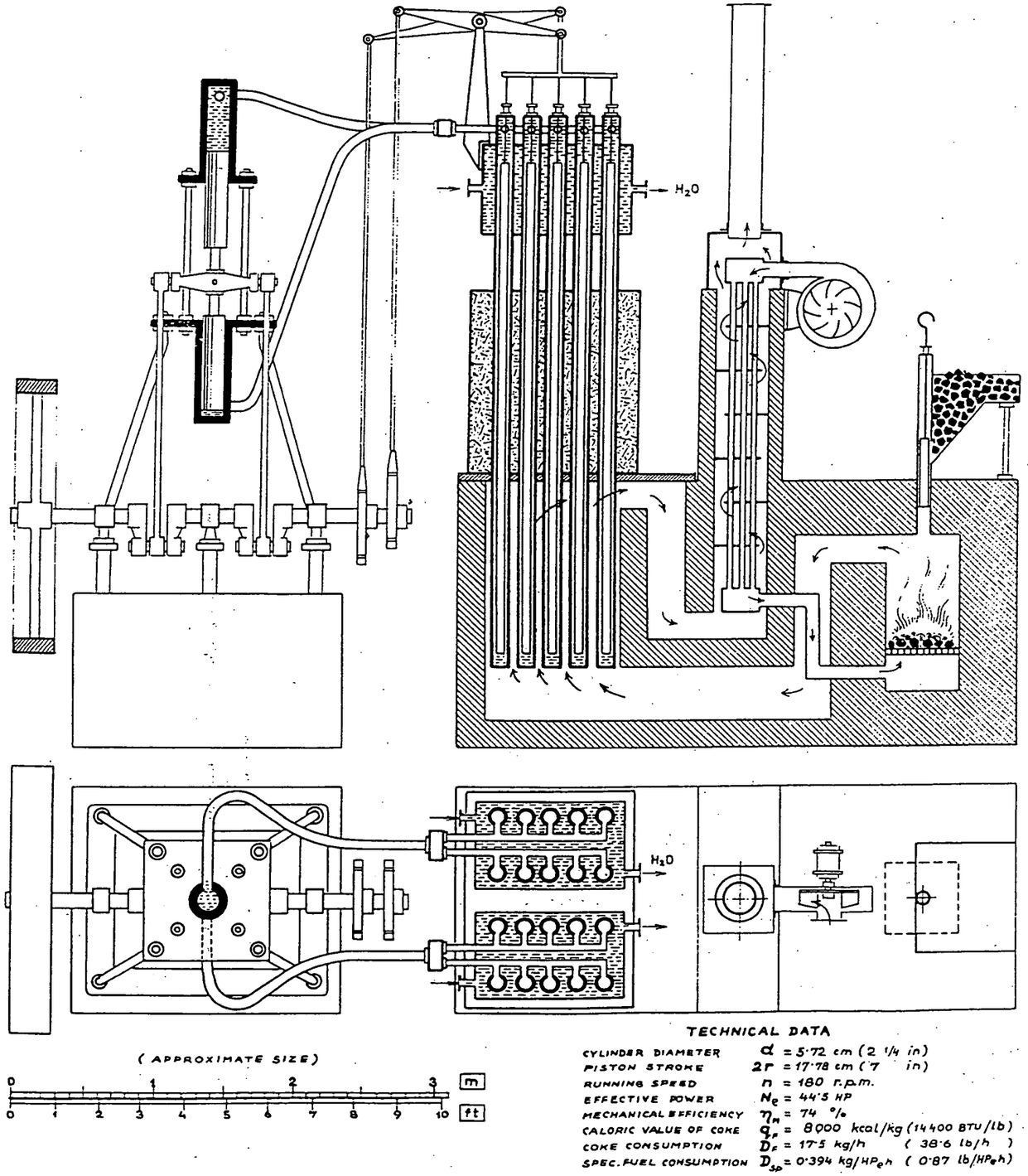
- The first problem is caused by the time lag between the change of input combustion power and the response of mechanical output power on the shaft. By designing engines with small thermal inertia and control over the dead volume,

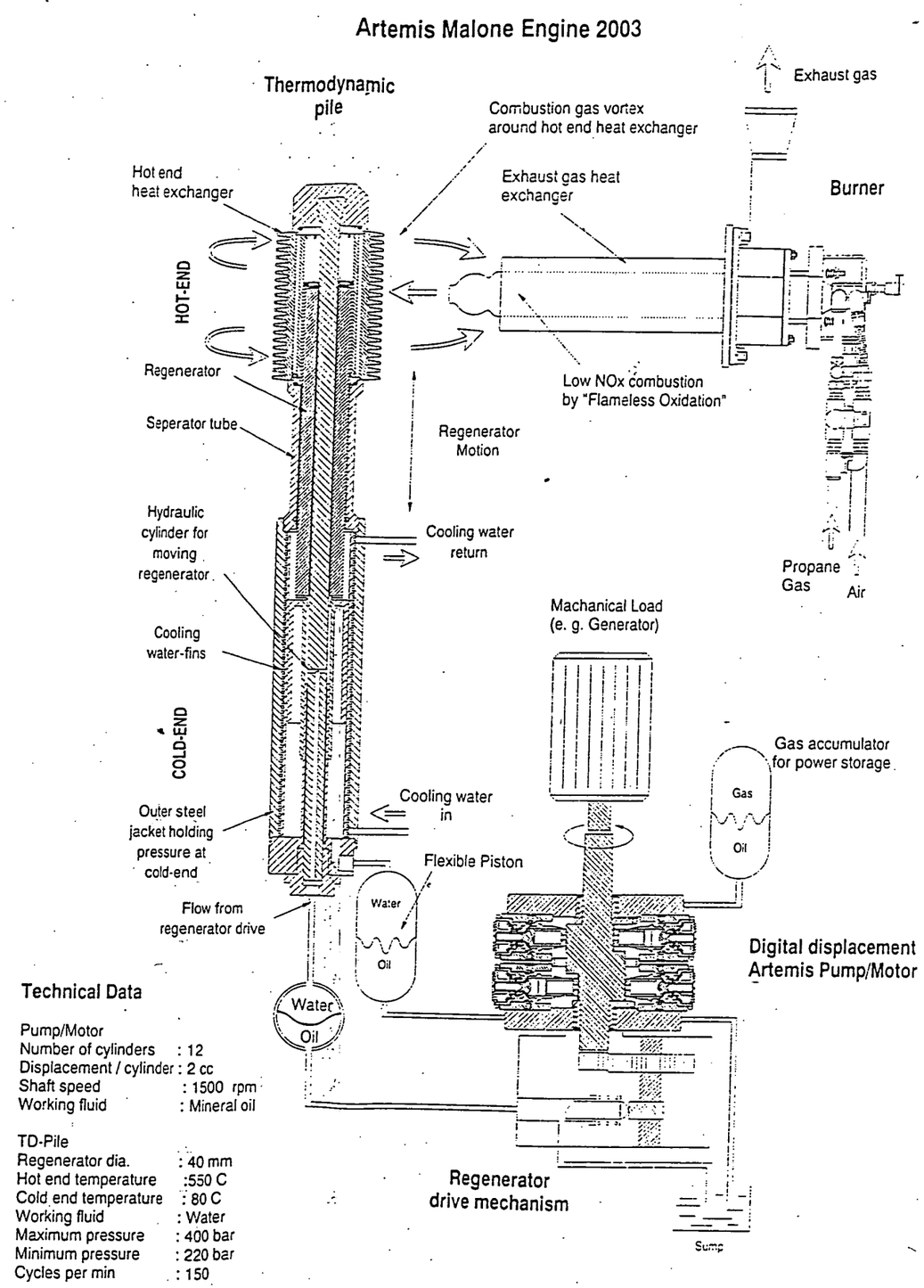
this time lag can be reduced significantly. It is still, however, unsuitable to be directly coupled into the vehicle drive train.

The Artemis hydraulic power take-off system is able to overcome this. Additional cylinders of the Artemis Digital Displacement™ pump/motor can be commanded to pump fluid into high-pressure accumulators at times of low power demand to buffer energy. This energy can be reused when instant power is required. A further advantage of the separate power take-off system is the flexible packing arrangement due to the modular nature of the components.

- The second problem arises from the difficulty of containing the pressurized working fluid in the engine space. To achieve reasonable high power densities and good thermodynamic efficiencies, it is necessary to compress the working gas to high pressures and, also, to use a gas with a very low viscosity such as hydrogen or helium. This gas then acts across the dynamic seal on the working piston and, unfortunately, no practical way of maintaining the seal for any length of time has been found.

  It is possible to solve the leakage problem on the working piston by transferring the pressure from the working fluid into hydraulic oil, with the help of a separator membrane. The Artemis digital hydraulic power take-off system then acts on the hydraulic oil side of the system (see figure 1.5). Due to the multi cylinder design of the hydraulic pump/motor and the controllability of individual cylinders, it is possible to replace any leakage by adding extra pumping cylinders during operation.





Technical Data

Pump/Motor	
Number of cylinders	: 12
Displacement / cylinder	: 2 cc
Shaft speed	: 1500 rpm
Working fluid	: Mineral oil
TD-Pile	
Regenerator dia.	: 40 mm
Hot end temperature	:550 C
Cold end temperature	: 80 C
Working fluid	: Water
Maximum pressure	: 400 bar
Minimum pressure	: 220 bar
Cycles per min	: 150

Figure 1.5 The left figure shows Malone's original engine from 1931. The engine had 20 thermodynamic piles, of which 10 were connected to each of the two working pistons. Malone used a mechanical linkage to operate the working pistons and the regenerators at synchronous speed. The engine was fired with coal and had an exhaust gas heat exchanger to preheat the incoming combustion air. Malone achieved an overall efficiency of 20 % at pressures between 220 and 700 bar and at a hot end temperature of 450 C.
The right figure shows the Artemis Malone Engine as analysed in this study. The engine works with one thermodynamic pile, which is connected, to the Artemis digital displacement pump/motor ™. The Pump/Motor is geared to the hydraulic regenerator drive system and runs at ten times the frequency of the thermodynamic pile. Each cylinder of the 12 cylinders can be commanded to pump, motor or idle within a shaft revolution via microprocessor control allowing non-sinusoidal working piston motion. This can be used for P-V diagram optimisation, replacement of leakage and optimisation of part power operation. Excess power can be stored in accumulators, allowing access to instant power when required. The combustion system works on the basis of flameless oxidation to minimise the production of NOx.

- The third and potentially the most difficult problem to tackle is the high cost of the hot end heat exchanger. Any efficient engine will have to work with a hot end temperature above the limits of conventional steels. This requires the use of high temperature alloys such as Ni-Superalloys or Ceramics, leading to high material and fabrication cost.

  The required surface area between the heat exchanger and the working fluid largely drives the complexity and required mass of high temperature materials. Supercritical water has favorable heat transfer properties, compared to gaseous working fluids, thus allowing simpler designs with less high temperature material per unit output power.

  The ability to crate an arbitrary working piston motion allows control of the P-V diagram such that work per stroke can be maximised whilst destructive pressure overshoot can be eliminated. This allows the maximum use of the metallurgical strength of the hot end heat exchanger.

In this early stage of development it would seem logical to apply the Artemis hydraulic technology to the much more advanced conventional Stirling engine. Attempts have been made to apply conventional hydraulic power take-off systems to a number of different Stirling engines. It has, however, always proven to be difficult to implement an efficient liquid power take-off system to the much higher cycle frequencies and lower pressures typically found in Stirling engines. Further, there is the need to avoid any extra dead volume in the Stirling engine due to the compressibility of the gaseous working medium. This problem does not exist in the Malone engine due to the incompressibility of the liquid working fluid in the cold end.

1.5 Overview of thesis structure

This thesis combines an experimental and theoretical study of aspects of the Artemis Malone Engine. It gives a detailed description of the regenerator and uses the results from the experimental and theoretical study to analyse the feasibility of such an engine.

The arrangement of the chapters largely follows the order of the energy flow through the engine. This starts from the heat source, describing the combustion, system followed by the thermodynamics of the Thermodynamic-Pile and ends with the hydraulic power take-off system.

More specifically:

Chapter two is a literature review

Chapter three addresses the design of the combustion chamber and demonstrates the energy flow outside the engine.

Chapter four describes the development work done in the area of hot end heat exchanger.

Chapter five comprises the main part of this work and gives a detailed description of the analysis and testing of the regenerator of the engine.

Chapter six describes the hydraulic power take off system and shows how the hydraulic system control is coupled to the thermodynamic pile performance.

In **chapter seven** a discussion of the results is made and recommendations for further development work are made.

2 Literature Review

2.1 Introduction

This Chapter describes the previously published work which is relevant to the different areas of research covered in this thesis. The research on the Artemis Malone Engine required a large amount of analytical work away from the main subject of the Stirling cycle engine and into the areas of thermodynamics, fluid power and combustion technology.

The review has been divided into three sections roughly corresponding to the main areas of research. The first section covers the fundamental theory behind the Stirling and Malone engine. It looks at the different theoretical and experimental studies that have been carried out in order to establish the fundamental principles and limits of these engines. The second section looks at the different mechanical arrangements described and tried in Stirling cycle engines, especially with regards to the use of hydraulic power take-off systems. The third and last part looks at the previously published work with regards to the combustion system in Stirling and Malone cycle engine.

Since the invention of the Stirling Engine in 1816 an immense and diverse amount of research has been done in order to understand the complex mechanics, fluid dynamics and thermodynamics of these engines. Conventionally the research took place in the form of experiments. More recently, with the aid of faster computer systems, the modeling of Stirling cycle engines has made a real contribution to our understanding of the complex fluid dynamics and thermodynamics. There is a vast amount of theoretical literature, which covers the basic function of the Stirling engine. In contrast to this, a surprisingly small amount of research and very few publications are available in both the field of the Malone Engine and that of the use of a liquid as the thermodynamic working medium.

2.2 Stirling cycle engine

Before we look at the more specific parts of research, the following publication are named for their importance in covering the general knowledge that has been collected in the field of the Stirling Engine.

In particular, the work by Walker gives a comprehensive review of the research in this field. In his books "Stirling Engines" (Walker 1994) and "The Stirling Alternative" (Walker 1980) a complete overview of the work done on Stirling engines is given.

In his book "The Philips Stirling Engine" C.M Hargreaves (1991) presents a complete collection of the work done by Philips between 1937 and 1979. He gives a detailed description of the different machines that have been developed by Philips and induces a comprehensive report on the theoretical background of the work.

Prof. T Finkelstein made a considerable contribution to the theoretical analysis of the regenerative Stirling cycle. In the book "Air Engine" (Finkelstein and Organ 2001), Finkelstein gives a comprehensive review of the development of the Stirling engine from the invention to the present day.

The work done by Allan J. Organ provides a detailed and complete description of the thermodynamics and kinematics in Stirling engines. In his books "The Thermodynamic and Gas Dynamics of the Stirling Cycle Machine" (Organ 1992) and "The regenerator and the Stirling engine" (Organ 1997) he provides a complete analysis of the gas dynamics and thermodynamics in Stirling engines.

2.3 Cycle analysis

In order to develop efficient Stirling cycle engines, it is essential to be able to describe the complex fluid dynamics and thermodynamics of the Stirling cycle. The main

problem with the analysis of the Stirling cycle comes from the fact that the different processes of compressing, heating, expanding and cooling merge into each other and happen simultaneously in different parts of the engine. For this reason, unlike the steam engine cycle, it is not possible to describe the Stirling cycle in a simple thermodynamic equation.

It was not until 30 years after the invention of the Stirling engine in 1816 that McQuorne Rankine was able to describe the thermodynamics of the Stirling cycle (Zarinchang, 1972).

G. Smith (1861) made the classical analysis of the Stirling cycle in 1861. The Smith cycle presumes isothermal condition in the compression and expansion strokes and has, therefore, to be seen as highly idealised. It is still useful however in order to get a rough approximation of the engine performance. In practical engines running at 1000-rpm it can be presumed that the process is nearly adiabatic. Walker (1980) states that, in this case, the indicated performance will be no better than 60% of the predicted Smith cycle performance.

T. Finkelstein (1960) made the next major development in the theoretical analysis of the Stirling cycle in 1960. Finkelstein introduced a model with limited heat transfer between the working fluid and the hot and cold end cylinder walls. Under the assumption of limited heat transfer during the compression and expansion stroke, the model becomes closer to the more adiabatic condition in the real engine.

J. Senft (1993) shows, in a simple model, which analyzes the ideal energy exchange in the engine, that it is possible for the engine to achieve Carnot efficiency. The model assumes ideal gas behaviour, and the absence of irreversible losses. Senft's simple analysis is important to the understanding of the Stirling engine and, therefore, a short description of it is made at this point.

The heat exchange from the fluid into the regenerator matrix happens in the isometric contraction stroke when the fluid is displaced from the hot end to the cold. The working medium passes through a matrix of large surface area, low thermal expansion

coefficient, and high thermal capacity. Under ideal conditions it is possible to transfer the complete enthalpy difference (Qa) of the fluid between T-hot to T-cold into the regenerator matrix. This stored energy can be returned into the working fluid (Qr) in the next isometric expansion stroke. This occurs when the fluid passes through the same matrix while it is being displaced from the cold end to the hot end.

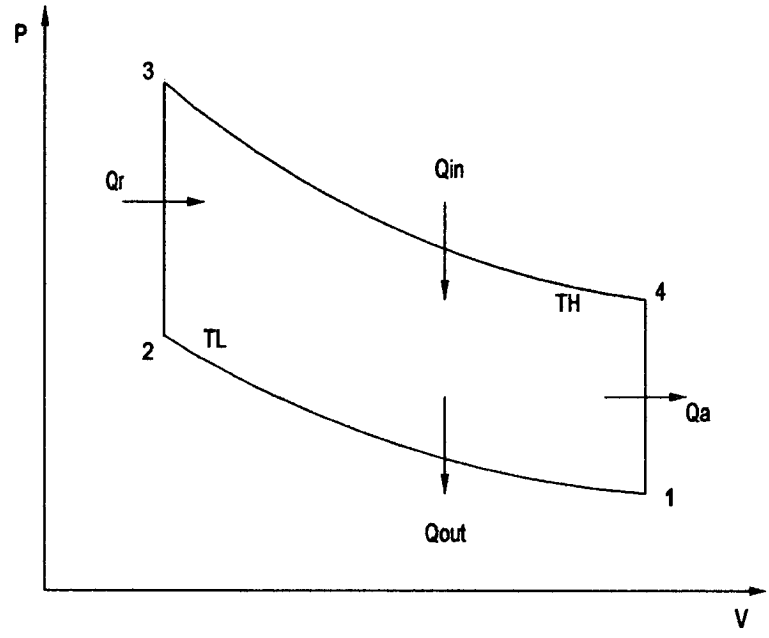


Figure 2.1. PV-diagram of the ideal Stirling cycle. 1-2 isothermal compression, 2-3 isometric heating, 3-4 isothermal expansion, 4-1 isometric cooling.

The energy Qr for the constant volume heating of the working fluid equals, under ideal conditions, the energy Qa released from the constant volume cooling of the working fluid.

$$Qr = Qa = mc_v\Delta T \qquad 2.1$$

m is hereby the mass of the working fluid, c_v the constant volume specific heat capacity, and T the temperature change.

Under this assumption of perfect thermal regeneration and an ideal gas behaviour the energies Qr and Qa do not have to be taken into account for the thermal efficiency calculation.

The heat absorbed *Qin* in the isothermal compression stroke 1-2 and the energy rejected *Qout* during the isothermal expansion stroke 1-2 can be described as:

$$Qin = mRT_H \ln r \qquad 2.2$$

$$Qout = mRT_C \ln r \qquad 2.3$$

R is hereby the gas constant of the working gas and r the compression ratio V_4/V_3. Senft is then able to show that the cycle efficiency can equal the Carnot efficiency. With the regenerator working perfectly, the thermal efficiency of the ideal Stirling cycle can be decried as:

$$\eta_{ideal} = \frac{Qin - Qout}{Qin} = 1 - \frac{T_{cold}}{T_{hot}} = \eta_{carnot} \qquad 2.4$$

A further step towards a more realistic model was taken by J. Smith in 1960 where he introduced the decoupled second order analysis. This analysis is based on the first order (isothermal or adiabatic) model but includes the mechanical and thermal losses of the engine. Organ (1997) gives a detailed description of Smith original work.

The fast advances in computing power over the past two decades made the nodal type analysis of the Stirling engine possible. Finkelstein (1975) introduced this type of analysis for Stirling cycles. The nodal type analysis divides the engine into a number of cells or nodes and assumes the condition inside the cells to be uniform. The individual cells are then analysed using the three basic conservation laws of mass, energy and momentum. Two different grid types are commonly used to define the nodes. The Eulerian grid, which divides the engine into nodes of fixed volumes and

position and the Langrangian grid, where the nodes are of fixed mass. A comprehensive review of the different numerical techniques is given by Organ (1992).

2.3.1 Stirling engine regenerator analysis

The regenerator can be seen as the most vital component in the Stirling engine. This becomes clear when observing the energy flow diagram of a typical Stirling engine with air preheater as shown by Walker (1980) in figure 2.2. The energy transferred in and out of the regenerator is a multiple larger then the energy supplied into the engine by the external heat source. Without a working regenerator, this energy would be transferred into the cold end and irreversibly lost.

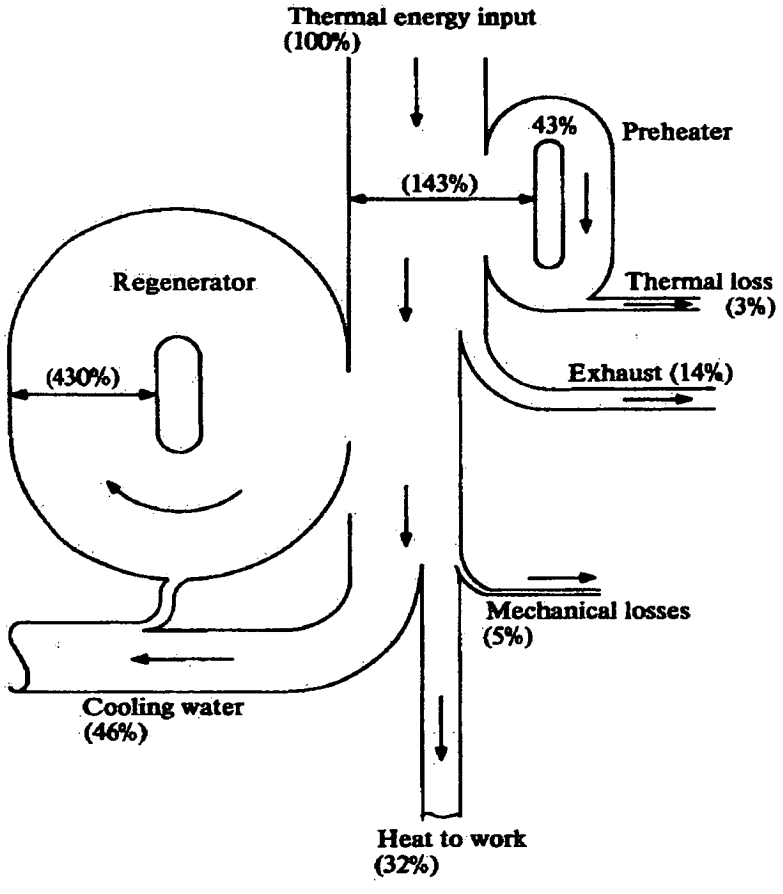


Figure 2.2. Energy flow in a typical Stirling cycle engine with inlet air preheater and working regenerator. It can clearly be seen that the regenerator shifts a multiple higher amount of energy around than the total energy supplied to the system. (Graph from Walkers book "Stirling Engines" 1980)

For any regenerator design, it is important to analyse the relationship between the energy that is transferred into the engine and the energy that is transferred in and out of the regenerator.

Hargreaves (1991) shows that this relationship can be described over equation 2.5.

$$\frac{Qr}{Qin} = \frac{\gamma}{\gamma - 1} * \frac{2*(\tau + r + 2s)}{\pi * \sqrt{\tau^2 + r^2 + 2\tau w \cos\phi} * \sin\theta} * (1 - \tau) \qquad 2.5$$

Qr	=	energy released from regenerator during each cycle
Qin	=	energy added to hot end during each cycle
γ	=	isotropic index cp/cv
τ	=	temperature ratio T_{hot}/T_{cold}
θ	=	phase shift of pressure cycle with respect to expansion space
ϕ	=	phase angle working piston/regenerator
r	=	compression ratio
s	=	reduced dead space volume

In a typical Stirling engine using hydrogen as its working fluid, with a hot end temperature of 1000 K and a cold end temperature of 300 K, and working with a phase angle of 90 deg, a dead space of 0.3, and a pressure phase shift of θ = 72 deg., the relation between Qe and Qr gives a result in the region of 3.5. In conclusion, the energy stored in the regenerator matrix in each cycle is 3.5 times the energy supplied to the hot end per cycle.

Further, it is important to analyse the factors that are defining the regenerator efficiency. The classical approach to defining the regenerator efficiency has been done by Hausen in 1929 (Hausen, 1983). Hausen analyzed the temperature deficit between the working fluid entering and leaving the regenerator in the return stroke on both the hot and the cold end site. In his calculation Hausen assumed a steady state

condition, whereby, after a number of cycles the temperature deficit is equalized by heating and cooling on the hot and cold side and the system has stabilized. Hausen proved that, under the assumption of ideal gas behaviour, the temperature deficit on both ends of the regenerator becomes equal and can be used to define the regenerator efficiency. Figure 2.3 shows the temperature profile along the regenerator, and at the points of entry and departure.

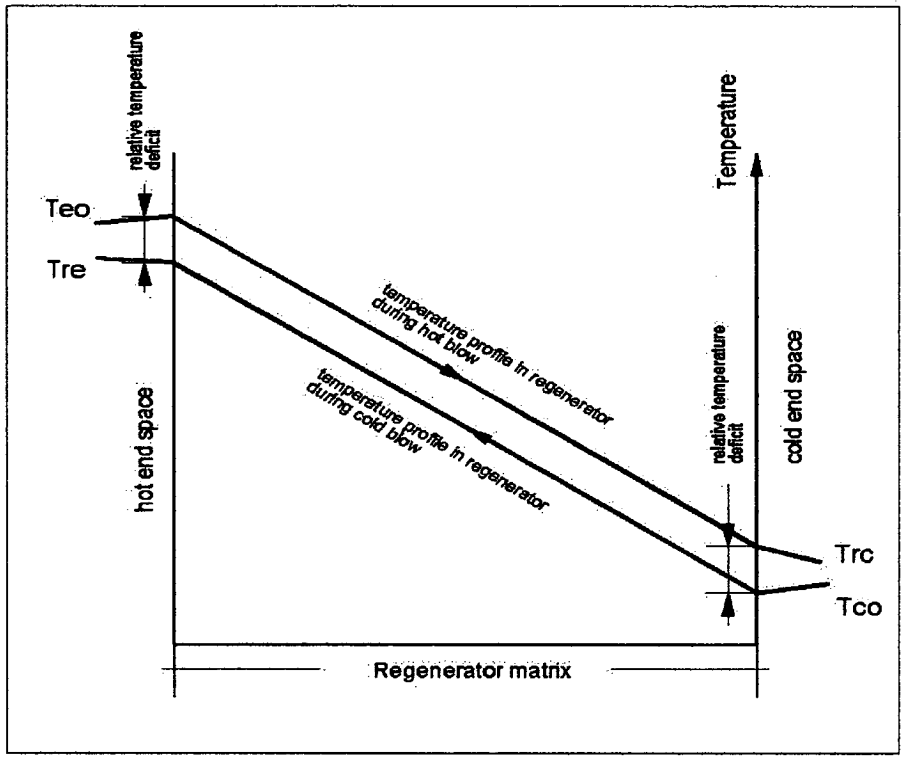


Figure 2.3. Inlet and outlet temperature of regenerator and temperature profile in regenerator during the constant volume heating and cooling stroke

Hausen is able to prove that the function defining the temperature deficit is the result of the two following conditions; (i) The heat exchange coefficient between the matrix and the fluid in relation to energy exchanged per stroke. (ii) The total heat capacity of the matrix material.

The regenerator efficiency then becomes a function of the two dimensionless numbers Λ and Γ.

$$\frac{Teo - Tre}{Teo - Tco} = \frac{Trc - Tco}{Teo - Tco} = f(\Lambda, U) \qquad 2.6$$

T_{eo} = temperature of fluid entering regenerator from hot end

T_{re} = temperature of fluid leaving regenerator at hot end

T_{co} = temperature of fluid entering regenerator from cold end

T_{rc} = temperature of fluid leaving regenerator at cold end

Λ and Γ are defined as:

$$\Lambda = h * \frac{total\ surface\ area\ of\ matrix}{heat\ capacity\ of\ gas\ flowing\ per\ second} \qquad 2.7$$

$$U = \frac{total\ heat\ capacity\ of\ matrix}{heat\ capacity\ of\ gas\ passing\ per\ stroke\ (half - cycle)} \qquad 2.8$$

Given the large difference in heat capacity per volume (ρcp) between gaseous working fluids and the matrix material, a high values for Γ is readily achievable. This allows the losses created through the temperature swing of the matrix material to be minimized. Hargreaves (1991) shows that for large values of U ($U > 10$) the influence from the matrix temperature swing becomes less important and the equation can be simplified to 2.5.

$$Teo - Tre = \frac{2}{\Lambda + 2}(Teo - Tco) \qquad 2.9$$

This equation shows that the regenerator efficiency in Stirling engines is mainly a function of the heat transfer between the working fluid and the matrix material.

A number of later works are based on Hausen`s theory of regenerative energy storage. W. Schmidt and J. Willmott (1981) give a comprehensive analysis of thermal energy

storage and regeneration. In his book "Dynamics of regenerative Heat transfer" Willmott (2001) provides a comprehensive coverage of the modeling of the processes of heat transfer in regenerative devices.

In real engines where the effects of flow losses in the regenerator, thermal conductivity losses and practical design limitations have to be taken into account, the optimization of the complete regenerator becomes very complex. Organ (1997) has dealt with this problem and gives, based on the Hausen equation, a comprehensive analysis for the regenerator in Stirling engines.

In his book "Stirling Engine" Walker (1980) describes the different characteristic properties that define the efficiency of the regenerator system.

He states that for heat transfer reasons, the ideal regenerator should have a dense matrix with high heat capacity. It is important that the heat capacity of the regenerator matrix is significantly higher than that of the fluid passing through it. This is to ensure that the fluid undergoes the full temperature swing without a significant change in matrix temperature.

Further, it is important that the size of the flow passages is chosen such that the balance of pumping losses and heat transfer rate between fluid and matrix is optimised. A large flow passage through the regenerator will create a minimum pressure drop for the passing fluid and, therefore, little energy is needed to drive the regenerator. It has to be remembered that the energy to drive the regenerator comes from the drive shaft and is, therefore, directly removed from the output power. Large flow passages, on the other hand, will create large temperature drops between the fluid and the regenerator, thus resulting in increased irreversible losses.

To minimize conductivity energy losses through the regenerator matrix from hot to cold end the matrix should have low heat conductivity in the longitudinal direction. The heat conductivity in the radial direction should be large enough to ensure complete use of the matrix material. Using a regenerator with a high length to

diameter ratio and creating thermal resistance in the longitudinal direction can generate this behavior.

For gaseous working fluid it is important to minimize the dead space in the regenerator. This, in turn, minimizes the amount of compressible fluid and, therefore, maximizes the cycle pressure fluctuation.

Given that it is not possible to fulfill all these various requirements, it is important to make sensible compromises, whereby the reduction in heat transfer balances the pumping and conductivity losses.

Continuous development and optimization work has made it possible to improve the regenerator efficiency while keeping the pumping losses to a minimum. The modern state of the art Stirling engine regenerators are made from hundreds of woven wire screens with wires thinner human hair. Test results from these regenerators show efficiencies of up to 99%, Organ (1997).

2.3.2 Malone engine development

The inventor of the engine J. F. Malone did all the original development work himself in the 1920s (Malone 1931). Operating his company as commercial enterprise Malone kept most of the test results of his research to himself.

In his book "The secrets of the Malone Engine" Richard Ford (1983) made a complete collection of all the available information about the original work. It includes a description of Malone's work in the "Journal of the Royal society of Arts" in 1931. In addition, he gives a description of Malone's work by David Brownlie and a number of the original patents.

It took a further 50 years after Malone's work came to an end in 1931 before John Wheatley, then at the University of California, rediscovered J.F. Malone's original

work and resumed the work on liquid engines (Allen et al., 1980). With the aim of applying modern materials and advanced scientific understanding of thermodynamics to the problem his group began with the systematic investigation of the principals behind Malone's engine. The later work of his group consisting of G. W. Swift, P. Allen, D. Paulson, G. Fisher produced a number of publications that greatly contributed to the understanding of the Malone engine.

G. W. Swift (1989b) conducted the first experimental work on Malone type liquid engines since Malone's original development work. In 1989 Swift was able to give the first simple theoretical model of the Malone engine. He was further able to give a detailed report on the results from his four-cylinder machine, which used liquid propane as a working medium. Swift's work in the early 1990s concentrates mainly on the development of Malone type refrigerators, which where developed under growing pressure to replace Ozone layer damaging cloro-fluoro-carbons.

G. W. Swift (1990, 1993) makes a comparison of the Malone refrigeration cycle with the Brayton refrigeration cycle. His publications include a comprehensive discussion on the limits and possibilities of the Malone refrigeration cycle. He concludes that it is possible to use the Malone cycle as a direct replacement for the vapor Brayton cycle and that gains in overall efficiency and system size can be made.

The main differences between Malone's engine and the Stirling engine are the use of a liquid in the supercritical region as the working fluid and a different type of regenerator arrangement. The following section looks at the research which is of specific importance in analysing the effect of these changes.

2.3.3 Malone engine regenerator

Malone's original experiments are the first recorded experiments conducted on a regenerator system working in the supercritical region. Malone was able to design and

build an advanced and working regenerator system which he optimised in the numerous experiments that he conducted on three different machines.

In his paper for the "Journal of the Royal Society of Arts", Malone (1931) gives a detailed description of the operating principle of the regenerator system but only limited information about the thermodynamics and limited test results. Malone's original description and later analysis do not describe the advantages or disadvantages of the contraflow arrangement. From discussion with Malone's son, we know that Malone tried to run his engines without the valve arrangement and experienced significant reduction in output power and overall system efficiencies.

P.C Allen et al. (1981) was the first to analyses the theory behind the heat transfer in the contraflow heat exchanger as used by Malone. Backed by practical experiments he is able to give a theoretical model of the thermodynamics in the heat regeneration process in Malone type liquid engines.

Reader and Hooper (1983) looked at the limitation of regenerator in liquid engines and state that the heat capacity of the matrix must be considerably higher than that of the chosen working fluid and, therefore, the use of regenerators is restricted to gaseous working fluids. This remains in direct contrast to the efficiency results achieved in one of the original Malone engines. In this case, indicated efficiencies have been found to be up to 27 %, thus indicating a working regenerator.

Gianfranco (2000) analyses the fluid dynamics and thermodynamics in the regenerator and describes the effects of real gas behavior in Stirling cycle engines. He compares the thermodynamic behavior of fluids in, and close to the supercritical region with the behavior of an ideal gas. In his theoretical model he is able to show that it is possible to use the nonlinear behavior of a non ideal gas to increase cycle efficiency.

A full discussion of the possibilities and limitations of the regenerator in an engine with a liquid working fluid is made in chapter 4.

2.3.4 Working fluid

In all heat engines, the working substance has to undergo a chemical or physical property change in order to convert thermal energy into mechanical energy. This is achieved, in internal combustion engines, through the expansion of the combustion gases and in steam engines, mainly through the phase change from water to steam in the boiler. In Stirling engines, the working piston is driven by the pressure cycle resulting from the expansion and contraction of the gaseous working fluid. J. R. Senft (1997) gives a complete model that describes the fundamental relation of the conversion of thermal energy into useful work.

The Stirling engine can, in principle, operate with any fluid of low viscosity and large thermal expansion coefficient. All early Stirling engines operated with air as their working fluid (Walker, 1980). Air is readily available, relatively easy to seal and any small leakage can be returned with the help of a compressor. In the 1950s and 60s there was a great deal of pressure to build Stirling engines which could compete with the internal combustion engine. This competition resulted in comprehensive research into the use of light gases and subsequently engines with high efficiencies, large power densities and fast response times were achieved (Hargreaves, 1991). Helium and Hydrogen have the advantage over air in having a better relation of thermal expansion coefficient to viscosity. When these gases are highly pressurized, it is possible to build engines with high efficiency and power density. The problem of how to seal these gases for any length of time remains to this day (Walker, 1980).

The thermodynamic and fluid dynamic processes in the Stirling cycle engine are so complex that it is difficult to compare the advantages and disadvantages of the different working fluids using simple mathematical relations. This analysis can be greatly simplified when comparing working fluids under steady flow conditions. Hall (1958) made a comprehensive comparison of different working fluids used for cooling of nuclear reactors. The requirement for the working fluid in nuclear reactors

is similar to that in Stirling engines. To achieve maximum work output for minimal pressure drop, the fluid must have low viscosity in relation to a high heat capacity and large thermal expansion. Hall was able to describe the relation of pumping power to transferred heat for steady flow condition through equation 2.10.

$$\frac{P}{Q} = \frac{Q^2}{\eta \rho^2 c^3 \Delta T (T_{in} - T_{out})^2 * A^2} \qquad 2.10$$

P = required pumping power

Q = energy transferred

η = pump efficiency

ρ = fluid density

c = heat capacity of fluid

ΔT = temperature difference between fluid and matrix

A = surface area

For a given heat exchanger geometry and temperature difference it is then possible to simplify this equation to the relation 2.11.

$$Q \propto \sqrt{\rho^2 c^3} \propto \sqrt{M^2 c^3} \qquad 2.11$$

M = molecular weight of fluid

This shows that the ability of the working fluid to transport energy with low pumping losses is mainly a function of the heat capacity and, secondarily, a function of the density. Hall (1958) points out that this equation has to be seen as highly simplified and only applies to ideal condition and tubular pipes. Walker (1980), however, describes the equation as a very useful relation in the comparison of the quality of different working fluids. He finds the results from the relation in line with those obtained from the experimental comparison of different working fluids.

Various experiments have been conducted in order to assess the possibility of two component working fluids. Walker et al. (1994) shows, in a theoretical model, that significant improvements in the power density of Stirling engines can be achieved by having a two-component, two-phase working fluid. The working fluid consists, in this case of a gaseous carrier and a component which is liquid in the cold space and which changes to vapor in the hot space of the engine. Wolgemouth (1969) investigated the effect of a chemically reactive working fluid. In experiments using nitrogen tetroxide (H_2O_4) as the working fluid Wolgemouth was able to show that the net work output can be increased by a factor of two compared to that of a non reactive gas.

Given the main requirement for the working fluid of low viscosity and large thermal expansion coefficient, the use of liquid seems utterly unsuitable as the working fluid. Taking the conventional view that liquids are thermodynamically inert, and virtually incompressible, it is difficult to understand how an engine can function with a liquid as its working substance (Swift, 1989a). This only becomes clear when the properties of liquids near the critical point and in the dense phase are analysed.

Allen et al. (1981) gives a practical analysis of liquids as a working medium for the Malone engine. Most of his research was driven by the aim of finding a replacement for the Rankine cycle. He analysed the heat regeneration in Malone type liquid engines using a parallel-plate contraflow regenerator. His paper describes the result of the experimental work and sets out equations to describe the heat exchange in the regenerator.

Swift (1989) states that the main properties that define the suitability of the working fluid are the thermal expansion coefficient, the heat capacity, the viscosity, and the compressibility. For external combustion engines, where the energy has to be transferred into the working fluid by some kind of heat exchanger, the Prandtl number is of importance. A high Prandtl number in combination with low viscosity is important in order to achieve high heat transfer and low pumping losses.

Walker (1980) characterized these properties as the "transport properties" of a fluid. He defines the best working fluid for the Stirling-cycle as the one that has a high ability to transport energy and, hence, high heat capacity in relation to low "pumping losses". This requires low viscosity and high Prandtl number.

Under these conditions, water at low temperatures would be unsuitable as a working fluid. Swift states that most liquids become suitable as working fluids the moment the temperature reaches 0.7 * $T_{critical}$. At around this temperature the transport properties of most fluids are significantly improved. Table 2.1 shows this effect using water as an example.

Fluid	Thermal expansion β [1/K]	Heat conductivity [W/m*K]	Heat capacity cp [KJ/kg*K]	Dynamic viscosity [10^{-6} Pa*s]	Isotropic index -
Saturated water 100°C, 1 bar	0.0007	0.7	4.2	279	1.3
Saturated water 300°C, 100 bar	0.0014	0.5	3.6	90	1.8
Supercritical water 350°C, 220 bar	0.0017	0.11	3.1	32	2.5
Supercritical water 500°C, 350 bar	0.0040	0.13	5.1	35	2.1
Supercritical water 700°C, 500 bar	0.0019	0.17	5.1	42	1.6
Helium 500°C, 100 bar	0.0016	-	20.8	39.5	1.7

Table 2-1 Properties of water at low temperature, 0.7 * $T_{critical}$ and in the dense phase. For comparison the properties of He are given.

At 100°C water has a low isotropic index and thermal expansion coefficient. This, combined with a high dynamic viscosity, makes is unsuitable as a thermodynamic working medium. At 0.7 * $T_{critical}$ the thermal expansion coefficient has already risen by a factor of two to 0.0014 and the isotropic index has exceeded that of an ideal gas. At this point the dynamic viscosity has fallen to 90 Pa*s which makes it only 1/3 of the viscosity at 100°C. This positive trend continues up to a temperature of around 500°C. When the temperature rises above 500 C, the falling isotropic index and thermal expansion begin to have a negative effect on the performance.

The main causes of losses in the Stirling cycle engine are derived from imperfect heat regeneration and the energy required to overcome flow friction. Hargreaves (1991) states that the gas with the best ratios of thermal expansion and heat transfer coefficient to viscosity will produce the highest engine efficiency.

The ratio of heat exchange between the working fluid and the regenerator matrix, to the amount of useful work, is mainly a function of the fluid properties. This has to be taken into account when quantifying the quality of the working fluid. The advantages of a high ratio of heat transfer coefficient to viscosity can easily be cancelled out by a poor ratio of energy input Qin to the regenerator matrix heat transfer Qr (see figure 2.1). This consideration established by Hargreaves (1991) is reflected in equation 2.5 shown above. The only working fluid specific value in this equation is the isotropic index γ, whereby it is advantageous to have a large isotropic index. This will result in a small amount of energy being shifted in and out of the regenerator and, therefore, result in decreased regenerator losses.

Zhaolin, Haruki and Feng (2000) make an important statement with regards to the operating pressures of liquid engines. For liquid engines to function efficiently it is important that the phase change happens between the liquid and the dense phase of the working fluid. This is achieved by holding the cycle pressure above the critical point at any time in the cycle.

If the pressure drops below the critical pressure, evaporation will occur in the working stroke, and condensation will occur in the compression stroke. As a result of the evaporation in the working stroke being under higher pressure and, therefore, at a higher temperature level than the condensation in the compression stroke, the regenerator cannot transfer the energy from condensation to evaporation. This becomes clear when the fluid and matrix temperature in a working Stirling engine regenerator, as shown in figure 2.4, are observed. At the point of BDC, the fluid temperature has to rise above the regenerator matrix temperature and keep constantly rising in order to reject the energy into the regenerator matrix. At TDC, the

temperature of the fluid passing the regenerator matrix has to fall, and constantly drop, so that the energy can be recovered by transferring it into the working fluid. If evaporation or condensation occurs at any point in this cycle, the fluid temperature will stagnate at the condensation temperature and the matrix temperature will then equalize. The fluid in the return stroke will then stagnate at the lower evaporation temperature and no energy can be extracted from the matrix.

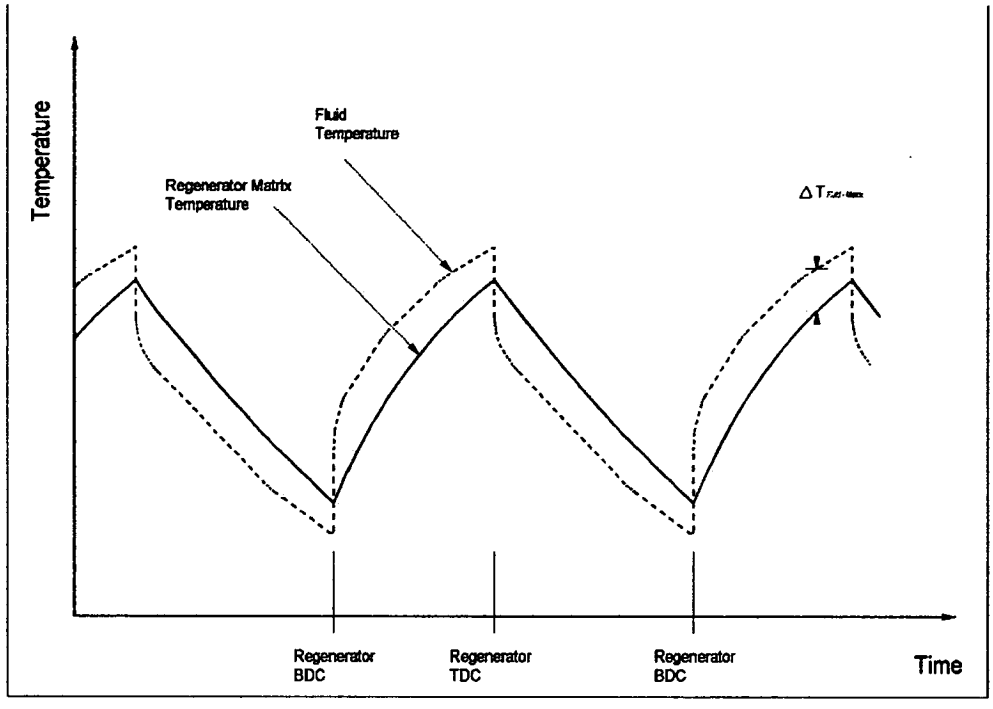


Figure 2.4. The typical matrix and fluid temperature inside a Stirling engine regenerator working with an ideal gas is shown. An ideal regenerator works with a minimum difference between matrix temperature (dotted line) and fluid temperature (solid line) and a small temperature swing of the matrix material in relation to the total temperature difference between T-hot and T-cold.

For modelling work it is essential to have equations to describe the transport properties of the fluid as a function of pressure and temperature. Ghajar (1980) presents expressions for determining the thermodynamic and transport properties of water, carbon dioxide and Refrigerant-114 in the supercritical region. For a given pressure it is possible to determine the density, specific heat, and absolute viscosity of the fluid as function of the temperature. The National Institute for Standards and Technology, Gaithersburg has provided the numbers for the thermal conductivity, and the specific heat capacity of supercritical water. Figure 2.5 shows the relevant properties of water as a function of temperature.

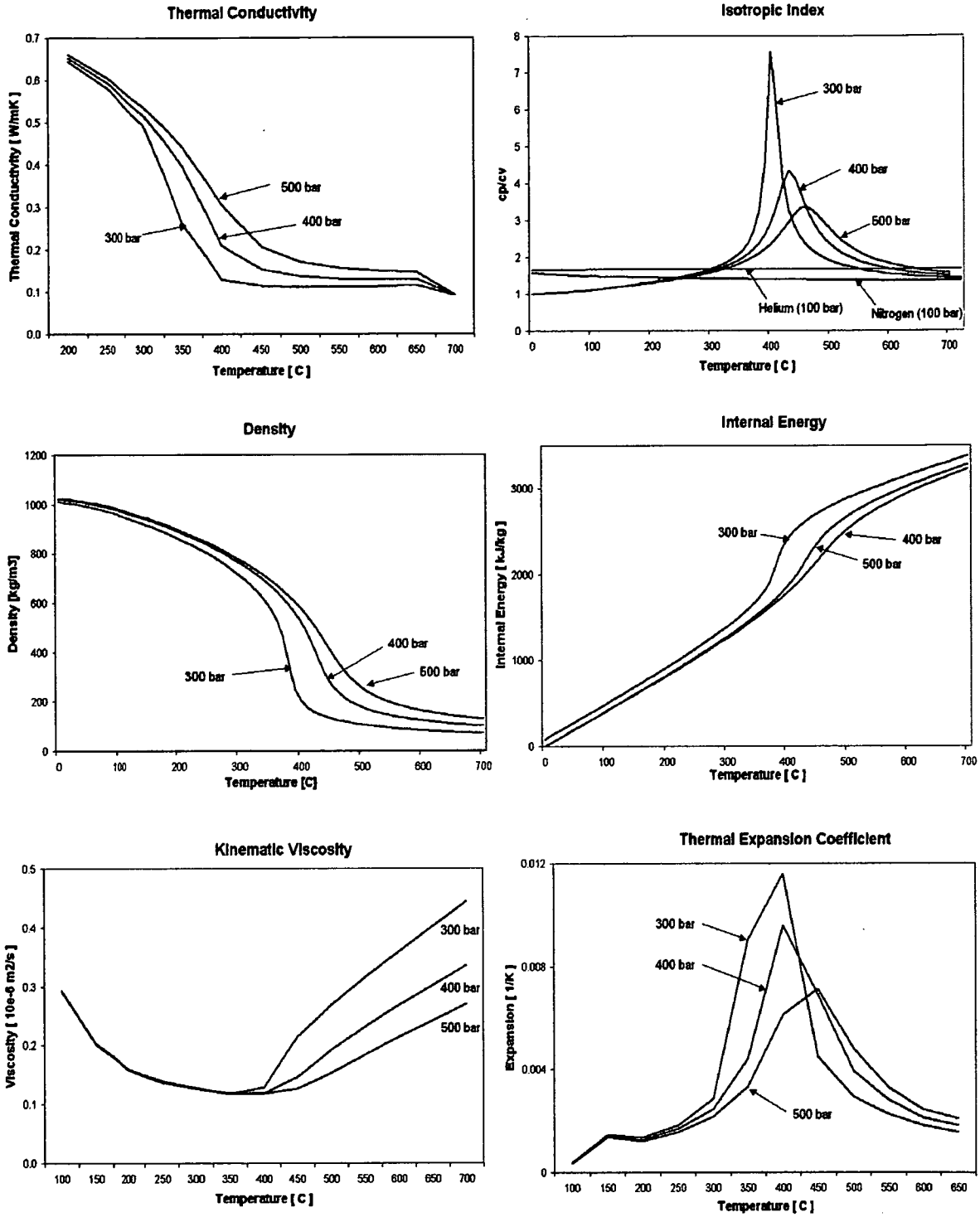


Figure 2.5 Fluid properties of water as a function of temperature at 300, 400, 500 bar. (source: Afshin J. Ghajar 1980, "Physical Properties Expressions for some fluids in the supercritical region")

2.3.5 Hot end heat exchanger

One of the fundamental difficulties with the Stirling cycle engine is found in the heat exchange from the combustion side of the engine into the working fluid (Walker, 1980). A large number of different hot end heat exchanger designs have been made and tested since the invention of the Stirling engine. With the introduction of high temperature alloys it is possible to overcome most of the technical difficulties. The technical advantages is offset, however, by high material and fabrication cost (Hargreaves, 1991).

The maximum theoretical efficiency of the Stirling engine is limited by the Carnot efficiency. Therefore, any engine with a high efficiency will have to work with a large temperature difference between the hot and cold side of the engine. With the cold end temperature set to be close above ambient temperature, the temperature of the fluid in the hot end determines the maximum theoretical efficiency of the engine.

Carlqvist (1977) divides the temperature levels and, therefore, the maximum efficiency of Stirling engines into three groups.

E1 Hot end gas temperatures in the range of 650 – 700°C. Engines of good efficiency (38 – 40 %) using established metallic materials for the hot end heat exchanger.

E2 Hot end gas temperature in the range of 700 – 750°C. Engines have improved efficiency (40 – 42) and are still able to use metallic but more advanced high temperature alloys.

H Hot end gas temperature in the range of 1000 – 1100°C. Engines of high efficiency (over 43 %). The hot end heat exchanger requires advanced materials such as ceramics. Such engines present a major development step.

Limited research has been undertaken with regards to heat exchangers for Malone engines. The original engines built by Malone in the 1920s worked with simple tubular hot end heat exchangers. To be able to withstand the high working pressures, Malone used long cast iron tubes of small diameter in order to minimise the stress in the wall. These heat exchangers had no means of improving the heat exchange between the hot combustion gasses and the hot end. To increase the heat transfer from the internal wall of the hot end into the working fluid, Malone used a dummy which was mounted onto the end of the regenerator. This increased the flow velocity along the internal wall and, therefore, the heat transfer from the wall into the fluid. The disadvantage of such a system is that, due to the travel of the regenerator, it is not possible to make use of the full length of the hot end heat exchanger.

The research on Malone engines, done at the laboratories in Los Alamos in the 1980s, was mainly focused on Malone refrigerators. The four-cylinder engine built by Swift in 1983 (Swift, 1989b) used an internal electrical heater and had, therefore, no need for a hot end heat exchanger. No further work with regard to heat exchangers in Malone engines was found in the literature.

It is important to analyse the communality between the hot end heat exchanger requirements for the Malone engine and the Stirling engine to see which parts of the research are of relevance. The Malone engine typically operates at much higher pressures than the Stirling cycle engine. This results in a larger wall thickness and, therefore, increased requirement for good heat conductivity and high temperature strength of the wall material. The problem of gas leakage through the heat exchanger material, found in engines using hydrogen, does not apply to the Malone engine. This may broaden the choice of suitable wall materials. The heat exchange from the combustion gas into the heat exchanger and from the heat exchanger into the working fluid follows, similar rules to the Stirling engine or other external combustion engines and it is possible to make use of the information gained from studies done in the field.

Most of the early Stirling engine heat exchangers were made from simple steel cylinders without any means of increasing heat transfer. Rathenau and Maijer (1973)

made one of the first steps towards more compact heat exchangers by developing a technique to braze aluminium-bronze to 18-8 stainless steel in 1946. This opened the way to composite structures such that it became possible to make pressure vessels from stainless steel and a fined structure from aluminium.

P. H. Clay introduced a technique that allowed further improvement in heat transfer for these finned heat exchangers. His technique is based on the principal that, for the same pressure drop, a large number of short ducts produces increased heat transfer coefficient compared to one long channel. This principal was successfully applied in a number of the early Philips Stirling engines by directing the combustion gas in radial direction towards, and away from the finned hot end heat exchanger. H. De Brey (1942) described Clay's principal and Hargreaves (1991) shows how this technique has been applied to the Stirling engine heat exchanger.

Most of the later Stirling engines use tubular hot end heat exchangers as introduced by De Brey in 1938 (Hargreaves 1991). The heat exchangers are typically made from a large number of U-tubes, which connect the expansion space to the regenerator. In most cases, these tubes have been located in a single array around the expansion space. The combustion space can then be located in the centre, with the hot combustion gas being forced outwards through the array of tubes. This technique is especially suitable for double acting machines, where there is already the need to connect the different compression and expansion spaces.

A number of different heat exchangers, using a third liquid or gaseous medium in heat pipes, have been developed and tried. The third medium is circulated to transport the heat from the combustion end of the heat pipe circuit to the hot end heat exchanger. Two different techniques have been used in Stirling engines in the past. Gaugler (1944) introduced a system, whereby, the fluid in the heat pipe is evaporated on the burner site and condensed on the hot end heat exchanger site. Dunn, Rice and Thring (1975) describe the results from the a engine using this technique.

The second type uses liquid metal as the transport fluid. A number of these systems were produced during the research at Philips. Asselman and Green (1973) and Hargreaves (1991) have reviewed this work.

Despite the extra complexity, there are a number of advantages of the systems that have previously been referred to. The heat can be uniformly applied to the hot end heater avoiding uneven heating and stressing of the heat exchanger material. The pressure in the heat pipe can be lower than the system pressure allowing the use of cheaper materials. High heat flux densities can be achieved. Further, it is possible to use the heat pipe system as a heat flux transformer by having different surface areas at the combustion and the working fluid site.

The heat pipe system might be of importance to the Malone engine where much higher heat transfer rates between the heater and the supercritical working fluid are expected than between the combustion gasses and the heater. A heat pipe system further allows the use of a small high-pressure vessel for the supercritical working fluid reducing the amount of high temperature high tensile strength material. No reference to the use of heat pipe systems in Malone engines could be found.

A number of books and papers are available that cover the general design of heat exchangers. In his book "Compact Heat Exchange" W Kays (1964) gives a good description of the available data on heat transfer and flow friction for compact heat exchangers. Webb (1994) provides a comprehensive overview of the different available techniques with regard to heat transfer enhancement.

2.4 Mechanical configuration

Various different piston-displacer arrangements, and drive mechanisms, have been proposed and tested since the invention of the Stirling Engine. Most of these are based on the conventional piston crank arrangement, connected to either two pistons or one piston and one displacer. Walker (1980) gives a complete description of the different

techniques that are commonly found in Stirling engines. Various developments have been made applying different techniques to create the required piston and displacer motion.

In principal, any of these systems can be adapted for use with the Malone engine but only a few have been built to date. These include crank and cam drives (Malone, 1924, 1929), free piston drives (Swift, 1989c), hydraulic drives (Rampen et al., 1997), and piezo-electric drives (Weldon, 2001)

The following description gives an overview of the different piston/displacer arrangements previously used in Stirling engines. In addition there will be a more detailed review of the different techniques used for driving the working piston and regenerator in Malone engines.

2.4.1 Classification of Piston/Displacer arrangement

Initially, all arrangements can de placed into two main groups:

1. Single acting machines
These machines only make use of one side of the piston. They use either one piston and one displacer (piston-displacer machines), or two pistons (two piston machines). The piston-displacer machines can be configured with an internal or external working piston.

2. Double acting machines
Double acting machines, first proposed by the French inventor Franchot in 1912, are multi cylinder machines, whereby, each cylinder is connected to two different Stirling-cycle systems by using both sides of the piston (Walker, 1980).

It is possible to divide the different types of piston/displacer arrangements into three main groups, the Alpha, Beta and Gamma arrangements.

Alpha

The Alpha type (figure 2.6) can be seen as, conceptually, the simplest Stirling engine but has the disadvantage of two separate pistons and, therefore, the need for two piston seals Senft (1993). This problem can be eliminated when the engine is used as a double acting engine. It is possible to configure the alpha type engine to compact double acting multi cylinder engines. These engines can achieve extremely high power densities as required for automotive applications. Philips used this type for the Ford Torino car in 1975.

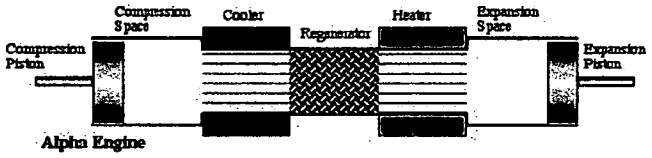


Figure 2.6. Alpha configuration (source: "Stirling Cycle Engine Analysis", I Urieli, 1984)

Beta type

Unlike the Alpha type machine, which has two power pistons, the Beta type engine (figure 2.7) has a single power piston and a displacer piston. Stirling's original engine from 1816 used the Beta configuration.

Rolf Meijer introduced the rhombic drive mechanisms for the Beta type engine in 1959, which removes any side load on the piston and reduces vibration to a minimum (Meijer, 1959).

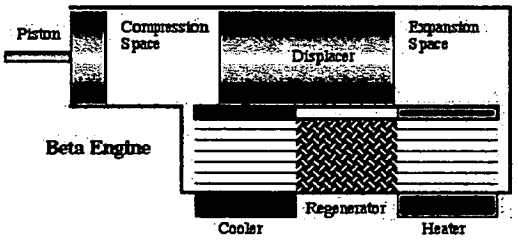


Figure 2.7. Beta configuration (source: "Stirling Cycle Engine Analysis", I Urieli, 1984)

Gamma Type

The Gamma type engine is similar to the beta type engine in that it has one working piston and one displacer piston (figure 2.8). In contrast to the beta type, the working and displacer piston are arranged in different cylinders. This arrangement has the advantages of the option of complete separation of the working cylinder from the thermodynamic parts of the engine. The disadvantage of the gamma type arrangement is the increased dead space that is created by the required connecting pipework.

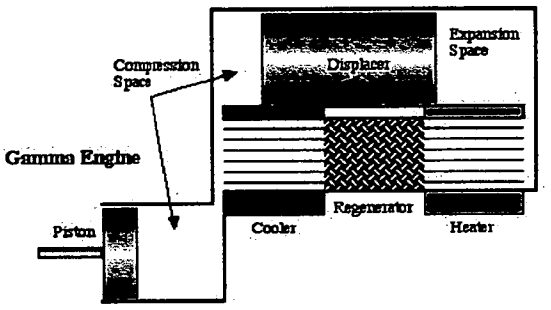


Figure 2.8. Gamma configuration (source: "Stirling Cycle Engine Analysis", I Urieli, 1984)

In all his original engines, Malone used the gamma type configuration as shown in 2.8. This system allowed him to connect one working piston to a number of displacer pistons.

2.4.2 Mechanical drive mechanisms for Malone engines

There is the need to move the piston and displacer in a reciprocating motion, irrespective of their arrangement. Conventionally, this is done with a crank/connecting rod arrangement, which results in a near sinusoidal motion. The phase angle between the piston and displacer can be created by working with two cranks from a common shaft.

Malone initially used a number of camshafts to drive the regenerators in the different TD-Piles, but later replaced these with crank mechanics. Senft (1993), states that piston-displacer arrangement, with the external piston, as chosen by Malone, is the simplest configuration because it can be driven from a single crankshaft. The

disadvantage for Stirling engines comes from the unavoidable extra volume in the connecting pipework. In liquid engines, this does not cause any problems because the fluid in the cold side of the engine is virtually incompressible.

Swift (1989b) chose the double acting piston arrangement for the Malone engine, which he constructed in the 1980s. He used a four cylinder double acting machine with a common crankshaft to conduct a number of tests. He states (Swift, 1989b) that the arrangement of his four-piston machine, running 90° out of phase, allowed him to operate the engine smoothly at low frequencies, without the need for a large flywheel.

Raetz (1984) describes in a patent, a Malone engine system whereby, the displacer is driven with an electromagnetic drive system and the linear motion of the working piston is directly used to pump water. No reports on the success of this system have been found.

Swift and Brown (1993) looked at the possibility of using Malone's liquid engine cycle in a Ringbom Type free piston engine for refrigeration. In their work they were able to show that the typically short stroke, low operating frequencies and high-pressure amplitudes of the Malone engine lend themselves to Ringbom operation.

Weldon (2001) presents a Malone refrigerator that uses a piezoceramic actuator to control the motion of the displacer and working piston. Due to the limited travel from the piezoceramic actuator, his system has to work with small displacements and large piston and displacer diameters.

The proposed hydraulic power take of system, using a multi cylinder hydraulic pump with independent control over each cylinder, offers compete control over the working piston motion profile and allows it to be change while the engine is in operation.

Md. Ehsan (1997) analyses the use of the Artemis Digital Displacement^{TM} pump motor as a power take-off system. In his model he is able to show that the control over the piston motion can be used to increase the power density of the engine without an

increased maximum cycle pressure. A detailed description of the digital displacement machine is given in the PhD work of Rampen (1992).

2.5 Combustion system

One advantage of Stirling cycle engines comes from their ability to use any kind of heat supplied from an external source. While most of the early Stirling engines were powered by coal, later engines used a variety of alternative heat sources. As a result of the flexibility of the heat source Stirling engines have been installed in areas where internal combustion engines are of limited use. Applications include: thermal energy storage Stirling engines for submarine power (Mattavi et al., 1969); solar and radioisotope powered engines for satellite (Parker and Malik, 1962) and radioisotope-powered Stirling engines for artificial hearts (Walker, 1980). C. Hargreaves (1991) gives a complete review of the different exotic heat sources that have been used to operate Stirling engines.

After the work by Malone on his original engines with a coal fired furnace system there is no evidence in the literature of any subsequent work on combustion systems in Malone engines. The combustion system for Malone engines is similar in its nature to the combustion system of Stirling engines. The high working pressures and high heat transfer rates achieved with supercritical water may result in a different hot end heat exchanger geometry which will effect the combustion system design.

For most mobile applications, where it is necessary to carry the fuel safely with the engine liquid hydrocarbons of high power density are the preferred fuel (Walker, 1980). The work in this study focuses on combustion systems for these fuels.

The combustion chamber geometry plays an important part in the design of an efficient low pollution and compact combustion system for Stirling engines. K. Eguchi (1984) defines the main parameters that are controlled by the combustion chamber geometry as:

- Low pressure losses
- Short stable flames
- Homogeneous temperature profile around hot end heat exchanger
- Efficient heat transfer onto hot end heat exchanger
- Long lifetime
- Low NO_x development

A great deal of effort has been put into the development of swirl flow combustion systems. In most later combustion systems, a part of the combustion gas (defined by the swirl number) is recirculated inside the combustion chamber to reduce peak flame temperature, flame length and improve heat transfer onto the hot end heat exchanger. The effect of the swirl has been analysed in a number of studies,Visser and Plessis (1990), Hidenori, Fujiwara and Sigimoto (1992).

2.5.1 Pollution reduction

Most of the development work on combustion systems done until the 1960s was aimed at increasing the overall engine efficiency. In the 1960s the regulations governing pollutants became much more stringent and as a result of this, comprehensive research into the reduction of emission from the combustion was undertaken (Hargreaves, 1991).

In efficient Stirling engines it is necessary to recover the energy from the exhaust gas to preheat the combustion air. This leads to high flame temperatures, often over 2000°C, which favour the formation of nitrogen oxide (Wuenning, 1997).

Two main strategies for avoiding the production of NO_x have been tried in the past. Firstly lowering of the flame temperature, and secondly reducing of the time that the combustion gases spends at the high temperature level.

A significant reduction in NO_x emission can be accomplished through exhaust gas recirculation (EGR), whereby, a part of the exhaust gas is mixed with the incoming combustion gas. The extra inert gas volume has the effect of lowering the adiabatic flame temperature. This technique was developed for both the Ford and MTI automobile programs in the 1970.

Philips developed a different technique in the early 1980s, the so-called combustion gas recirculation (CGR) see figure 2.9 (Hargreaves, 1991) . In this system a part of the gas that has already passed the hot end heat exchanger is mixed with the combustion gas between the preheater and the burner. With this technique it is possible to reduce the NO_x emission to a minimum without compromising the overall system performance (Walker, 1994).

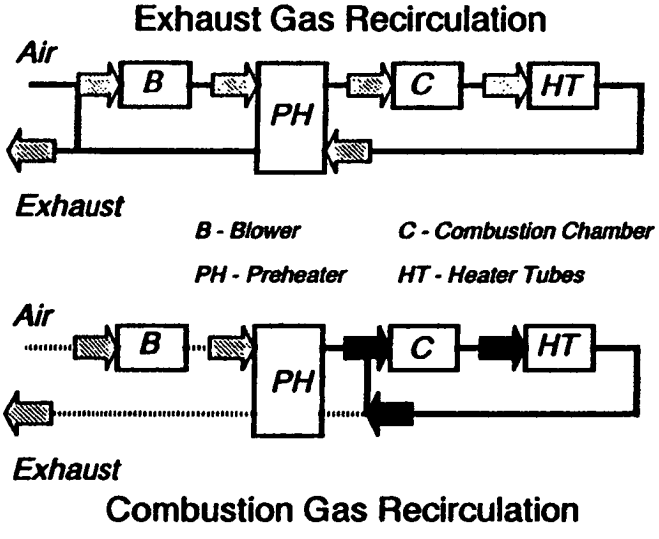


Figure 2.9. Exhaust gas recirculation (EGR) and combustion gas recirculation (CGR) have been used to reduce NO_x development. (source: Hargreaves, "The Philips Stirling Engine" 1991)

The investigation done by A. Michel (1971) shows the effect of the time that the combustion gas spends at the high temperature level on the growth of NO. (see Figure 2.10)

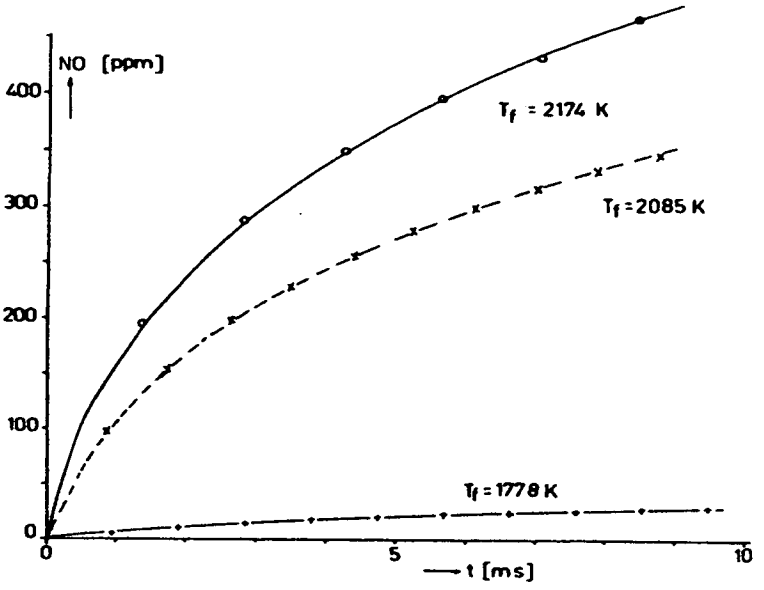


Figure 2.10. The graph shows the development of NO depending on temperature and time at high temperature level. (A.P.J. Michel 1971)

An investigation done Magnus Palsson (1997) on a United Stirling V 160 engine using combustion gas recirculation (CGR) shows that it is possible to reduce the NO_x emission to levels below 0.5 g per kg of burned fuel.

Hidenori, Fujiwara and Sigimoto (1992) analyse the possibility of NO_x reduction through minimum flame length, and without exhaust gas recirculation (EGR). They are able to show that, through optimum combustion chamber geometry, it is possible to reduce the NO_x to 0.34 ppmV/K at hot end temperatures of 1000K.

A further method to reduce the production of NO_x is presented by Wuenning (1997). Typically it is not possible to work with exhaust gas recirculation values above 30 %, due to flame stability limits. Wuenning found that at high combustion space temperatures, as typically found in Stirling engines, it is possible to have stable flame condition at very high recirculation rates. In the so-called flameless oxidation™, the combustion occurs with no visible flame and at significantly reduced NO_x production.

3 Combustion System

This chapter discuses the combustion system for the proposed Artemis Malone engine and analyses the key parameters that define the performance of the combustion system and the hot end heat exchanger.

A description of the two combustion systems produced during the study is given, and the theoretical and experimental results are presented. Further, the results from a room temperature flow test rig are described.

3.1 Introduction

With increasing political pressure to achieve good fuel economy and low emissions, the Stirling engine has often been described as a potential competitor for the internal combustion engine.

In most engine designs, much greater attention is paid to the design of the internal heat exchangers and the mechanical arrangements than to the design of the combustion system. In order to achieve the often promised high efficiencies and low emissions, however, the design of the burner, combustion chamber and exhaust gas heat exchanger are crucial.

It is important to maximize the potential of the more controllable external combustion, of the Stirling cycle engine, compared to the often intermittent and more difficult to control internal combustion. In an external combustion system the emission of carbon monoxide (CO), nitrogen oxides (NO_x) and hydrocarbons (HC) can be kept to significantly lower levels than they would in the less controllable internal combustion engine. External combustion also offers the attraction of a wide choice of fuels.

It has to be pointed out that catalytic converters, as used to clean exhaust gases from internal combustion engines, are very good at removing the bulk of carbon monoxide (CO) and hydrocarbons (HC) but show generally poor performance in removing thermal nitrogen oxides (NO_x). The real advantages of Stirling engines, as compared to internal combustion engines, can be seen only when the combustion produces lower values of these gases than it is possible to achieve with catalytic converters in the internal combustion engine.

In principle, it is possible to use any external heat source with a temperature level above the sink temperature to run a Stirling type engine. Low temperature differential Stirling engines, operating across a few degrees Celsius, have been made successfully in the past (Senft 1996). However, as in all heat engines, the efficiency of the Stirling engine is limited by the Carnot efficiency. High efficiencies are possible only when there is a large temperature difference between the heat source and heat sink temperature.

In contrast to other cycles, for example the steam engine cycle, the Stirling cycle uses a regenerator to preheat the working fluid before it enters the hot end heat exchanger. This limits the lowest possible temperature of the hot end heat exchanger to the temperature at which the working fluid leaves the regenerator. The combustion products can, therefore, only transfer heat against this already high temperature level. The result is that the gas leaving the combustion chambers must be at a higher temperature level than the preheated working fluid. To avoid the resulting high exhaust gas losses, it is important to recover the energy from the exhaust gas.

Without any exhaust gas heat recovery, and under the assumption of constant heat capacity, the maximum theoretical efficiency of the combustion system can be described through equation 3.1:

$$\eta = 1 - \frac{exhaust\ gas\ losses}{fuel\ energy} = 1 - \frac{T_{Exhaust} - T_0}{T_{adiabatic} - T_0} \qquad 3.1$$

$T_{exhaust}$ = exhaust gas temperature [K]

$T_{adiabatic}$ = adiabatic combustion temperature [K]

T_0 = ambient temperature [K]

The proposed Artemis Malone engine works with propane gas as fuel and has a calculated hot end fin base temperature of around 700°C. Propane gas has an adiabatic combustion temperature of around 2000°C when combusted with 10% excess air. With the hot end fin temperature of 700°C, the highest theoretical efficiency for the combustion system becomes only 65% with 35 % of the input energy lost through the exhaust. This makes exhaust gas heat recovery an essential part of an efficient combustion system.

A recuperative or a regenerative exhaust gas to inlet air heat exchanger can be employed for this exhaust gas heat recovery. The recuperative type of heat exchanger consists of separate flow channels for the incoming gas and the exhaust gas. The channels are separated by a wall with good heat conductivity. The regenerative type works on the principle of passing the incoming air and exhaust gas alternately through the same matrix of a large surface area and high heat capacity.

With exhaust gas heat exchangers it is possible to preheat the inlet air to a temperature level close to that of the exhaust gas and to recover most of the exhaust gas losses. The problem of this method comes from the resulting high flame temperatures. The flame temperature of the combustion system increases to the sum of the adiabatic combustion temperature and the air preheat temperature. In the proposed engine, this would result in a flame temperature of over 2500°C. At these high temperature levels large amounts of thermal NO_x are produced (see also figure 2.10), erasing the advantage of the clean external combustion over the internal combustion. A further problem comes from the temperature limits of the available materials for the combustion chamber and hot end heat exchanger. The high flame temperatures, when working with preheated combustion gas, will almost certainly result in a combustion gas temperature that is too high to be directly applied to the heat exchanger fins and combustion chamber walls without causing damage.

There are a number of arrangements through which it is possible to lower the flame temperature and to minimize the production of thermal NO_x. One way to overcome this problem is to increase the amount of extra air in the combustion (high Lambda number, Λ). A high Lambda number will lower the flame temperature and, therefore, reduce the production of NO_x. This further ensures complete combustion and low CO and HC emissions. Operating with a high Lambda number requires a larger blower with increased energy consumption. The exhaust gas volume will be increased and, therefore, the size of the exhaust gas heat exchanger also increases and adds extra cost and weight to the system and will increase the machine size. It is, therefore, preferable to work with the lowest possible Lambda number which still ensures complete combustion.

An alternative way to lower the flame temperature is to recirculate some of the combustion gas which has already passed through the heat exchanger back into the high temperature combustion gas. This results in the combustion gas being at a lower and more constant temperature and also increases the volume and velocity of the combustion gas passing the hot end. It further helps to minimize the temperature difference between the combustion gas and the heat exchanger fins. Two different techniques have been described in the past; (I) the exhaust gas recirculation (EGR) and (II) the combustion gas recirculation (CGR) technique. A description of these systems has already been made in chapter 2.4.

For the proposed Artemis Malone engine, a combustion system working with a low Lambda number to minimize the size of the blower and the exhaust gas heat exchanger together with a combination out of both the EGR and the CGR was chosen. A description of this system is given in the following sections.

Combustion chamber geometry

Most modern Stirling engines use tubular hot end heat exchangers, with the burner located in the center of the heat exchanger. The combustion gas flow can then be

passed in a radial direction through the heat exchanger tubes. To avoid the high number of required brazed joints on the tube ends, and a large hot end dead volume, the Artemis Malone engine uses a single tube with an external fin structure for the hot end heat exchanger. This lay out is similar to that chosen by Malone for his original engine, but differs in that it has a fin structure at the outside of the tube. This arrangement does not allow the typical central location of the burner and requires high heat flow per area due to the limited surface area available. Working with a supercritical fluid as the working fluid results in much smaller swept volumes inside the engine, than working with a gas, as the working fluid, would. This results in smaller acceptable hot end dead volumes and, therefore, a smaller hot end heat exchanger per unit power. This makes the development of a good combustion chamber geometry an essential part in the development of the Artemis Malone engine.

The heat energy from the combustion gas can be transferred into the hot end fins by both convection and radiation. To achieve good heat transfer it is important to have the combustion gas passing the hot end fins with a high velocity and, if possible, in turbulent flow. The combustion chamber wall should have a large surface, at a high temperature level, directed towards the hot end fins. It is advantageous to use a material with a high radiation coefficient for this wall. The combustion chamber has to be designed so that the heat exchanger is evenly heated to avoid `hot spots`. Further, it is important to keep the pressure drop small to minimize the size, and energy consumption, of the blower. These considerations have been taken into account in the design of the combustion chamber for the Artemis Malone engine. The resulting combustion chamber design is described in section 3.2 and 3.3.

3.2 Experimental study of the combustion system

The aim of the study was to develop and test a heater system for the first Artemis Malone Engine. The engine was designed to have an output power of about 5 kW at around 30% overall efficiency. This required approximately 15 kW of input power from the combustion system. It was decided that the test rig should, at the end of the development process, incorporate all the features of an efficient, low pollution heater

system as described above. Prior to this combustion system, a simple combustion system was constructed to analyse the hot end heat exchanger materials.

3.2.1 First combustion system

The first combustion test rig was built with the aim to study the hot end heat exchanger for the proposed engine. The focus of this study was to test the different joining and sealing techniques and to analyze the behavior of the different hot end materials in terms of corrosion, creep and fatigue. It was further proposed that the heat transfer from the combustion gas into the hot end heat exchanger would be analysed. For these tests it was only important to create a combustion gas flow of the representative temperature and flow rate. The optimization of the combustion system for high thermal efficiency and low pollution was to be studied in the second test rig.

The test rig was designed to hold a hot end heat exchanger with an outside diameter of 80 mm as in the final test engine, but only one third of the 120-mm length of the first test engine. To achieve the right combustion gas temperature the burner had an independent controls for the air and gas flow rates. By controlling the excess air in the combustion, it was possible to create the required flame temperature. A single cylinder digital hydraulic pump motor (for details see chapter 5.3) was used to simulate the high oscillating internal pressures. Figure 3.1 shows the components of the first test rig and picture 3.2 shows the combustion system with two of the test heat exchangers.

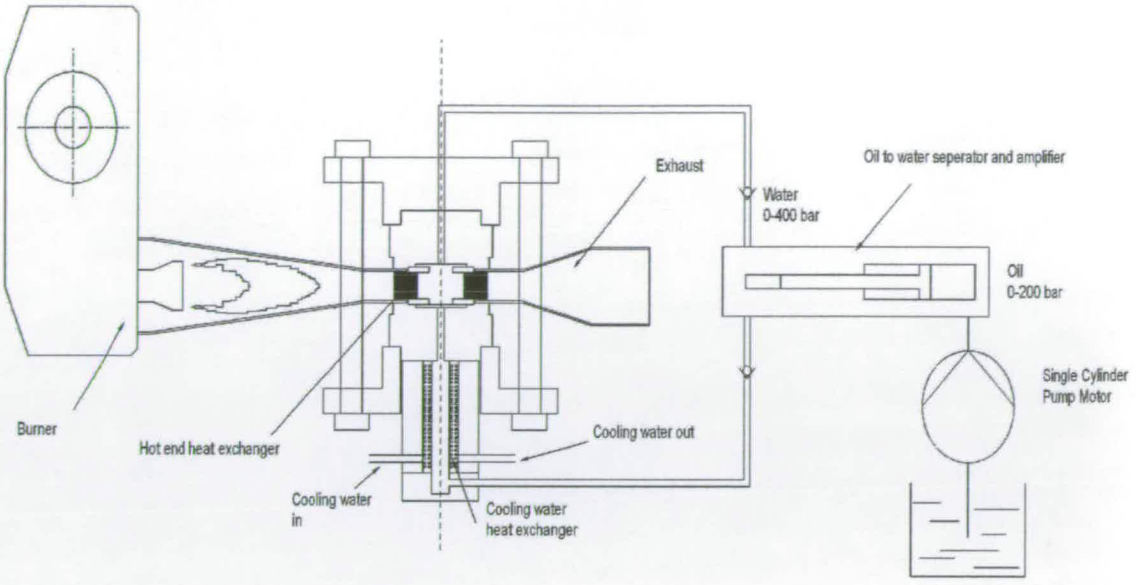


Figure 3.1. Layout of the first test rig with the burner to the left the combustion chamber, the hot-end heat exchanger in the center, and the pressurizing pump to the right of the drawing.

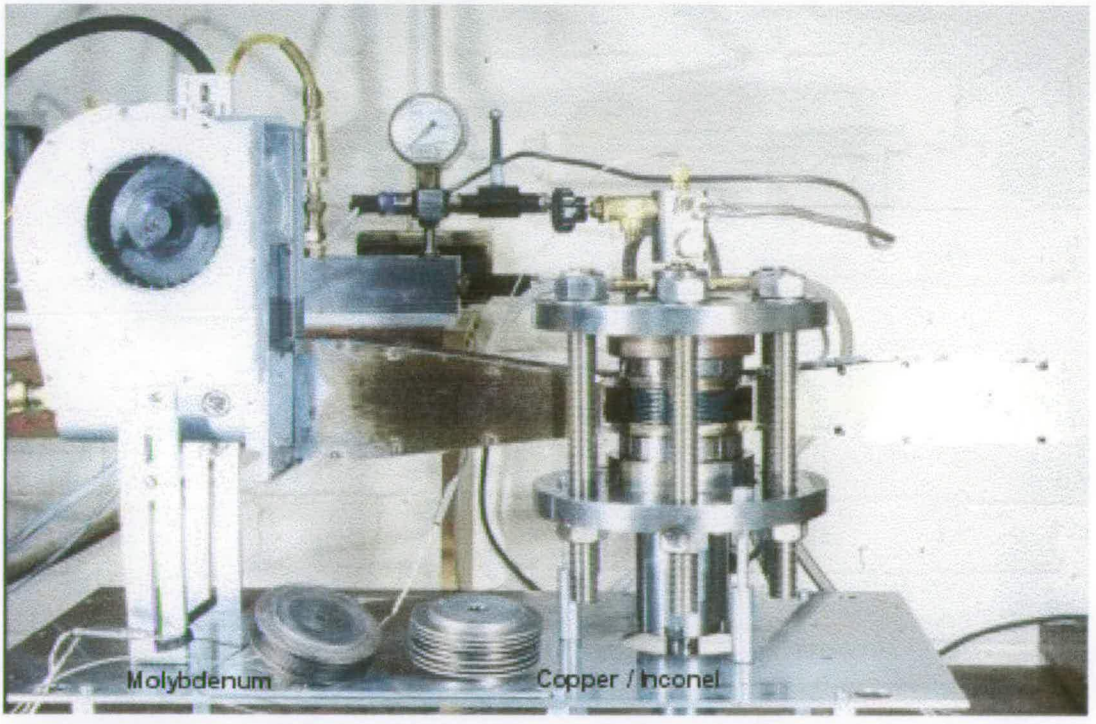


Figure 3.2. The fully assembled test rig with two of the test hot-end heat exchangers in the front of the picture is shown.

In this design, the combustion gas is channeled along the hot-end fins in tangential direction, as shown in figure 3.1. The idea is that the combustion gas flow is accelerated when it passes the hot-end fins and then becomes turbulent in order to increase the heat transfer.

A data sampling system was employed in order to measure temperatures and flow rates (see Appendix E). The signals from the transducers were passed either directly, or through pre- amplifiers, to the sampling computer via a data acquisition card. With this system it was possible to log the combustion gas temperature before and after it passes through the hot-end heat exchanger. The temperature of the hot-end fins, the fluid temperature inside the hot-end and the flow rate of the combustion gas and inlet air, were also logged.

It became clear early during testing, that there was a design fault in that the combustion gas being blown from one side, through the fin structure, was causing a temperature imbalance in the hot-end. The fin area, towards the inlet, was rising to a significantly higher temperature level than the area towards the outlet. The higher gas temperature of the incoming combustion gas on the inlet creates this effect, while heat transfer through radiation from the extremely hot inlet walls adds to the problem. While the rig was unsatisfactory in terms of heat transfer, it was still possible to compare the different materials, coatings and joining techniques used. The results are described in Chapter 4.2.

Due to insufficient insulation and leakage of the combustion chamber it was not possible to get reliable measurements of the heat transfer from the combustion gas into the hot-end. It was decided that this area would only be analysed in the final combustion chamber design.

3.2.2 Second test rig

The combustion chamber of the second test rig was designed to hold the hot-end of the first test engine with an output power of 5 kW. It had a fundamentally different layout from that of the first test rig. In this combustion system, the hot-end heat exchanger is located in the center of the combustion chamber, with the combustion gas swirling tangentially around it (see figure 3.3).

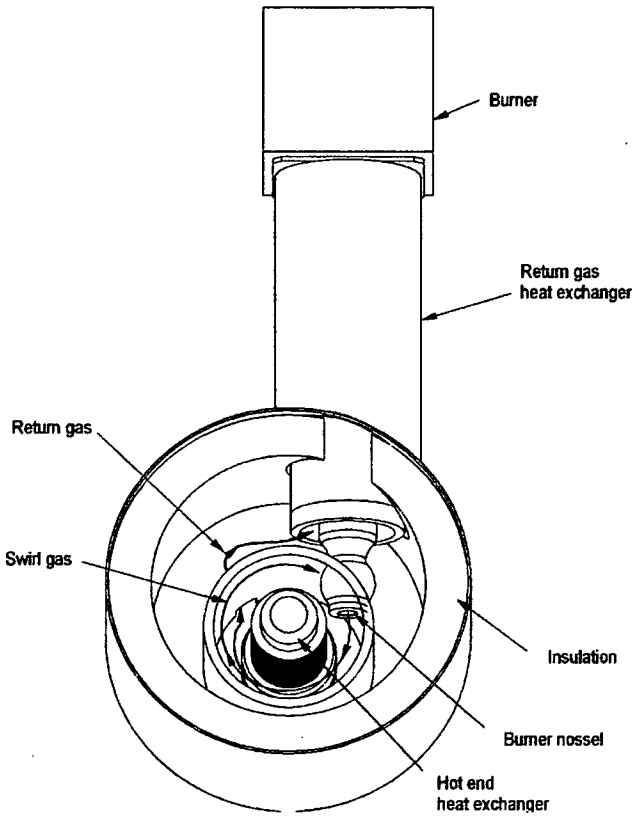


Figure 3.3. The gas passage inside the swirl chamber of the combustion system is shown. The gas swirls for a number of times around the hot-end of the engine before is passes through the exit on the bottom of the inner combustion chamber and enters the exhaust gas heat exchanger.

From the different methods of reducing NOx formation, which were described earlier in the chapter, the recirculation of a fraction of the combustion gas was chosen. A special low NOx burner was also employed. The recirculating method has the advantages of increased flow rates along the hot-end heat exchanger, without the disadvantage of the necessary increase in the size of the blower and exhaust gas heat. The high flow rate of the combustion gas is especially important because of the single tube hot-end heat exchanger with its limited surface area and the high power density of the proposed engine.

The combustion gas recirculation was achieved by injecting the combustion gas in a tangential direction through the burner nozzle, with high velocity, into the circular combustion space. The hot-end heat exchanger is located in the center of the combustion space, with the burner inlet near the top, and the exit at the bottom. In this design, the combustion products have to circulate around the hot-end heat exchanger, whereby, the shape of the combustion chamber geometry will define the average number of turns that the combustion products have to make before leaving the combustion space. A further advantage of this design, compared to the cross flow design, is the relatively even temperature profile around the hot-end and the large wall area which can radiate heat onto the fins. Figure 3.4 shows the general arrangement of the hot-end structure, burner, combustion chamber, and the exhaust gas heat exchanger of this test rig. The schematic of the data sampling is shown in appendix E.

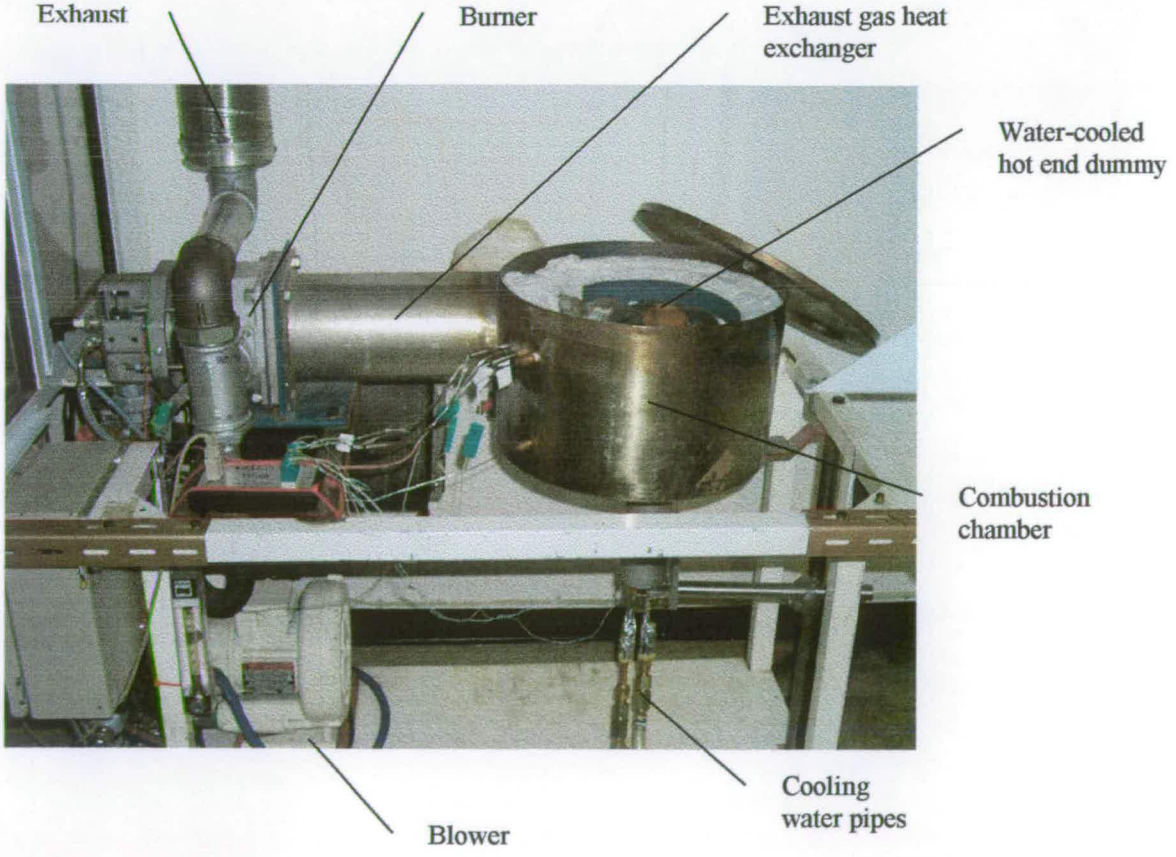


Figure 3.4. The 15 kW low NOx combustion system with the water cooled dummy hot-end is shown.

The relation of the hot-end diameter to the combustion wall diameter, and the entry and exit point for the combustion products, is important in this design and has to be carefully chosen to optimize the following factors.

- The amount of combustion gas that combines with the incoming combustion gas, after circulating around the hot-end heat exchanger. This will, from now on, be refered to as the recirculation factor (*Rf*).
- The volume flow and velocity of the combustion gas passing along the hot-end heat exchanger.
- The amount of heat that is transferred onto the hot-end fins by radiation from the combustion chamber wall depends on the combustion chamber diameter.

In practice, it is difficult to measure actual flow rates at the high combustion temperatures. A model of the combustion space was built in order to analyze the flow rates at room temperature with Reynolds number similitude. The model test and results are described in section 3.3.

With the aim of high efficiency and low emissions, it was important to use a burner with the ability to achieve complete combustion while avoiding the production of thermal NO_x. For the second test rig a "FLOX-Burner", type Recumat C100 made by the Germany company WS-Wärmetechnik, was chosen. The burner uses propane gas as fuel and has a variable output power of 12 – 20 kW. The burner can be operated in conventional flame, and in flameless oxidation, mode. When operated on the principle of flameless oxidation, the combustion air and gas are slowly mixed through the length of the flame. In this system, the flame temperature rises to its maximum temperature without creating any high temperature zones. Fig 3.5 shows the temperature distribution when the burner is operated in conventional flame mode and in FLOX mode (data provided by WS- Wärmetechnik). With a Lambda number of 1.3, and an air preheat temperature of 650°C, the burner is still able to keep the NOx emission down to about 6 ppm, compared to about 160 ppm when used in flame mode.

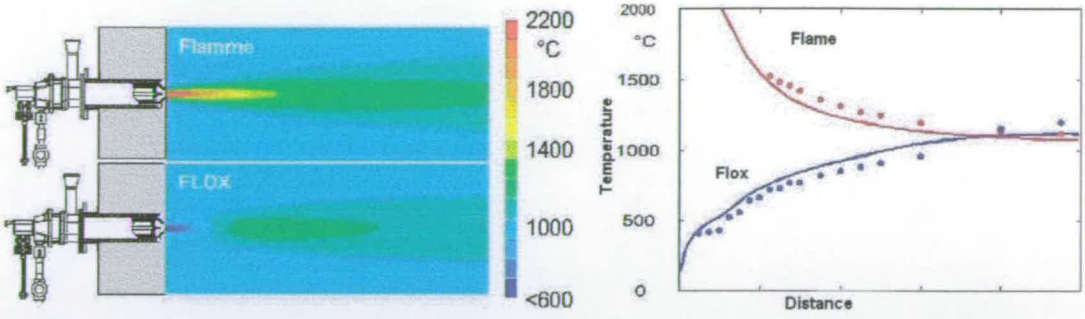


Figure 3.5. Comparison of the temperature profiles in conventional combustion and flameless oxidation. The temperature of the combustion gas in flameless oxidation mode is slowly rising to its maximum temperature, whereas in conventional flame mode the combustion gas temperature peaks at the burner nozzle.

To avoid losses due to heat leakage from the combustion chamber to the surrounding air a minimum insulation thickness of 30-mm ceramic fiber was chosen. By choosing a single centre pin of high tensile steel to clamp the TD-Pile together it was possible to minimize the heat leakage through the support structure of the TD-Pile.

3.3 *Energy flow*

For a given combustion system it is possible to calculate the gas temperature, mass flow rate, and energy flow at any point in the combustion system. The following calculation analyzes the energy flow in the combustion system of the proposed engine. The calculations have been done using the software package Math-Cad and are presented in Appendix C. The following discussion explains the method used in these calculations.

For a given heat flow into the hot-end of the engine, it is possible to calculate the required output power from the burner. In a combustion system with an exhaust gas heat exchanger, the required fuel supply rate ($\dot{m}_f$) to the burner for a given output power depends on the air preheat temperature, which is a function of the exhaust gas losses (Q_{ex}). This requires the use of iterative calculations. The process is begun by initially setting a value for the exhaust gas losses (Q_{ex}) and later correcting the value to solve the loop.

The mass flow rate of fuel for the required input power can be calculated using the heat value of the chosen fuel.

$$\dot{m}f = \frac{Q_{sup} + Q_{ex} + Q_{loss}}{CV * \eta} \qquad 3.2$$

$\dot{m}_f$ = fuel mass flow rate

Q_{sup} = heat energy supplied to TD Pile

Q_{ex} = exhaust gas losses

Q_{loss} = heat energy losses in combustion system

CV = specific heat value of fuel [J/kg]

η = combustion efficiency

With the combustion equation for Propane gas and air it is now possible to calculate the required amount of combustion air.

$$C_3H_8 + 5O_2 + 20N_2 = 3CO_2 + 4H_2O + 20N_2 \qquad 3.3$$

$$\dot{m}_{fa} = \dot{m}f * \frac{44 + (5 * 32 + 20 * 28) * \Lambda}{44} \qquad 3.4$$

$\dot{m}_{fa}$ = mass flow rate Air + Propane gas

Λ = Lambda number (amount of extra air in combustion)

It is important to determine the temperature of the air and combustion gases at each point in the combustion system. This can be done using the specific heat capacity, mass flow rate, and energy either added or subtracted.

$$T_2 = T_1 + \frac{\dot{Q}}{cp * \dot{m}} \qquad 3.5$$

T_1 = Temperature of gas before energy exchange

T_2 = Temperature of gas after heat exchange

Q = Exchanged energy

cp = specific heat capacity of gas (average) [J/kg*K]

With the results from the Math-Cad model it was then possible to show the temperature and mass flow rate at each point in the combustion system. The results are presented graphically in figure 3.6. The calculations have been done with the same design parameters as chosen for the test rig, so that it is possible to compare the theoretical results with the measurements from the test rig. The calculations were done using Propane gas and a Lambda number of 1.3. The thermal load was set as 11.4 kW which results in an input power from the burner of 16.2 kW at an exhaust gas temperature of 400°C.

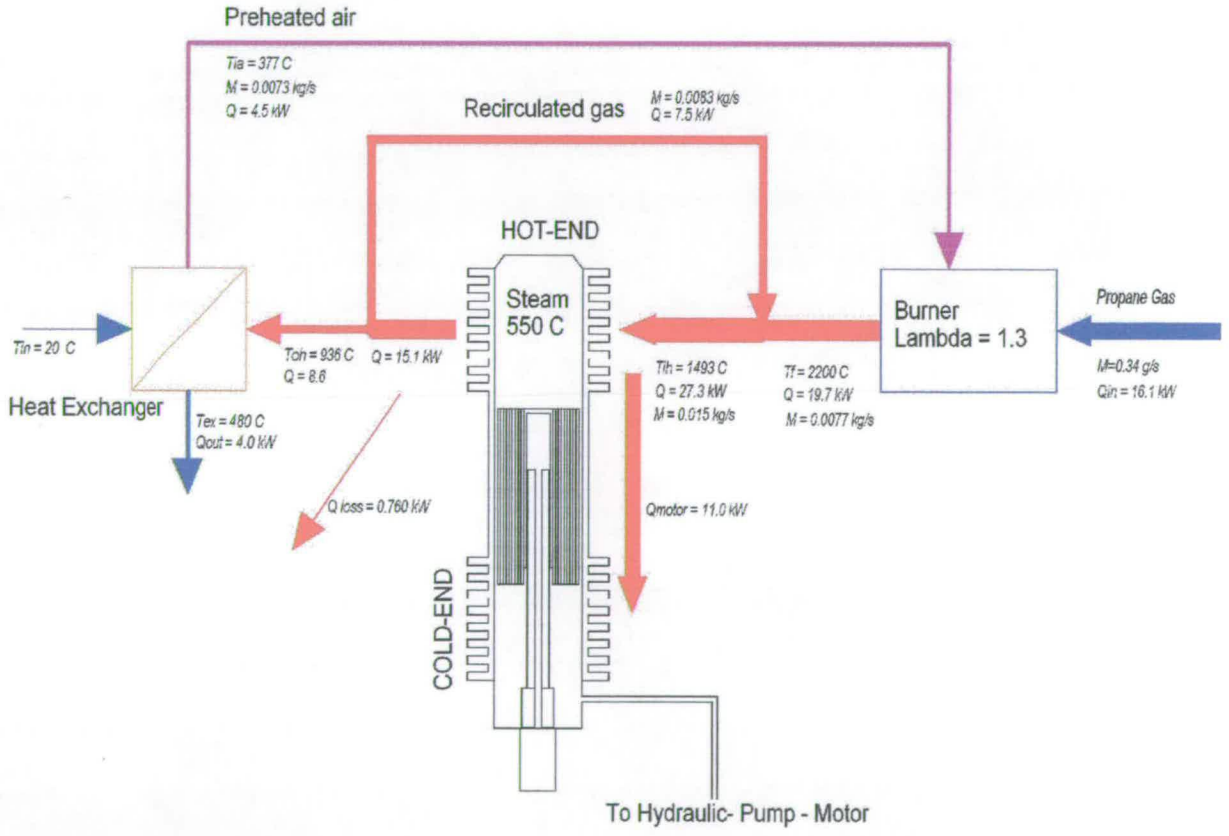


Figure 3.6. The results from the Math-Cad model of the combustion system are presented. It is possible to see the combustion gas temperature and mass flow at each point in the system. The line width represents the energy flow rate. The calculations are done on basis of a lambda number of 1.3 and a recirculation factor of two.

3.4 Flow test rig

An experimental model was constructed to analyse and optimize the recirculation factor and the flow velocity around the hot-end heat exchanger. The model was built to the same dimensions as the proposed combustion space but employed room temperature air as the flow medium.

With this rig it was possible to vary the diameter of the combustion chamber and to analyse the effect on the flow velocity profile inside the combustion chamber and around the hot-end heat exchanger fins. Figure 3.7 shows the combustion chamber flow test rig with a number of flow sensors and the different wall tubes that have been used during the test.



Figure 3.7. Room temperature test rig with flow measurement probes to the left of the test chamber the hot-end heat exchanger in the center. Two further combustion chamber walls with different diameters are shown on the right.

To allow for the different density and viscosity of the air at room temperature, the mass flow rate was scaled so that the Reynolds Number (Re) in the model and in the real combustion chamber were the same.

The hot combustion gas has a density of only around one fifth of the density of air at room temperature. At the same time the dynamic viscosity increases by a factor of about three.

It is possible to calculate the mass flow rate and velocity to achieve the same Reynolds number using the equation 3.6.

$$\dot{m}c = \frac{\dot{m}h}{\mu h} * \mu c \qquad 3.6$$

$\dot{m}c$ = mass flow rate room temperature air [kg/s]

$\dot{m}h$ = mass flow rate hot combustion gasses [kg/s]

μh = dynamic viscosity prototype [kg/s*m]

μc = dynamic viscosity cold test [kg/s*m]

By connecting the test rig to a variable speed fan unit it was possible to create the same Reynolds numbers as expected in the real combustion chamber. To measure the flow rates in the combustion chamber, a hot wire flow anemometer was built and used. Figure 3.8 shows the anemometer probes positioned around the hot-end heat exchanger fins.

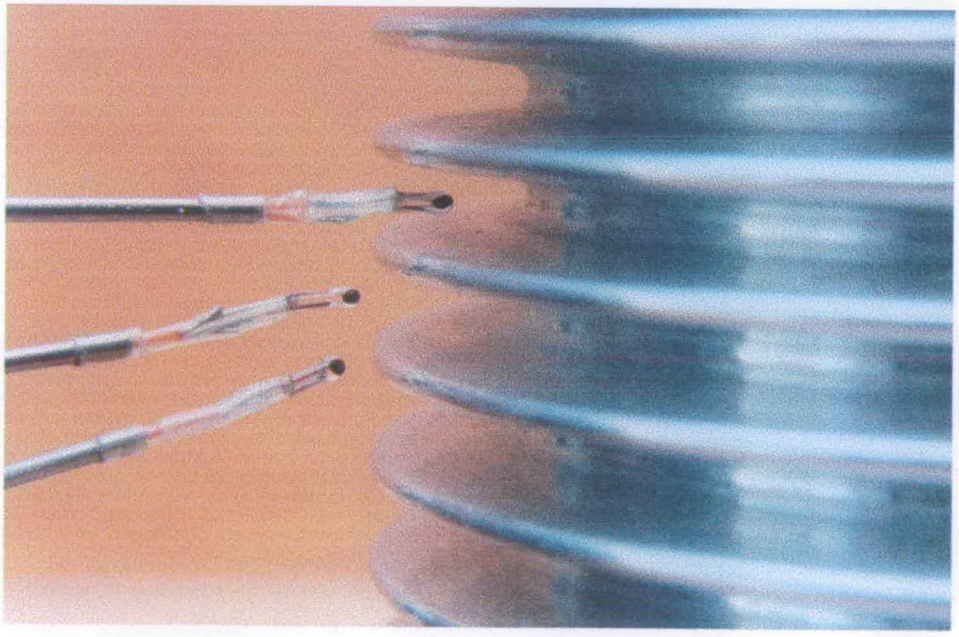


Figure 3.8. Photograph of three hot wire anemometer probes positioned to analyse the flow velocity around the outer fins of the hot-end heat exchanger.

With this test set up, it was possible to analyse the flow velocities around the fins and inside the combustion chamber. Further, it was possible to calculate the recirculation factor (*Rf*) by measuring the total volume of gas circulating the hot-end heat exchanger.

Table 3.1, 3.2 and 3.3 illustrate the results from the air velocity measurement between the hot-end heat exchanger and the combustion chamber wall for the three different combustion chamber wall diameters. The air velocities have been measured at three different planes, 30°, 150° and 270° past the inlet tube (see figure 3.9 left). At each plane, the flow velocities were measured at a number of different heights and distances from the hot-end fins (see figure 3.9 right) to form a measurement grid across the flow area. The flow velocities at the surface were presumed to be zero.

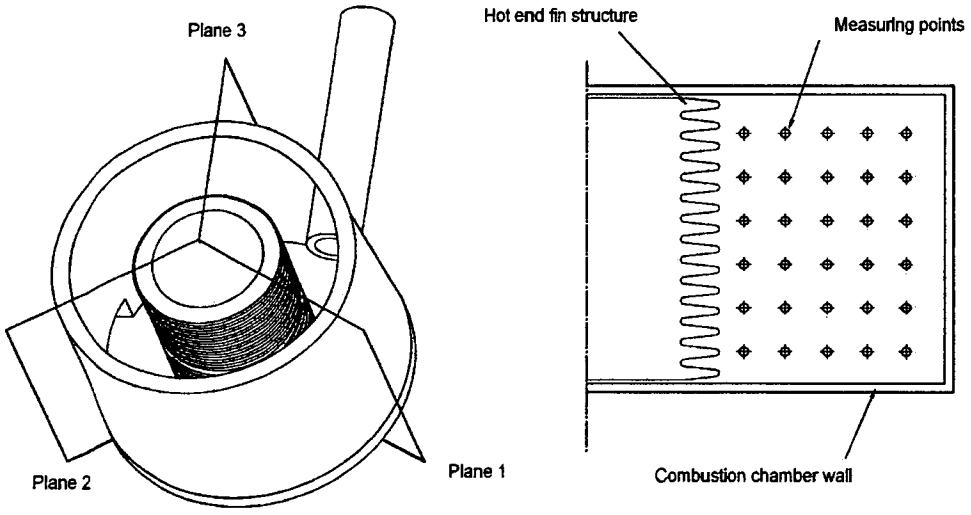


Figure 3.9. The left figure shows the measuring planes in relation to the combustion chamber and inlet tube. Plane one is, hereby, 30°, plane two 150° and plan three 270° past the burner inlet. The right figure shows the location of the measuring points in each plane.

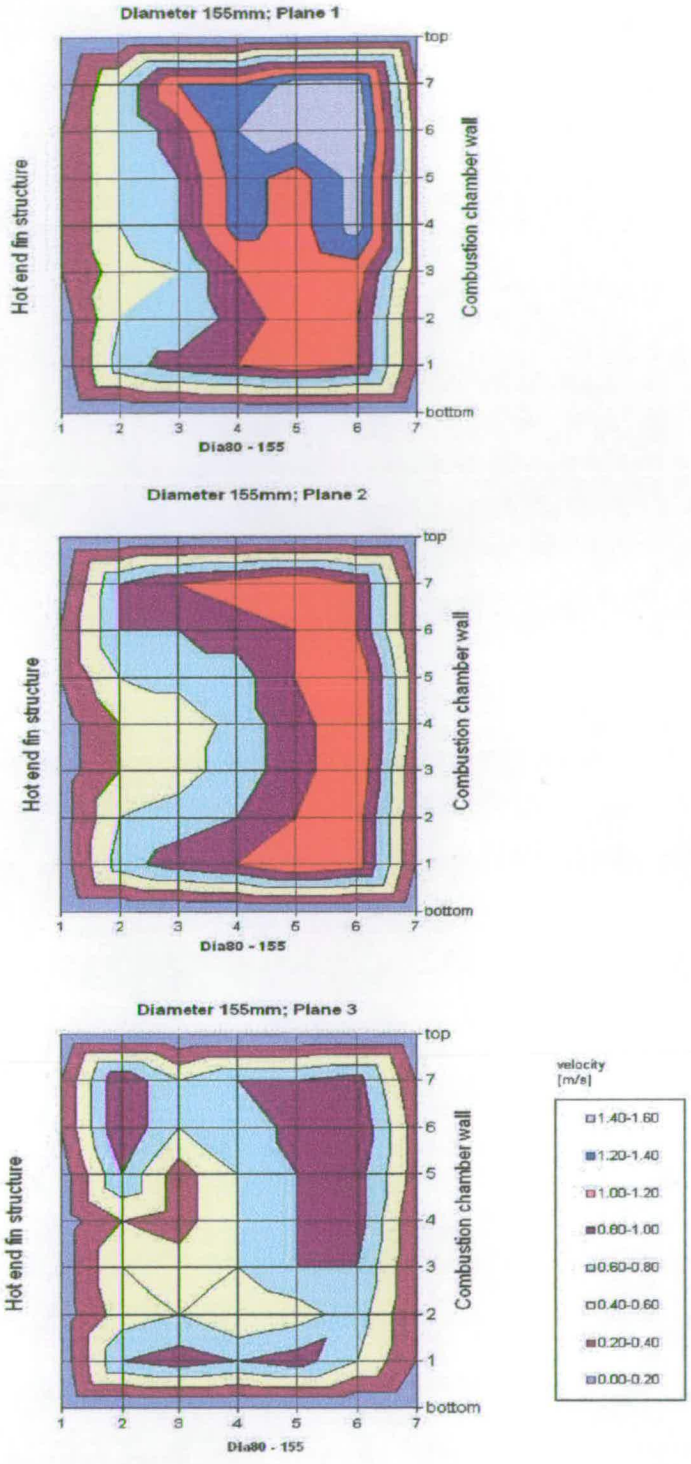


Table 3-1 shows the air velocity profile in the area between the hot-end heat exchanger fins and the combustion chamber wall, for a hot-end heat exchanger diameter of 80 mm and an inner combustion chamber diameter of 155 mm. The velocity profiles are measured at 30, 150 and 270 degrees past the burner inlet (see drawing 3.9).

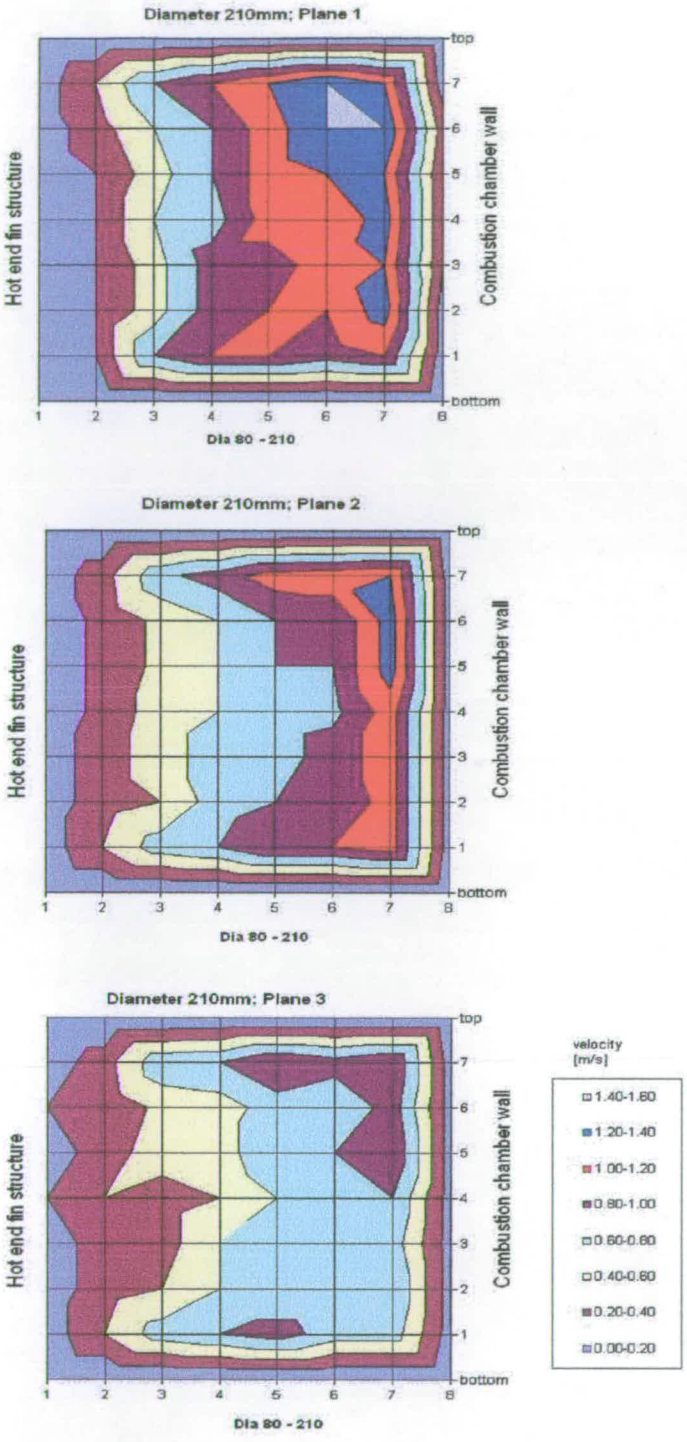
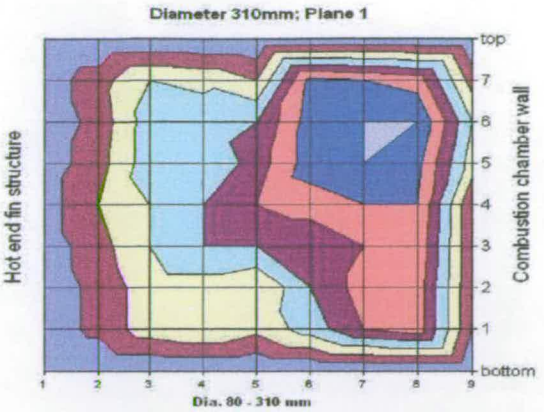
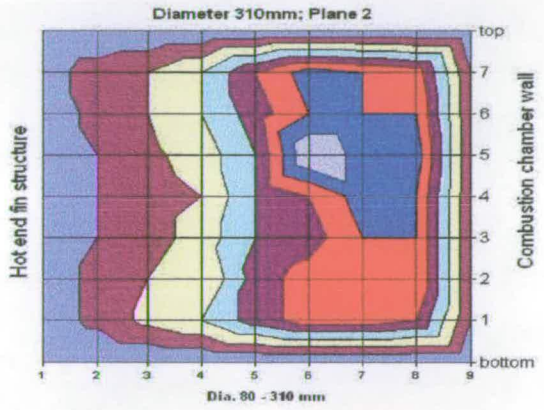


Table 3-2 shows the air velocity profile in the area between the hot-end heat exchanger fins and the combustion chamber wall, for a hot-end heat exchanger diameter of 80 mm and an inner combustion chamber diameter of 210 mm. The velocity profiles are measured at 30, 150 and 270 degrees past the burner inlet (see drawing 3.9).





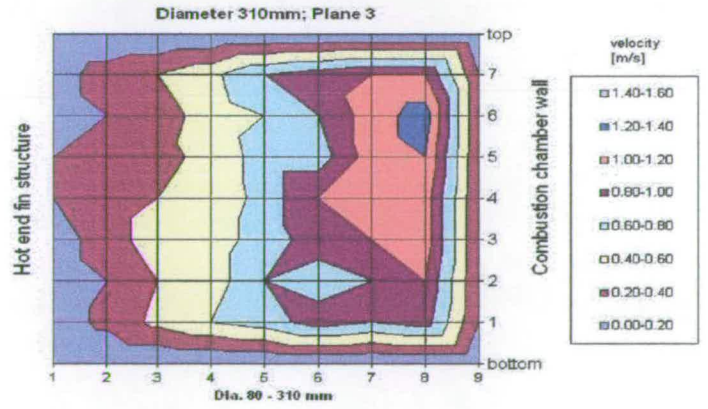


Table 3-3 shows the air velocity profile in the area between the hot-end heat exchanger fins and the combustion chamber wall, for a hot-end heat exchanger diameter of 80 mm and an inner combustion chamber diameter of 310 mm. The velocity profiles are measured at 30, 150 and 270 degrees past the burner inlet (see drawing 3.9).

With the results from the velocity measurements, it is possible to calculate the total air volume flow between the hot-end heat exchanger and the combustion chamber. Sector one presents, the recirculated and the newly entered combustion gas volumes. Sector three presents the recirculated combustion gas volume. Sector two overlaps with the exit and the results can not be used to calculate the volume flow.

Average air velocity in each sector

	Air velocity [m/s] 155 mm diameter	Air velocity [m/s] 310 mm diameter	Air velocity [m/s] 210 mm diameter
Sector 1	0.770	0.610	0.660
Sector 3	0.540	0.440	0.550

Table 3-4 Average flow velocity in sector 1 and 3 for three different combustion chamber diameters

By comparing the volume flow in sector one with the volume flow that enters the combustion chamber through the inlet tube, it is possible to calculate the recirculation factor.

155 mm Combustion chamber diameter

	Sector 1	Inlet tube	Recirculation factor
Flow area [m2]	0.00570	0.00038	
Flow velocity [m/s]	0.770	5.000	
Flow rate [m3/s]	0.004	0.002	2.3

210 mm Combustion chamber diameter

	Sector 1	Inlet tube	Recirculation factor
Flow area [m2]	0.00900	0.00038	
Flow velocity [m/s]	0.610	5.000	
Flow rate [m3/s]	0.005	0.002	2.9

310 mm Combustion chamber diameter

	Sector 1	Inlet tube	Recirculation factor
Flow area [m2]	0.01500	0.00038	
Flow velocity [m/s]	0.660	5.000	
Flow rate [m3/s]	0.010	0.002	5.2

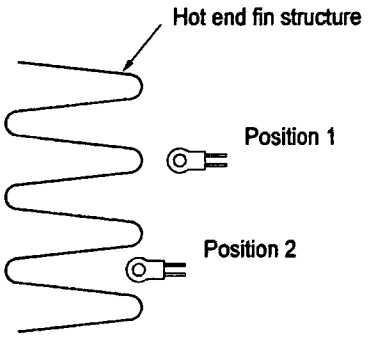
Table 3-5 Recirculation factor for 155 mm, 210 mm and 310 mm combustion chamber diameter calculated from volume flow in inlet tube and volume flow in Sector 1.

The results from the cold test rig show an increase for the recirculation factor from 2.3 for the 155-mm combustion chamber diameter, to 2.9 for the 210-mm combustion chamber diameter, and to 5.2 for the 310-mm combustion chamber diameter.

At the same time, a clear decrease in flow velocity along the hot-end fins was found. A further set of measurements had been taken close to the fin structure. The results are presented in table 3.6.

155 mm Combustion chamber diameter

Probe position	Air velocity [m/s]
Position 1	0.15
Position 2	0.1



210 mm Combustion chamber diameter

Probe position	Air velocity [m/s]
Position 1	0.1
Position 2	0.06

310 mm Combustion chamber diameter

Probe position	Air velocity [m/s]
Position 1	0.1
Position 2	0.05

Table 3-6 Air flow velocity at fin tip and between hot-end fins for 155 mm, 210 mm and 310 mm combustion chamber diameter. The air velocities are measured at the middle fin of the hot-end in sector three.

To find the optimum combustion chamber diameter, it is important to analyse the effect on the heat transfer into the hot-end, and the temperature profile and peak temperature in the combustion chamber. The fraction of recirculated combustion gas has to be large enough to lower the gas temperature to a level where the production of thermal NO_x is low and the material limits of the combustion chamber wall and hot-end fins structure are not exceeded. It was decided that a recirculation factor larger than two would guarantee this, and could also create an even temperature profile inside the combustion chamber. The temperatures of the combustion gas, for a recirculation factor of two, have already been calculated in section 3.2. The incoming combustion gas with a temperature of around 2200°C would mix with an equal amount of combustion gas that had passed the fin structure. This will produce a combustion gas temperature of around 1500°C, which is low enough to be directly applied to the combustion chamber wall, made from Nimonic sheet metal grade Inconel 718. Further the production of thermal NO_x will be kept to a minimum (see

also figure 2.10). The combustion chamber outer wall diameter choice was then made on the basis of optimum heat transfer.

Two main effects, resulting from the above decision, have to be taken into consideration. The heat transfer through radiation is a function of the combustion wall area and, therefore, a function of the combustion chamber diameter. The flow velocity and Reynolds number dominates the heat transfer through convection and it is, therefore, preferable to have a high flow velocity along the fins and, hence, the smallest possible combustion chamber diameter. Due to the large variation in flow velocity and gas temperature inside the swirling flow, and the complex geometry of the hot-end heat exchanger, conventional heat transfer equations could not be applied to calculate the heat transfer by convection. The experimental results would be used to study the heat transfer.

Under the simplified assumption of plane walls for the hot-end heat exchanger and combustion chamber wall, it is possible to calculate the heat transfer by radiation from the wall onto the heat exchanger. Due to the finned structure of the real hot-end this calculation has to be seen as simplified. It does, however, give a clear indication of the effect of the combustion chamber diameter on the proportion of heat transfer by radiation, to the heat transfer by convection.

The heat transfer between two cylinders, where, the smaller one is located inside the larger one, can be described by equation 3.5 (Siegel and Howell 1992).

$$Q_R = \frac{\sigma\left[(T_1)^4 - (T_2)^4\right]}{\left[\left(\frac{1-\varepsilon_1}{\varepsilon_1 * A_1}\right) + \left(\frac{1}{A_1 * F_1}\right) + \left(\frac{1-\varepsilon_2}{\varepsilon_2 * A_2}\right)\right]} \qquad 3.5$$

Q_R = heat transfer by radiation [W]

$T_{1,2}$ = temperature of each cylinder [K]

$A_{1,2}$ = surface area of each cylinder [m^2]

$\varepsilon_{1,2}$ = emissivity of each surface

σ = Stephan-Bolzmann Constant

The total emissivity of the different materials that have been chosen for the structure of the combustion chamber and hot end heat exchanger are given in table 3-7.

Material	Temperature [°C]	Total emissivity
Inconel 718		
Inconel 718 Oxid. @ 815 °C for 15 min	425	0.6
Inconel 718 Oxid. @ 815 °C for 15 min	650	0.67
Inconel 718 Oxid. @ 815 °C for 15 min	900	0.72
Monel		
Monel, Ni-Cu	400	0.44
Monel, Ni-Cu Oxid. at 800 °C	600	0.46
Copper		
Copper oxidised	327	0.5
Copper oxidised	527	0.58
Copper oxidised	727	0.8
Nickel Plated	38-260	0.37
Molybdenum		
Molybdenum	260	0.08
Molybdenum	538	0.11
Molybdenum Oxid. @ 550 °C for 15 min	316	0.8
Molybdenum Oxid. @ 550 °C for 15 min	538	0.82

Table 3-7 Emissivity of combustion chamber and hot end heat exchanger materials at elevated temperatures. (source: Greene and Finfrock (2000) [Inconel 718]; Siegel and Howell (1992) [Monel]; Incropera and Dewitt (1990) [Copper]; Plansee (1992) [Molybdenum])

The heat transfer by radiation for the three different combustion chamber wall diameters has been calculated for a combustion chamber wall temperature of 1300, 1400 and 1500 K and a mean hot-end surface temperature of 900 K. The results are presented in table 3.8. The full calculations are given in appendix D.

	Heat transfer [W] at 1300 K wall temperature	Heat transfer [W] at 1400 K wall temperature	Heat transfer [W] at 1500 K wall temperature
155 combustion chamber diameter	1650	2390	3305
210 combustion chamber diameter	1661	2405	3327
310 combustion chamber diameter	1671	2420	3348

Table 3-8 Heat transfer by radiation from the combustion chamber wall to the hot-end. The heat transfer is calculated for 1300, 1400 and 1500 K combustion chamber wall temperature and 900 K hot-end temperature for three different wall diameters.

The result clearly indicates that the effect of increased wall diameter is of little significance compared to the increase in combustion chamber wall temperature. Further, a small combustion chamber diameter will have less thermal losses through the insulation and smaller space requirement. The results show that a small combustion chamber diameter has a clear advantage for heat transfer reasons. A diameter of less than 155 mm results in a recirculation factor of less than two with insufficient recirculation of combustion gas.

3.5 Experimental test results

Before the combustion system was used to test the prototype engine, it was important to validate the results from the theoretical calculations shown in section 3.3 and to ensure that the system was capable of transferring the calculated power into the hot-end. This would be especially important for interpreting efficiency measurements of the engine later in the project. To test the combustion system a dummy hot-end, as shown in drawing 3.10, was constructed. The dummy hot-end was designed so that the external fin temperature and geometry was similar to that of the proposed engine. This has been achieved by using a material of higher heat resistance for the structure, combined with low temperature cooling water on the inside of the structure. The heat exchanger in the final hot-end has a calculated fluid temperature of 500°C on the internal fin structure, combined with a wall thickness of around 5 mm to the base of the flame fin. The temperature drop from working the working fluid to the base of the flame fin was calculated to be around 150°C. With a working fluid temperature of 500°C, this results in a flame fin base temperature of around 650°C. The dummy hot-end was constructed to work with a much lower fluid temperature of 15 – 30°C on the internal side of the heat exchanger, making it possible to use tap water as the cooling media. The wall thickness was chosen so that the temperature drop in the dummy hot-end wall would compensate for the lower fluid temperature. A wall of 15 mm martenistic stainless steel, with lower heat conductivity, was calculated to give a temperature drop of around 600°C, at full output power of 10 kW. By changing the cooling water flow rate it was possible to vary the temperature drop between the cooling water and the internal wall of the dummy hot-end. This has been used to

adjust the flame fin base temperature to 650°C, the calculated value for the proposed engine.



Figure 3.10. The dummy hot-end as used to simulate the thermal load of the engine is shown. The dummy hot-end is internally water-cooled. The wall thickness and material is chosen to create an increased thermal resistance in the wall, resulting in the same fin base temperature as the proposed test engine.

A number of thermocouples were used during the test to measure the temperatures at the key points in the system. A flow sensor was installed in the propane gas line to monitor the gas flow rate and, therefore, the energy input. An airflow sensor was used to measure the air mass flow to the combustion and to calculate the Lambda number and mass flow rates in the system. A schematic of the data sampling system is shown in appendix E. From the flow and temperature measurements in the cooling water system it was possible to determine the heat flow that was transferred into the dummy cold end. The results from the temperature measurements are shown in figure 3.11. The energy flow rates have been calculated from the temperature and flow rate measurements and are presented in figure 3.12.

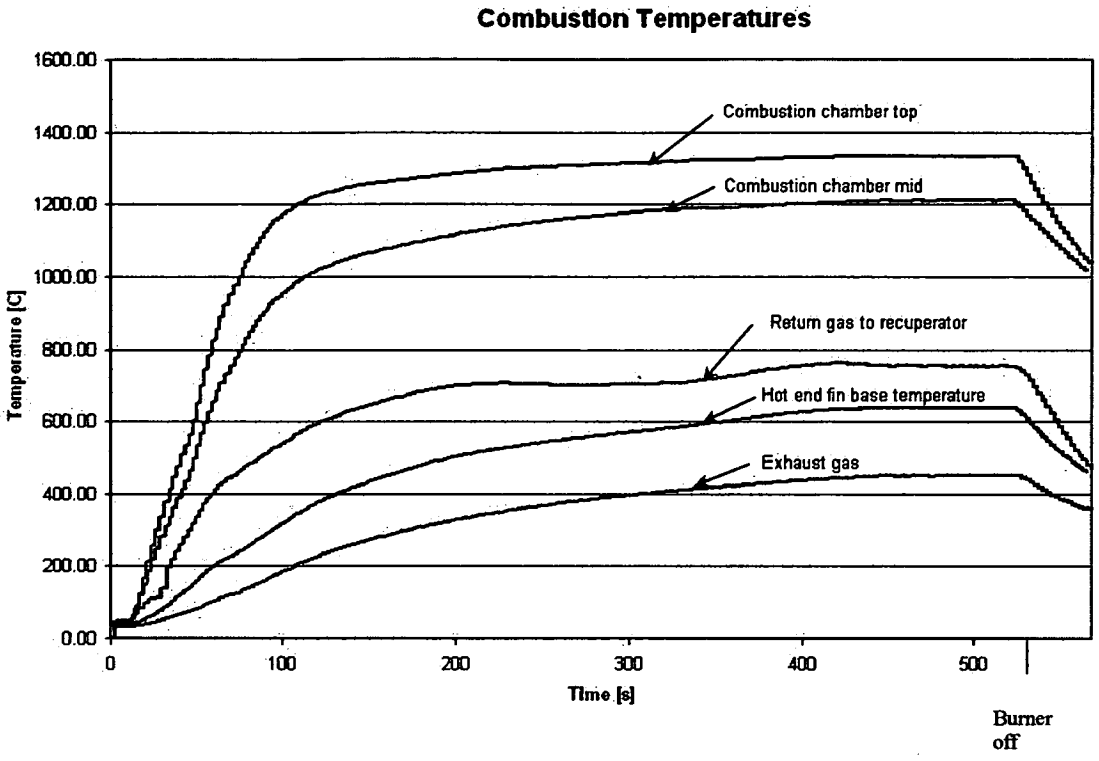


Figure 3.11. Temperature profiles at different points in the combustion system during a 500 s long test.

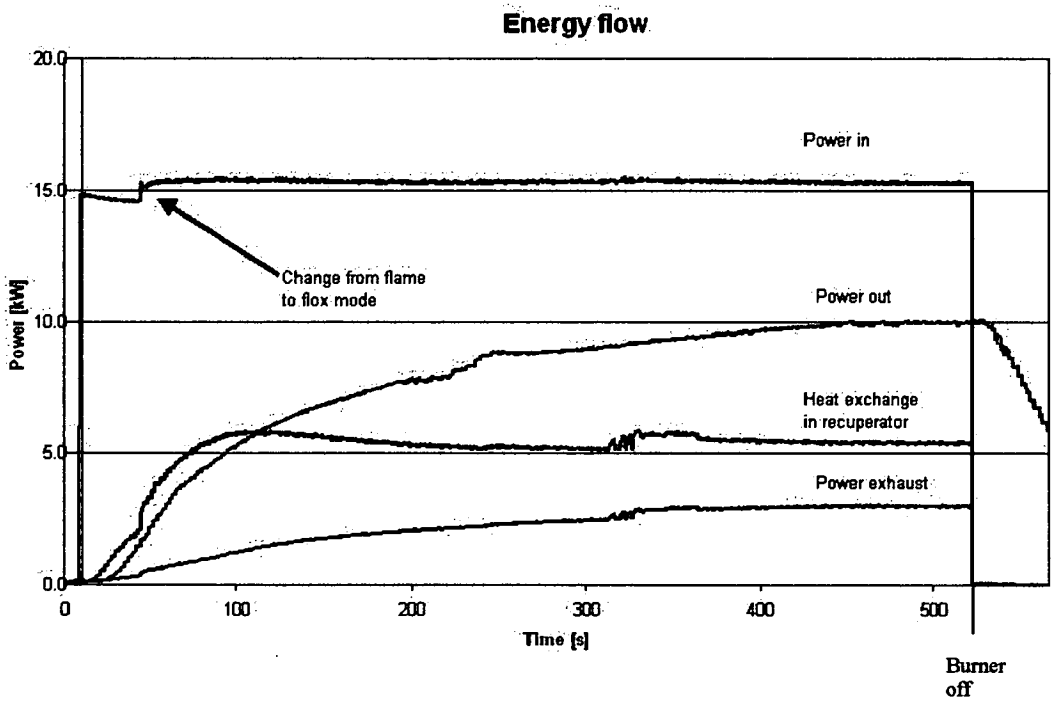


Figure 3.12. The main results for the energy flow in the combustion system are illustrated. The different energy flows are calculated from the measured temperatures and mass flow rates.

3.6 Discussion of results

The results from the combustion test rig show that it is possible to transfer the required energy into a finned single tube heat exchanger as prefered for the Malone engine. With the chosen design of swirling the combustion gas around the central heat exchanger, it was possible to create an even temperature profile in the hot-end heat exchanger and to reach heat transfer rates of over 500 kW per m^2. The required power for the combustion air blower was less than one percent of the input power. The low overall efficiency of 68% was mainly due to the insufficient exhaust gas heat recovery. Complete exhaust gas heat recovery would result in a combustion system efficiency of around 90%. The extent to which further exhaust gas heat recovery is economical, is determined by the application.

Generally, the test results were found to agree with the results predicted from the theoretical calculations presented in figure 3.6. A small discrepancy was found in the form of a higher thermal efficiency of the combustion chamber calculated than found in the test. The theoretical calculation predicted that it would be possible to transfer 11 kW into the dummy hot-end when working with 16 kW input energy and an exhaust gas temperature of 400°C. The losses, due to incomplete combustion, and the thermal losses had, hereby, been set to 0.75 kW resulting in a burner efficiency of 95%. At an exhaust gas temperature of 400°C, as specified by the burner manufacturer, the resulting exhaust gas losses are around 4 kW, giving an overall efficiency of 70 %. The test results show that, at an input of 16 kW to the burner, only 10 kW could be transferred into the dummy hot-end, resulting in an overall efficiency of 62%. This was partly explained by the slightly higher exhaust gas temperature of 420°C. The remaining lower efficiency of the combustion system is expected to come from insufficient insulation.

With the limited ability to measure flow rates in the hot parts of the combustion chamber, it is difficult to confirm the predicted recirculation factor of 2.3 from the cold test rig. The calculated combustion gas temperature after the remix of the gas that has already passed the combustion space is 1298°C, for a recirculation factor of two. This is in good agreement with the measured value of 1300°C.

4 Hot-end heat exchanger

This chapter presents a general discussion of the work undertaken in the development of the hot-end heat exchanger for the proposed engine. An introduction to the subject, and a short explanation of the Thermodynamic Pile of the proposed engine is given in order to clarify the general layout and position of the hot-end heat exchanger.

A description of the work on the different hot-end heat exchangers is also presented. This section focuses on the various materials and fabrication techniques employed in the heat exchanger design. The results from a number of tests carried out on these heat exchangers are presented.

4.1 Introduction

A description of the general layout of Malone's engine is already given in section 1.3 and Figure 1.2 shows the Thermodynamic-Pile as used by Malone in his original engine. Malone introduced the term Thermodynamic Pile or short TD-Pile for the core element of his engine. The TD-Pile can be seen as the heart of the Malone engine. It is here that part of the thermal energy, which comes from the combustion system, is converted into mechanical energy, with the remainder being transferred into the cooling system. The main components of the TD-Pile are the hot-end heat exchanger, the regenerator and the cold end heat exchanger. Compared to the Stirling engine, where the working piston and the mechanical linkages are an integral part of the engine, Malone's arrangement is such that these components are separated from thermodynamic parts of the engine.

The TD-Pile of the proposed engine incorporates all the main components found in Malone's TD-Pile, but differs substantially in the design of the individual components. Figure 4.1 shows the TD-Pile of the proposed Artemis Malone engine. The general arrangement chosen is the same as Malone's, with the regenerator, and the hot and cold end dummy traveling between the hot and the cold end space. There

are a number of differences between the TD-Pile of the proposed Artemis Malone engine and that of Malone`s original TD-Pile. (i) The use of a hot-end heat exchanger made from advanced materials and with fins on the inside and outside (ii) A different arrangement of the hot and cold end dummy (iii) The use of a conventional regenerator, without valves, to direct the flow through different flow passages.

At the beginning of the study a large amount of research was conducted in the field of the hot-end heat exchanger. During this time a number of different heat exchangers were designed and made. It eventually became apparent that the biggest difficulty lay in the design of an efficient regenerator system. As a result of this, the focus of the study shifted away from the hot-end heat exchanger development in order to concentrate on the regenerator. It was decided that the work on the hot-end heat exchanger would be resumed once the development phase of the regenerator was completed. At the time of submission, an experimental program to evaluate the heat transfer in the hot-end heat exchanger is ongoing. For this reason the results of these experiments are not included in this thesis which is, therefore, restricted to the initial development work, which considers the various feasible materials and fabrication techniques. The results from the experimental studies, carried out in the TD-pile test rig as shown in figure 4.1, are presented at the end of the chapter.

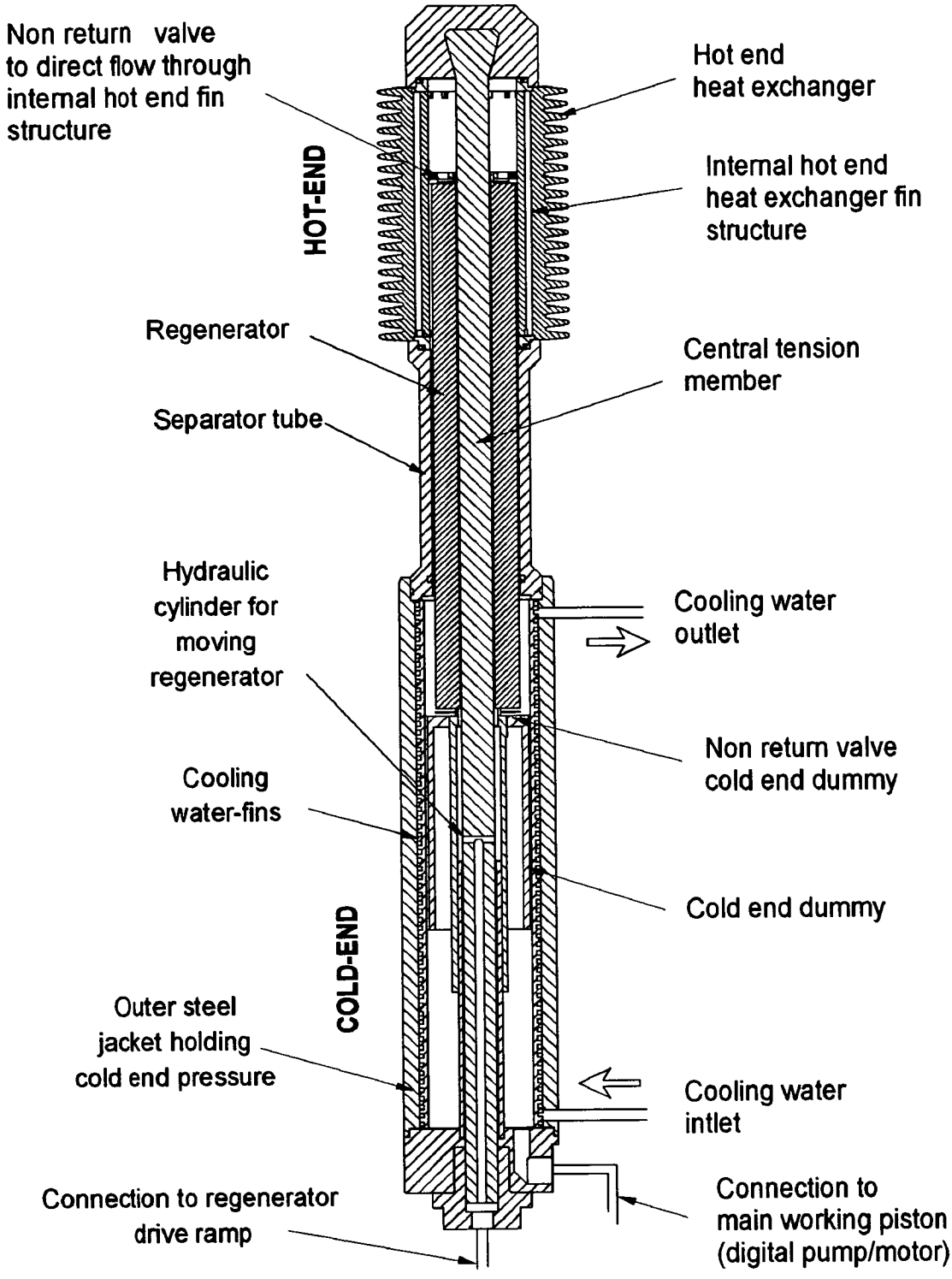


Figure 4.1 Thermodynamic pile of the proposed Artemis Malone engine as used for the experimental study on the hot-end heat exchanger and the regenerator. It was possible to work with internal pressures of up to 400 bar and hot-end fluid temperatures of up to 550 °C.

4.2 Hot-end heat exchanger

In external combustion engines, it is necessary to transfer the heat energy through the hot-end heat exchanger into the engine. It is, therefore, important to keep the temperature difference between the combustion gas on the outside, and the fluid on the inside as small as possible, in order to avoid a damaging increase in fin or exhaust gas temperature.

The main requirements for an optimised heat exchanger are summarized as follows:

- The material must be able to withstand the high internal pressure cycles at a high temperature. The peak cycle pressure in the proposed engine is 400 bar at a mid wall temperature of over 600°C.
- The wall must be made from a material with good heat conductivity so that the temperature drop through the heat exchanger wall is kept to a minimum.
- The material must be resistant to corrosion from the combustion gas on the outer side as well as from the supercritical water on the inner side.
- There must be a large surface area on the inner side with the working media passing at a high velocity along it.
- There must be a large surface area on the outer side with the combustion gas passing at a high velocity along it.
- The material must be able to go through repeated temperature cycles without deforming or cracking.

Given that there is no material commercially available that has all the right properties, compromises in some areas have to be made, or composite structures made from two or more different materials have to be produced.

In the following section a comparison between Malone's original hot-end heat exchanger and the heat exchanger as proposed for the Artemis Malone engine is made.

Malone's original engine used a long cast steel tube with a small diameter to length ratio for the hot-end heat exchanger. This design was mainly driven by the fact that cast steel, had limited high temperature strength. The subsequent development of high temperature metals has opened up many new possibilities for constructing the hot-end heat exchanger. It is now possible to work with larger diameters and smaller wall thickness, increased thermal conductivity in the wall and smaller temperature drops at the interface from gas to heat exchanger and to the working fluid. During the course of the study a number of different designs for the hot-end heat exchanger of the Artemis Malone engine were proposed. The development of a heat exchanger with an increased energy flow per unit wall area, allowing the building of compact engines of increased power to weight ratio, was the main aim of these designs. Different material combinations were tested in order to try to improve the thermal conductivity. These included the use of Nickel Super Alloys, Copper, Monel and Molybdenum. A number of different designs for the internal and external fin structure have been analysed.

Malone used pistons he called dummies, which were mounted onto the ends of the regenerator to increase the heat transfer from the internal wall of the hot and cold end into the working fluid. The dummies increased the flow velocity along the internal wall and, therefore, enhanced the heat transfer from the wall into the fluid. The main disadvantage of such a system is that, due to the travel of the regenerator, it is not possible to make use of the full length of the hot-end heat exchanger surface.

In the Artemis Malone engine one-way valves have been installed in the hot and cold end dummy so that the fluid only passes the heat exchanger when it is leaving the regenerator in either direction. In the return stroke the fluid is passed through the centre of the hot or cold end dummy.

During the heating stroke, the fluid leaving the regenerator passes through the hot-end heat exchanger fin structure to be heated. The hot-end heat exchanger is by-passed

during the hot blow, where further heating of the working fluid would be disadvantageous and would create extra pumping losses. The same principle, in reverse, is applied to the cold end.

During the project a number of different hot-end structures and materials were analysed. In this analysis two main alternatives were considered. The first concerns structures made from only one material, while the second concerns composite structures made from two or more different materials, each used for its desirable properties and to negate the deficiencies of the other.

The development started off with a composite structure made from copper and Inconel as proposed by Salter. Further structures made from Molybdenum, Copper-Molybdenum, Copper-Monel, and Monel were also produced and evaluated.

4.2.1 Heat exchanger materials

There is a large choice of suitable materials for heat exchangers, all of them offering advantages in some areas and disadvantages in others. It is important to obtain the fine balance between heat conductivity, high temperature strength, corrosion resistance, availability and machineability. Table 4.1 gives an overview of a number of different available materials properties.

Material	Heat conductivity at 600 C [w/mK]	Tensile Strength at 600 C [N/mm^2]	Machineability	High temperature Corrosion resistance	Price	Availability
Copper	360	60	fair	poor	cheap	good
Inconel 718	20.4	989	good	very good	expensive	fair
Monel 500K	33.3	612	good	very good	expensive	fair
Stainless Steel 304	23.9	106	good	good	cheap	good
Molybdenum TZM	112	900	poor	poor	expensive	poor
Tungsten VM	125	1100	very poor	poor	expensive	poor

Table 4.1. The advantages and disadvantages of a number of different possible materials for the use in the hot-end heat exchanger are illustrated (Inco Alloy Intl. 1984, 1985a, 1985b; Howard and Timothy 1984; Plansee 1992, Copper Development Association 1994).

It can be concluded that none of these materials has a clear advantage over the others. Looking at the work done on Stirling engines in the past decades, most of the high temperature heat exchangers are made from thin wall tubes of high temperature Nickel super alloys like Inconel 718 (Walker 1980; Hargreaves 1991). These alloys offer a satisfactory combination of the different parameters in all aspects except conductivity (see table 4.1). The consequences of this deficiency are minimized by using small tubes with thin walls.

In the Malone engine, due to the higher heat conductivity and heat capacity of supercritical water, an increased heat flow rate in the heat exchanger wall is expected. Further, due to the high internal pressures, an increased wall thickness is required. This results in increased temperature drops in the wall, making the right choice of the wall materials crucial in the design of a thermodynamically and cost efficient engine.

Initially a basic analysis of the proposed engine was made, in order to acquire an understanding of the magnitude of the temperature drop, and to compare the different materials with each other. The proposed hot-end heat exchanger has a length of 120 mm and an internal diameter of 45 mm. From stress analysis on the heat exchanger wall it was found that at the wall thickness of 5 mm in the prototype design a maximum stress of around 230 N/mm^2 occurs. This is within the stress limit of Inconel 718, Monel K500, Molybdenum and Tungsten. With the maximum stress in a thick wall cylinder occurring at the inner wall, even extreme thick walls would not permit the use of stainless steel or copper at these temperatures.

It is now possible to calculate the temperature drop in the heat exchanger wall for the different materials using equation 4.1 (Incropera and Dewitt 1990).

$$\Delta T = \frac{Q * \ln \frac{R_{out}}{R_{in}}}{k_m * 2 * \pi * L} \qquad 4.1$$

Q = heat flow through wall [W]

ΔT = temperature drop in wall [K]

k_m = thermal conductivity in wall material [W/m*K]

R_{out} = outer tube radius [m]

R_{in} = inner tube radius [m]

L = heat exchanger length [m]

The temperature drop in the heat exchanger wall of the proposed engine with 10 kW heat flow and 5 mm wall thickness was found as:

Inconel 718	=	118 °C
Monel K500	=	72.6 °C
Molybdenum TZM	=	21.5 °C
Tungsten VM	=	29.4 °C

It can clearly be seen that a heat exchanger wall made from Inconel or Monel would result in a significantly larger temperature drop than in the wall made from Molybdenum or Tungsten. On the other hand Inconel and Monel have a clear advantage in their better machineability, corrosion resistance, availability and lower cost, making them the more feasible materials for actual production.

A further possibility for the design of heat exchanger is the use of composite structures. There are a number of advantages in using composite structures compared to structures made from a single material. It is possible to combine materials with good high temperature strength and good corrosion resistance such as nickel-super alloys, with materials of good thermal conductivity such as copper. The problem with these designs is that the different values in thermal expansion, modulus of elasticity and corrosion behaviour make it extremely difficult to join the individual parts without eventual leakage.

Prior to any work on a complete TD-Pile, a number of studies using the first combustion system test rig, already described in section 3.2.1, were conducted. These tests were primarily intended to study the behaviour in terms of corrosion, sealing and creep of the hot-end heat exchanger, at the temperatures and pressures of the proposed engine. Unfortunately with this test set up, it was not possible to study the heat

transfer in the heat exchanger. The rig was primarily used to analyse the different heat exchanger designs with respect to their corrosion and sealing performance.

4.2.2 Initial Copper-Inconel heat exchanger

The first design was a structure made entirely from Copper and Inconel washers, which were brazed together. In this structure, the Copper is used for its heat conductivity and the Inconel for its high temperature strength. A photograph of the first prototype is shown in figure 4.2 left and the design of the heat exchanger can be seen to the right. In this type, it is important that there is a good bond between the Inconel washers and the copper to ensure a leakage free vessel and good transfer of stress.



Figure 4.2 First hot-end heat exchanger made from copper and Inconel washers. The washers were laser cut and then vacuum brazed together.

The thickness ratio between the Copper and Inconel washers defines the sheer stress in the copper as well as the thermal resistance of the hot-end. It is important to optimise this ratio so that the maximum amount of Copper is used to minimise the thermal resistance while the stress in the copper does not exceed its creep stress limit. The expected shear at 400 bar with an Inconel to copper ratio of about one to one has been calculated to be around 2 N/mm^2. A number of studies concerning the creep behavior of copper at high temperatures have been found in the literature (Copper Development Association, 1994; Howard, 1984). None of these extends to the temperatures of over 500°C in the proposed engine. Figure 4.3 illustrates the results from creep tests on electrical grade Copper in a 1000h test at temperatures of up to

260°C (Copper Development Association, 1994). Extrapolating these results to temperature of over 500°C indicates the possibility of creep at very low tensile stress.

It was decided that tests on the creep properties of copper above 500°C would have to be done prior to any further work on this design. The tests were carried out on electrical grade copper strips of 5 mm width and 0.15 mm thickness. The strips were accurately marked, at two points 50 mm apart, using a milling machine with digital read out with an accuracy of plus and minus 0.05%. The strips were then clamped in a rig and ballasted with weights to the tensile stress of 2.5 and 4.7 N/mm^2. The rig was then placed in an oven. With the help of a microscope attachment on a milling machine (with a digital read out), it was possible to measure the change in length before and after the test to plus or minus 0.05%.

The creep tests were carried out in an electrically heated furnace. An extra thermocouple was used to measure the temperature close to the copper thus allowing accurate control of plus and minus 2°C. Unfortunately the initial tests failed due to the extensive corrosion on the copper at the test temperature of 550°C. The tests were then repeated after the copper strips had been nickel plated. Initially, this prevented corrosion but the coating failed during the tests and oxidation started again along cracks in the nickel plating. Further tests were carried out in a nitrogen atmosphere and it was then possible to stop the copper from corroding and to measure the creep in the copper. These tests were carried out on two copper strips for each loading case giving an error of less than 10% between the strips. The average results are presented in table 4-2.

Time	2.74 N/mm^2	4.57 N/mm^2
24 h	0.1 %	0.4 %
48 h	0.4 %	0.6 %
72 h	0.5 %	0.7 %

Table 4-2 Creep on electrical grade Copper at 550 °C. Tests were carried out on strips of pure copper in a nitrogen atmosphere and with nickel coating to prevent corrosion.

There is a clear indication that significant creep occurs at the shear stress and temperature levels required in the proposed engine. A further reduction of the Copper to Inconel ratio would, eventually, help to overcome this problem. This would ultimately result in an increased thermal resistance. Further, it would leave little margin for any local overheating in operation. Figure 4.3 shows the 550°C test results extrapolated to 1000h in comparison to available creep data at lower temperatures.

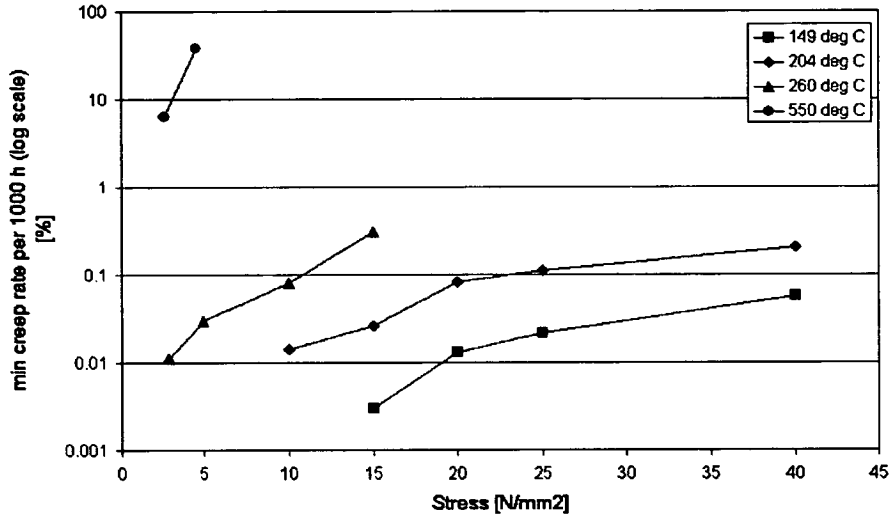


Figure 4.3 Creep on electrical grade Copper per 1000h at elevated temperatures. (source for 149°C, 204°C and 260°C : Copper Development Association (1994))

As a result of this, and the difficulty experienced with the corrosion, the decision was made to look at different arrangements avoiding the use of copper in direct contact with the flame, and to further reduce the tensile stress in the copper.

4.2.3 Revised Copper-Inconel heat exchanger

It was concluded that the secure protection of copper against corrosion at the temperature and the stresses in the hot-end heat exchanger was not possible. Therefore, a complete redesign of the structure was undertaken.

In this new design, the Copper washers are completely enclosed between Inconel washers. The Inconel acts as the corrosion protection layer and provides the strength to resist the internal pressure. Figure 4.4 shows the design and the first prototype of this structure.

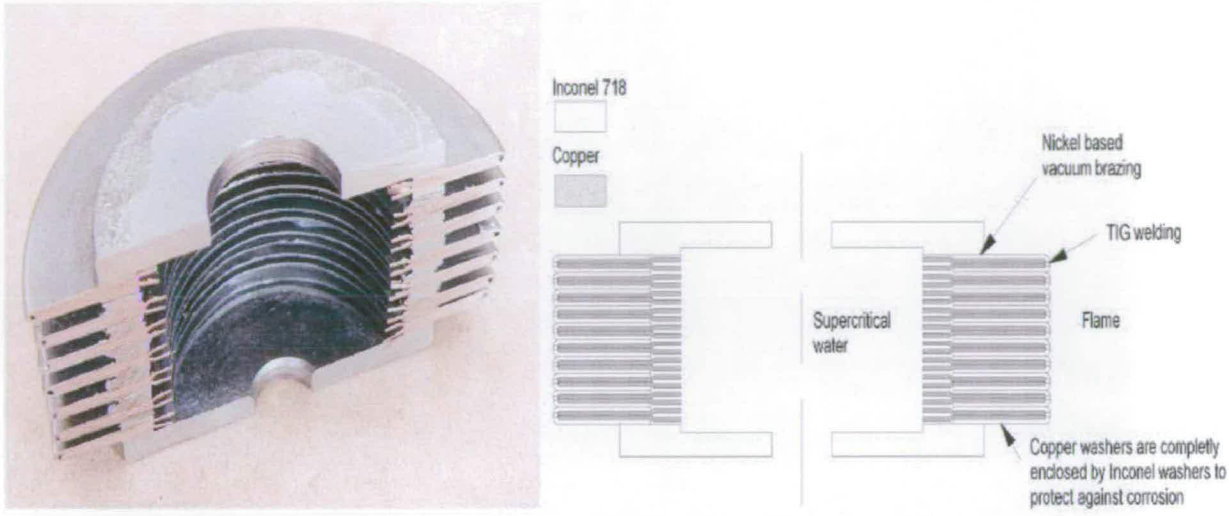


Figure 4.4 Revised copper Inconel hot-end heat exchanger with completely enclosed copper washers. The edges of the Inconel washers were TIG welded. Two copper washers were used for each external fin and spaced apart along the inner radius to increase the surface area of the internal fins.

By passing the heat flow through the thin Inconel sheet at the large external fin area, the temperature drop is kept to a minimum. The thermal conductivity of the copper is then used to transfer the heat through the hot-end wall to the internal fin structure.

The Inconel and copper washers were laser cut from sheet material. After mechanical and chemical cleaning of the surface, the washers were stacked up in a jig and vacuum brazed together. In a second process, the outer ends of the Inconel washers were folded together and TIG welded.

Pressure tests on the first hot-end showed a number of leaks on the brazing between the washers. Further investigation by slitting the structure and observing the brazing under the microscope showed that the brazing compound had completely wetted the copper surface but not properly flowed on the Inconel surfaces. After studying literature it became clear that it is virtually impossible to achieve complete wetting on alloys containing more than 0.5 % aluminum or titanium.

The type of alloy Inconel 617 that was used for the washers had been chosen for its high temperature strength and corrosion resistance. The high temperature corrosion resistance is achieved through the aluminum content that forms an oxide layer on the surface. Inconel 617 contains 1.2 % of aluminum and 0.3 % of titanium. This explains the poor result from the brazing.

It was decided that the design had become too complicated and, even with more suitable materials for the brazing process, the problem of controlling a large sealing area would remain. Therefore, no further work on the design of copper and Inconel was done.

4.2.4 Molybdenum washer heat exchanger

The first hot-end heat exchanger made from one type of material was built by stacking up washers of Molybdenum (grade TZM). The washers were cut in alternating sizes to create the internal and external fin structure. Figure 4.5 shows the design and a photo of the first prototype.

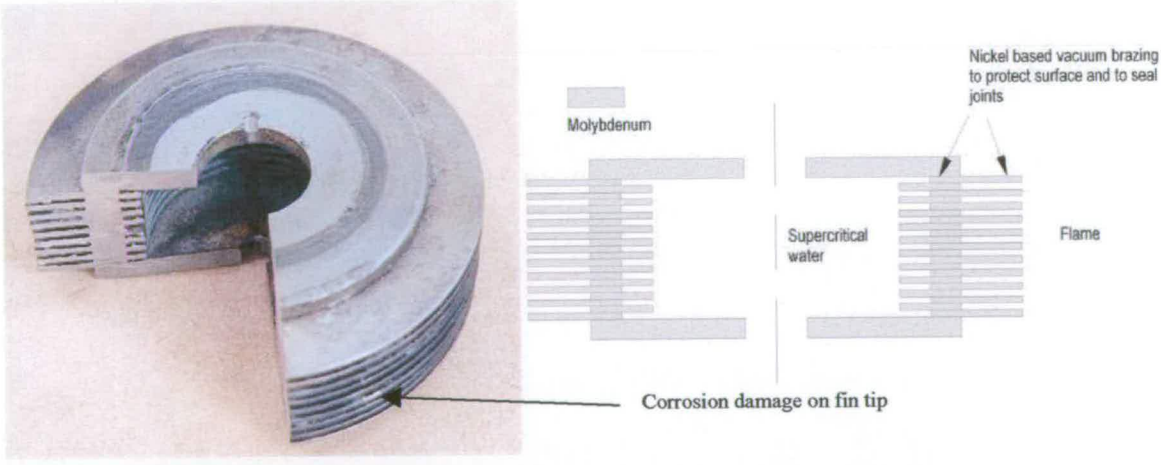


Figure 4.5. First hot-end heat exchanger made from Molybdenum. The washers were machined from Molybdenum grade TZM sheet material of 1 mm thickness. The complete surface was then coated with nickel based compound and vacuum brazed.

Initially, it was important to develop the different machining and coating techniques to ensure a leakage free and corrosion resistant structure. Molybdenum starts to oxidize in oxygen containing atmosphere at temperatures over 400°C, with the oxidation becoming intense at temperatures over 600°C. It is, therefore, essential to protect the Molybdenum against corrosion. For this reason the complete surface of the washers was coated with nickel brazing powder and then vacuum brazed. Tests carried out on small pieces, coated in this way, showed corrosion resistance to temperatures of over 900 C in a Bunsen burner flame with low oxygen content.

The heat exchanger was constructed from washers that were machined from sheet material. After the laser cutting, the washers were ground to size to avoid any cracking on the edges. In the next process the surfaces of the washers were cleaned with emery paper and completely degreased. After this, a thin layer of brazing compound type "Nicrobraze 30" was applied to the complete washer surface with the help of an adhesive. The washers were then assembled in a jig and vacuum brazed for ten minutes at 1125°C.

A number of tests on this heat exchanger were carried out using the first combustion test rig. The heat exchanger was pressurized to pressures of up to 400 bar and heated to temperatures of up to 350°C in the center, and up to700°C at the fin tips. During these tests a number of problems with the design were experienced.

The coating was initially able to protect the surface from corrosion but, after a number of tests, cracks in the coating appeared and corrosion of the molybdenum became visible in the form of white molybdenum trioxide (see figure 4.5). The seal between the washers started leaking. Through repeated brazing it was temporarily possible to overcome these problems but continued testing showed further evidence of corrosion. Also the leakage problem recurred.

The failure of the seal on the brazed joints may be a result of high local stresses between the washers. The washer stack is highly stressed from internal pressure and the compression from the clamping rig. This together with a likely uneven thermal

expansion of the washers in the heating and cooling of the rig, could produce high local shear stresses in the joints.

The main reason for the failure in the protective nickel-brazing layer is found in the corrosion behaviour of Molybdenum. At temperatures of around 700°C Molybdenum trioxide begins to sublimate. At these temperatures, a micro crack in the coating is enough to start oxidation which, due to the sublimation of the oxide layer, starts uncontrollably to corrode the base material.

As a result of the problems experienced with the sealing and corrosion on the different hot-end heat exchangers made so far, the decision was made that any further design would have to meet requirements. Firstly; working with a large number of brazed joints in the main pressure vessel would have to be avoided. Secondly; only corrosion resistant materials or proven coating techniques would be used. With these principles, and the experience from this initial investigation, three different hot-end heat exchangers for the first engine were designed and produced.

4.2.5 Heat exchangers for the proposed engine

The heat exchangers made for the proposed engine were designed to transfer 10 kW of thermal energy from the flame into the supercritical water. The inside diameter was determined by the regenerator diameter as 40 mm, and the outside diameter was chosen as 80 mm. The length of the hot-end heat exchanger was set by the regenerator stroke of 120 mm.

An initial test of the external fin structure had already been carried out during the development of the combustion system. From this it was possible to demonstrate heat transfer rates of up to 10 kW into the dummy hot-end. Further improvements, due to geometry changes, may help to improve the heat transfer in this area but no further investigation was done in this study as the objective were met.

The design of the internal fin structure was utterly different to that of Malone's original engine. Malone's engine used a moving hot-end dummy to force the fluid through an annulus between the plain internal wall of the heat exchanger and the dummy at high velocity.

The design chosen for the proposed engine again uses the regenerator motion to propel the fluid but this time employs a non-return valve to direct the fluid through an internal fin structure in the heat exchanger wall. The valve is located on top of the regenerator. The fluid that leaves the regenerator during the hot blow is directed downwards, alongside the regenerator, until it enters the heat exchanger channels at the bottom of the hot-end. The fluid then travels upwards, through the hot-end fin structure in the heat exchanger wall, until it enters the space above the regenerator.

The fluid bypasses the heat exchanger in the return stroke and enters the regenerator directly through the non-return valve. This helps to minimize pumping losses and avoids further heating of the fluid in the cold blow. Figure 4.6 shows this principle, as designed for the proposed engine.

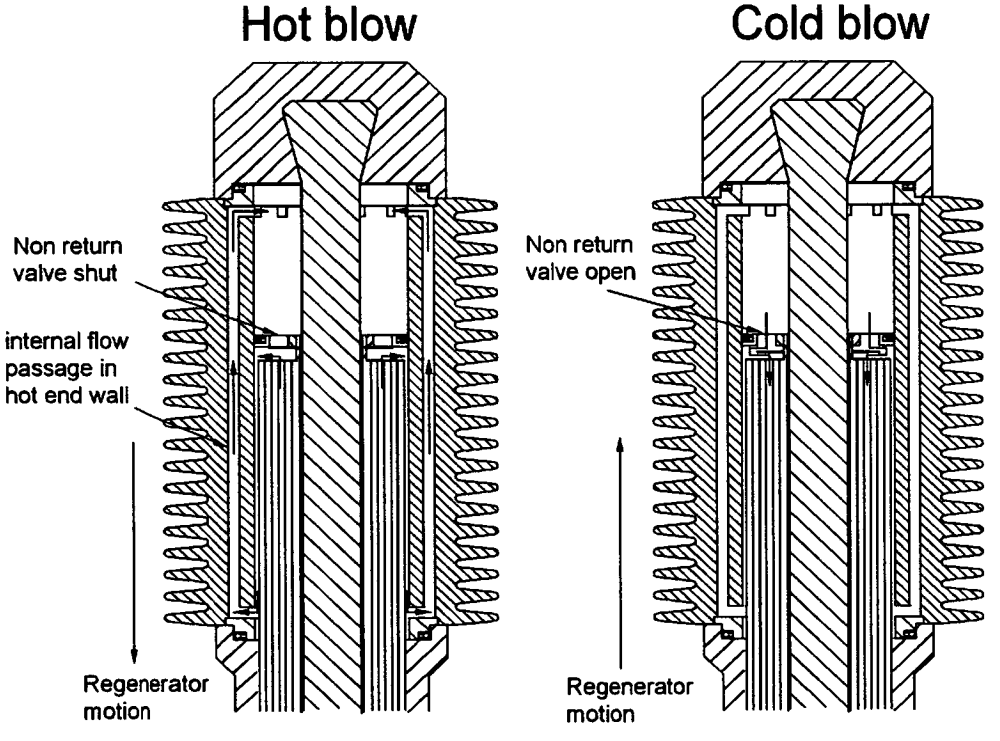


Figure 4.6 The non return valve on top of the regenerator directs the fluid in the hot blow, through the flow passages in the heat exchanger wall. In the cold blow, the valve opens and most of the fluid bypasses the heat exchanger directly entering the regenerator.

The advantage of this system, compared to the hot-end dummy design, is that the heat exchange happens along the full length of the hot-end heat exchanger. In the dummy design it would never be possible to achieve this because the dummy loses contact with the top part of the heat exchanger during the stroke.

The internal flow passage structure leaves a wide choice of passage geometries. This allows the optimisation of heat exchange and pumping losses for a specific design.

The first design, using this technique, was made from a solid piece of Monel type K500. After the initial machining of the external fin structure and the internal bore for the regenerator the internal fin structure was added by the drilling of longitudinal holes between the top and bottom half of the hot-end.
From heat transfer calculations, it was found that a large number of holes with a diameter of less than 1.5 mm are required to achieve the required heat transfer coefficient and surface areas (see appendix F). An attempt was then made to connect a number of holes in series by channelling the flow upwards and downward before leaving the heat exchanger. This showed a significant increase in hole diameter and had the further advantage of a reduced temperature difference between the top and bottom end of the heat exchanger. It was found, however, that the hole diameter was still too small to be drilled over the full length. Finally, a design using wires inside the holes, to increase the flow velocity, was proposed and it was found that it was possible to work with around 50 holes of 3.0 mm diameter if a wire of 2.0 mm was inserted. In this design three axial passages are always connected in series. The flow entering the heat exchanger has, therefore, to travel over a total distance of 330 mm before leaving the fin structure. Figure 4.7 right shows a solid Monel hot-end heat exchanger exchangers using this principle. The temperature drop between the matrix and the fluid was then calculated to be less than 100°C at 10 kW of heat transfer (full calculations are shown in appendix F). To further enhance the heat transfer in the

channels, the wires were rolled to an oval cross section of around 2 by 3 mm and then twisted (see figure 4.7 left).

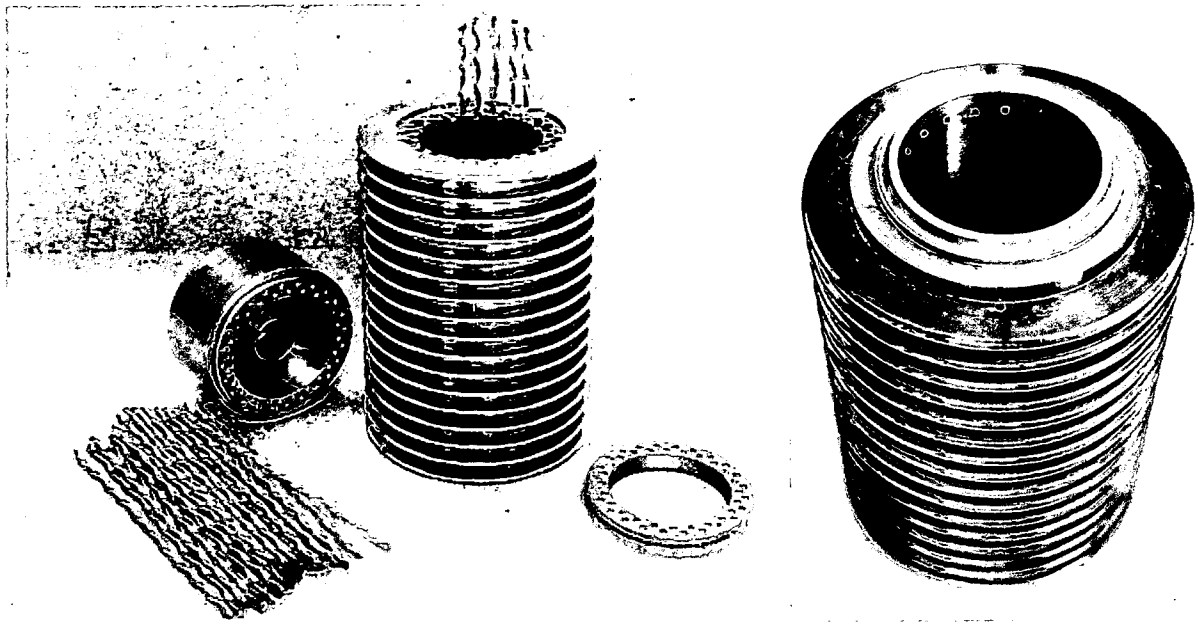


Figure 4.7 Shows the solid Monel hot-end heat exchanger during assembly left and fully assembled right. The end caps are vacuum brazed onto the heat exchanger after the twisted wires are inserted into the holes.

A number of experiments in the TD-Pile test rig, using the full combustion system and the pump motor, were carried out during the study. The experimental results are described together with the results of the regenerator in section 5.2.

A further technique analysed during the study, used heat exchangers made from two different materials. These were constructed from an internal section made of copper and an external section made from either molybdenum or Monel washers.

The inner copper section was made from two coaxial tubes. It was possible to machine a channel structure onto the inner tube before the tubes were assembled. To assemble the inner structure the tubes were, firstly, nickel-plated and then pressed together using a cryogenic fit by cooling the inner tube in liquid nitrogen. Finally, the end of the tubes were vacuum brazed. This design, using two individual parts, allowed, the machining of smaller flow channels and, therefore, did not require the extra wire to reduce the flow area, as in the solid Monel design. Again, three flow

channels, the wires were rolled to an oval cross section of around 2 by 3 mm and then twisted (see figure 4.7 left).

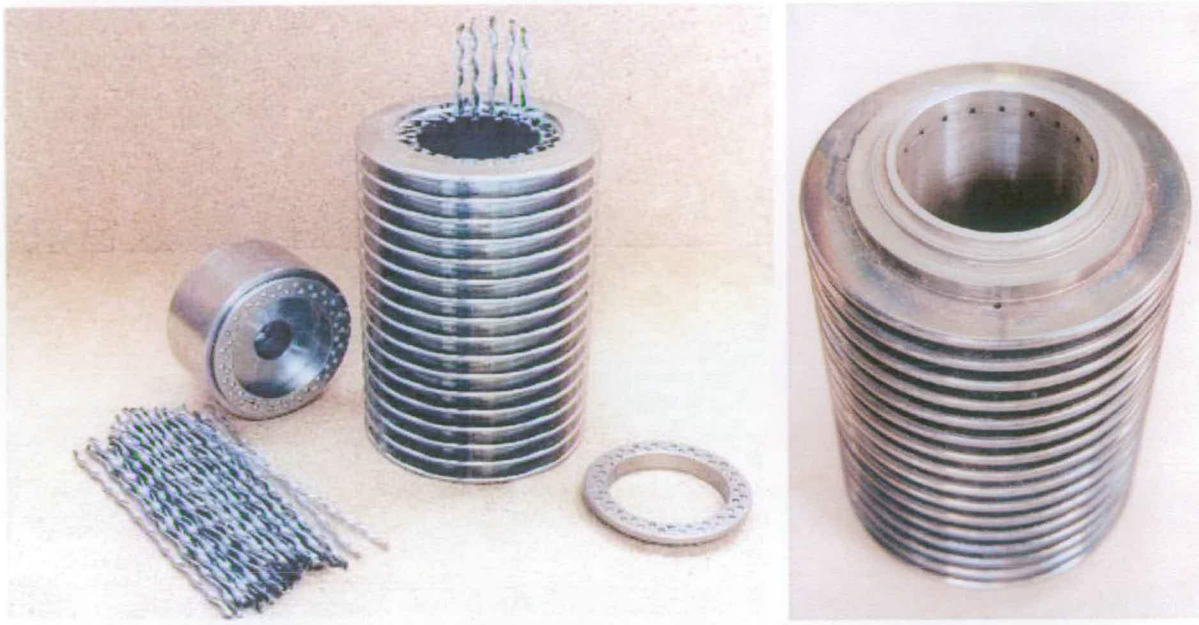


Figure 4.7 Shows the solid Monel hot-end heat exchanger during assembly left and fully assembled right. The end caps are vacuum brazed onto the heat exchanger after the twisted wires are inserted into the holes.

A number of experiments in the TD-Pile test rig, using the full combustion system and the pump motor, were carried out during the study. The experimental results are described together with the results of the regenerator in section 5.2.

A further technique analysed during the study, used heat exchangers made from two different materials. These were constructed from an internal section made of copper and an external section made from either molybdenum or Monel washers.

The inner copper section was made from two coaxial tubes. It was possible to machine a channel structure onto the inner tube before the tubes were assembled. To assemble the inner structure the tubes were, firstly, nickel-plated and then pressed together using a cryogenic fit by cooling the inner tube in liquid nitrogen. Finally, the end of the tubes were vacuum brazed. This design, using two individual parts, allowed, the machining of smaller flow channels and, therefore, did not require the extra wire to reduce the flow area, as in the solid Monel design. Again, three flow

passages were connected in series to increase the flow velocity. Figure 4.8 shows the inner fin structure before and after assembly.

After the inner section was made, the outer fin structure was added to achieve the required radial strength. This was done by sliding washers of alternating size onto the inner section. Two different materials for the outer fin structure were tried. The first one was made by laser cutting washers from Monel K500 sheet material. After the laser cutting, the internal diameter of the washers was machined to give an interference fit to the inner fin structure and the washers were then pressed onto the structure.



Figure 4.8 The picture shows the inner fin structure of the hot-end heat exchanger. It is possible to see the fine flow passages that have been milled into the inner copper part. To the right, a section of a complete inner structure can be seen.

The second heat exchanger was made from stamped molybdenum washers. A special ceramic coating type "Durak B" that had been developed in the 60s in USA by Commanday (1960) was used to protect the molybdenum from corrosion. The "Durak B" type coating creates a thin ceramic layer on the surface of the Molybdenum, protecting it against corrosion. Chomalloy in the US, Los Angeles, carried out this process.

In contrast to the solid Monel heat exchanger, a square shape was chosen for the external fin structure in order to enhance turbulence in the combustion gas stream. Each washer was rotated 90° relative to the next one. Figure 4.9 shows the two different hot-ends.



Figure 4.9. Hot-end heat exchanger prototypes made from copper inner section and washer stack for the external fin structure. Left: heat exchanger made from Monel washers after use in TD-Pile test rig. Right: unused heat exchanger made from molybdenum washers that have been coated with the "Durak B" process.

4.3 Test results

A number of tests were carried out on these hot-end heat exchangers. The hot-end heat exchangers were mounted into the TD-Pile, as shown in figure 4.1. The photograph in figure 4.10 shows the complete assembly of the TD-Pile.

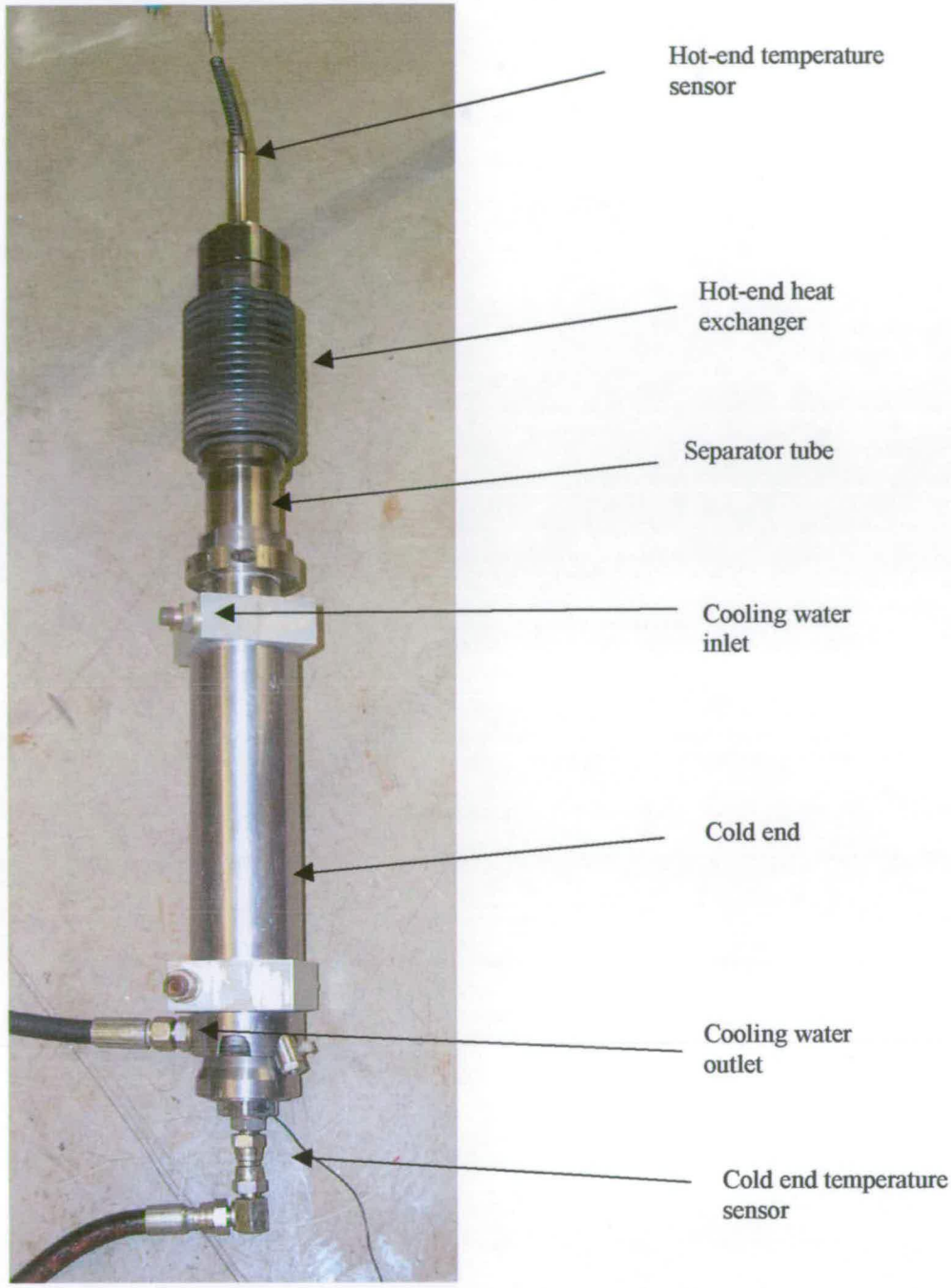


Figure 4.10. Completely assembled TD-Pile with solid Monel hot-end heat exchanger.

The combustion system described in section 3.2, and shown in figure 3.4, was employed as the heat source, allowing an input power into the hot-end of up to 10 kW. A 12 cylinder digital displacement pump/motor, described in chapter six, was used as the power take off system. A data sampling system was employed to sample the different pressures, motions and temperatures during the tests (see apendix E). Figure 6.11 shows the complete engine, as used in the tests.

The main problem encountered during the tests was the failure of the seals between the heat exchanger and the TD-pile structure. Metal C-Rings produced by Sealco Ltd in the UK were used. The rings were made from Inconel with Silver or Copper coating and were used on both ends of the heat exchanger. It was found that, even when the seals were used within their design specification, the seals would only work for one heating cycle and only for a limited number of pressure cycles. The large thermal expansion and pressure fluctuation caused the Silver or Copper coating to rupture, resulting in leaks. This problem was especially apparent on the hot-end heat exchangers made from Monel or Molybdenum washers with Copper as the inner tube. The different thermal expansions and modulus of elasticity, in this design, caused increased damage to the seal. With a number of alterations to the geometry and surface finish of the sealing surfaces, and by adding of extra compliance to the central tension member, it was possible to achieve some improvements to the seal lifetime. It was then possible to conduct a limited number of tests allowing the measurement of the heat flow through the hot-end heat exchanger.

Due to problems arising from low regenerator efficiency, it was not possible to analyse the heat transfer through the hot-end at full regenerator frequency and amplitude. Under these conditions the hot-end temperature would fall to temperatures of around 200°C. This problem will be further addressed in section 6.2.

With a reduced regenerator cycle frequency it was possible to achieve stable conditions in the TD-Pile. For these tests, the system was initially completely filled with water. The burner was then started and operated at a fixed input power of 15 kW. As a result of this, the pressure in the system rose steadily. A pressure relief valve was used to limit the pressure to values between 200 and 400 bar. With the frequency of the regenerator motion, it was then possible to control the heat flow from the hot to the cold end. It was found that the hot-end temperature would stabilize at the required temperature of around 500°C for regenerator frequencies of around 0.5 Hz.

It was then possible to measure the heat flow through the hot-end by analyzing the energy flows in the combustion and cooling system. A heat flow into the hot-end, of

around 10 kW, was calculated from the Propane gas and combustion air flow towards the burner, and the temperature of the exhaust gas. Through the measurement of the cooling water flow and temperature difference it was further possible to confirm these results. The calculated cooling water energy output, was found to be around 9 kW. These measurements clearly show the ability of the hot-end heat exchanger to transfer the required amount of energy into the working fluid. At full cycle frequencies, a reduction in temperature drop from the internal hot-end fin structure into the working fluid can be expected due to the increased heat transfer rate, from the higher fluid velocities in the axial passages.

The previously mentioned sealing problems meant that it was only possible to collect a limited amount of data. As a result of this a comparison of the different hot-end exchangers could not be made.

When it became apparent that the metal C-Rings could not guarantee a reliable seal between the hot-end and TD-Pile, further work was carried out in order to find different ways of overcoming this problem. The most promising approach was the use of friction welding. Initial tests carried out by Thomson Friction Welding Ltd showed that reliable sealing between Monel K500 tubes could be made in this way. Figure 4.11 shows a test piece, which has been friction welded and then sectioned to observe the weld.

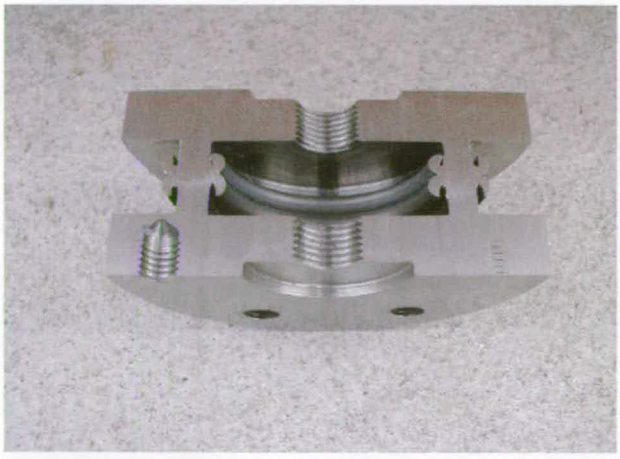


Figure 4.11 Section view of a Monel K500 part that has been friction welded. No recrystallization in the weld could be observed and initial high-pressure tests at room temperature showed no leaks.

Tests carried out with water at room temperature and pressures of up to 600 bars showed that a leakage free seal between the friction-welded parts could be maintained. Further work at elevated temperatures and cycling pressures is still ongoing at the time of submission.

4.4 Conclusion

A study on different materials, coating and joining techniques for the hot-end heat exchanger is presented. It was found that a significant reduction in temperature drop can be achieved by combining materials of high temperature strength, with materials of high thermal conductivity. Unfortunately a number of unsolved problems with regard to corrosion protection and sealing were experienced. It was found that it is not possible to sufficiently protect copper against corrosion through nickel-plating at temperatures over 600°C. It was further found that copper starts to creep at temperature over 550°C with tensile stresses as low as 1.5 N/mm^2. A number of hot-end heat exchangers were then made, avoiding larger sealing areas and with improved corrosion protection.

Tests conducted with these heat exchangers, suggest that it is possible to transfer up to 10 kW into the working fluid of 550°C. In these tests it was possible to keep the flame fin base temperature at around 700°C. This was within the corrosion resistance of the chosen heat exchanger materials.

Substantial problems were encountered at the seal between the hot-end heat exchanger and the TD-Pile. With the metal C-Rings used, it was not possible to maintain a seal over any number of thermal and pressure cycles. An investigation into the use of friction welding showed promising results on early test pieces. Further work to analyse this technique in a complete system is still to be done.

5 Malone engine regenerator

This chapter contains the main essence of the research. A detailed study of the regenerator in the Malone engine is presented.

The results from the analysis of the regenerator, using the TD-Pile are presented. A theoretical investigation of the regenerator system was then undertaken on the basis of the test results.

This theoretical study is concerned with the fundamental relations between the different regenerator design parameters. These are demonstrated using the example of the proposed engine. The results of a theoretical study, which optimises the main variables that define the regenerator system, are given.

The chapter concludes with a discussion of the results gained from the theoretical and practical analyses.

5.1 Introduction

The regenerator is the central element in the Malone engine and has a large influence on the overall efficiency of the engine. Most of the irreversible thermodynamic, and pumping, losses can be expected to come from it. Due to the high viscosity and heat capacity of liquids, it is not possible to use the same regenerator as is used in the Stirling cycle engine. This has to be taken into account when designing an efficient regenerator system. Malone addressed this problem by inventing a regenerator system, which used different flow passages for the fluid entering from the hot-end and that entering from cold-end of the engine. He installed non-return valves in order to direct the fluids into the different flow passages. The principle of Malone's regenerator has already been described in section 1.3.

This study details an investigation of the regenerator for engines using water as the working medium in, and below, the supercritical phase. The initial analysis is based on the parameters of the proposed Artemis Malone engine, as already described in section 1.4.

The regenerator of the proposed engine differs substantially in its design from the regenerator used by Malone. A conventional regenerator arrangement was used which had no valves for directing the flow into separate channels. The matrix was made from coiled stainless steel foil, which was dimpled, to create the required spacing for the flow channels. Figure 5.1 shows the regenerator of the proposed Artemis Malone engine.

In contrast to Malone`s engine, which uses a crank drive to create the regenerator motion, the Artemis Malone engine employs a hydraulic drive. The hydraulic drive consists of a single acting ram in the center of the cold-end dummy. It is connected to an external drive system, which is linked to the power take-off system (see figure 4.1). The internal pressure in the TD-Pile is used to return the regenerator in the heating stroke. The interface with the pump/motor is described in chapter 6.

5.2 Regenerator test rig

At the beginning of the study, a number of tests were carried out to analyse the regenerator system. The test rig as used, for the study on the hot-end heat exchanger and already described in section 4.3, was employed for these tests. The initial thermodynamic design of the regenerator was based on the analysis done by Ehsan (1997).

The regenerator matrix was fabricated from 0.2 mm thick stainless steel foil, which was dimpled to create a constant flow channel width of 0.1 mm. Figure 5.1 shows this first regenerator. The regenerator had an unrolled shim length of around 10 m and an axial length of 240 mm.

The total mass of the stainless steel matrix was 0.9 kg. The main parameters used during the tests are:

- hot-end temperature : 550 °C
- cold-end temperature : 100 °C
- regenerator stroke : 80 mm
- regenerator displacement : 100 cc
- phase angle : 0 – 90 deg
- swept working fluid mass : 40 g @ 90 deg
- cycle frequency : 0.5 - 2.4 Hz
- maximum input power : 10 kW

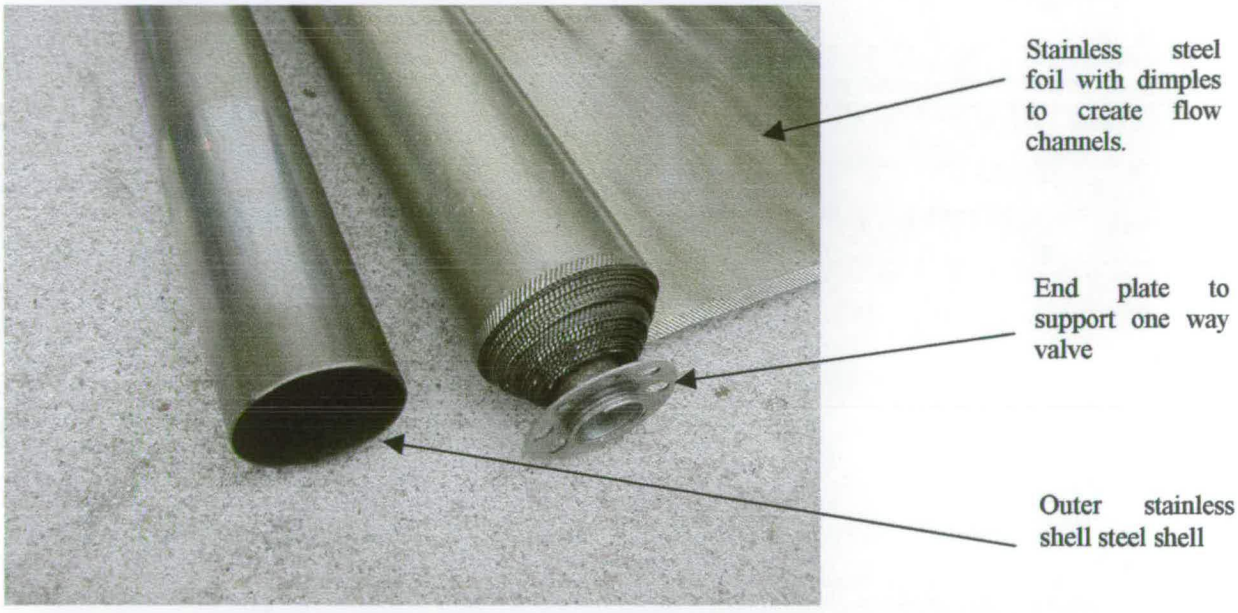


Figure 5.1. Regenerator made from 0.2 mm stainless steel foil. The foil has been dimpled to create constant flow channel width. The entry and exits have been corrugated to avoid blockage.

It became apparent that there was a large discrepancy between the test rig results and the initial theoretical prediction. The regenerator efficiency was found to be much lower than predicted by the theoretical model. It spite of this, the experience gained during these tests contributed greatly to the later analysis of the regenerator system. Given the poor performance of this first test engine, only a brief description of the results is made at this point.

Initially, a large number of unsuccessful attempts at extracting power from the system were carried out. It was not possible to maintain the required temperature difference between the hot and cold-end of the engine during the tests. Further, it was found that the pressure cycle was purely a reflection of the displacement of the working piston motion. A number of different phase angles and displacement ratios between regenerator and working piston were tried, without any significant improvement.

A further series of tests, with zero displacement from the power take-off system, were then carried out in order to separate the operation of the regenerator from the effect of the working piston motion. In a system with an efficient regenerator system, a large pressure fluctuation, in phase with the regenerator motion, was expected. In addition, a small heat flow from the hot-end to the cold-end, as a result of the missing compression and expansion stroke, was predicted.

Tests, with zero displacement from the power take-off system, showed that, at a cycle frequency of 2.4 Hz, constant pressures around 300 bar and full regenerator amplitude of 80 mm, it was not possible to maintain the required hot-end temperature. The temperature in the hot-end space would drop far below the critical temperature of 374°C, to around 200°C. It was found that the hot-end fluid temperature of around 500°C could only be maintained during the first few shaft revolutions. At this point, the temperature difference between the hot and cold-end would be reduced to around 100°C. The cold-end temperature had then risen from 20 °C to 100°C. A small pressure cycle, up to 50 bar, was observed during the first few shaft revolutions. After that, the pressure fluctuation was reduced to only a few bars. For very low cycle frequencies, of less than 0.5 Hz, it was possible to maintain a hot-end temperature above the critical point and to produce some limited pressure fluctuation. The heat flow from the hot to the cold-end of the engine was found through the measured input power from the combustion system and energy released into the cooling water flow. From the measured propane gas flow towards the burner and the measured temperature and volume flow of the exhaust gas the energy input into the hot end was found to be around 10-kW. This was further confirmed through the measurement of

the cooling water flow and temperature difference before and after the cold end heat exchanger.

Under the assumption of constant pressure during the cycle, and perfect regeneration, the heat flow from the hot to the cold-end should be reduced to the thermal conductivity losses through the regenerator and the TD-Pile structure. The calculated heat flow through the matrix material, center pin and TD-Pile shell predicted heat flows of less then 1 kW. The measured heat flow loss of around 10 kW clearly indicated low regenerator efficiency. The lack of pressure fluctuation further confirmed this hypothesis.

As already described in chapter 4.2, the energy absorbed and rejected from the regenerator matrix during each cycle is a multiple larger than the total energy input into the TD-Pile. A low regenerator efficiency can, therefore, result in energy flows from the hot to the cold-end greater than the energy required to operate the engine with an efficient regenerator. This explains how a regenerator, with a lower than predicted efficiency, can produce such large irreversible losses.

The thermal inertia of the hot and cold-end will help to maintain a stable temperature in the hot and cold space for the first few shaft revolutions. This could explain the pressure fluctuation observed during the start up.

The results from this first test set up were then used as the basis of a full theoretical investigation into the operation of regenerator in Malone type engines.

5.3 Regenerator analysis

The alternating process of heating and cooling, in both the regenerator matrix and the fluid, makes the analysis of the regenerator system a difficult task. The resulting complex thermodynamics and fluid dynamics in the regenerator, do not allow to quantify and optimise the performance of the regenerator with simple universal equations. There are a number of theoretical approaches for determining the

efficiency of a Stirling regenerator system. Most of them are made under the assumption of ideal gas behavior, a high ratio of matrix heat capacity to heat capacity of the passing fluid, minimal heat losses through the matrix material, and a small dead volume in comparison to the swept volume. For engines using gaseous working fluids it is possible to assume these conditions and to produce results with reasonable accuracy.

Section 2.3 already describes the fundamental principle and importance of the regenerator in the Stirling cycle engine. The following study looks at the specific aspect of the regenerator in the Malone engine. Previous studies done by Allen (1980) analysed regenerators in low temperature Malone-type heat pumps with organic fluids as the working media. This study focuses on regenerators in engines with a large temperature span between the hot and cold-end and fluids of high heat capacity. The results are presented, as far as possible, in a generic way, allowing them to be applied to any Malone-type liquid engine.

There are a number of reasons why it is not possible to use the applied Stirling engines assumptions when working with water in the liquid and supercritical state as the working fluid. The obvious difference for the regenerator in the Malone cycle engine, as compared to that in the Stirling cycle engine, is the increased viscosity and high heat capacity of the liquid working fluid. Not so obvious, but of equal importance, are the following two differences: Firstly, the fluid properties of liquids change drastically around the critical point as can be seen in figure 2.5. In engines that work with a liquid below the critical temperature in the cold-end, and above it in the hot-end, it is not possible to presume ideal gas behaviour of the working fluid.

Secondly, the fluid in the cold-end of the regenerator and in the compression space of the engine is liquid and, therefore, virtually incompressible. This results in a different flow profile through the regenerator from that in the Stirling engine.

Taking these facts into account, a fundamentally different design for the regenerator in the Malone engine is required. In the following section a detailed examination of

the key design parameters is presented. For each parameter, a short calculation, using the example of the proposed engine, is shown in order to highlight its importance.

The requirements for an efficient regenerator system have already been described in section 2.3. The main requirements can be summarised as:

- The heat capacity of the regenerator matrix should be significantly higher than that of the fluid passing through it, so as to minimise temperature swing in the regenerator matrix. Any temperature swing in the regenerator matrix results in an irreversible loss.

- The pressure drop in the passing fluid should be kept to a minimum to avoid large pumping losses. Pumping losses must be supplied from the net power output and, therefore, multiply losses by the thermodynamic efficiency of the cycle.

- The matrix should have a sufficient surface area with small flow channels to minimise the temperature drop from fluid to the matrix. Any temperature drop between fluid and regenerator matrix results in an irreversible loss.

- The fluid volume inside the regenerator matrix should be small, in relation to the swept fluid, so as to avoid any extra volume of compressible fluid. Large fluid volumes inside the regenerator matrix reduce the amplitude of fluid oscillations in the matrix and result in reduced regenerator efficiency and constitute an irreversible loss.

While it is possible to fulfill these requirements to an acceptable degree for gaseous working fluids, it proves more difficult for liquids. In the following section these fundamental requirements of an efficient regenerator system are discussed with respect to an engine with a liquid as the working fluid.

- Due to the high thermal capacity per unit volume of fluids, it is difficult to achieve a large heat capacity of the matrix in relation to the passing fluid.

- The swept working fluid volume is small in relation to the large amount of energy that has to be exchanged with the matrix. This results in, either a densely packed matrix, or a large regenerator dead volume.

- The large surface areas, required to ensure minimal temperature drop, result in flow channels of small hydraulic diameter. This, together with the high viscosity of the fluid, can cause significant pressure drops and, therefore, large pumping losses.

- With the large matrix mass densely packed into the regenerator, the heat losses through the regenerator in the longitudinal direction can become significant.

Figure 5.2 further illustrates the difference between the regenerator in the Malone and the Stirling engines. It can be seen that, in the Malone engine, a much larger regenerator matrix volume is required for a similar swept working fluid volume.

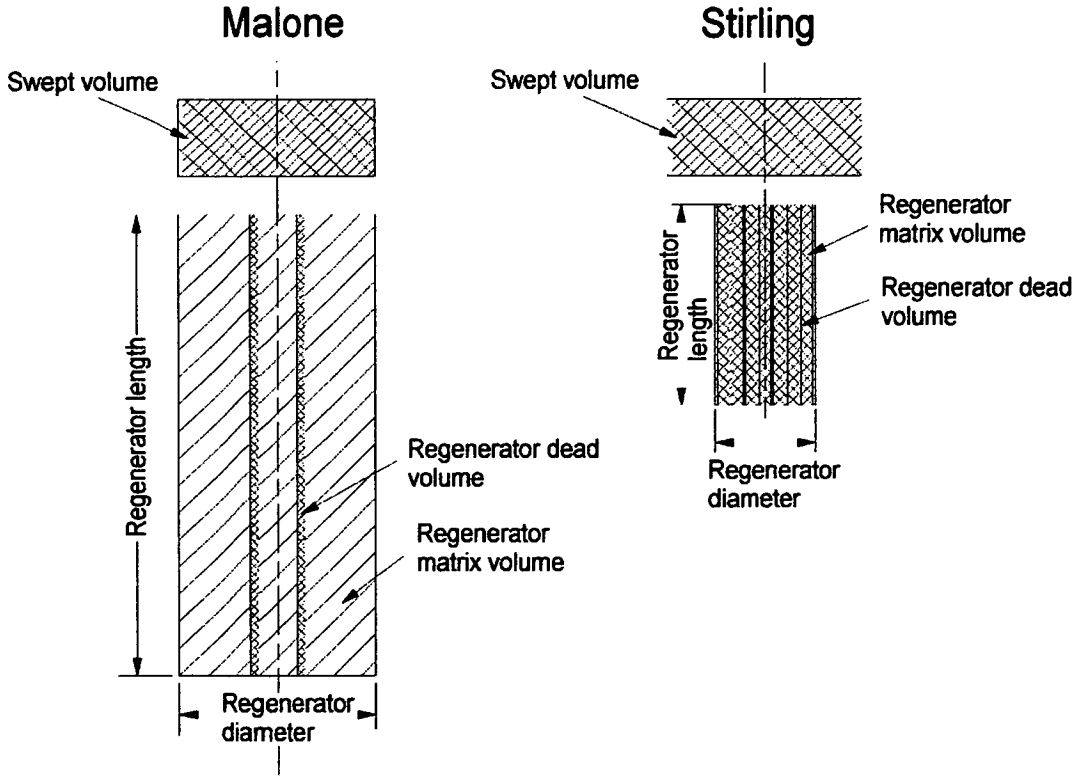


Figure 5.2. Regenerator matrix and regenerator dead volume for a given swept volume in a Stirling and a Malone engine. The areas represent the volumes for a similar heat capacity ratio of swept fluid to matrix volume and flush ratio.

Before it is possible to look at the individual parameters that define the functioning of the regenerator, it is important to analyse the actual flow and temperature profile in the regenerator. For Stirling engines, it is typically presumed that the temperature distribution in the regenerator is linear between T_{hot} and T_{cold} which, for ideal gas behaviour, is close enough to the real temperature profile. Given that the behaviour of fluids around the supercritical phase is far from uniform, it is not possible to make this assumption in the Malone cycle. The heat capacity and, therefore, the energy required to heat or cool the fluid temperature changes significantly along the regenerator.

In the case of the proposed engine, the working fluid has to exchange 2835 kJ/kg with the matrix material in order to cool the swept mass from 550°C to 100°C, at a constant pressure of 350 bar. A significant increase in thermal capacity is found around the critical point. One third of the total energy is required to cool the fluid through one ninth of the total temperature swing between 425°C to 375°C. It becomes clear that this will have a significant effect on the temperature profile in the regenerator. If a constant heat transfer rate between the matrix and the fluid is presumed, then the temperature distribution in the regenerator becomes more a function of the heat capacity of the fluid than a linear distribution between the hot and cold temperature.

Under real conditions, the heat transfer rate between the fluid and matrix alters due to the fact that variation in the fluid properties has an effect on the temperature distribution. The initial analysis of the regenerator was done using the mean fluid properties. This is not an accurate representation of real conditions but allows an initial comparison of the different parameters. Later, the regenerator is split into a series of different sections and each one is analysed individually, giving a more accurate result.

It is important to predict the mass and volume flow inside the regenerator. To a certain extent this is simpler in Malone engines than in Stirling engines. The fluid in the cold-end space (compression space in Stirling engines) is virtually incompressible. The mass of working fluid entering and leaving the regenerator at the cold-end site is,

therefore, not affected by the pressure and temperature change and is only a function of the differential motion from working piston and regenerator. Under the assumption of small fluid volumes inside the regenerator, it is possible to assume a constant mass flow through the regenerator with the volume flow becoming only a function of density at each point.

With the hydraulic power take-off system as the working piston, it is possible to create any kind of differential motion between the regenerator and the working piston, allowing complete control over the flow inside the regenerator. For the initial study on the regenerator, it is assumed that the motion profile from the hydraulic power take-off system creates a constant mass flow rate during the stroke of the regenerator.

The following section looks at the individual requirements and analyzes the coupled effects between the different parameters. The study is largely based on the existing theory of countraflow regenerators. Due to the importance of this theory, with regards to regenerator design, a short introduction is given at the beginning of the section.

5.3.1 Basic theory in contraflow regenerators

We begin by analysing the change in matrix and fluid temperature for the case of a single blow of fluid through a bed of higher or lower uniform temperature. Willmott (2001) presents the main differential equations that describe the change in fluid and matrix temperature as:

$$\frac{\partial t_f}{\partial y} = \frac{h^* A_r}{\dot{m}_f * c_p * L_b}(T_s - T_f) - \frac{m_f}{\dot{m}_f * L_b} * \frac{\partial t_f}{\partial_\tau} \qquad 5.1$$

$$\frac{\partial t_s}{\partial_\tau} = \frac{h^* A_r}{M * C_s}(T_s - T_f) \qquad 5.2$$

A_r = regenerator matrix surface area [m^2]

T_s = Temperature solid (regenerator matrix) [K]

T_f = Temperature fluid [K]

m_f = mass of working fluid in regenerator [kg]

$\dot{m}_f$ = mass flow working fluid [kg/s]

C_s = specific heat of regenerator matrix [J/kg*K]

L_b = time of hot or cold blow [s]

Equation 5.1 describes the change of the fluid temperature during a single blow as a function of the distance from the entrance.
Equation 5.2 describes the change in matrix temperature as a function of time.

If the only requirement is to find the relative change in fluid or matrix temperature with regard to the total initial temperature difference from fluid to matrix, then it is possible to simplify the equations by introducing the dimensionless temperature.
The parameter ξ can be used as the dimensionless distance from the entrance and the parameter η as the dimensionless time from the beginning of the stroke (Willmott 2001).

$$\xi = \frac{h * A}{\dot{m}_f * c_p * L} y \qquad 5.3$$

$$\eta = \frac{h * A}{M * C_s} * \left(\tau - \frac{m_f y}{\dot{m}_f L_b} \right) \qquad 5.4$$

y = distance from entrance of regenerator matrix [m]

From the two parameters ξ and η it is possible to develop universal design parameters that define the efficiency of any regenerator system. By introducing dimensionless parameters for the length and time, it is possible to further reduce the equations to the reduced length Λ and the reduced time Π (Willmott 2001). These parameters are sometimes named as dimensionless distance and dimensionless period (Hargreaves 1991)!

$$\Lambda = \frac{h^* A}{\dot{m}_f * c_p} = \frac{heat\ transfer\ coefficient * total\ surface\ area}{heat\ capacity\ of\ gas\ flowing\ per\ second} \qquad 5.5$$

$$\Pi = \frac{h^* A}{M^* C_s}\left(P - \frac{m_f}{\dot{m}_f}\right) = \frac{heat\ transfer\ coefficient * total\ surface\ area}{heat\ capacity\ of\ matrix\ material} * \left(period - \frac{fluid\ mass}{fluid\ mass\ flow}\right) \qquad 5.6$$

P = duration of period [s]

Hausen (1983) used these equations to predict the efficiency of a contraflow regenerator system. He quantifies the regenerator efficiency by predicting the temperature deficit between the working fluid after a return stroke. Hausen proved that, under the assumption of ideal gas behaviour and steady state conditions, the temperature deficit on both ends of the regenerator becomes equal and can be used to define the regenerator efficiency.

Hausen (1983) was further able to prove that the function defining the temperature deficit is the result of the two following conditions; (i) The heat exchange coefficient between the matrix and the fluid in relation to energy exchanged per stroke. (ii) The total heat capacity of the matrix material.

The regenerator efficiency then becomes a function of the two dimensionless numbers for the reduced length Λ and the reduced period Π.

$$\frac{Teo - Tre}{Teo - Tco} = \frac{Trc - Tco}{Teo - Tco} = f(\Lambda, \Pi) \qquad 5.7$$

Hausen (1983) presented the results as a family of various curves, allowing the efficiency of the regenerator to be determined. Figure 5.3 shows the regenerator efficiency as a function of the reduced length and reduced period.

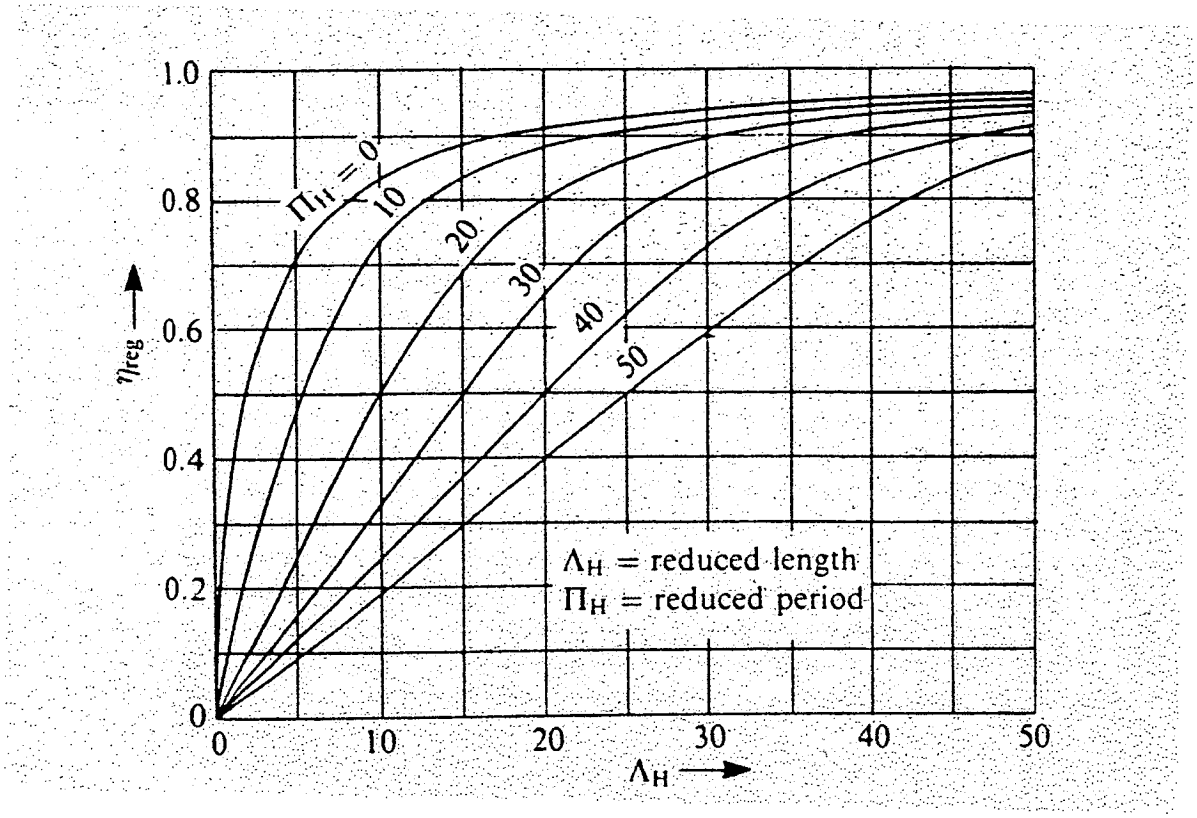


Figure 5.3 shows the reduced regenerator efficiency as a function of the reduced length and reduced period. (source: Hausen 1983)

It can be seen that it is advantageous to (i) design a system with a large value for the reduced length, hence maximum temperature change of the working fluid and, (ii) to achieve a low value for the reduced period, hence small temperature change in the matrix.

With the quotient of the two dimensionless numbers Λ and Π it is possible to calculate the utilization factor U, which describes the heat capacity ratio between the matrix material and the fluid. In practice the utilization factor is often used as a measure for the temperature swing in the matrix (Orgen 1997).

$$U = \frac{\Lambda}{\Pi} = \frac{\textit{heat capacity of gas passing per stroke}}{\textit{total heat capacity in matrix material}} \qquad 5.8$$

It is important to achieve small values for the utilization factor hence a large heat capacity of the matrix relative to the passing fluid.

Given the large difference in heat capacity per volume (ρcp) between gaseous working fluids and the matrix material in Stirling engines, a low value for the utilization factor U is readily achievable. This allows the losses created through the temperature swing of the matrix material to be minimized. Hausen (1983) shows, that for low values of U (U < 0.1), the influence from the temperature swing becomes unimportant. It is possible to describe the regenerator temperature deficit and, therefore, the regenerator efficiency through equation 5.9. This equation shows that the regenerator efficiency in Stirling engines is mainly a function of the heat transfer between the working fluid and the matrix material.

$$Teo - Tre = \frac{2}{\Lambda + 2}(Teo - Tco) \qquad 5.9$$

Due to the high heat capacity of water, it is unlikely that low enough values for the utilization factor would be achieved and, it is therefore, not possible to work directly with equation 5.9

Schalkwijk introduced a simple approximation in 1959 that adds the correction number Ω into Hausen`s original equation 5.10. (Hargreaves 1991). At a low value for the utilization factor, the equation for the regenerator temperature deficit then becomes:

$$Teo - Tre = \frac{2}{\Lambda + 2 - \Omega} * Teo - Tco \qquad 5.10$$

Through a number of experiences, Schalkwijk was able to establish a simple approximation formula for Ω:

$$\Omega = \Pi + 2 - 2.35\sqrt{\Pi} = \frac{\Lambda}{\Gamma} + 2 - 2.35\left(\frac{\Lambda}{\Gamma}\right)^{1/2} \qquad 5.11$$

The temperature deficit after a full cycle of the regenerator using the reduced period can be described as (Hargreaves 1991):

$$Teo - Tre = \frac{2}{\Lambda + 2 - \left[\Pi + 2 - 2.35\sqrt{\Pi}\right]} * Teo - Tco \qquad 5.12$$

With equation 5.12, it is now possible to predict and subsequently optimise the efficiency of the regenerator in the proposed engine. Before this process is done, an initial study on the effect of the individual geometric and material parameters is made using the example of the proposed engine. This is important for the understanding of the basic relations and limitations of the regenerator system in liquid engines.

5.3.2 Utilization factor

The high heat capacity of supercritical and liquid water, as compared to gas, makes it difficult to achieve low values for the utilization factor U, the result of which is a significant temperature swing of the regenerator matrix. This, in turn, will result in increased irreversible regenerator losses. The heat capacity per unit volume of water at supercritical pressure and temperature is 2275 $^{kJ}/_{m^3K}$. This is around 2/3 of that of Stainless Steel at 3500 $^{kJ}/_{m^3K}$. Compared to this, the gaseous working fluids used in Stirling engines have, depending on type, temperature and pressure, heat capacities per unit volume of 100 to 1000 times smaller than that of Stainless Steel.

In the proposed engine the working fluid changes from around 100°C in the cold end to around 550 in the hot end of the engine. The enthalpy in water changes from 437 kJ/kg*K at 100°C to 3337 kJ/kg*K at 550°C, under the assumption of constant

pressure of 300 bar (Haywood 1990). This results in a mean working fluid heat capacity of 6.5 kJ/kg*K.

The heat capacity of stainless steel is only about 1/13 of this at 0.5 kJ/kg*K. To achieve a utilization factor of 0.1 would require a regenerator matrix mass 130 times larger than that of the swept fluid. In the example of the proposed engine, with a swept mass of 40g, the regenerator mass becomes 5.2 kg if a value of 0.1 is required for the utilization factor.

Even though a decreased regenerator efficiency, due to a higher value for the utilization factor, is inevitable, a liquid engine must have a much higher ratio of regenerator matrix volume to swept fluid volume than that of a Stirling engine to work at all. This makes it difficult to achieve small fluid dead volumes in the regenerator. The effect of this is discussed in section 5.3.4

5.3.3 Fluid to matrix heat transfer

With the large matrix mass it is, in principle, possible to create a large enough surface area and a high value for the heat transfer coefficient **h** in order to ensure high values for the reduced length **Λ**. The problem then occurs of needing to get the small swept fluid volume into contact with the large amount of matrix material.

Using the same type of regenerator as in Stirling engines, with a minimum of dead space and a high number of fine flow passages, we would expect a massive increase in pumping losses in a Malone engine. This is a particular problem in the cold region of the regenerator where water is a liquid and has a high viscosity. If a regenerator with a small number of larger flow passages is used, this will minimise the flow losses but will make the provision of the required surface area difficult. In addition to this, the problem of a possible temperature drop through the matrix is introduced due to the increase in matrix shim thickness.

It is possible to demonstrate this using the example of the proposed engine. As we have seen earlier, the heat capacity per unit volume of supercritical water is around 2/3 of that of stainless steel. A utilization factor of 0.1 results in a matrix volume eight times larger than the swept volume. To achieve the same small regenerator dead volumes, as typically found in Stirling engines, the packing ratio of the regenerator has to be over 90%. If the proposed test engine is to have a regenerator dead volume of half the swept volume or less, at a value for the utilization factor of 0.1, this would result in a packing ratio of 95 % or more.

Applying such packing ratios to a regenerator made from 0.1 mm thick metal shim, results in a fluid passage of 0.005 mm. With the relatively high viscosity of supercritical water, such small flow channels would certainly result in unacceptable pumping losses. Choosing a shim thickness of a few millimeters would allow an increase of the flow passage but would result in larger temperature drops inside the shim, and also in a smaller surface area. If, for example, we chose a shim thickness of 3 mm, the flow passage would 0.15 mm. At this shim thickness, it is important to observe the temperature drop through the shim thickness, which will reduce the regenerator efficiency. Using a metal which has high thermal conductivity, in relation to its heat capacity, reduces the effect of the temperature drop in the shim. Figure 5.4 shows the heat capacity per unit volume and the thermal conductivity properties of a number of possible metals for the regenerator matrix.

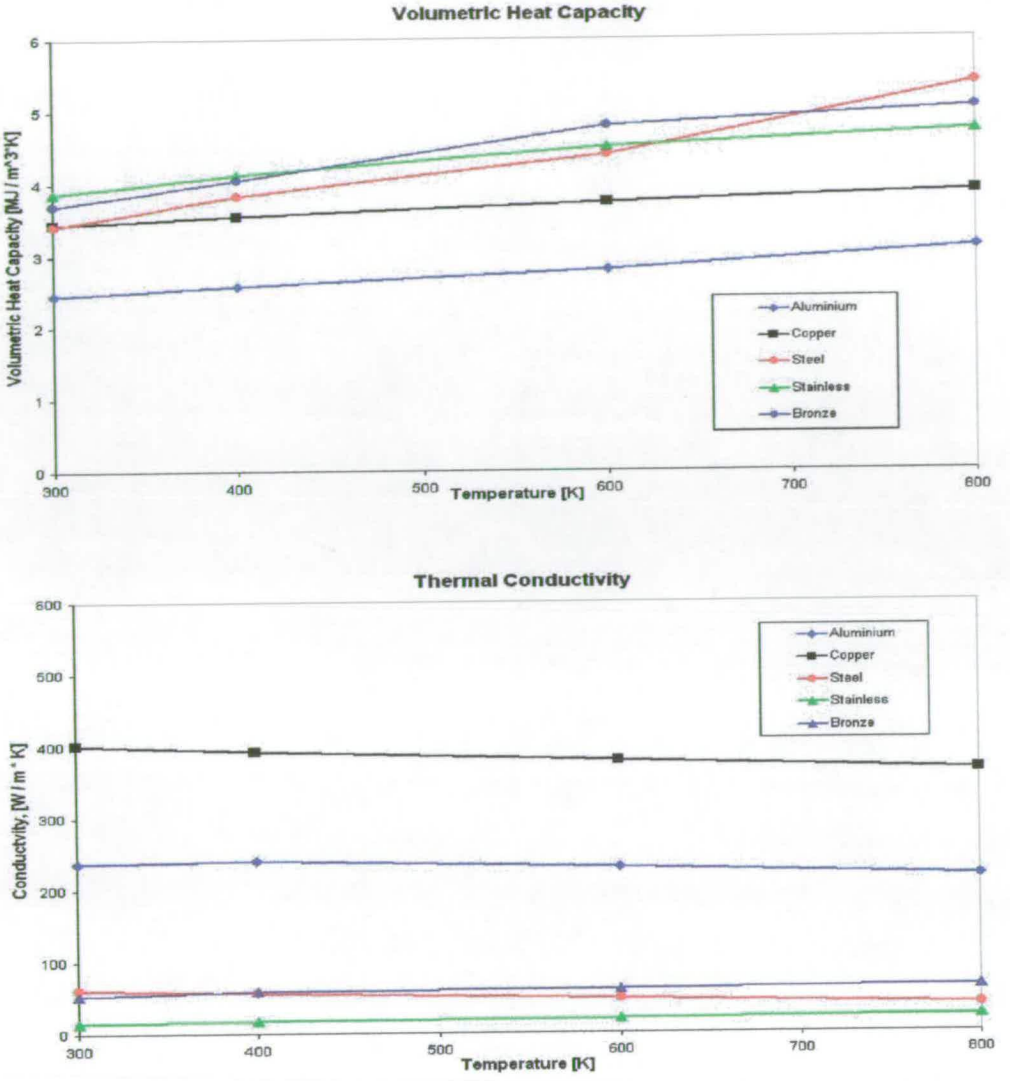


Figure 5.4. Volumetric heat capacity and heat conductivity data for possible regenerator metals at elevated temperatures illustrated (source: Howard and Timothy 1984; Incropera, 1990; Copper Development Association 1994).

From figure 5.4 it can be seen that the heat capacity per unit volume is similar for most metals, with aluminum being the lowest among them. Thermal conductivity in comparison varies significantly between the different metals. Copper has the best ratio of heat capacity to thermal conductivity.

The effect of the temperature drop in the matrix material on the regenerator efficiency can be quantified through the Biot number.

$$Bi = \frac{h * w}{k} \qquad 5.13$$

Bi	=	Biot number
h	=	convection heat transfer [W/m^{2}K] (Hausen uses α instead of h!)
w	=	semithickness of matrix material [m]
k	=	thermal conductivity of matrix material [W/m*K]

Schmidt and Willmott (1981) show that for a Biot number smaller than 0.1 the error through internal heat resistance is small enough to be, in most cases, ignored.

For Biot numbers larger than this, it is possible to correct for the temperature drop in the matrix by using modified values for h, Λ and Π. Hausen (1983), and based on this Smith and Willmott (1981) have established the relationship between these numbers and the Biot number.

The Biot number used in the following equations has to be calculated using equation 5.14 for the case of flow between two parallel surfaces (Schmidt 1981).

$$Bi_{\Delta} = \frac{h * w}{3k} \qquad 5.14$$

The modified heat transfer coefficient for flow between two surfaces can then be described through equation 5.15 (Schmidt 1981).

$$\frac{1}{\overline{h}} = \frac{1}{h} + \frac{w}{3k} \qquad 5.15$$

The modified reduced length can then be described through equation 5.16 (Schmidt 1981).

$$\overline{\Lambda} = \frac{\Lambda}{\Lambda + Bi_{\Delta}} \qquad 5.16$$

The reduced period can, thus, be described by equation 5.17 (Schmidt 1981).

$$\overline{\Pi} = \frac{\Pi}{1 + Bi_{\Delta}} \qquad 5.17$$

In addition, it is important to realise that the available surface area becomes smaller as the thickness of the shim increases. To achieve the same heat exchange between the matrix and the fluid at a smaller surface area, a larger heat transfer coefficient is required. The Biot number, is a function of the shim thickness, and of the heat transfer coefficient, with the result that the Biot number changes with the square of the shim thickness.

This effect can be shown in the example of the proposed engine. The surface area, in the test engine with a matrix mass of 5.5 kg and shim thickness of 0.1 mm has been calculated to be 13.2 m^2. For the same matrix mass, using a 3.0 mm shim, the surface area is reduced to 0.44 m^2.

At the proposed cycle frequency of 4 Hz, the time for each stroke becomes 0.125 s. Under the assumption of a constant pressure of 300 bar, the enthalpy change in the working fluid from hot to cold is 2835 kJ/kg (see figure 2.5). With a working fluid mass of 40g, this results in 113 kJ heat exchange during each stroke which results in a mean heat flow between the fluid and regenerator matrix of around 900 kW.

The regenerator using the 0.1 mm shim gives a heat flow rate of around 70 kW/m^2. In the regenerator using the 3.0 mm shim, the heat transfer rate is increased to around 2100 kW/m^2.

For a design temperature difference between the fluid and the matrix, it is possible to calculate the required value for the heat transfer coefficient **h** using equation 5.18.

$$h = \frac{\dot{Q}}{A * \Delta T} \qquad 5.18$$

Selecting, for example, a maximum temperature difference between fluid and matrix of 1% of the total difference, gives a maximum temperature drop from the fluid to the matrix of 4.5°C. Using equation 5.6, the value the heat transfer coefficient at this temperature difference becomes 14822 W/m^2K for the 0.05 mm shim. The heat transfer coefficient for the 3.0 mm thick shim becomes 454000 W/m^2K.

It is now possible to calculate the Biot number for these two cases using equation 5.5. The Biot number for the 0.1 mm shim becomes 0.05. The Biot number for the 3.0 mm shim becomes 45.

As far as the function of the regenerator is concerned, the temperature drop inside the 3.0 mm shim is significantly larger than the temperature drop from shim to fluid. The result being that the heat capacity of the center part of the matrix material is not fully used, giving rise to reduced regenerator efficiency. In the case of the 0.1 mm shim, the low Biot number of 0.05 results in a significantly smaller temperature drop in the matrix, with most of this being between the fluid and the matrix. In this case it is possible to assume a constant temperature distribution inside the matrix material.

It is possible to make some improvement by using a material for the regenerator matrix which has larger heat conductivity than stainless steel. Copper has around 80% less heat capacity, but around 20 times the heat conductivity of stainless steel. By adjusting the shim thickness to give the same heat capacity per area, it is possible to analyse the change of the Biot number in the example used earlier. The Biot number for the regenerator with the 0.1 mm shim is reduced to 0.0025. The Biot number for the regenerator with the 3 mm shim is reduced to 2.1.

These values demonstrate the importance of the matrix shim thickness and the matrix material. If this factor is applied to an alternative regenerator geometry, made from wire mesh for example, similar results would be expected.

5.3.4 Flush ratio

The flush ratio is defined as the ratio of the working fluid mass, passed through the regenerator, to the working fluid mass inside the regenerator. If constant pressure is assumed, it is possible to calculate the flush ratio from the volume passed through the regenerator, to the volume inside the regenerator.

Typically, the Stirling engine regenerator works with a minimum of regenerator dead volume in order to avoid a reduction in cycle pressure change and regenerator efficiency. The first aspect is not of the same importance in the Malone engine. Here a large fraction of the fluid in the regenerator is below the critical point and, therefore, virtually incompressible. Further the fluid in the cold-end can be treated as incompressible, resulting in a stiff system. Later in the study it will be shown that, even with a large regenerator dead volume, it is possible to achieve the required change in cycle pressure. As a result of this, only the reduction in regenerator efficiency will be considered at this point.

The problem of reduced regenerator efficiency, due to a small flush ratio, is of equal importance in Stirling and Malone engines. In engines with a small flush ratio, the fluid entering the regenerator from the hot-end, and that entering the regenerator from the cold-end, will only penetrate into the regenerator by some fraction of its length.

As described earlier, the matrix volume in Malone engines has to be significantly larger than the swept working fluid volume to achieve an acceptable value for the utilization factor. For a small flush ratio, this results in a very high packing ratios and, therefore, small flow passages. It is possible to solve this problem with a regenerator of large flush ratio but this has the disadvantages of decreased regenerator efficiency. It is difficult to visualize the effect on the regenerator efficiency from equation 5.5 and 5.6. The following description aims to clarify this effect.

With the following calculation, it is possible to show that a small flush ratio causes a decrease in the maximum temperature swing of each individual part of the working fluid. As a result of this, the temperature swing of the regenerator matrix and the

temperature difference between regenerator matrix and fluid, become more significant, and causes large irreversible losses.

If constant heat capacity of the fluid is assumed, the energy exchanged between the fluid and matrix becomes a function of the temperature change and fluid mass.

$$Q = c_p * m * \Delta T \qquad 5.19$$

In a regenerator system with a small flush ratio, the oscillating mass of fluid increases, due to the added fluid mass inside the regenerator. The amplitude and, therefore the temperature swing of the fluid are reduced. The simple block diagram in figure 5.5 demonstrates this effect.

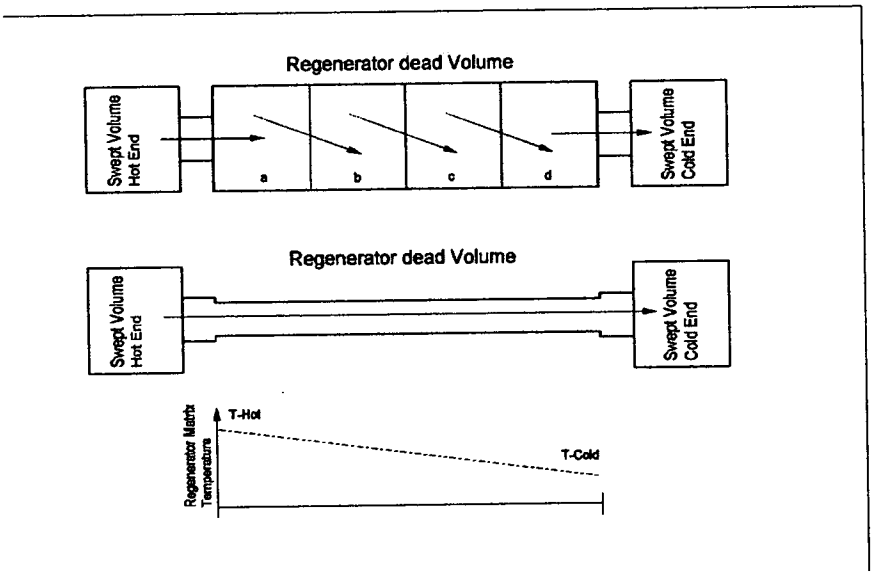


Figure 5.5. In engines with large regenerator dead volumes, compared to swept volumes, each particle of fluid passes only through a part of the regenerator (top). The exchange can be divided into boxes, whereby, the shifts between the hot space and box (a), and the fluid from a shifts between box (a) and (b), and so on. In engines with small swept volumes (bottom), the majority of the fluid shifts between the hot and cold space of the engine.

If a regenerator with perfect heat transfer, and infinitely high heat capacity of the regenerator matrix is assumed, there are no thermodynamic disadvantages for either case. If a large mass of fluid moves through a small temperature difference, or a small mass of fluid is moves a large temperature difference, the net heat exchange and,

therefore, change in volume remains constant. This is valid for real working fluids, with different properties over the temperature span, because the temperature change occurs at all temperature levels.

This effect can be demonstrated further by examining the extreme cases. If the dead volume is infinitely large, then the mass m in equation 2.1 becomes infinitely large. With Q and c_p unchanged, the temperature change ΔT has to become infinitely small. This change is caused by the fact that the fluid travels an infinitely small distance through the regenerator.

On the other hand, when working with an infinitely small swept volume, the entire swept fluid shifts from the hot to the cold space. The mass m in Equation 2.1 then becomes the mass of the swept volume, and ΔT the temperature difference between the hot and cold-end. This, then results in the same net energy exchange.

In real conditions, it is not possible to presume perfect heat transfer between fluid and matrix. Depending on the heat transfer coefficient, a temperature difference between the fluid and the matrix is required so that the heat transfer occurs. If the fluid undergoes a reduced temperature swing, due to the larger regenerator dead volume, the temperature drop between matrix and fluid becomes more significant. This will result in a reduction of the ratio of temperature change, dT, to the distance the fluid has traveled through the regenerator matrix, dx, hence a reduction in the characteristic length presented in equation 5.1. Figure 5.6 demonstrates this using the example of a regenerator with a large and a small value for the heat transfer coefficient. The irreversible loss is shown as the length of the horizontal path in the temperature swing of the fluid.

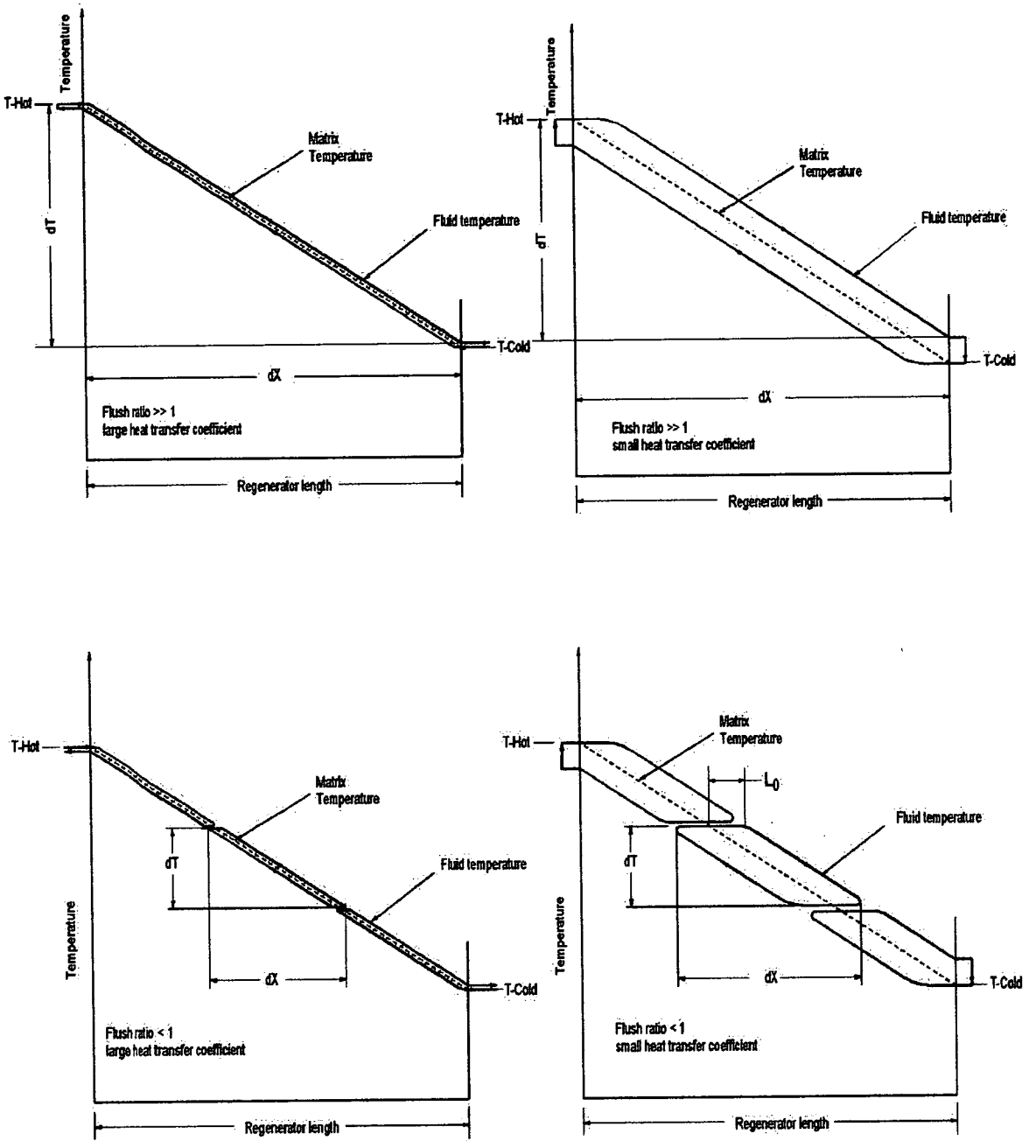


Figure 5.6. The effect of the regenerator dead volume for regenerators with large heat transfer coefficient to the left and with a poor heat transfer coefficient to the right is shown. While for the regenerator with a large heat transfer coefficient the ratio of temperature change in the fluid **dT** to length traveled **dX** remains unchanged in the case of poor heat transfer coefficient a reduction in the ratio **dT** to **dX** can be seen.

Under real conditions, the maximum available temperature difference from the fluid to the matrix becomes the fraction by which the fluid shifts through the regenerator, multiplied by the total temperature difference.

$$\Delta T_{fluid-matrix} = \Delta T_{hot-cold} * \frac{v_{swept}}{v_{dead}} \qquad 5.20$$

V_{swept} = working fluid volume swept through regenerator

V_{dead} = working fluid volume inside regenerator

Even a relatively small change in the regenerator matrix temperature during the cycle, or a small temperature drop from regenerator matrix to working fluid, will result in a significant reduction of exchanged energy. This occurs if the dead volume is large and, therefore, the maximum temperature differences small.

This effect will now be demonstrated on the regenerator of the proposed engine. For a regenerator with a flush ratio of 0.2, the fluid only shifts through one fifth of the total length of the regenerator. The maximum temperature swing of the fluid is reduced from 450°C to 90°C. A temperature drop between fluid and matrix of 4.5°C, for both the heating and the cooling, as used in the example earlier, would result in a decreased temperature swing of 10%.

Practically, such a regenerator is still densely packed. If we use a value of 0.1 for the utilization factor and stainless steel as the matrix material, the matrix volume becomes 660 cc. For a flush ratio of 0.2 the regenerator dead volume becomes 450 cc, resulting in a packing ratio of 75%. It is still difficult to achieve such high packing ratios with round wire mesh.

5.3.5 Length over diameter ratio

The correct choice is of importance because it has a significant effect on the open flow area and, therefore, flow velocity in the regenerator. It is important to understand the effect of this variable in order to optimise the regenerator effectively.

For a particular regenerator design, with a given packing ratio, matrix volume and displacement - doubling of the length over diameter ratio results in:

- the fluid velocity in the flow channels being doubled
- the Reynolds number being doubled
- the matrix surface area being unaffected
- the regenerator stroke being reduced by half
- the static heat loss through the regenerator matrix being increased by a factor of four.

This shows that the length to diameter ratio has a significant effect on the fluid and thermodynamics in the regenerator. It makes it an important parameter for later optimisation, giving control over the relation between pumping losses and decreased regenerator efficiency. A short and wide regenerator has short channels and a large open flow area, resulting in low flow velocities and low pressure drops can be expected. On the other hand, the heat losses in axial direction are high and the heat transfer between fluid and matrix can be poor due to the low Reynolds numbers.

5.3.6 Pumping losses

The energy to drive the regenerator comes from the output shaft and, therefore, directly reduces the output power. It is important that the size of the flow passages and the length over diameter ratio is chosen such that the balance between pumping losses and heat transfer rate between fluid and matrix is optimised. The properties of the working fluid change very significantly around the critical point. Consequently, reaching the optimum for the regenerator of the liquid engine proves difficult unless the regenerator geometry is altered along its length.

To calculate the pressure drop for the example of the proposed engine, it is initially important to establish whether the regenerator works in the turbulent or in the laminar region.

With a cycle frequency of 2.4 Hz, and a swept mass of 40 g, the mass flow rate of working fluid through the regenerator becomes 0.192 kg/s. Under the assumption of constant mass flow rate, it is possible to describe the fluid velocity inside the regenerator as a function of density and opening area. With the kinematic viscosity, it is then possible to calculate the Reynolds number.

$$\mathrm{Re} = \frac{\omega * d}{\upsilon} = \frac{\frac{\dot{m}_f}{\rho * A_f} * 2 * tf}{\upsilon} \qquad 5.20$$

Re	=	Reynolds number
w	=	fluid velocity ($w = \dot{m}_f / * \rho A_f$) [m/s]
d	=	hydraulic diameter [m]
ρ	=	mass density [kg/m^3]
A_f	=	open flow area in regenerator [m^2]
tf	=	gap between regenerator shim [m]

For a given flow area in the regenerator, the Reynolds number becomes a function of the density and the kinematic viscosity.

In the proposed engine with 100°C in the cold-end of the regenerator, the density is 972 kg/m^3 and the kinematic viscosity is $0.25*10^{-6}$ m^2/s. In the hot-end of the regenerator, at 550°C, the density is reduced to 98 kg/m^3 and the kinematic viscosity has changed to $0.3*10^{-6}$ m^2/s. This results in a reduction of the Reynolds number of nearly 10 from the hot to the cold-end of the engine.

For the proposed engine it is possible to calculate the Reynolds number for a given flow area. Taking into account the need to keep the thermodynamic losses within limits, the following factors are used for an initial calculation of the flow area:

- Utilization factor : 0.1
- Flush ratio : 1

- Shim thickness : 0.5 mm
- Length to diameter ratio : 3

With the required matrix mass of 5.2 kg, the matrix volume becomes 660 cc. With a flush ratio of 1, the regenerator dead volume is 100 cc resulting in a packing ratio of 87%.

With a shim thickness of 0.5 mm, the flow gap between the shims becomes 0.065 mm. For a length to diameter ratio of 3, the total regenerator volume is 760 cc.

The regenerator diameter becomes 0.066 m resulting in a frontal area of 0.0034 m^2. With the packing ratio of 87% this results in a open flow area of 0.00044 m^2.

The unrolled length of the regenerator foil can be calculated from the matrix volume, the shim thickness and the regenerator length. The calculated shim length for the example is 6.6 m.

Using equation 5.21, it is now possible to calculate the Reynolds number in the regenerator. Reynolds number for the cold-end of the regenerator at 350 bar, with a density of 974 kg/m^3, and a kinematic viscosity of $0.25*10^{-6}$ m/s^2.

$$\mathrm{Re} = \frac{\frac{0.192\ kg/s}{974\ kg/m^3 * 0.00044\ m^2} * 2 * 0.000065\ m}{0.25*10^{-6}\ m^2/s} = 233$$

Reynolds number for the hot-end of the regenerator at 350 bar with a density of 98 kg/m^3, and a kinematic viscosity of $0.30*10^{-6}$ m/s^2.

$$\mathrm{Re} = \frac{\frac{0.192\ kg/s}{98\ kg/m^3 * 0.00044\ m^2} * 2 * 0.000065\ m}{0.30*10^{-6}\ m^2/s} = 1932$$

As it is below the transitional point of 2000, it can be assumed that the flow in the regenerator is completely laminar and it is possible to calculate the pressure drop as a function of the fluid shear.

For laminar flow, the pressure drop of flow between two parallel plates is described through equation 5.22. The volume flow rate can be described as the mass flow rate over the density, and the kinematic viscosity as the dynamic viscosity times the density. The density falls out of the equation and the pressure drop only changes with the kinematic viscosity. Graph 2.5 shows that the kinematic viscosity of water at 300 bar has a fairly constant value of $0.12*10^{-6}$ m^2/s for most of the working area, with an increase at the hot and the cold-end.

$$\Delta P = \frac{12*Q_f*L_r*\mu}{tf^3*L_s} = \frac{12*\frac{m_f}{o}*L_r*\upsilon*o}{tf^3*L_s} = \frac{12*m_f*L_r*\nu}{tf^3*L_s} \qquad 5.22$$

ΔP = pressure drop in regenerator [Pa]

L_r = length of regenerator [m]

ρ = fluid density [kg/m^3]

μ = dynamic viscosity [Pa*s]

ν = kinematic viscosity [m^2/s]

L_s = length of regenerator shim [m]

It is then possible to calculate the pressure drop per length of regenerator matrix, for a given temperature in the regenerator fluid.

This has been done using the example of the proposed engine for the cold-end temperature, the regenerator mid temperature, and the hot-end temperature. It is worth noting that the regenerator mid temperature is not necessarily at the mid point of the regenerator!

Pressure drop in Pa per mm length at 100°C working fluid temperature.

$$\Delta P = \frac{12*0.45kg/s*0.001m*0.25*10^{-6}\,m^2/s}{0.000065m^3*6.6\,m} = 744 \text{ Pa}$$

Pressure drop in Pa per mm length at 320°C working fluid temperature

$$\Delta P = \frac{12 * 0.45 kg/s * 0.001 m * 0.12 * 10^{-6}\ m^2/s}{0.000065 m^3 * 6.6 m} = 357\,\text{Pa}$$

Pressure drop in Pa per mm length at 550°C working fluid temperature

$$\Delta P = \frac{12 * 0.45 kg/s * 0.001 m * 0.3 * 10^{-6}\ m^2/s}{0.000065\ m^3 * 6.6\ m} = 794\,\text{Pa}$$

It can be seen that the pressure drop is increased at the hot and cold-end of the regenerator with a lower region in the middle. The mean value for the kinematic viscosity between 100°C and 550°C has been calculated as $0.19*10^{-6}$ m^2/s. Under the simplified assumption of linear temperature distribution inside the regenerator, this results in a mean pressure drop of around 5600 Pa per mm regenerator length.

In the example engine, with a regenerator length of 200 mm, this results in a peak pressure drop of around 1.1 bar. The pumping losses are expected to be of some significance at this pressure drop and it is expected that, in an optimised system, other compromises in the thermodynamics will have to be made in order to reduce the pressure drop in the regenerator.

Heat transfer coefficient

With the Reynolds number showing laminar flow, it is now possible to calculate the heat transfer coefficient **h.** The heat transfer coefficient becomes a function of the thermal conductivity and the gap between the shim layers. For laminar flow, the Nusselt number is independent of the Reynolds number. Incropera and Dewitt (1990) give the Nusselt number for laminar flow between parallel plates as 7.54.

$$Nu = \frac{h * tf}{k} = 7.54 \qquad 5.23$$

Nu = Nusselt number

k_f = thermal conductivity of working fluid [W/mK]

The heat transfer coefficient can then be calculated through equation 5.24.

$$h = 7.54 * \frac{k_f}{tf} \qquad 5.24$$

Graph 2.5 shows a significant decrease in thermal conductivity above the critical temperature. At 100°C, water has a thermal conductivity of 0.7 W/mK. With a gap between the shims of 0.065 mm, the resulting in a heat transfer coefficient is around 80000 W/m^{2}K. At the hot-end of the regenerator, with a temperature of 550°C, the thermal conductivity has dropped to 0.12 W/mK, resulting in a heat transfer coefficient of 14000 W/m^{2}K.

It is now possible to calculate the temperature drop, from the fluid to the shim, for the example used earlier to calculate the pressure drop. The surface area of the regenerator can be calculated from the matrix volume and shim thickness. With a regenerator shim thickness of 0.5 mm, and a matrix volume of 660 cc, the resulting surface area is 1.32 m^2. As shown in 5.3.3, the mean heat transfer between fluid and matrix is at a value of around 900 kW.

With the temperature drop being described through equation 5.12 it is now possible to calculate the temperature drop from fluid to matrix in the proposed engine.

$$\Delta T = \frac{\dot{Q}}{h * A} \qquad 5.25$$

This temperature drop becomes 8.5°C at the hot-end and 49°C at the cold-end of the regenerator, which would not result in a useful engine.

From these initial calculations, it becomes clear that a careful optimisation of the different parameters is crucial for any successful regenerator design in liquid engines. Due to the large number of cross coupled variables, it is difficult to manually optimise the system. A computer-assisted optimisation is, therefore, presented in following section.

5.4 Theoretical regenerator optimization

The main difficulty found in designing and optimizing a regenerator system is the large number of variables and the coupling effects between them. Even when these numbers are carefully analysed on their own, it is difficult to predict their effect on the overall engine performance. This problem can be demonstrated in the following example. The energy to displace the working fluid through the regenerator is taken from the driveshaft and, has therefore, to be subtracted from the output power. The resulting extra requirement in input energy then becomes a function of the engine efficiency and, consequently, a function of the regenerator efficiency.

A further example of this problem comes from the regenerator efficiency itself. The effect of the regenerator efficiency on the overall system efficiency depends, largely, on the relationship of energy supplied to the system and the energy shifted in and out of the regenerator in each cycle. With a calculated regenerator efficiency, it is possible to predict the irreversible loss in the regenerator. To establish the effect on the engine efficiency, it is first necessary to establish the ratio between the energy supplied to the system and the energy stored and released by regenerator.

The optimisation method used was to analyse the key parameters that affect performance, and to quantify their effect on overall efficiency. It was then possible to put a weighting factor on each of these parameters in order to quantify their effect on input power. This gave a common parameter, and allowed a solution, which generated the minimum input power and, therefore, the highest efficiency.

The key quantities that affect the input power are the thermodynamic regenerator efficiency (ηre), and the pumping losses (Qpl). For a small length to diameter ratio and matrix material of large thermal conductivity, the thermal losses through the regenerator (Qth) become significant. The regenerator efficiency can be calculated from the temperature deficit in the fluid within one complete regenerator cycle, under adiabatic conditions. The regenerator efficiency is defined as the temperature difference between the fluid entering and leaving the regenerator on the return stroke,

over the total temperature difference from the hot to the cold-end. The increase in input power can then be calculated by multiplying the temperature deficit by the heat capacity of the fluid at the hot-end temperature. The effect of the pumping losses can be estimated by multiplying the expected pumping losses by the inverse of the expected thermal efficiency of the TD-Pile. The overall thermal efficiency of the TD-Pile can be estimated by the product of the Carnot efficiency and the regenerator efficiency

For a specific engine, it is then possible to compare the effect of pumping losses, irreversible regenerator loses and thermal conduction losses through the matrix. Due to large number of variables in the complete system, it is not possible to optimise all parameters in a single step. Initially, the variables that have the least coupling, and that are fairly constrained in their range of values, were independently analysed and fixed. The remaining variables were then optimised using the Math-Cad model presented in appendix A.

Figure 5.7 shows the different parameters that define the regenerator geometry and the fluid and thermodynamics of the system. It can be seen that about half of the parameters have been set to a fixed value for simplicity. The criteria for the individual choices are given in the following section.

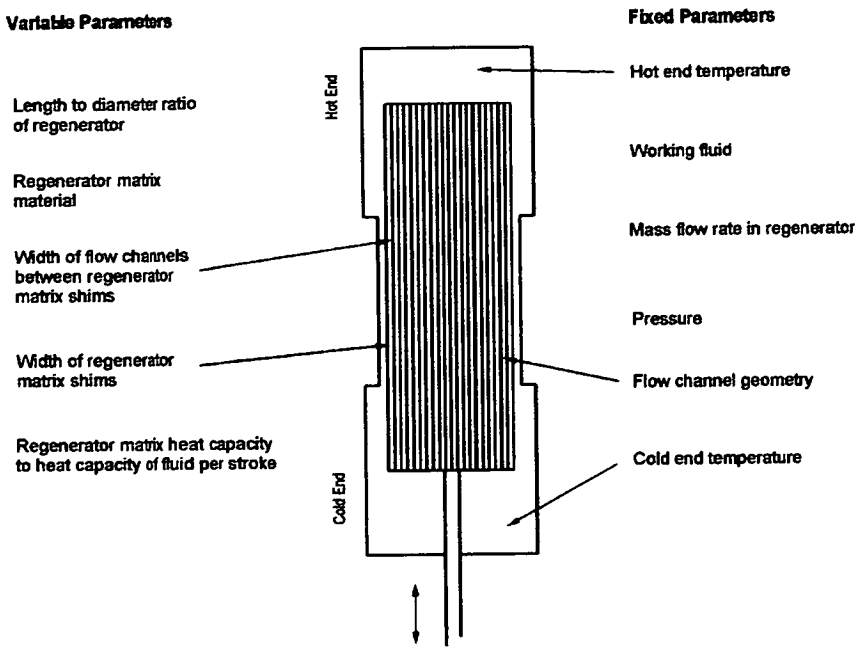


Figure 5.7. The different parameters that define the geometry, fluid and thermodynamics of the regenerator system are displayed. To simplify the process, about half the parameters have been set to fixed values leaving five variables to be optimised.

5.4.1 Fixed parameters

Working fluid

To achieve a high Carnot efficiency, it is important to work with high temperatures in the hot-end. This excludes virtually all organic fluids from use as the working fluid. Malone experimented with a number of different liquids including Sodium and Potassium, and their alloys, and Mercury. He concluded that water is the most suitable thermodynamic medium for this type of engine.

Water has a critical temperature of 420°C, around which the largest thermal expansion is expected. With 420°C the critical temperature is well placed between the ambient temperature and the strength limit of nickel super alloys, which can provide sufficient tensile strength up to over 700°C. This allows the use of the large thermal expansion above and below the critical temperature. In addition, it is cheap, non-reactive, non-

toxic and thermally stable. All the work in this study has been based on water as the working fluid.

Temperature range

Given that the cold-end temperature must be above the ambient temperature, and the hot-end temperature is constrained by the material limits of the hot-end heat exchanger, the choice of minimum and maximum temperature is fairly restricted. Taking into account the far from ideal behaviour of water, it is important to establish which temperature range gives the most favorable set of fluid properties. From Hall's work described, in 2.3.4, we know that a high ratio of thermal expansion to viscosity is an advantage. From graph 2.4, we can see that the isotropic index and, therefore, the thermal expansion of water is at its peak around 400°C. The thermal expansion has higher values than that of an ideal gas at temperatures between 200°C and 600°C. With the value for the kinematic viscosity steadily rising and that of the density steadily falling the dynamic viscosity remains fairly constant above 400°C. It can, therefore, be presumed that the optimum working range is between 200°C and 600°C. A cold-end temperature of 200°C is far enough above the ambient temperature to allow a compact cold-end design. A hot-end temperature of 600°C is within the permissible heating range of high temperature alloys. Lowering the cold-end temperature to values of less than 200°C is unlikely to increase the output power. The ratio of thermal expansion to heat capacity of water, at this temperature, is very poor and the viscosity is high. In this case it is difficult to extract more energy from the expansion than is required in pumping energy to achieve the heat exchange. On the basis of these factors, a hot-end temperature of 600°C and a cold-end temperature of 200°C have been selected as the optimum.

Regenerator matrix geometry

With an expected packing ratio of over 90%, most typical regenerator matrix designs cannot be used. For example it is not possible to use wire mesh as typically used in modern Stirling engines, because it is not possible to achieve the required packing ratios for a high flush ratio. A design, which makes use of wound sheet metal, gives

good control over the flow channel width, and guarantees constant matrix thickness. For the optimisation, it has the advantages of simplifying the flow, and heat transfer calculation to the condition of flow between parallel plates. In the future, a matrix design that enhances turbulence in the flow, in order to increase the heat transfer, might be required. Increased surface roughness, for example, could have a positive effect. The initial optimisation is restricted to the flow between hydraulically smooth parallel plates.

Flow profile in regenerator

The flow in the regenerator is created from the differential motion between the working piston and the regenerator. With the hydraulic power take-off system it is, therefore, possible to create any arbitrary flow profile in the regenerator. This is most likely to be used such that high peak flows in the regenerator are avoided, creating rather long periods of constant flow. Under this assumption, and due to the significant simplification in the calculations, the initial optimisation of the regenerator is based on constant flow during the stroke. The value for the mass flow rate is chosen as the mean flow rate.

Cycle frequency

The cycle frequency has a large effect on the regenerator efficiency as well as on the output power per displaced working fluid volume. Purely from the viewpoint of high regenerator efficiency and low pumping losses a very low cycle frequency in conjunction with a long regenerator to minimize the conductivity losses would result in the highest system efficiency. Practically it is however important to achieve high power densities and, therefore, to work at higher cycle frequencies. A cycle frequency of 4 Hz for the initial analysis has been chosen. At this frequency a reasonably high power density is expected and the frequency is still within the bandwidth of the hydraulic power take-off system.

5.4.2 Variable Parameters

The main variables that are optimised are those that have a significant effect on (i) the regenerator efficiency and (ii) the pumping losses in the regenerator.
These were found to be:

- Flow channel width
- Shim metal width
- Regenerator mass
- Regenerator length over diameter ratio
- Matrix material / fluid insulating gaps

Beside the main geometric variables a further variable was introduced and investigated during the optimization. It was tried to reduce the axial thermal losses through the regenerator material, by introducing extra thermal resistance in the regenerator matrix. It was found that these losses could be greatly reduced by introducing a number of thin fluid gaps along the length of the regenerator. This for example could be achieved with a number of matrix coils which are spaced away from each other. The required spacing was found to be only a very small fraction of the regenerator length and, therefore, would not affect the regenerator dead volume in a significant way. This technique was included in the regenerator optimization.

5.4.3 Optimization results

By limiting the optimisation to these five variables, it is possible to display the effect of the different variables in a series of tables. This was done by choosing two variables for the subtable axis, allowing two further variables to be used for the main table. Each value has been allocated a different color for ease of identification.

The equations, which describe the losses in the system, have been developed from the equations for the pumping losses and the reduced regenerator efficiency used in the

previous section. Therefore, no repeat of these equations is given at this point. The full set of calculations is displayed in appendix A.

The analysis is restricted to the case of flow between parallel plates at a constant pressure of 350 bar. The mass flow rate along the regenerator is presumed constant. The regenerator has been divided into four different temperature regions, which have been analysed individually. The fluid properties in each section have been presumed constant (see appendix A).

Three values were chosen for each of the variable parameters. With these values, and the values from the fixed parameters, it was then possible to calculate the thermal losses arising in each of the four sections. Using the results from this calculations, it was possible to optimize the system by altering the input data in each section to minimize the required input power. The values that have been used for the final step of the optimization are presented in table 5.1.

Flow channel	tf 1	0.01	mm
	tf 2	0.02	mm
	tf 3	0.03	mm
Shim thickness	ts 1	0.1	mm
	ts 2	0.15	mm
	ts 3	0.2	mm
Matrix mass	ms 1	0.75	kg
	ms 2	1.75	kg
	ms 3	2.75	kg
Regenerator length	rl1	50	mm
	rl 2	100	mm
	rl 3	150	mm

Parameter	Value	Unit
swept mass	25	g
freq	4	HZ
T-hot	600	C
T-cold	200	C
Number of fluid gaps in regenerator	3	
thickness of gaps	0.01	mm
Matrix material	Stainless Steel	

Table 5.1 Input values as used in the final step of regenerator optimisation.

Initially it was necessary to calculate the different geometric parameters such as matrix volume, matrix surface area and length over diameter ratio. The different calculations are shown in appendix A and the results are presented in table 5.2.

Length over diameter ratio

		rl1			rl2			rl3		
		ts1	ts2	ts3	ts1	ts2	ts3	ts1	ts2	ts3
ms1	tf1	0.25	0.24	0.23	0.16	0.16	0.15	0.13	0.12	0.12
	tf2	2.76	2.64	2.54	1.81	1.73	1.66	1.44	1.38	1.33
	tf3	6.67	6.38	6.13	4.36	4.18	4.01	3.48	3.33	3.20
ms2	tf1	0.25	0.24	0.24	0.16	0.16	0.16	0.13	0.13	0.12
	tf2	2.80	2.72	2.64	1.84	1.78	1.73	1.46	1.42	1.38
	tf3	6.77	6.57	6.38	4.43	4.30	4.18	3.53	3.43	3.33
ms3	tf1	0.25	0.25	0.24	0.17	0.16	0.16	0.13	0.13	0.13
	tf2	2.83	2.76	2.70	1.85	1.81	1.77	1.48	1.44	1.41
	tf3	6.82	6.67	6.52	4.47	4.36	4.27	3.56	3.48	3.40

Matrix surface [m2]

	ts1	ts2	ts3
ms1	1.88	1.25	0.94
ms2	4.38	2.92	2.19
ms3	6.88	4.58	3.44

Matrix volume [cc]

ms1	94
ms2	219
ms3	344

Table 5.2. Values found for geometric regenerator parameters at the different input values. The values used for flow channel width *tf*, shim thickness *ts*, matrix mass *ms* and the regenerator length *rl* are shown in table 5.1 (calculations are shown in appendix A).

With the help of these geometric parameters, it was possible to calculate the different thermodynamic and fluid dynamic parameters as the Reynolds number, Reduced length, Reduced period and Flush ratio. The different calculations are shown in appendix A and the results are presented in table 5.3 to table 5.5.

Reynolds Number

550 C section

		rl1			rl2			rl3		
		ts1	ts2	ts3	ts1	ts2	ts3	ts1	ts2	ts3
ms1	tf1	112	150	187	168	225	281	225	299	374
	tf2	112	150	187	168	225	281	225	299	374
	tf3	112	150	187	168	225	281	225	299	374
ms2	tf1	75	100	125	112	150	187	150	200	250
	tf2	75	100	125	112	150	187	150	200	250
	tf3	75	100	125	112	150	187	150	200	250
ms3	tf1	56	75	94	84	112	140	112	150	187
	tf2	56	75	94	84	112	140	112	150	187
	tf3	56	75	94	84	112	140	112	150	187

450 C section

		rl1			rl2			rl3		
		ts1	ts2	ts3	ts1	ts2	ts3	ts1	ts2	ts3
ms1	tf1	133	177	221	199	266	332	266	354	442
	tf2	133	177	221	199	266	332	266	354	442
	tf3	133	177	221	199	266	332	266	354	442
ms2	tf1	88	118	147	133	177	221	177	236	295
	tf2	88	118	147	133	177	221	177	236	295
	tf3	88	118	147	133	177	221	177	236	295
ms3	tf1	66	88	111	100	133	166	133	177	221
	tf2	66	88	111	100	133	166	133	177	221
	tf3	66	88	111	100	133	166	133	177	221

350 C section

		rl1			rl2			rl3		
		ts1	ts2	ts3	ts1	ts2	ts3	ts1	ts2	ts3
ms1	tf1	46	61	76	69	92	114	92	122	153
	tf2	46	61	76	69	92	114	92	122	153
	tf3	46	61	76	69	92	114	92	122	153
ms2	tf1	31	41	51	46	61	76	61	81	102
	tf2	31	41	51	46	61	76	61	81	102
	tf3	31	41	51	46	61	76	61	81	102
ms3	tf1	23	31	38	34	46	57	46	61	76
	tf2	23	31	38	34	46	57	46	61	76
	tf3	23	31	38	34	46	57	46	61	76

250 C section

		rl1			rl2			rl3		
		ts1	ts2	ts3	ts1	ts2	ts3	ts1	ts2	ts3
ms1	tf1	31	41	51	46	61	76	61	82	102
	tf2	31	41	51	46	61	76	61	82	102
	tf3	31	41	51	46	61	76	61	82	102
ms2	tf1	20	27	34	31	41	51	41	54	68
	tf2	20	27	34	31	41	51	41	54	68
	tf3	20	27	34	31	41	51	41	54	68
ms3	tf1	15	20	25	23	31	38	31	41	51
	tf2	15	20	25	23	31	38	31	41	51
	tf3	15	20	25	23	31	38	31	41	51

Table 5.3 Reynolds numbers in the regenerator matrix for different regenerator geometries and different temperature sections. The input values for the different parameters are shown in table 5.1 (calculations are shown in appendix A).

Reduced Period

	550 C section			450 C section			350 C section			250 C section		
	ts1	ts2	ts3	ts1	ts2	ts3	ts1	ts2	ts3	ts1	ts2	ts3
ms1 tf1	77	58	46	77	63	50	175	132	107	385	293	236
ms1 tf2	38	29	23	41	31	25	84	64	52	182	140	114
ms1 tf3	25	19	15	27	21	17	53	41	34	114	90	74
ms2 tf1	76	57	46	82	62	50	165	127	103	357	277	226
ms2 tf2	37	28	23	40	31	25	74	59	48	154	125	104
ms2 tf3	25	19	15	26	20	16	44	36	30	86	74	64
ms3 tf1	75	57	46	81	61	49	155	121	100	329	261	216
ms3 tf2	37	28	23	39	30	24	64	53	45	126	109	94
ms3 tf3	24	18	15	25	19	16	34	30	27	59	58	54

Reduced Length

	550 C section			450 C section			350 C section			250 C section		
	ts1	ts2	ts3	ts1	ts2	ts3	ts1	ts2	ts3	ts1	ts2	ts3
ms1 tf1	314	236	189	314	138	111	418	313	251	1297	973	778
ms1 tf2	157	118	94	92	69	55	209	157	125	649	486	389
ms1 tf3	105	79	63	61	46	37	139	104	84	432	324	259
ms2 tf1	733	550	440	430	322	258	975	731	585	3027	2270	1816
ms2 tf2	367	275	220	215	161	129	488	366	293	1513	1135	908
ms2 tf3	244	183	147	143	107	86	325	244	195	1009	757	605
ms3 tf1	1153	864	692	676	507	405	1532	1149	919	4756	3567	2854
ms3 tf2	576	432	346	338	253	203	766	575	460	2378	1784	1427
ms3 tf3	384	288	231	225	169	135	511	383	306	1585	1189	951

Table 5.4 Reduced periods and reduced lengths for different regenerator geometries and temperature sections. The reduced periods and reduced length are not effected by the length to diameter ratio. The input values for the different parameters are shown in table 5.1 (calculations are shown in appendix A).

Flush ratio

	550 C section			450 C section			350 C section			250 C section		
	ts1	ts2	ts3	ts1	ts2	ts3	ts1	ts2	ts3	ts1	ts2	ts3
ms1 tf1	81.3	108.4	135.5	81.3	72.1	90.1	12.4	16.6	20.7	9.7	12.9	16.1
ms1 tf2	40.7	54.2	67.8	27.0	36.0	45.0	6.2	8.3	10.4	4.8	6.5	8.1
ms1 tf3	27.1	36.1	45.2	18.0	24.0	30.0	4.1	5.5	6.9	3.2	4.3	5.4
ms2 tf1	34.8	46.5	58.1	23.2	30.9	38.6	5.3	7.1	8.9	4.2	5.5	6.9
ms2 tf2	17.4	23.2	29.0	11.6	15.4	19.3	2.7	3.5	4.4	2.1	2.8	3.5
ms2 tf3	11.6	15.5	19.4	7.7	10.3	12.9	1.8	2.4	3.0	1.4	1.8	2.3
ms3 tf1	22.2	29.6	37.0	14.7	19.7	24.6	3.4	4.5	5.6	2.6	3.5	4.4
ms3 tf2	11.1	14.8	18.5	7.4	9.8	12.3	1.7	2.3	2.8	1.3	1.8	2.2
ms3 tf3	7.4	9.9	12.3	4.9	6.6	8.2	1.1	1.5	1.9	0.9	1.2	1.5

Table 5.5 Flush ratio for different regenerator geometries and different temperature section. The flush ratio is not affected by the length to diameter ratio. The input values for the different parameters are shown in table 5.1(calculations are shown in appendix A).

With these numbers, the different losses arising from the reduced regenerator efficiency, the regenerator drive and the thermal conductivity through the matrix could be determined. It was further possible to calculate the total energy required to maintain the full temperature difference between the hot and cold-end. The different

calculations are shown in appendix A and the results are presented in table 5.6 to table 5.10.

Thermal conductivity losses [W]

	rl1			rl2			rl3		
	ts1	ts2	ts3	ts1	ts2	ts3	ts1	ts2	ts3
ms1 tf1	516	500	492	52	50	49	19	19	18
ms1 tf2	563	531	516	56	53	52	21	20	19
ms1 tf3	609	563	539	61	56	54	23	21	20
ms2 tf1	1203	1167	1148	120	117	115	45	43	43
ms2 tf2	1313	1240	1203	131	124	120	49	46	45
ms2 tf3	1422	1313	1258	142	131	126	53	49	47
ms3 tf1	1891	1833	1805	189	183	180	70	68	67
ms3 tf2	2063	1948	1891	206	195	189	76	72	70
ms3 tf3	2234	2063	1977	223	206	198	83	76	73

Table 5.6 Losses arising from thermal conductivity in the axial direction for different regenerator geometries. The input values for the different parameters are shown in table 5.1 (calculations are shown in appendix A).

Regenerator losses [W]

	550 C section			450 C section			350 C section			250 C section		
	ts1	ts2	ts3	ts1	ts2	ts3	ts1	ts2	ts3	ts1	ts2	ts3
ms1 tf1	279	367	454	279	20	19	426	830	1217	14	14	13
ms1 tf2	539	707	871	75	73	71	1193	2294	3325	52	50	49
ms1 tf3	788	1031	1267	160	154	149	1894	3623	5219	110	106	103
ms2 tf1	106	141	345	16	16	60	174	345	1476	11	11	41
ms2 tf2	209	278	511	61	60	131	505	426	2391	42	41	90
ms2 tf3	311	176	68	134	15	15	820	513	109	92	11	10
ms3 tf1	130	173	215	58	58	57	320	637	949	40	40	39
ms3 tf2	194	257	320	129	128	127	523	1043	1551	88	88	87
ms3 tf3	87	109	10	15	15	10	218	325	949	10	10	20

Table 5.7 Irreversible regenerator losses arising from imperfect heat exchange and matrix temperature swing for the different regenerator geometries. The length to diameter ratio does not affect the heat exchange for the case of laminar flow. The input values for the different parameters are shown in table 5.1 (calculations are shown in appendix A).

Pumping losses [W]

550 C section

		rl1			rl2			rl3		
		ts1	ts2	ts3	ts1	ts2	ts3	ts1	ts2	ts3
ms1	tf1	125	167	208	3122	4163	5203	10115	13487	16859
	tf2	16	21	26	390	520	650	1264	1686	2107
	tf3	5	6	8	116	154	193	375	500	624
ms2	tf1	54	71	89	1338	1784	2230	4335	5780	7225
	tf2	7	9	11	167	223	279	542	723	903
	tf3	2	3	3	50	66	83	161	214	268
ms3	tf1	34	45	57	851	1135	1419	2759	3678	4598
	tf2	4	6	7	106	142	177	345	460	575
	tf3	1	2	2	32	42	53	102	136	170

450 C section

		rl1			rl2			rl3		
		ts1	ts2	ts3	ts1	ts2	ts3	ts1	ts2	ts3
ms1	tf1	133	177	221	199	265	332	265	354	442
	tf2	133	177	221	199	265	332	265	354	442
	tf3	133	177	221	199	265	332	265	354	442
ms2	tf1	88	118	147	133	177	221	177	236	295
	tf2	88	118	147	133	177	221	177	236	295
	tf3	88	118	147	133	177	221	177	236	295
ms3	tf1	66	88	111	100	133	166	133	177	221
	tf2	66	88	111	100	133	166	133	177	221
	tf3	66	88	111	100	133	166	133	177	221

350 C section

		rl1			rl2			rl3		
		ts1	ts2	ts3	ts1	ts2	ts3	ts1	ts2	ts3
ms1	tf1	7	10	12	179	239	298	580	773	966
	tf2	1	1	1	22	30	37	72	97	121
	tf3	0.3	0.4	0.4	7	9	11	21	29	36
ms2	tf1	3	4	6	77	102	128	248	331	414
	tf2	0.4	1	1	10	13	16	31	41	52
	tf3	0.1	0.2	0.2	3	4	5	9	12	16
ms3	tf1	2	3	3	49	65	81	158	211	263
	tf2	0.2	0.3	0.4	6	8	10	20	26	33
	tf3	0.1	0.1	0.1	2	2	3	6	8	10

250 C section

		rl1			rl2			rl3		
		ts1	ts2	ts3	ts1	ts2	ts3	ts1	ts2	ts3
ms1	tf1	7	9	11	163	217	271	527	703	879
	tf2	1	1	1	20	27	34	66	88	110
	tf3	0.2	0.3	0.4	6	8	10	20	26	33
ms2	tf1	3	4	5	70	93	116	226	301	377
	tf2	0.3	0.5	1	9	12	15	28	38	47
	tf3	0.1	0.1	0.2	3	3	4	8	11	14
ms3	tf1	2	2	3	44	59	74	144	192	240
	tf2	0.2	0.3	0.4	6	7	9	18	24	30
	tf3	0.1	0.1	0.1	2	2	3	5	7	9

Table 5.8 Shows the losses arising from the pressure drop in the regenerator for the different regenerator geometries. The input values for the different parameters are shown in table 5.1 (calculations are shown in appendix A).

Total regenerator losses [W]

550 C section

		rl1			rl2			rl3		
		ts1	ts2	ts3	ts1	ts2	ts3	ts1	ts2	ts3
ms1	tf1	856	1207	1555	9462	14176	18887	29804	44694	59579
	tf2	880	1221	1554	1844	2737	3618	4379	6544	8698
	tf3	1169	1632	2081	1355	1990	2606	2099	3112	4105
ms2	tf1	595	732	874	4062	6076	8091	12764	19140	25516
	tf2	614	740	873	780	1162	1537	1855	2778	3698
	tf3	748	922	1106	565	834	1100	867	1298	1726
ms3	tf1	656	734	820	2609	3890	5171	8130	12186	16242
	tf2	690	752	828	523	780	997	1184	1770	2355
	tf3	796	991	984	381	548	715	552	824	1096

450 C section

		rl1			rl2			rl3		
		ts1	ts2	ts3	ts1	ts2	ts3	ts1	ts2	ts3
ms1	tf1	1674	2361	3017	4820	7141	9429	12422	18550	24643
	tf2	2731	3837	4871	3012	4329	5570	3954	5748	7465
	tf3	3763	5280	6682	3747	5335	6803	4019	5749	7358
ms2	tf1	829	1080	1330	1956	2914	3867	5199	7788	10373
	tf2	1229	1656	2079	1109	1639	2158	1496	2231	2954
	tf3	1642	2256	2863	1374	2038	2684	1472	2199	2905
ms3	tf1	788	934	1085	1253	1856	2458	3299	4941	6581
	tf2	1051	1299	1557	699	1028	1354	926	1386	1843
	tf3	1321	1681	2056	851	1266	1677	893	1349	1799

350 C section

		rl1			rl2			rl3		
		ts1	ts2	ts3	ts1	ts2	ts3	ts1	ts2	ts3
ms1	tf1	1496	2098	2669	1879	2735	3558	3037	4476	5882
	tf2	2601	3651	4631	2537	3625	4640	2674	3835	4923
	tf3	3598	5044	6381	3479	4945	6297	3513	5001	6375
ms2	tf1	759	974	1190	702	1033	1360	1183	1764	2341
	tf2	1183	1587	1988	915	1348	1771	956	1422	1877
	tf3	1583	2167	2746	1271	1883	2478	1267	1891	2496
ms3	tf1	743	869	997	456	690	864	744	1109	1471
	tf2	1024	1257	1501	577	845	1110	584	874	1160
	tf3	1286	1627	1983	788	1171	1549	765	1156	1541

250 C section

		rl1			rl2			rl3		
		ts1	ts2	ts3	ts1	ts2	ts3	ts1	ts2	ts3
ms1	tf1	1115	1549	1961	1454	2118	2759	2506	3701	4873
	tf2	1910	2662	3366	1840	2628	3363	1964	2818	3621
	tf3	2629	3665	4625	2508	3564	4537	2538	3614	4607
ms2	tf1	632	785	939	558	815	1071	991	1478	1962
	tf2	943	1228	1514	672	985	1292	708	1051	1387
	tf3	1238	1650	2062	925	1365	1793	919	1370	1807
ms3	tf1	670	755	846	368	528	688	628	933	1238
	tf2	891	1041	1212	432	626	818	436	648	860
	tf3	1081	1315	1565	583	857	1129	559	841	1119

Table 5.9 Effect on the input power arising from conductivity losses, flow losses and imperfect regeneration in each section of the regenerator. The input values for the different parameters are shown in table 5.1 (calculations are shown in appendix A).

Total regenerator losses [W]

		rl1			rl2			rl3		
		ts1	ts2	ts3	ts1	ts2	ts3	ts1	ts2	ts3
ms1	tf1	5141	7215	9201	17614	26171	34633	47769	71421	94977
	tf2	8121	11371	14421	9232	13319	17192	12970	18946	24706
	tf3	11158	15621	19769	11089	15834	20242	12169	17476	22444
ms2	tf1	2814	3571	4333	4687	6935	9180	20138	30171	40191
	tf2	3969	5210	6454	3258	2231	4279	5015	7482	9916
	tf3	5210	6994	8776	2604	3843	5070	4525	6757	8934
ms3	tf1	2860	3292	3748	7276	10838	14388	12801	19169	25533
	tf2	3646	4350	5099	3481	6121	6757	3130	4679	6218
	tf3	4484	5503	6588	5134	4136	8055	2768	4170	5556

Table 5.10 Effect on the input power arising from conductivity losses, flow losses and imperfect regeneration. The input values for the different parameters are shown in table 5.1 (calculations are shown in appendix A).

Initially it was predicted that the optimum would be in a regenerator design with turbulent flow in the channels. It was expected that the high heat transfer coefficients in the turbulent region would outweigh the increased pressure drops and, therefore, produce the highest system efficiencies. To start with, regenerator designs with large lengths to diameter ratios were tried. To achieve high heat transfer coefficients, very high flow velocities in the channels were used. At these high velocities, the pressure drops became significant, resulting in poor overall efficiencies.

During the optimization, it was then found that a reduction in the length to diameter ratio and the use of much smaller flow channels (resulting in fully laminar flow in the regenerator) produced much higher regenerator efficiencies. With a certain value for the thermal conductivity of the working fluid and the Nusselt number being constant in the laminar region, it was possible to increase the heat transfer coefficient by reducing the flow channel width. If, at the same time, the length to diameter ratio is reduced it is possible to keep the pumping losses to a minimum. This was only possible to the point at which the thermal losses through the regenerator become significant.

By introducing a number of thin fluid gaps along the length of the regenerator, these losses could be greatly reduced. It was found that the required spacing had to be only 0.01 mm with three gaps along the length for the thermal losses to become less than 10% of the total losses.

It was, further, found that the Biot numbers for stainless steel, as a matrix material, are in all cases smaller than 0.2, indicating a minimal reduction in the reduced length (see equations 5.13 to 5.17). This means that materials with high thermal conductivity have no advantages while a material of low thermal conductivity consequently, has the advantage of a low axial conductivity losses through the matrix. For this reason, there was no reason to carry out an optimization for materials of high thermal conductivity.

A further discussion of the results is made at the end of the chapter.

5.5 Malone regenerator variants

As we have seen in the previous section, the use of conventional regenerators in engines with working fluids of large heat capacity is limited. It might be possible to optimise the regenerator design in order to achieve an acceptable performance, but there will always be a compromise between heat exchange and pumping losses as it is the case for the Stirling engine. The requirement of large matrix volume and the high viscosity, together with the large variation in fluid properties, however, causes reduction in performance. With increased complexity of the regenerator system, it may be possible to compensate for some of the limitations caused by the liquid working fluid. The following section looks at some of the methods previously described and those which were proposed during the study.

5.5.1 Constant heat transfer regenerator

The simplest, and, therefore, probably the first step, is to design a regenerator that is optimised for the different properties of the working fluid along the length of the regenerator. A logical step, therefore, is to have a variation in matrix geometry that creates a constant heat transfer rate along this length. This allows the matrix material

to be optimised, for the required heat capacity, over the full length. If this was not the case, we would see a large energy exchange between the fluid and matrix in areas where the heat transfer coefficient is high. This would result in a large temperature swing in some parts of the matrix and, therefore, increased losses. In areas of low heat transfer rate, the smaller heat transfer between the fluid and the matrix would result in a decreased temperature swing of the matrix and, therefore, would not use the heat capacity of the matrix to its full extent. If we look at the example on the proposed engine in 5.3.6 we see that the heat transfer coefficient for a non-optimised regenerator is about six times greater at the cold-end than at the hot-end. The matrix material at the top of the regenerator will have, therefore, a significantly smaller heat exchange with the fluid and a, larger than required, heat capacity. In contrast to this, the cold-end of the regenerator will exchange significantly more energy with the matrix and undergo an increased temperature swing, causing increased losses. There are various ways to generate a more constant heat transfer coefficient over the full length of the regenerator.

The simplest would be to change the hydraulic diameter of the flow channel. It might also be possible to change the matrix material, the flow channel geometry or the surface roughness to achieve the required heat transfer coefficient.

5.5.2 Malone contraflow regenerator

Malone`s original engine had an indicated efficiency of 27%, which is evidence of his regenerator working efficiently. This section examines the technique which Malone used to overcome the problem of large matrix volume and high fluid viscosity.

As we have seen earlier, it is crucial to find the right balance of matrix mass, dead volume, and surface area in a conventional regenerator. The large required matrix volume, in relation to the swept volume always results in either a small matrix surface area, a small flow channel size, a large regenerator dead volume, or a combination of the three. When working with small flow channels, in order to create the large surface area required, the pumping loss increase. When working with a small surface area, to

increases the flow channel size, the temperature drop between fluid and matrix increases. When working with a large added fluid mass, to achieve the first two requirements, the maximum temperature swing of the fluid decreases, causing a relative increase in temperature drop from fluid to matrix.

To overcome this fundamental limitation of the regenerator in liquid engines, Malone choose an entirely new design, allowing him to optimise the regenerator for a high matrix mass, large regenerator dead volume and wide flow channels. From the original drawings, as shown in Figure 5.8, the packing ratio can be worked back to be around 80% matrix to fluid. He describes the regenerator dead volume as three to four times the swept volume. The wide flow channels caused minimal pressure drop and, therefore, small pumping losses. He was then left with the fundamental problem of having a small maximum temperature difference between the fluid and the matrix, a result of the large regenerator dead volume.

With a conventional regenerator, a significant efficiency decrease, due to the large dead volume, would be expected. The fluid entering the regenerator would only penetrate into it by a small fraction of its total length. Following equation 2.2, the maximum temperature difference between matrix and fluid becomes, therefore, only around one quarter of the total temperature difference, hence 75°C. A relatively small temperature swing of the regenerator matrix, and temperature drop from fluid to matrix, would cause a significant reduction in regenerator efficiency.

Malone managed to overcome the problem of the limited maximum temperature difference between fluid and regenerator matrix by installing non-return valves to direct the flow in the regenerator.

The hot fluid would now travel over a series of strokes unidirectionally along the flow channels until the temperature difference towards the cold fluid in the adjacent passage became large enough for the heat transfer to occur. In this way Malone was able to avoid the reduction of the maximum temperature difference caused by the

large dead volume, and to use the full temperature span from hot-end to cold-end temperature.

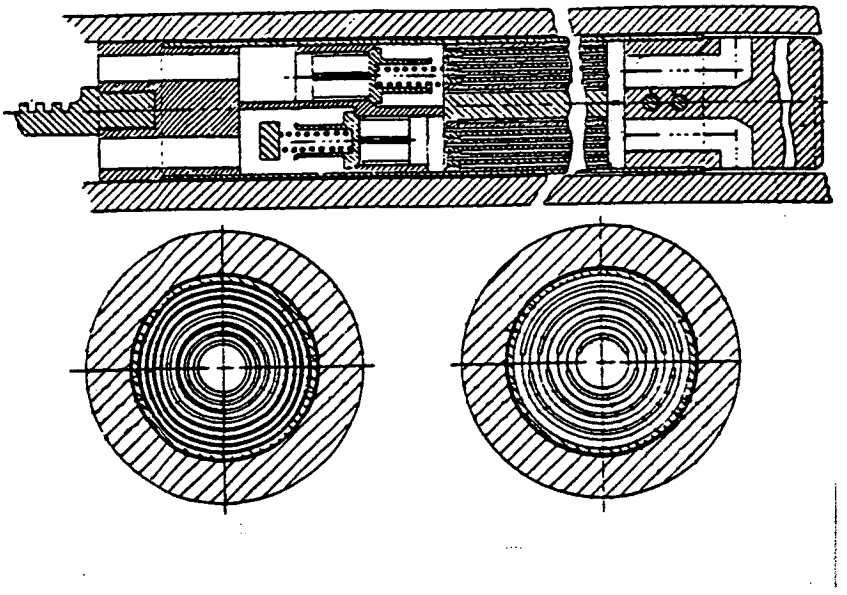


Figure 5.8. Section view of the TD-pile as used by Malone. Malone used two, one-way, valves on the cold side of the regenerator to direct the fluid to and from the hot-end into different flow passages. The flow passages were created by coiling steel sheets with cut outs for the different flow channels. (Drawing from Malone's report in the "Journal of the Royal Society of Arts", June 1931)

Malone's original description, and later analysis, do not address the advantages or disadvantages of such an arrangement. From discussion with Malone's son, we know that Malone tried to run his engines without the valve arrangement and experienced significant reduction in output power. This further confirms the prediction of poor regenerator efficiency expected with a conventional regenerator design and a large dead volume.

In the literature (Swift 1989a; Kolin 1972), the regenerator as used by Malone has been described as a contraflow heat exchanger. Looking at the basic function of the regenerator in the Stirling cycle, it becomes clear that the regenerator performs a totally different function than that of a contraflow heat exchanger. The function of the regenerator is to store thermal energy in a material of a much smaller thermal expansion coefficient than the working fluid. This is what causes the thermal contraction of the working fluid in the isometric compression stroke.

The contraflow heat exchanger transfers thermal energy between two continuous fluid flows. The dividing matrix is, thereby, staying at constant temperature and not performing the function of storing and releasing thermal energy.

With the heat transfer coefficient for turbulent flow being a function of the Reynolds number and, therefore, a function of the flow rate in the channels, it can be assumed that the heat transfer between matrix and the fluid becomes very small at times of zero flow. Under this assumption, Malone`s regenerator, can perform the same function as the regenerator in a Stirling engine. At the time that the regenerator is driven towards the hot-end, the flow velocity in the channels, with the fluid from the hot-end, becomes high and the thermal energy can be transferred into the matrix in order to cause the thermal contraction. The fluid in the channels coming from the cold-end is stationary and little heat transfer from the matrix into the fluid can be expected. In the return stroke the flow velocity in the channel, with the fluid from the cold-end, becomes high and the thermal energy from the matrix can be returned into the fluid, to create thermal expansion.

Because the flow is prevented from reversing within the regenerator, the effect of the large dead volume becomes largely irrelevant. The fluid will now travel through the full length of the regenerator and has, therefore, the full temperature difference available in order to transfer thermal energy into the matrix. The only difference is that the stroke is divided into a series of motions.

5.5.3 Collapsible regenerator

A further novel way to overcome the problem, arising from the large regenerator matrix volume, has been considered in this study. As described earlier in the chapter, a large regenerator dead volume, hence small flush ratio, reduces the distance that the fluid travels through the regenerator and, therefore, reduces the regenerator efficiency.

If, it were possible to pass the fluid through the full length of the regenerator and, at the same time, work with a large dead volume, then this configuration would be at a clear advantage. As we have seen previously it is only possible to create a large

surface area by working with small flow channel size. This then, especially at the time of peak working fluid flow, causes high pressure drops, subsequently resulting in unacceptably high pumping losses. A regenerator system that increases the flow channel size, hence increases the dead volume during the stroke, and reduces the size around the time of zero fluid flow, can generate the required behaviour.

This could be produced by use of an expanding and contracting regenerator matrix. A number of different possible designs for such a regenerator system have been proposed and considerate in the study. These regenerator systems can be divided in two groups:

I. Systems with a mechanical linkage that change the regenerator dead volume depending on the shaft position.

II. Systems that change the regenerator dead volume depending on the flow rate and/or pressure drop in the regenerator

The fundamental limitation in either of these configurations is that it is not possible to increase the dead volume by more than the swept volume. If we presume an equal, fixed dead volume at the beginning and the end of the stroke, then it is only possible to absorb the swept volume into the increasing regenerator dead volume during the expansion stroke of the regenerator. At the time of mid stroke, all the swept volume will be contained by the regenerator. During the second half of the stroke, it would be possible to displace this volume out of the regenerator. If the volume that entered the regenerator during the expansion stroke were larger than the swept volume this would create a reverse flow in the regenerator during the contraction stroke, causing large irreversible losses.

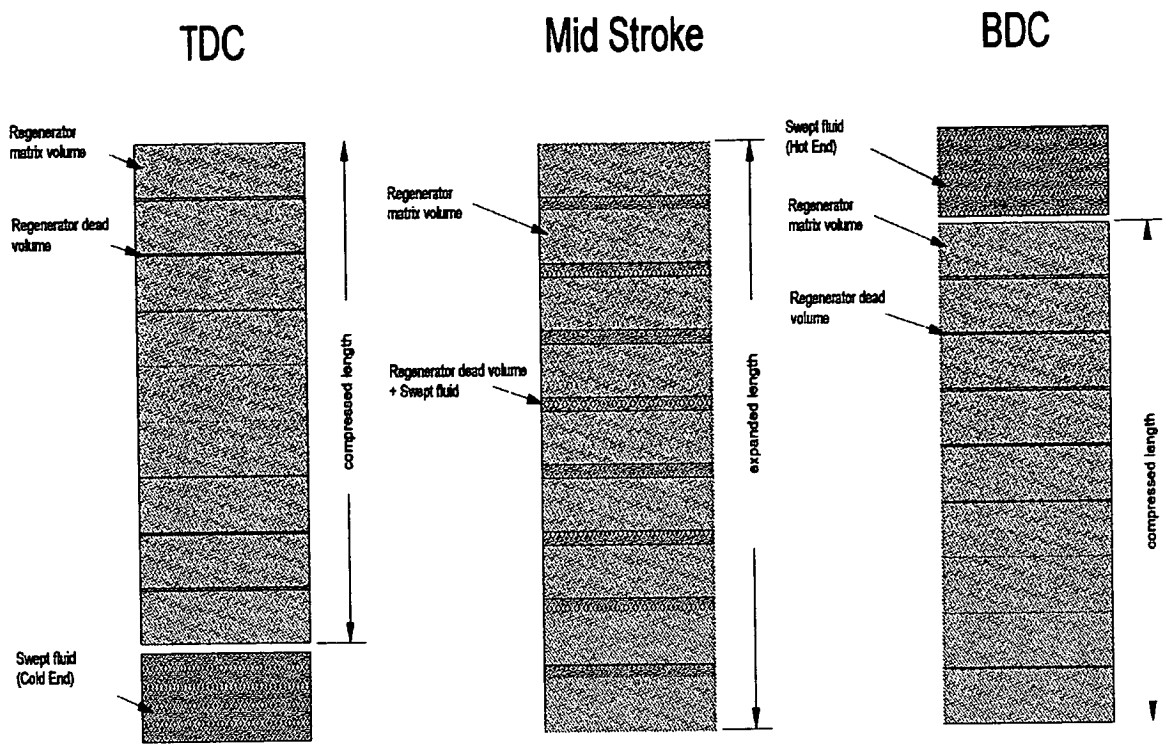


Figure 5.9. shows the collapsible regenerator during the stroke from hot to cold-end. The initial regenerator position is at the top dead center with a minimum of dead volume in the compressed regenerator, and the swept volume in the cold-end space. In the first half of the stroke the swept fluid enters the expanding regenerator matrix until, at mid stroke, all the fluid has been absorbed into the matrix. In the second half of the stroke, the regenerator empties the swept fluid into the hot-end space.

Further, it is important to realise that the regenerator motion is not in phase with the flow through the regenerator. In the case of the Malone engine, it is purely a function of the differential motion between the regenerator and the working piston. To make maximum use of the expansion and contraction of the regenerator, the flow and expansion motion have to be synchronised.

For any heat transfer calculations this has to be taken into account and it is, therefore, no longer possible to presume constant mass flow through the length of the regenerator. The mass flow in the regenerator becomes a function of the actual regenerator displacement and the change of dead volume. In the case of equal regenerator expansion volume and swept volume, for example, the mass flow into the regenerator during its expansion consists of the full swept volume, while the flow out of the regenerator at the other end becomes zero. In the second half of the stroke,

during the regenerator compression stroke, the flow out of the regenerator consists of the full swept volume, and the flow into the regenerator becomes zero.

5.5.3.1 Mechanically controlled dead volume

Designs using a fixed mechanical linkage to control the regenerator dead space can either use the regenerator motion directly, or employ a further drive system to control the regenerator dead volume.

The advantage of such systems is that no further eccentric drive system is required. The disadvantage in using the regenerator motion to control the dead volume comes from the fact the flow through the regenerator is a function of both the working piston and the regenerator motions. The time of zero flow in the regenerator is not in phase with the regenerator top dead centre, and bottom centre and the time of peak flow through the regenerator is not in phase with regenerator mid stroke. It will, therefore, not be possible to change the regenerator dead space by the same amount as the swept volume.

Figure 5.10 and 5.11 present the ideas of two different systems that use the regenerator motion to control the dead volume. The first system has a regenerator matrix made from metal cones or shim that is coiled up around a cone. The connection rod angle is used to control the spacing of the individual metal sheets. With the largest angle between the regenerator and the connecting rod accruing during mid stroke, the regenerator dead volume reaches its maximum at this point. During top and bottom dead centre of the regenerator, the angle between the connecting rod and the regenerator becomes zero, resulting in the minimum dead volume.

The second system is made from a stack of thin washers, arranged in a way that the flow passes the washers alternately between the inside and the outside. It is possible to use stack of washers in parallel and series to create the optimum flow channel characteristics. The required spacing between the washers is maintained through spring elements between them, which for example, could be achieved through a slight

bending of the washers. The linear motion of the regenerator compresses the washer stack towards the end of each stroke, by running into a mechanical end stop. It is possible to control the amount of compression through the position of the end stop.

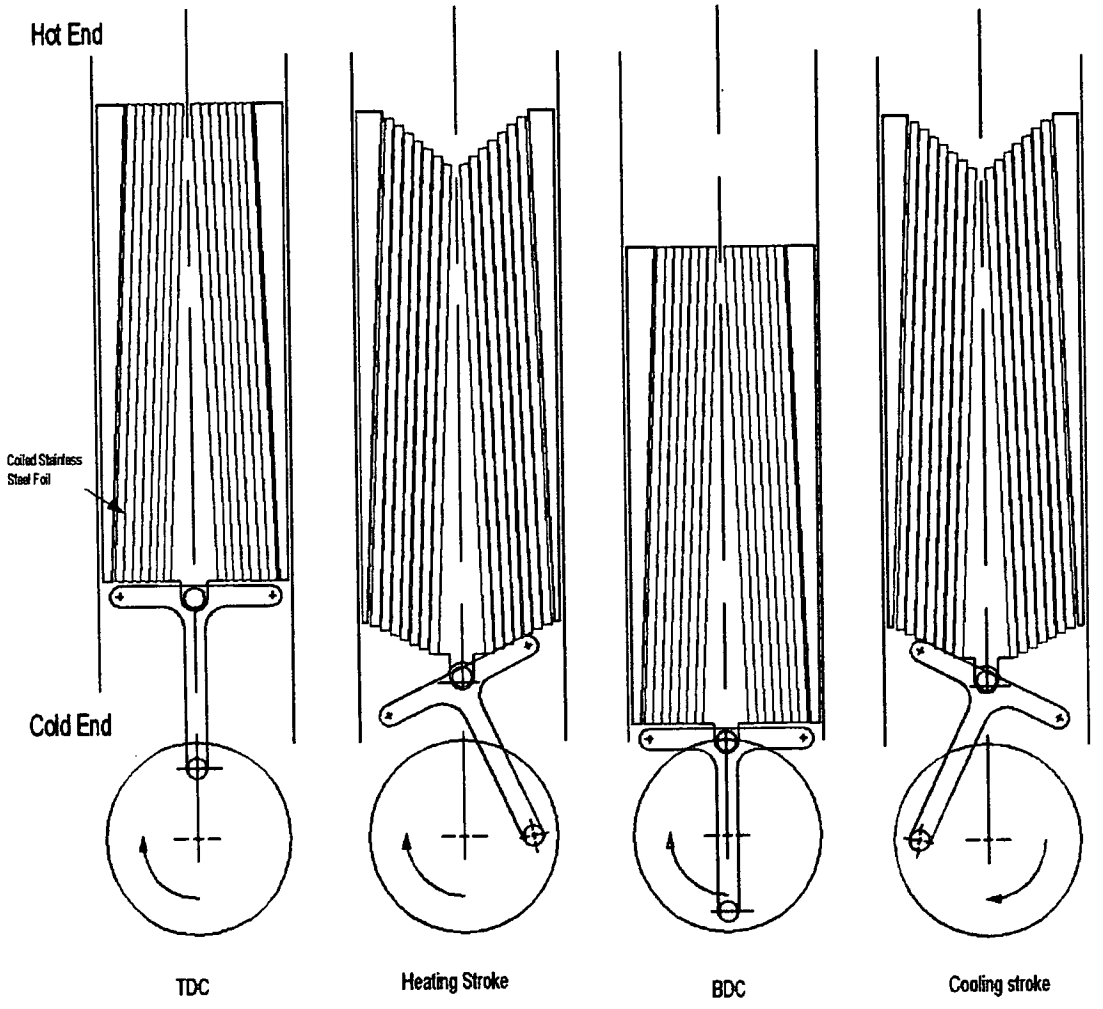


Figure 5.10. Proposed technique to minimise dead volume in the regenerator at times of TDC and BDC. The angle of the connecting rod is used to control the dead volume in the regenerator. At times of maximum flow through the regenerator, the connectiong rod angle is at its maximum with a large opening between the matrix layers. At times of minimum flow, around TDC and BDC the connecting rod angle is zero with a minimum space between matrix layers.

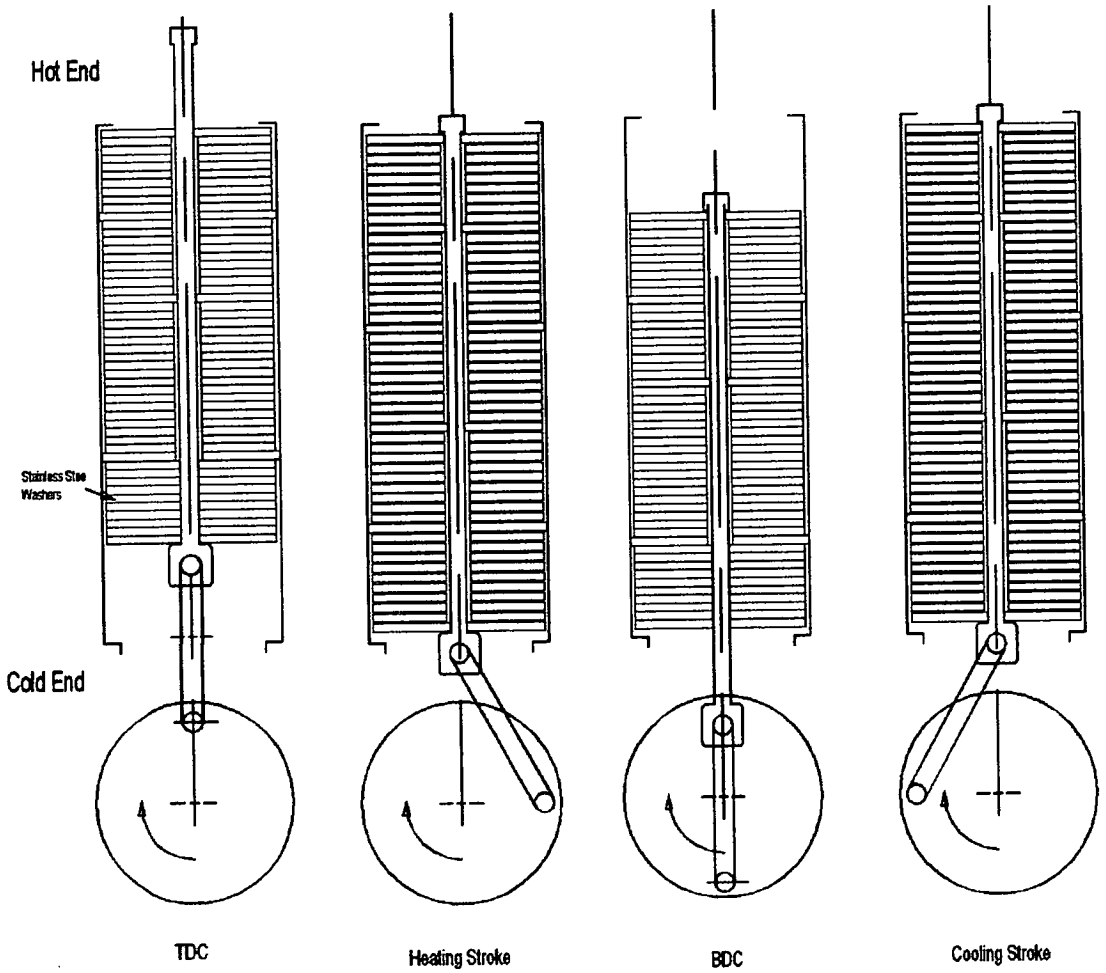


Figure 5.11. Springs between the washers cause the regenerator matrix to expand at mid stroke. End stops at the hot and cold-end are used to compress the regenerator at TDC and BDC to minimise dead volume. The flow is channeled in alternating direction over the washers, whereby, a number of washers are connected in parallel. By changing the number of washers used in parallel, it is possible to optimise between pressure drop and heat transfer. It is further possible to vary the numbers of washers connected in parallel, along the regenerator to optimise for different fluid properties between the hot and cold-end.

Instead of using the regenerator motion to control the dead volume, it would also be possible to use an independent mechanical drive, which can then work out of phase from the regenerator and in phase with the expected flow. A camshaft, for example, could be used to create the required motion profile. Such a system would, however, increase the complexity and cost of the engine. No further studies have been carried out in this area.

5.5.3.2 Flow controlled regenerator dead volume

A method of controlling the dead volume in the regenerator by expanding the matrix, using the pressure drop created through the flow in the regenerator was considered. The advantage of this arrangement is that it always adjusts to the current flow in each part of the regenerator. It could be further designed to maintain a specified pressure drop for each part in the regenerator. This could then be used to create a constant heat transfer along the length. Practically it would, however, require quite a complex system of well-balanced spring and piston elements. Given the difficulties presented by the high hot-end temperature, the reversing flow and the tight tolerances, it is not possible to propose a viable practical design.

5.6 Discussion of results

When the findings in this section are reviewed, it can be seen that the main design challenge for an efficient regenerator system comes from the high heat capacity of the working fluid around the critical point, and the large variation of properties during the cycle. This brings two fundamental problems to the design of any efficient regenerator system. Firstly, there is the problem of bringing the relative small swept volumes in contact with the large required matrix mass. The high flush ratios, which are required in order to maximize the temperature swing of the fluid then results in high packing ratios. This excludes the use of wire meshes, as typically found in the Stirling engine, and requires a precisely manufactured regenerator structure. Secondly, the fluid properties vary to such an extent, from the hot to the cold-end temperature, that an efficient regenerator requires a different matrix geometry along its length.

A theoretical analysis of the regenerator in the Malone type engine was done, such that, in theory, it was possible to optimize the different parameters for an efficient regenerator system. It was possible to find an optimum for the four main variables defining the regenerator geometry.

- For water as the working fluid, a matrix mass, which is around 60 times larger than that of the swept fluid mass, was required. At this matrix mass to fluid ratio, the temperature swing in the matrix becomes less significant and a further increase in matrix mass has only a small effect.

- Observing only the regenerator efficiency and flow losses, the optimum for the length to diameter ratio was found to be a very short and wide regenerator construction. Taking the thermal conductivity losses through the matrix into account, the optimum for stainless steel as the matrix material was found at an length/diameter ratio of 1.5. It was possible to show that thin fluid isolating gaps, along the length of the regenerator, can allow for the use of shorter regenerator constructions, without high axial conduction losses.

- The optimum flow channel width was found to be around 0.01 mm towards the cold-end, and 0.02 mm towards the hot-end. At this thickness, it is possible to create a large enough heat transfer coefficient to minimize the temperature drop from the fluid into the matrix. For a short and wide regenerator construction, it is still possible to keep the pumping losses within acceptable levels.

- The optimum shim thickness for a matrix to swept mass ratio of 60 was found to be around 0.15 mm. An increase in shim thickness, from this point, will have the negative effect of reduced surface area. A decrease of shim thickness results in an increased regenerator dead volume, with the negative effect of reduced temperature swing of the working fluid.

A number of different systems to overcome the fundamental problem of trapped fluid volumes in the regenerator were considered. It was thereby found, that it is, to a

certain extent, possible to overcome this problem through expanding matrix constructions which collapse towards the end of the stroke in order to reduce the dead volume. In addition Malone`s original contraflow regenerator was analysed. It was found that this system removes the problem arising from large dead volumes and, therefore, allows regenerator constructions with lower packing ratios.

6 Hydraulic power take-off systems

In this chapter, an analysis of possible power take-off systems for the Malone cycle engine is presented. Both the Artemis digital displacement^{TM} power take-off system, and conventional crank arrangements are considered. The various theoretical models and experimental set ups made during the study are described and the results presented.

The chapter ends with a discussion of the advantages and disadvantages of the different systems.

6.1 Introduction

In order to achieve the required regenerator and piston motion in Stirling engines, a large number of different mechanical linkages have been proposed and developed in the past. Most of these systems work on the basis of conventional crank drives. For the Malone engine, the number of power take-off systems which are described in the past is restricted to Malone`s original work and a few different experimental machines working with organic fluids at low pressures. (see also chapter 2.3).

The demand on the mechanical power take-off system for the Malone engine differs considerably to that of the Stirling engine. The reason for this is mainly found in the low compressibility and high critical pressure of suitable working fluids. This results in two fundamental differences between the power take-off system for the Malone cycle engine and that of the Stirling cycle engine. Firstly, to avoid evaporation and condensation of the working fluid in the regenerator, the working pressure has to be maintained above the critical pressure throughout the cycle. Secondly, due to the incompressibility of the fluid in the compression space, the sinusoidal piston and regenerator motion profiles, as typically used in the Stirling cycle, are of limited use. Sections 6.2 and 6.3 deal with these fundamental requirements in greater detail.

There is a further difference between the two engines, which gives the Malone cycle engine a clear advantage over the Stirling cycle engine. Due to the low compressibility of the working fluid in the compression space, the absolute amount of trapped fluid in the cold-end does not effect the functioning of the system. There is no disadvantage to work with a large volume of working fluid in the cold-end space of the engine. This gives an increased flexibility in the design of the power take-off and regenerator drive system making it, for example, possible to couple fluid separators, extra pipework, pressure intensifiers and crank arrangements to the cold-end working fluid circuit without penalty.

The study presented in this thesis is an examination and performance analysis of a number of different mechanical arrangements, which have been designed to achieve the required motion profiles. During the study two types of power take-off systems have been analysed. The first type is based on the Artemis digital displacement technology, which allows full control over the working piston motion. The second type is based on a conventional crank piston arrangement. A number of different crank arrangements, with different techniques for reducing the torque pulsation in the output shaft, are described.

6.2 High bottoming cycle pressure

In the Malone engine, the operating pressure has to be maintained above the critical pressure throughout the cycle to avoid evaporation or condensation in the regenerator (a full explanation for this has been given in 2.2.5). There is the practical requirement of the cold-end temperature to be above ambient temperature. The hot-end temperature is limited by high temperature strength of the hot-end heat exchanger material. Further there is the desire to work around the critical point, where the maximum thermal expansion of the fluid is. This restricts the choice for working fluids with water having been found as the most suitable fluid (see also 4.3). The critical point then dictates a minimum cycle pressure of 220 bar. This requires not only a design for the power take-off system that can cope with high cycle pressures, but also one that has to be very efficient given the extra losses encountered from the high pressure during the compression stroke.

If the pressure during the compression stroke is far above ambient pressure, and it is not possible to work with a significantly higher maximum cycle pressure, the resulting power take-off system efficiency will be reduced significantly. Figure 6.1 shows the energy losses encountered during a compression and expansion stroke in relation to the cycle work output.

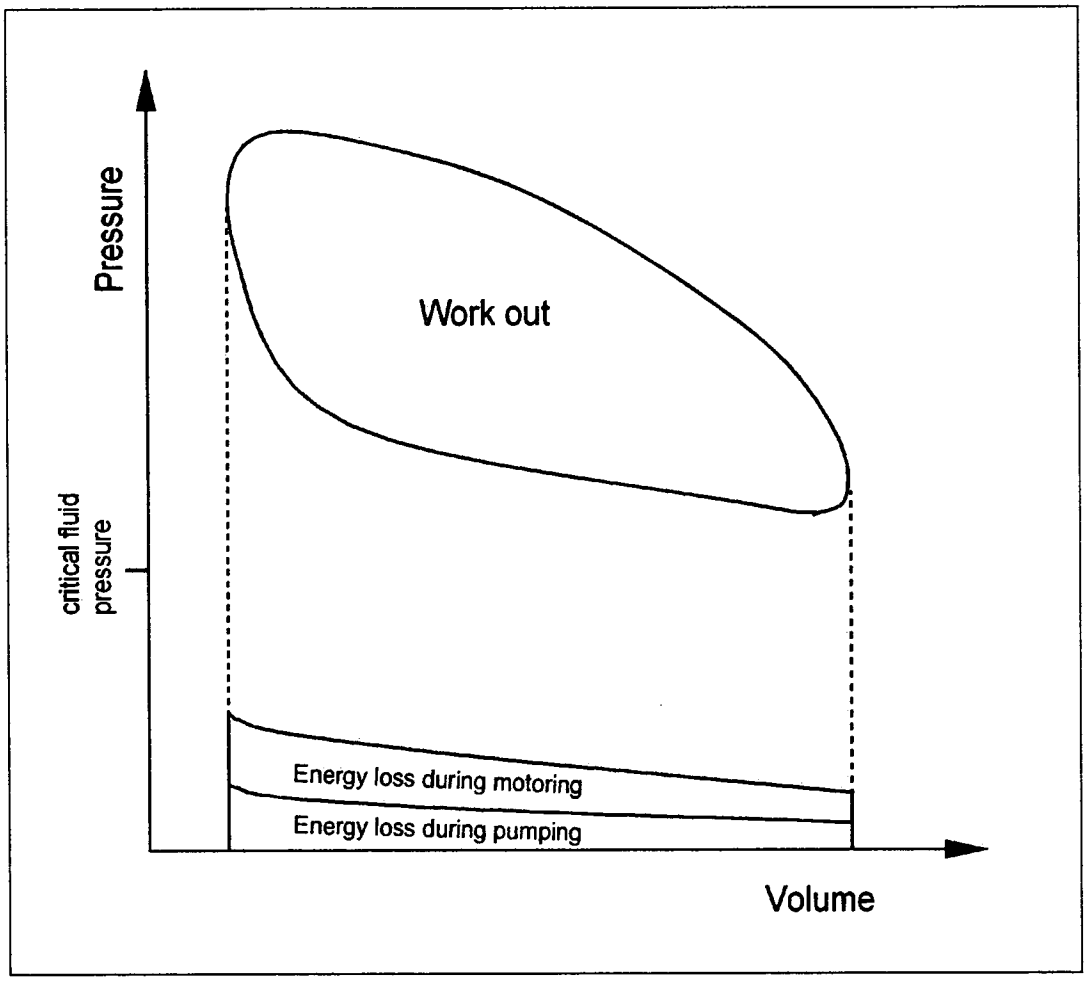


Figure 6.1. PV-diagram of Malone type engine working with high critical pressure in relation to peak cycle pressure. In such systems small losses in the power take-off system can create significant losses in relation to the output power.

For a given power take-off machine efficiency, it is possible to calculate the overall mechanical efficiency as a function of the ratio between compression and expansion pressure. The energy extracted during a cycle can be calculated by subtracting the

energy required for the compression stroke from the energy extracted during the expansion stroke (equation 6.1).

$$Q_{out} = \left[\Delta V * P_{E\,mean} * \eta_M\right] - \left[\Delta V * P_{C\,mean} * 1/\eta_P\right] \qquad 6.1$$

Q_{out} = Energy extracted during expansion stroke

ΔV = displaced volume during expansion or compression stroke

P_{Emean} = mean pressure during expansion stroke

P_{Cmean} = mean pressure during compression stroke

η_M = efficiency during expansion (motoring) stroke

η_P = efficiency during compression (pumping) stroke

The energy lost in the power take-off system during the same working stroke can be calculated using equation 6.2.

$$Q_{loss} = \left[\Delta V * P_{C\,mean} * (1-\eta_P)\right] + \left[\Delta V * P_{E\,mean} * (1-\eta_M)\right] \qquad 6.2$$

It is now possible to calculate the efficiency of the power take-off system.

$$\eta_{system} = \frac{Q_{out}}{Q_{out} + Q_{loss}} \qquad 6.3$$

With the displacement present in all terms, it is possible to simplify equation 6.3 to equation 6.4.

$$\eta_{system} = \frac{P_{Emean} * \eta_M - P_{Cmean} * 1/\eta_P}{P_{Emean} - P_{Cmean}} \qquad 6.4$$

For conventional crank-piston arrangements, the piston efficiency during the compression and expansion stroke can be expected to be of similar value. With equation 6.4 it is possible to calculate the overall system efficiency for different power take-off efficiencies at a given mean pressure in the compression and

expansion stroke. This has been done for three different power take-off systems all having equal efficiencies in the expansion and compression stroke and working at a mean pressure during the compression stroke of 250 bar. The results are presented in graph 6.2.

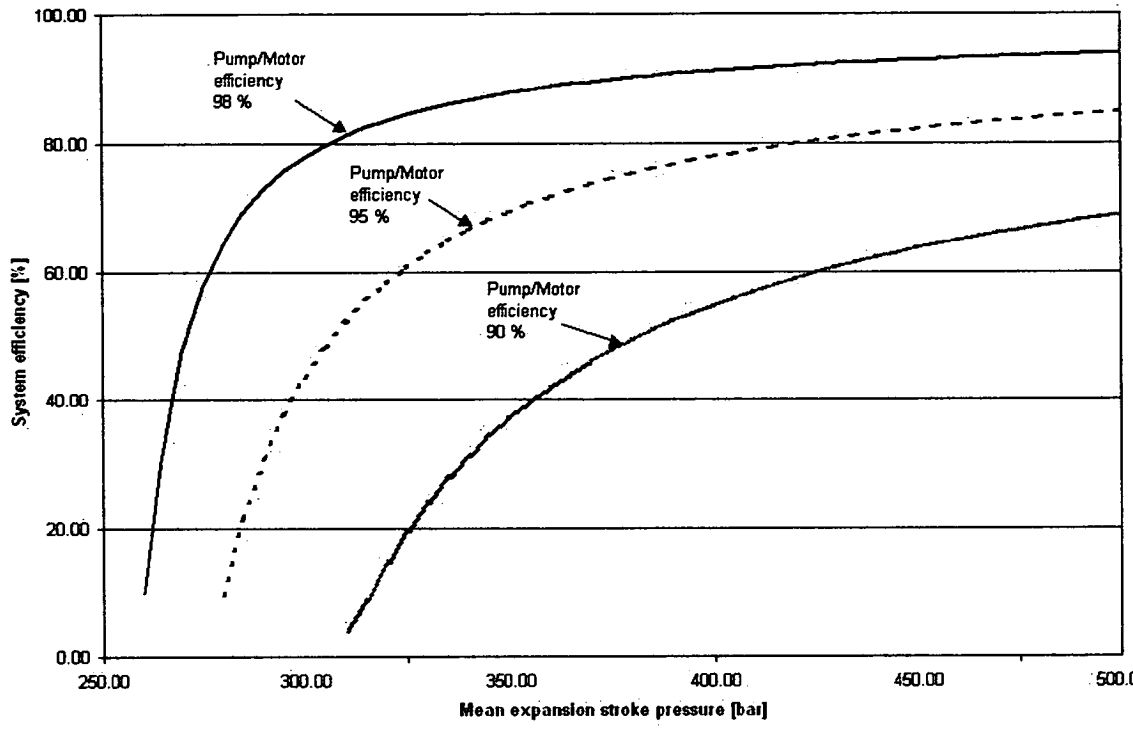


Figure 6.2. Theoretical power take-off system efficiency for system working at 250 bar mean compression stroke pressure. The efficiency is shown as a function of mean expansion stroke pressure for pump/motor efficiencies of 90 %, 95 % and 98 %.

The critical pressure of water at 220 bar dictates the absolute minimum cycle pressure of the engine. The upper pressure is limited by the mechanical strength of the pressure vessel, especially in the hot-end heat exchanger. Also, Malone managed to work at extremely high pressures of up to 800 bar thought it is difficult to see how to design a compact and economical engine for these pressures. The efficiency of the power take-off system becomes, therefore, a crucial factor in the functioning of the engine. Later in the chapter it will be shown that elevating the tank pressure, to reduce the cycle pressure offset, can help to solve this fundamental limitation, resulting in an increase in the power take-off system efficiency.

6.3 Piston motion profiles

In Stirling cycle engines the gaseous working fluid stays compressible when it is present in the cold-end space of the engine. In Malone type engines the working fluid becomes liquid in the cold-end space and is, therefore, virtually incompressible. For an efficient engine with a minimum dead volume in the regenerator and the hot-end space, this results in a hydraulically stiff system at times when the fluid is in the compression space. When reviewing the typical Stirling cycle, as presented in figure 2.1, it becomes clear that, due to the incompressibility of the fluid in the isothermal compression phase 1-2, this stroke would be not possible. With a conventional crank arrangement operating 90° out of phase from the regenerator, and small hot-end dead volumes, we would expect large pressure spikes during the compression stroke. This problem has already been discussed by Ehsan (1997). He was able to show that it is possible to overcome this problem by using a non-sinusoidal motion profile for the working piston. This motion profile can be created by the Artemis digital displacement pump/motor.

Malone, as we know, used a simple crank arrangement and stated that the phase angle between regenerator and working piston was 90° in his engines. If, during the compression stroke, all the working fluid were in the cold-end it would not be possible to compress the fluid. When drawings of Malone's original engine are studied, it can be surmised that the dead volume around the hot-end dummy and in the upper end of the regenerator will be larger than the volume displaced by the working piston. This volume remains at temperatures above the critical temperature during the cycle and adds, therefore, significant compliance to the system. From figure 6.3 it can be seen that the compressibility of water is at its peak around the critical pressure.

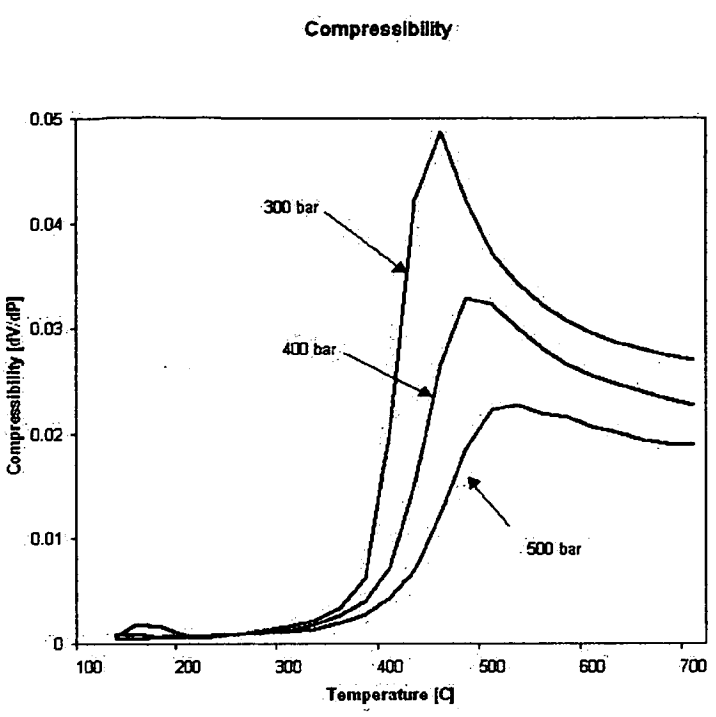


Figure 6.3. Compressibility of water as a function of pressure and temperature. It can be seen that the fluid in the cold-end and in the cold part of the regenerator is virtually incompressible.

To analyse the relation between the system pressure, the phase angle and the different volumes, a numerical computer model of the Malone engine has been made, using AMESim® 4.0.1 (2002). The AMESim® model is highly simplified thermodynamically and presumes, like the Smith classical model, isothermal conditions in the engine. The conditions in the real engine are expected to be partly adiabatic but, with the isothermal model, it is still possible to analyse the effect of the low compressibility of the working fluid in the cold-end. Further, the model allows the study of effects from the change in phase angle, regenerator and hot-end dead volumes, and the relation of swept volume to the volume displaced by the working piston. The model presumes sinusoidal motion of regenerator and working piston. A numerical approach of the model is presented in appendix B.

The parameters of Malone's original engine are analysed before any study on the proposed engine is made. Unfortunately Malone kept most of his test results to himself but, from the material that is available, it is still possible to analyse his engine. Malone stated that the dead volume in his regenerator equals three times the swept

volume and that the phase angle between regenerator and working piston was 90°. From the drawings and descriptions available it was further possible to see, that the dead volume in the hot-end was much smaller than the swept volume.

Using a working piston displacement of similar value to the swept volume, the isothermal simulation model produces a PV-Diagram similar to that presented by Malone in 1931. Even with slightly larger or smaller values for the different presumed parameters, the result stays remarkably close to that presented by Malone.

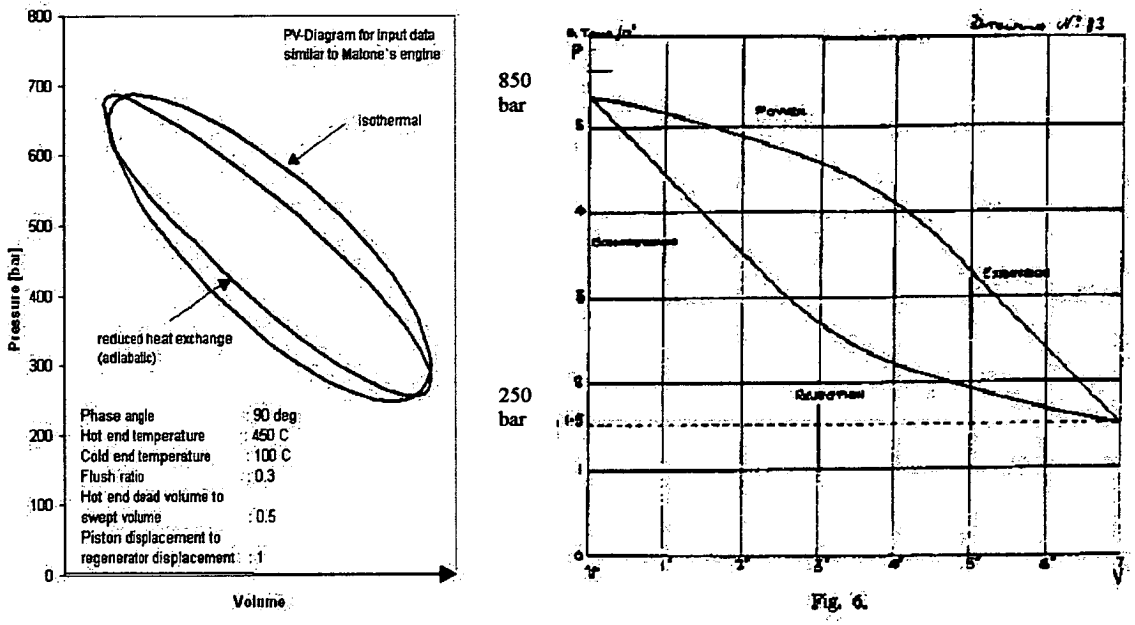


Figure 6.4 PV-Diagram of Malone's engine. Left, predicted PV-Diagram from the AMESim® model. Right, PV-Diagram presented by Malone in 1931.

The main difference between the predicted PV-Diagram and the measurements by Malone are found in the areas towards the TDC and BDC of the working piston. A possible explanation for this can be found in the simplified isothermal conditions used in the simulation. If we presume a low regenerator efficiency and poor heat transfer in the hot and cold-end heat exchanger, the conditions in the engine become more adiabatic. The shape of the PV-Diagram would then be reduced to a very slim profile between the point of maximum pressure and minimum volume, and the point of minimum pressure and maximum volume. To simulate this effect with the isothermal model, the actual volume of fluid undergoing the temperature change in the

regenerator has been reduced. By reducing the swept volume to 75% of the value used in the initial assumption, the area inside the PV-Diagram becomes smaller with the same corner points at the TDC and BDC of the working piston (see figure 6.4).

When Malone`s measured PV-Diagram is compared with the modeled one of reduced swept volume, the indications are, that the conditions of Malone`s engine were closer to adiabatic around TDC and BDC. This could well be a result of the poor heat transfer in the regenerator at times of small flow rates. A further reason might be hysteresis in Malone`s measurements due to limitation of measurement instruments at the time.

Following this initial investigation of Malone`s engine, the AMESim® model was used to analyse the limits to which a conventional crank power take-off system could be used in the proposed Artemis-Malone engine. The effects of the phase angle, the hot-end dead volume, and the working piston displacement in relation to the swept volume were, analysed. It became instantly clear that, with the small regenerator dead volume in the proposed engine, it is not possible to create a PV-Diagram within the pressure limits of any engine. If the volume in the engine model is increased so that the bottoming cycle pressure is over the critical pressure, the peak cycle pressure rises to values of thousands of bar. This proves the theory, proposed earlier, that with all the working fluid in the cold-end and, thus incompressible, it was not possible to use the same crank and regenerator motions as are typically found in Stirling engines. Simulations with reduced phase angles, down to a few degrees, and reduced working piston strokes to only a fraction of the swept volumes, still showed unacceptable pressure peaks during the cycle.

As described earlier, and as analysed by Ehsan (1997), it is possible to overcome this problem through non-sinusoidal working piston motion profiles. Ehsan was, hereby, able to show that it is possible to create working piston motion profiles that allow sinusoidal regenerator motion without significant pressure peaks.

Another way to overcome the fundamental problem of the large pressure fluctuation in Malone engines with small regenerator dead volumes has been analysed in the study. It can be shown that it is possible to add the required compliance to the system by working with an increased dead volume in the hot-end space, allowing the use of conventional crank arrangements. This volume can, for example, be controlled over the position of the top dead center of the regenerator and, therefore, the hot-end dead volume. In this way it is possible to control the volume of compressible media in the engine during the compression stroke and, therefore, the peak cycle pressure.

As well as the effect of the increased hot-end dead volume, the effects of decreased phase angle and of change in working piston displacement have been analysed in the simulation. The hot and cold-end temperatures, and the regenerator flush ratio have been kept to a constant value. The simulation used a hot-end temperature of, 550°C and a cold-end temperature of 150°C. The regenerator dead volume was only one tenth of the swept volume, resulting in a flush ratio of 10.

Initially a fixed phase angle of 90 degrees and equal displacement of the regenerator and working piston were used to analyse the effect of the hot-end dead volume. The results from this simulation are presented in figure 6.5.

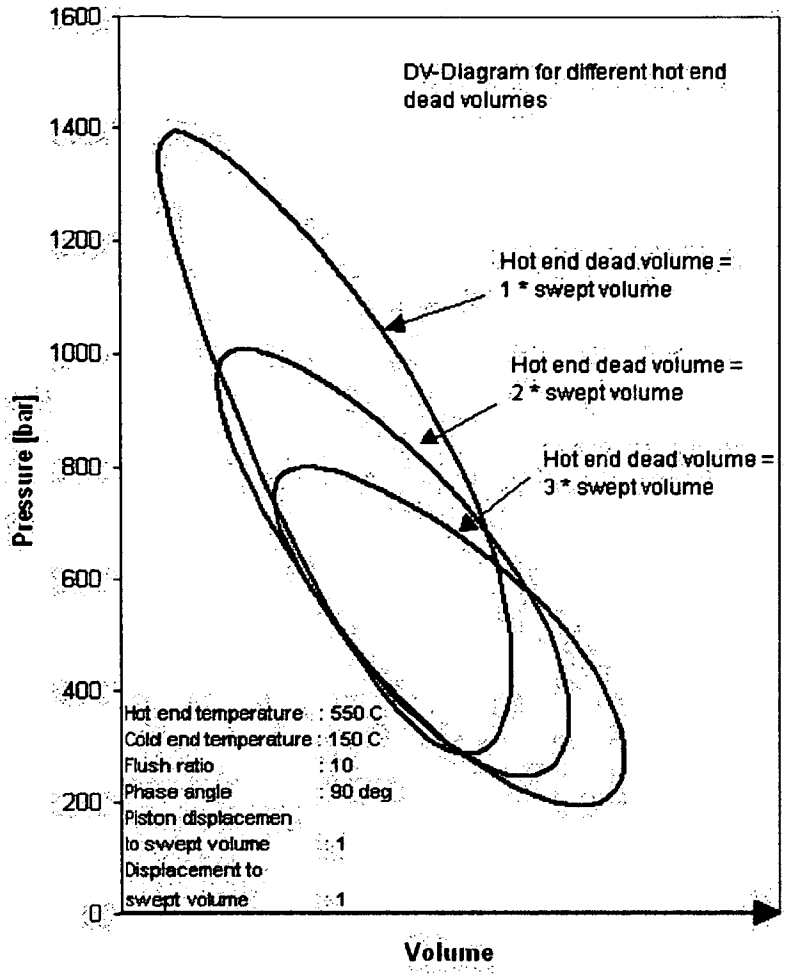


Figure 6.5 Results from the simulation showing the effect of change in hot-end dead volume on the PV-diagram.

In the simulation it was found that for a phase angle of 90 degree, a hot-end dead volume of at least three times the swept volume is required to keep the working pressure within the same limits as in Malone's engine of 800 bar. Any smaller dead volumes result in increased maximum cycle pressures.

The second simulation was done over a range of phase angles varying from 90 to 30 deg. The hot-end dead volume was held constant at two times the swept volume and an equal working piston and regenerator displacement ratio was used.

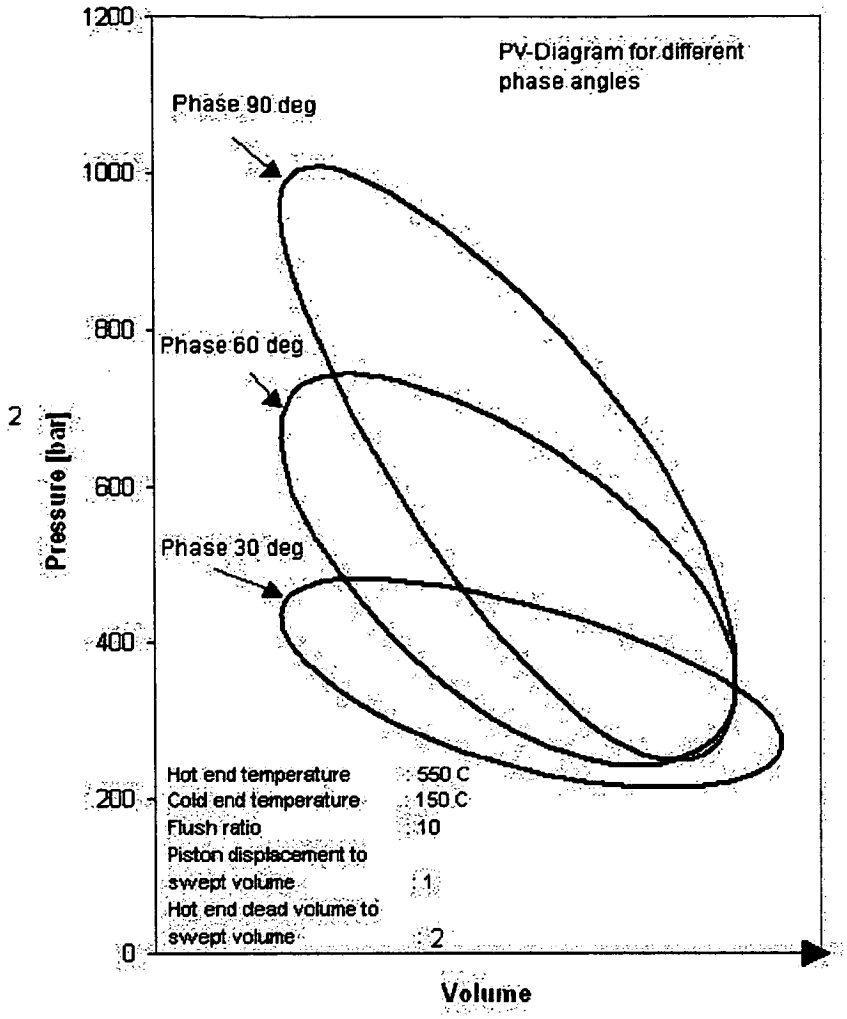


Figure 6.6 Results from the simulation showing the effect of change in phase angle on the PV-diagram.

With this simulation it was found that a significant reduction in the peak cycle pressure is achieved through reduction of the phase angle. If the phase angle is reduced to 30 degrees it is possible to keep the peak cycle pressure to less than 500 bar. The reason for this is found in the reduced differential motion between the working piston and regenerator, at reduced phase angles. A small phase angle results in a reduced rate of compression when the regenerator is at its top dead center and there is the least of compressible fluid in the system.

The third simulation was done over a range of working piston displacements varying from half to twice the displacement of the regenerator. The hot-end dead volume was held constant at two times the swept volume and a fixed phase angle of 90 degrees was used.

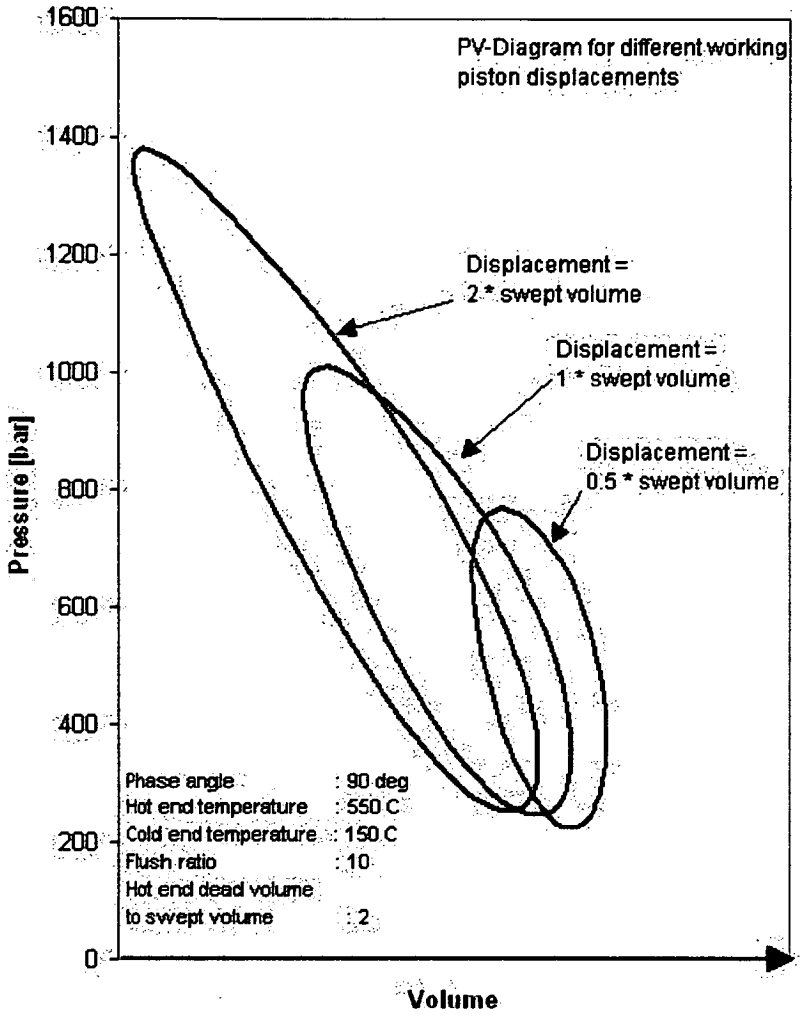


Figure 6.7 Results from the simulation showing the effect of change in working piston displacement on the PV-diagram.

With the reduction in working piston displacement the absolute change in cycle pressure falls but the pressure change in relation to the displacement increases resulting in a slim, high PV-Diagram. It can be assumed that a decrease in phase angle and increase in hot-end dead volume are more efficient ways of reducing the peak cycle pressure.

6.1.1 Digital displacement power-take off system

The subject of the digital displacement technology has been thoroughly covered by Rampen and Salter (1990; 1994; 1995) and, therefore, this description is limited to the parts that are required for the basic understanding of the system.

The Artemis Digital Displacement^{TM} pump motor is based on a multi-cylinder piston machine. The inlet and outlet valves of each cylinder are of poppet type and controlled by solenoids. Figure 6.8 shows a piston-cylinder group with its solenoid controlled low and high pressure valves. With the help of microprocessor-control, it is possible to command each cylinder to function in one of five distinct modes:

Idle: neither the high-pressure nor the low-pressure valve is activated at any point in the cycle. The low-pressure valve remains latched open and the high-pressure valve remains shut. The fluid is displaced in and out off the low-pressure gallery. The flow losses are minimal.

Full Pump: the solenoid in the low pressure valve is activated to shut the valve at BDC and the full piston displacement is pumped into the high-pressure gallery. At TDC the low pressure valve opens and the high pressure valve fall shut.

Part Pump: the solenoid in the low pressure valve is activated to shut the valve shortly before TDC so that only a fraction of the cylinder displacement is pumped into the high-pressure gallery.

Full Motor: the solenoid in the low pressure valve is activated to shut the valve just before TDC. When the cylinder pressure has reached the pressure in the high pressure gallery, the high-pressure valve is actively opened. The high pressure valve is actively held open for the inlet stroke and falls shut shortly before BDC so that the low pressure valve can open.

Part Motor: the part motor cycle starts the same way as the full motor cycle. The high-pressure valve is then released in the middle of the inlet stroke so that only a

fraction of the full displacement is taken from the high-pressure gallery. The low-pressure valve will immediately open and the rest of the inlet stroke will be taken from the low-pressure gallery.

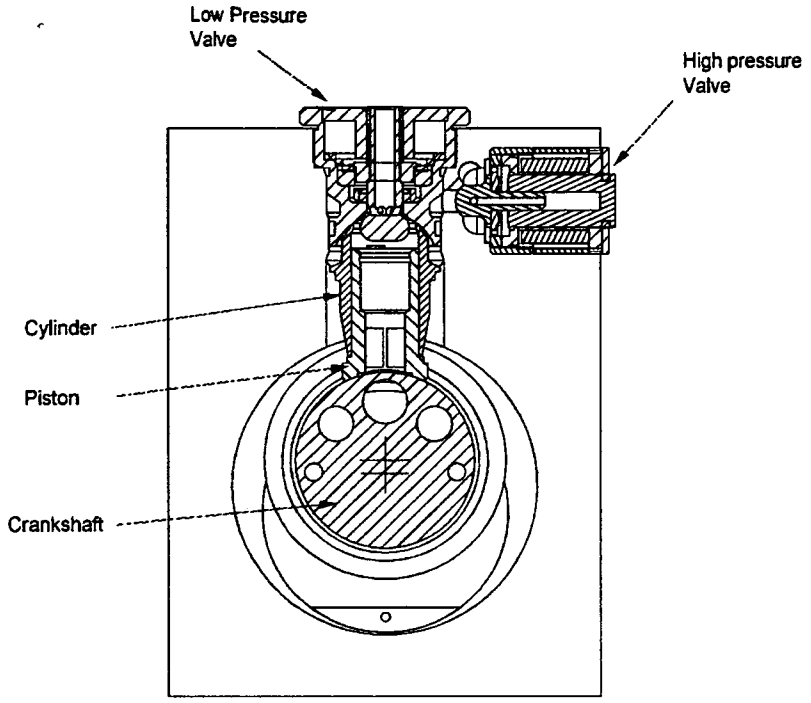


Figure 6.8. Schematic of the digital displacement pump motor arrangement. The low and high pressure valves are solenoid actuated allowing full control over displacement in each shaft revolution.

The micro controller can demand any of these five distinct modes on each shaft revolution. This enables the creation of a controllable bi-directional flow with high efficiency and fast response times. The selection of cylinders allows the output power of the pump/motor to behave like a fluid function generator capable of very high levels of power transmission.

Two different hydraulic pump motors have been produced and tested during the study. The first machine was a 12-cylinder pump motor with an integrated regenerator drive system. Each cylinder had a displacement of 2 cc giving a total of 24 cc per shaft revolution at a maximum working pressure of 200 bar. The second machine is of single cylinder configuration with 2 cc displacement. This machine can be operated with supercharge pressures of up to 200 bar on the low-pressure side of the system, allowing a maximum output working pressure of 400 bar.

An analysis of the efficiency of the digital displacement technology was carried out by N. Caldwell, as part of a separate investigation. His efficiency measurements are based on a 6-cylinder machine using the same 2cc piston-cylinder units as in the machines used in this study. The efficiencies of the machines used in this study are expected to be close to these results. The efficiency results from this study are presented in figure 6.9.

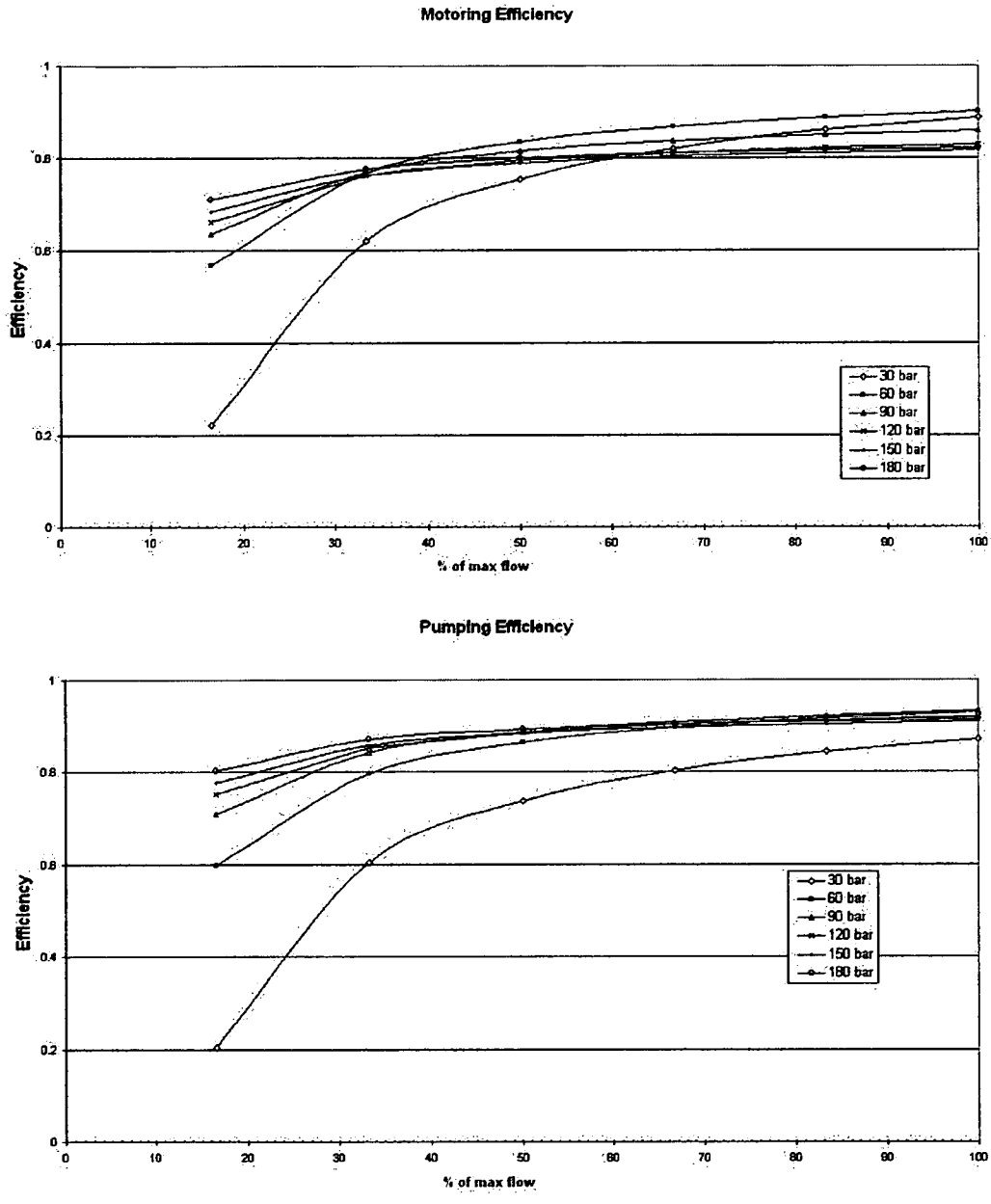


Figure 6.9. Efficiency from 6-cylinder digital displacement pump/motor. The pump motor has 2 cc displacement per piston and is operated with mineral oil at 1500 rpm. (Results are provided by N. Caldwell, Artemis Intelligent Power Ltd)

The machines show good part load efficiency down to half of the maximum output flow, which is the expected load on the machine when used in the power take-off system. The efficiency is shown to be fairly pressure independent down to a small fraction of the maximum working pressure. The efficiency in the motoring cycle is, in general, lower than the efficiency in the pumping cycle, which is a disadvantage for any power take-off system because the energy transferred in the expansion stroke is larger than the energy transferred in the compression stroke. The efficiency of the complete system is analysed later in this chapter.

6.1.2 Multi cylinder test machine

The first digital displacement hydraulic machine built during this study was designed to work as the power take-off system for the 5 kW prototype Artemis Malone engine described in the previous chapters. The hydraulic system was designed to work as a "stand-alone" system independent from the other parts of the engine. This allowed the separate development and testing of the hydraulic machine prior to testing in conjunction with the thermodynamic parts of the engine.

The key parameters were defined as:

Shaft speed	: 1500 rpm
Displacement per cylinder	: 2 cc
Number of cylinders	: 12
Pressure range at pump	: 0 – 200 bar
Working fluid	: mineral oil
Reductions gear for regenerator drive	: 10:1
No of cylinders available in each thermodynamic cycle	: 120

The layout of the hydraulic circuit can be seen in figure 6.10. Due to the 200 bar limit in maximum working pressure of the hydraulic machine it was required to intensify

the output pressure to suit that of the thermodynamic cycle. A piston type pressure intensifier was used to raise the output pressure from 200 to 350 bar, reducing the effective displacement to 1.2 cc per cylinder. The intensifier was also used as the separator between the water in the engine and the mineral oil in the hydraulic circuit and to monitor the actual displacement.

A reduction gear was mounted to the end of the pump/motor shaft and connected to an eccentric. This was then used to drive a hydraulic ram. The output from this ramp was used to control the motion of the regenerator. A double acting ram was used to decouple the high TD-Pile pressure from the regenerator drive system. A picture of the complete system is presented in figure 6.11.

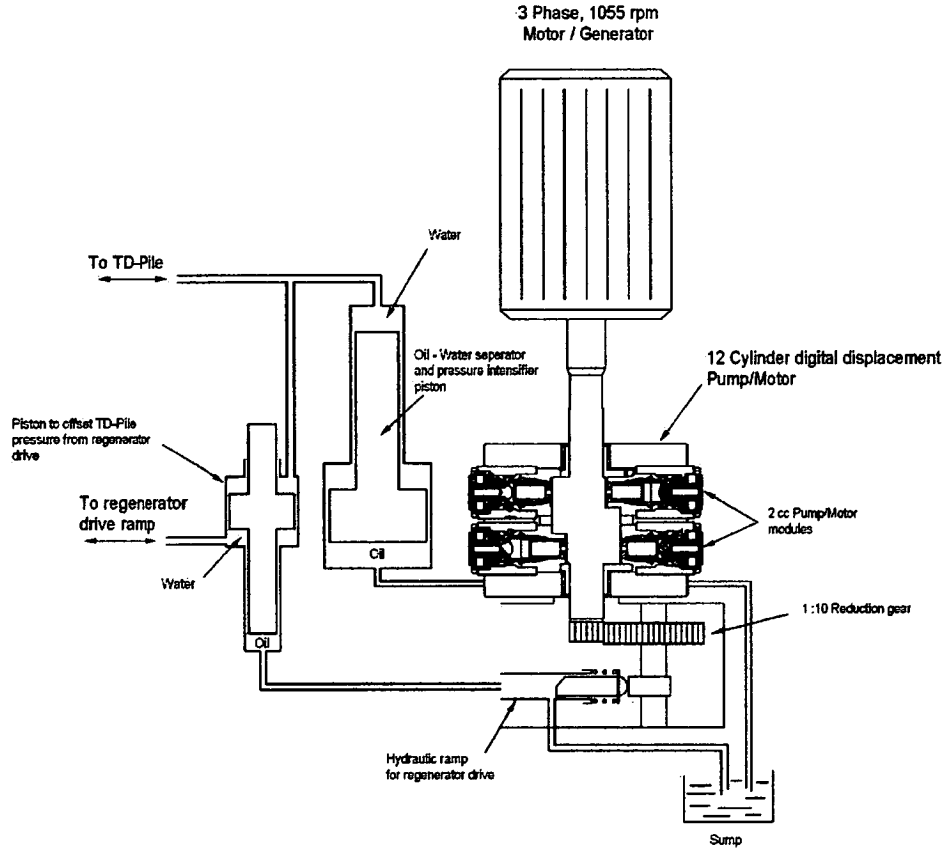


Figure 6.10. Digital displacement power take-off system for Artemis Malone engine. The 12 cylinder Pump/Motor operates at 10 times the shaft speed of the Thermodynamic Pile, allowing up to 120 pump or motor actuations in each thermodynamic cycle.

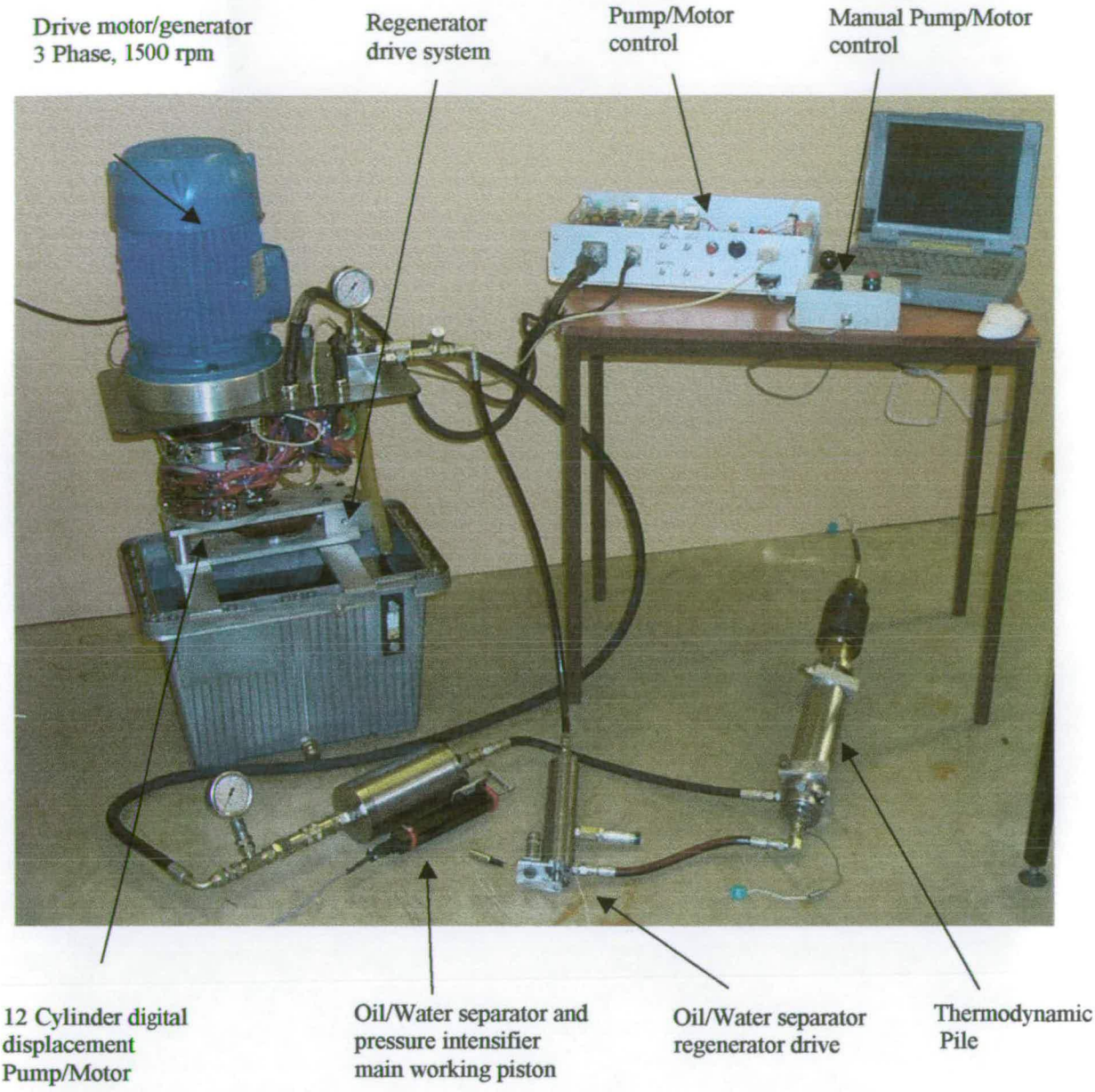


Figure 6.11. Shows this machine with the control system to the left, and the different oil water separators, and the TD-Pile to the front of the picture.

Software control

The software control of the pump motor for the power take-off system was mainly developed by J. Almond, Artemis Intelligent Power Ltd. Only a brief description of the complex control system is made at this point.

The control system for the pump/motor is based on two Intel 196 microprocessors each controlling a bank of 6 cylinders. The software is written in C allowing full control over the function of each of the 120 cylinders available during each thermodynamic cycle. The software is then able to choose one from up to ten

different lookup tables to generate each thermodynamic cycle. Each lookup table consisted of an array of 120 lines defining the relevant mode for each of the available cylinders. The decision on which table is to be used for the next cycle is made as a result of external settings and depends on the system pressure and the separator position measurement. This arrangement allowed the selection from a number of different motion profiles and the use of pressure and position feed back in order to control the system between certain position and pressure limits.

Due to the problems with the regenerator in the TD-Pile, it was never possible to demonstrate the extraction of power from the engine. It was possible, however, to use the compressibility of the supercritical fluid in the hot-end as a load, and to use the different lookup table to create different motion profiles and pressure curves. Figure 6.12 shows the displacement results from a test.

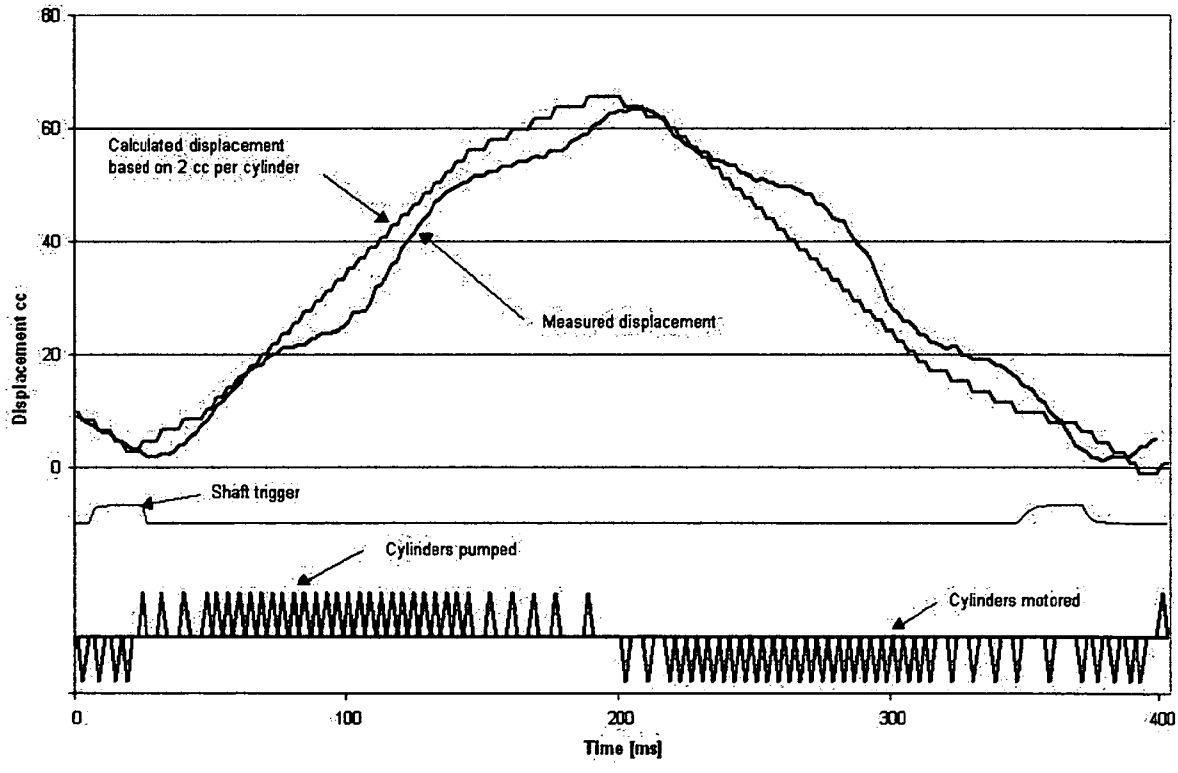


Figure 6.12. Calculated and measured separator motion profile of intensifier piston. 32 of the 120 cylinders available were pumped and 37 were motored to compensate for the difference in volumetric efficiency.

From the displacement measurements, it can be seen that the pump/motor is able to follow the theoretical displacement closely. The error between the measured and the calculated displacement might be a combination of variation in cylinder efficiency and inaccuracy in the position measurement. In further tests it was possible to show that the system is able to create any other motion profile with the limitation of the maximum slope angle limited by the maximum output flow-rate of the machine.

With the efficiency results presented in figure 6.9 it is now possible to predict the efficiency of the system when it is connected to a working TD-Pile. We can presume that the use of 50% of the number of available cylinders gives enough resolution to create most motion profiles. The maximum cycle pressure is restricted to 350 bar by the maximum pressure capability of the system. The minimum pressure of 220 bar is dictated by the critical pressure of water. The pump/motor efficiency at these flow rates and pressures are ~ 85% for the motoring cycle and ~ 90% for the pumping cycle. In the ideal case, with the pressure during the compression stroke at the critical pressure, and during the expansion stroke at the maximum pressure, equation 6.2 predicts a system efficiency of around 41%.

$$\eta_{system} = \frac{350 * 0.85 - 20 * 1/0.9}{350 - 220} = 0.41$$

In reality it is unlikely that it is possible to maintain constant pressures during the compression and expansion stroke, resulting in a further reduction in efficiency. Even with improvements to the efficiency of the pump/motor it is unlikely that acceptable system efficiencies would be achievable with the current set up. As a result an investigation into different methods to overcome this problem was undertaken. A system was proposed which uses an increased tank pressure to offset the high bottoming cycle pressure. Such a system is described in the following section.

6.1.3 Digital displacement with elevated tank pressure

One way to overcome the fundamental problem of reduced efficiency through high bottoming cycle pressure is by lifting the tank pressure of the pump/motor with the help of an extra boost pump. With the help of an accumulator, it is then possible to maintain a fairly constant pressure in the crankcase during a cycle with the boost pump only being required to replace any leakage. By setting the tank pressure to the minimum cycle pressure, the work output in the expansion stroke becomes significantly larger in relation to the work transferred during the compression stroke. This results in a take-off efficiency close to the motoring efficiency of the pump/motor.

In the framework of a different study done by the author, a single cylinder test machine with elevated crankcase pressure was constructed. This machine was of single cylinder nature and had, therefore, a much smaller bandwidth than the 12-cylinder machine. At the maximum possible shaft speed of 2500 rpm it was, however, still possible to create motion profiles of up to 3 Hz.

The machine used the same piston-cylinder and valve arrangement as the multi-cylinder unit and the efficiency of this machine was expected to be similar to that of the multi cylinder machine. As a result of pressurizing the complete system, the forces on the bearings and the leakage flows in the machine were not affected. The pumping and motoring efficiency was, therefore, presumed to be the same as in the non-pressurized machine. A small increase in idle losses, however, occurred as the result of the power consumption from the boost pump, which had to return oil leakage from the drive shaft seal. Figure 6.13 shows a picture of the single cylinder test rig and the hydraulic flow diagram.

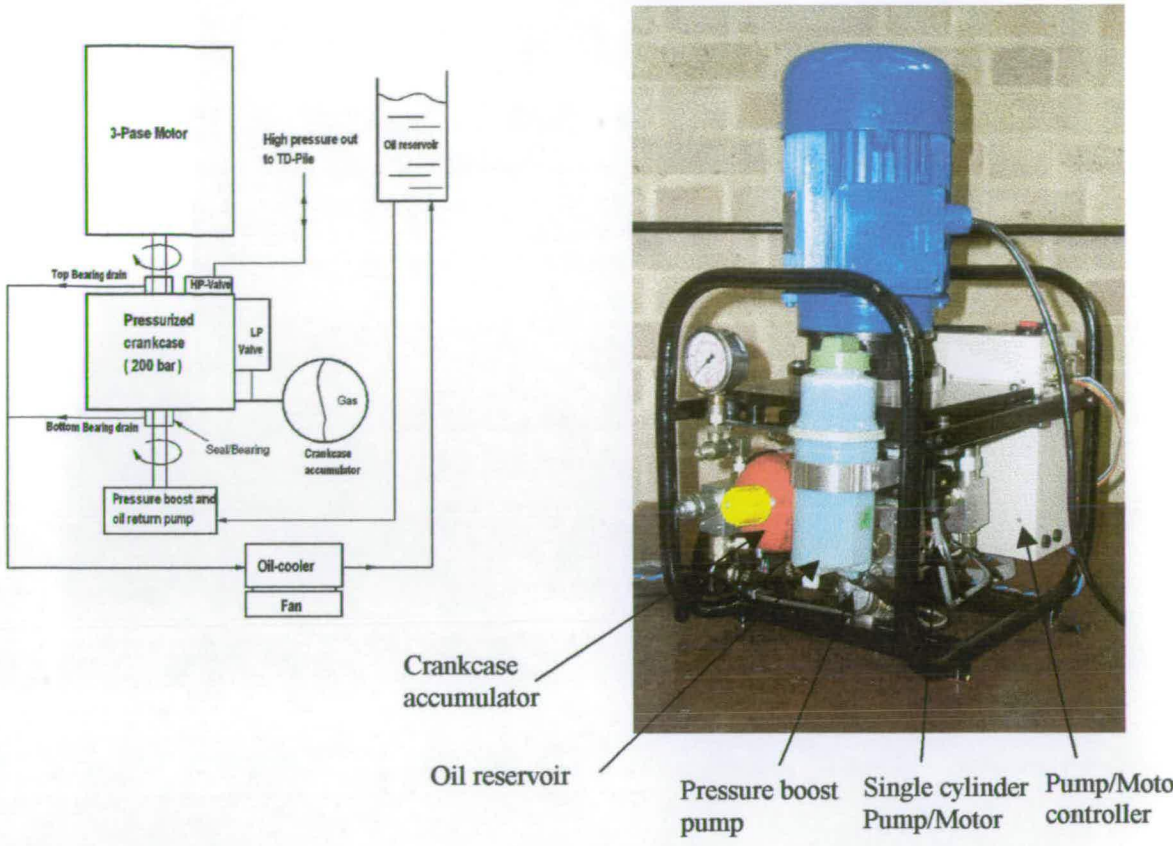


Figure 6.13. Hydraulic circuit and photo of the single cylinder digital displacement Pump/Motor with elevated crankcase pressure. The crankcase pressure could be lifted to a maximum of 200 bar allowing output pressures of up to 400 bar. The Pump/Motor could supply flow of up to 6 l/min at 300 rpm shaft speed.

6.1.4 Test results

A large number of tests were carried out with the super charged test pump which showed that the increase of the tank pressure had no effect on the operation of the digital displacement technology. It was further found that the tank pressure does not significantly affect the volumetric efficiency of the pumping and motoring cycle.

To assess the performance of the super charged system tests have been carried out, whereby, the output from the pump/motor was connected to a gas filled accumulator. The size and pre charge of the accumulator was chosen so that the pressure changes in the accumulator were similar to that in the engine. Figure 6.14 shows the measured pressure change in an accumulator for a flow demand of 1 and 3 Hz.

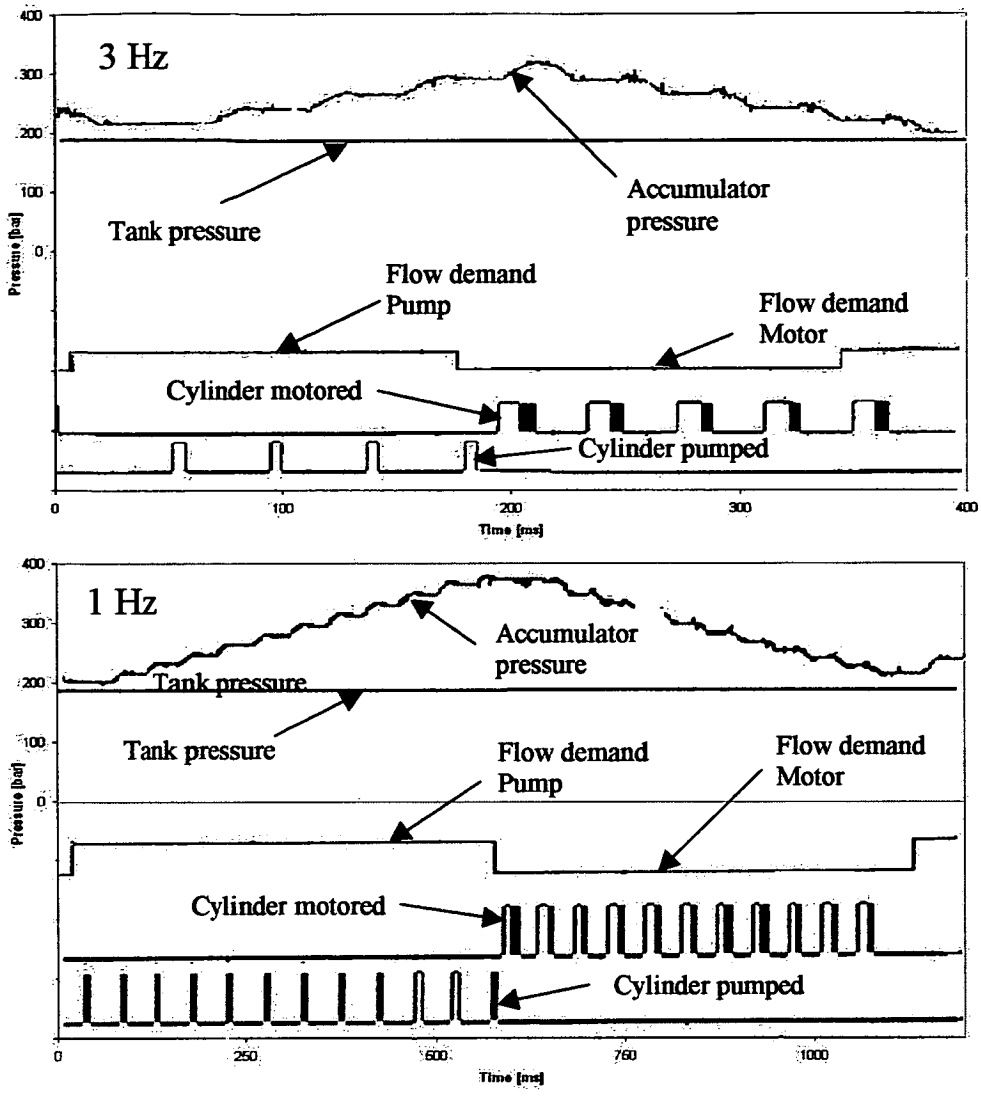


Figure 6.14. Test results from single cylinder Pump/Motor. The output from the pump motor has been connected to an accumulator and the pressure change was recorded for a flow demand of 1 and 3 Hz.

It is possible to calculate the system efficiency by referencing the compression and expansion stroke pressure to the increased tank pressure. This has been done for a tank pressure of 200 bar with, otherwise, the same conditions as in the example on the 12-cylinder machine. The relative expansion pressure then becomes 150 bar, with a motoring efficiency of 80% and the relative compression pressure becomes 20 bar, with a pumping efficiency of 70%. The calculated system efficiency using equation 6.3 is then 71%

$$\eta_{system} = \frac{150 * 0.8 - 20 * 1/0.7}{150 - 20} = 0.71$$

The system with the increased tank pressure shows clear advantages of over the non-pressurized system, which showed a system efficiency of only 41%. A power take-off efficiency of 71% is certainly still too low for use in an engine. It is important to realise, however, that the hydraulic machines are still in the development phase and an increase of efficiency due to improvements in material choice, bearing arrangements and general tolerances is expected.

6.4 Crank drive power take-off system

This section will show some of the general design concepts for crank arrangements in the Malone engine, proposed during the study. The high bottoming pressure has already been identified as one of the fundamental problems in the Malone cycle engine. This will not only result in increased losses for any mechanical piston arrangement, it will also result in large reverse torque on the output shaft during the compression stroke. This is, in principle, no different to any other Stirling engine, but the effect becomes more significant with a smaller ratio of peak to minimum cycle pressure. The maximum pressure in the proposed engine is, with only 350 bar, 1.6 times larger than the minimum cycle pressure of 220 bar. This results in a large reverse torque during the compression stroke.

In general it is possible to reduce the torque reversal through the use of multi-cylinder double-acting machines. For single cylinder machines there is the need for large shaft inertia to provide the required compression energy. This is especially problematic at the low shaft speeds expected of Malone engines.

In the following section a comparison of the conventional simple crank arrangement, as used by Malone, with two further configurations using extra pistons to reduce the reverse torque is made.

6.1.5 Conventional crank arrangement

An AMESim® computer model has been made to predict the force on the working piston and the torque on the output shaft. The model presumes a sinusoidal change of system pressure with the peak pressure in the middle of the working stroke. Initially, a simple crank piston arrangement, as used by Malone, was analysed. The general arrangement of the engine and the results from this simulation is shown in figure 6.15.

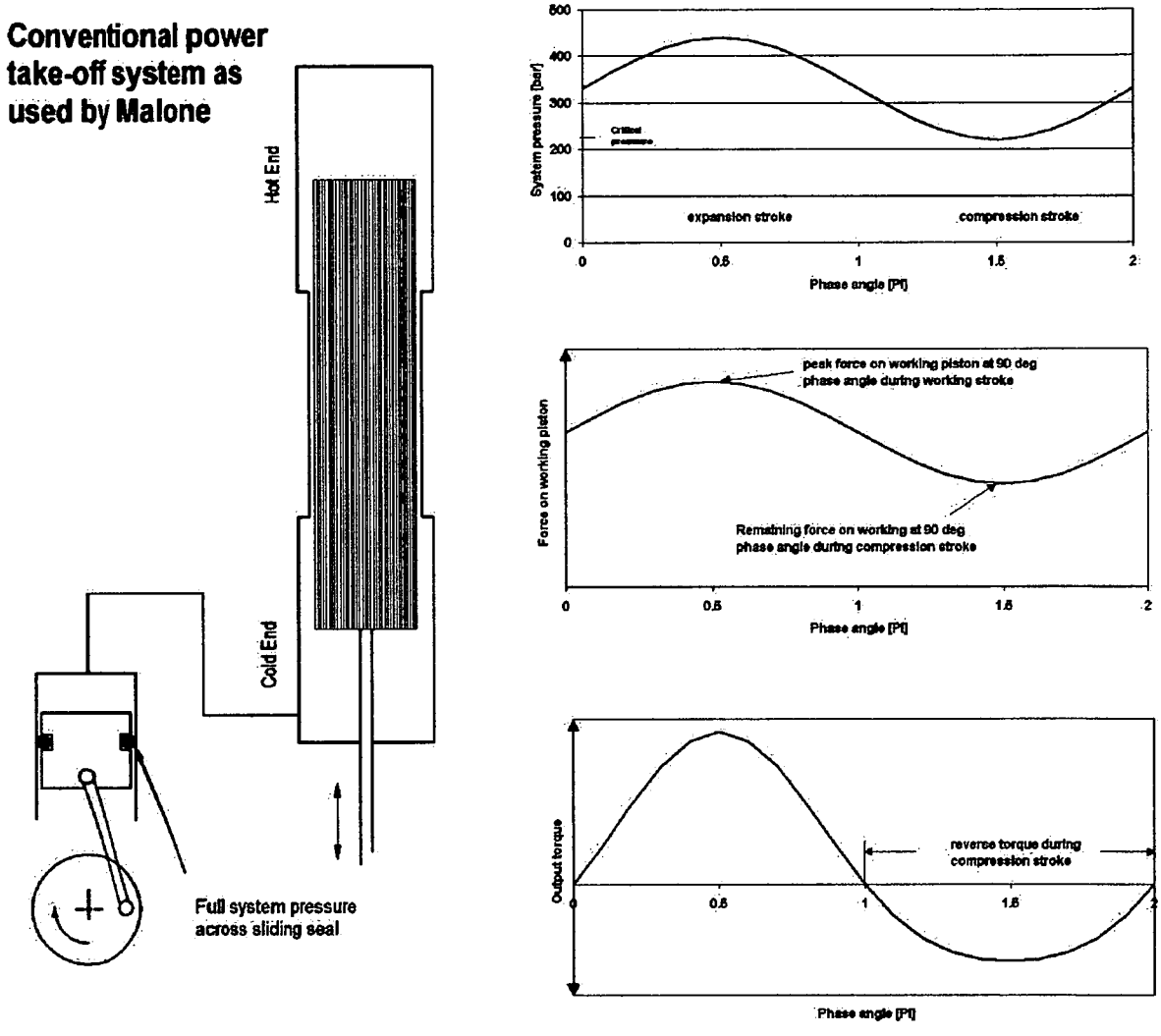


Figure 6.15. The conventional crank arrangement for the working piston, as used by Malone, can be seen to the left of the figure. The force on the working piston and torque on output shaft during the cycle are shown to the right of the figure.

From the results presented in figure 6.15, it can be clearly seen that the required work for the compression stroke is a large fraction of the work output in the expansion stroke. In the proposed engine with a peak to bottom pressure ratio of 1.6, the maximum reverse torque is 62 % of the maximum positive torque! Malone`s original engine had a peak to mean pressure ratio of 3.4 resulting in a maximum reverse torque of only 30% of the maximum positive torque. His engines still had to work with large flywheels to ensure smooth operation at the low shaft speeds.

Two different arrangements to overcome this fundamental problem are presented in the following section.

6.1.6 Partially balanced piston arrangement

The partially balanced piston arrangement uses the principle that an accumulator, connected to the working pressure through a flow impedance, adjusts to the mean cycle pressure over a number of shaft revolutions. The impedance has, to be chosen in a way that allows the accumulator to adjust fast enough to mean cycle pressure changes during operation, but is small enough that the flow through the impedance during one cycle is minimal to avoid throttling losses. In the partially balanced system, the mean pressure from the accumulator is then applied to the crankcase side of a double-acting working piston reducing the otherwise large reverse torque from the compression stroke.

Figure 6.16 shows schematic of this arrangement and also illustrates the resulting force on the working piston and torque in the output shaft as a function of the rotation.

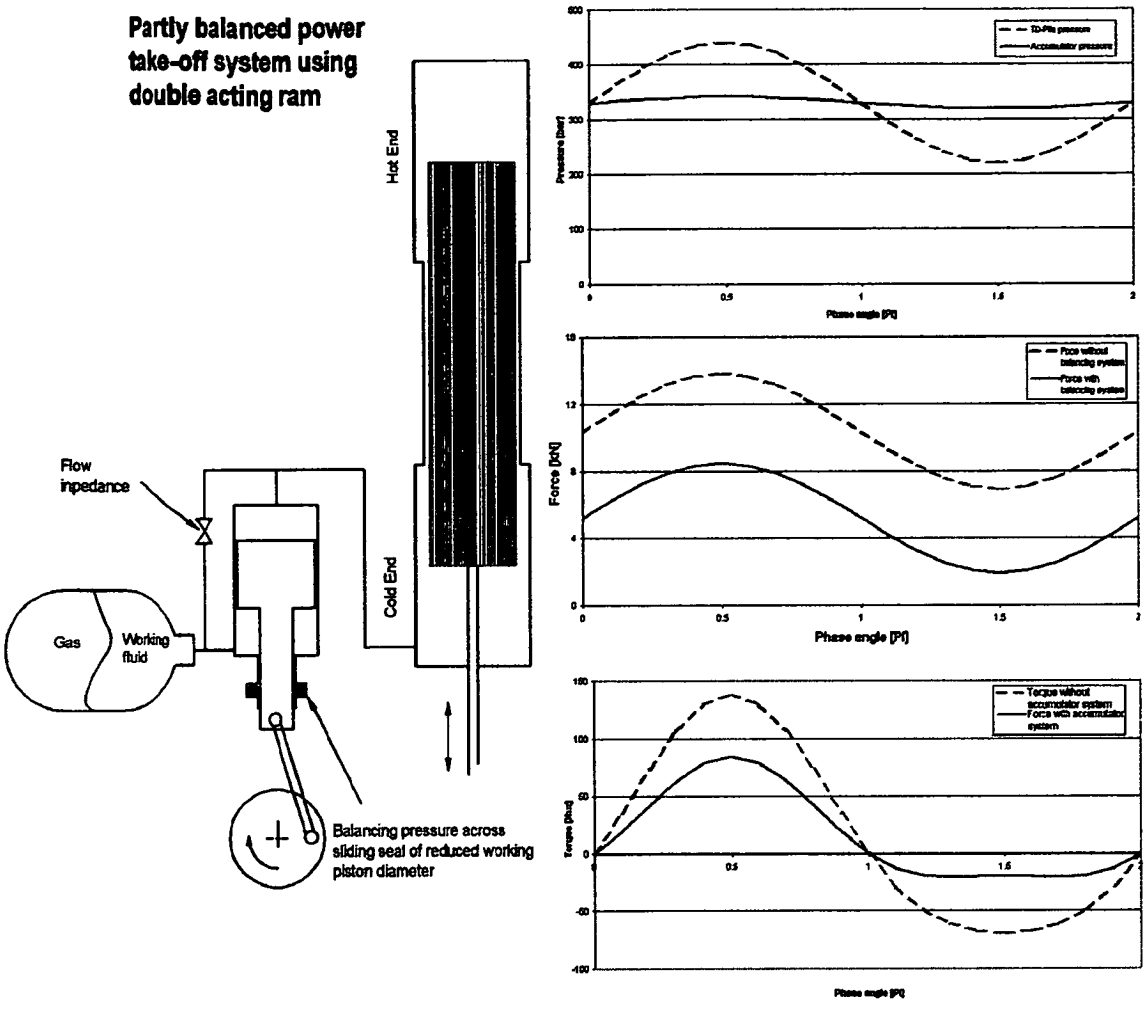


Figure 6.16. The part-balanced piston arrangement can be seen to the left of the figure. The force on the working piston and torque on the output shaft during the cycle are shown to the right of the figure.

It can be clearly seen that, compared to the conventional system, a drastic reduction in reverse torque is achieved. A further advantage of this system is the reduced seal friction due to its smaller seal diameter and, therefore, an increase of efficiency. The sealing on the main working piston uses a simple sliding fit, with the mean cycle pressure from the accumulator on the crankcase side. Any leakage will, in principle, occur in equal amounts in both directions. Practically, it might be possible to use the leakage from a simple sliding fit between cylinder and working piston as the impedance to adjust the accumulator pressure thus eliminating the need for an extra

external impedance. The remaining seal on the drive rod is of smaller diameter and, therefore, reduced friction losses can be expected.

In the partially-balanced system the area of the balancing piston is chosen so that it offsets most of the force in the compression stroke, but remains a positive force on the working piston during the cycle. The advantage of this design over any design where the area of the offsetting piston is chosen to create negative force on the working piston is the more flexible choice of mechanical linkages between the piston and the drive shaft. If a positive force is maintained at all times, it is possible to work with a cam type eccentric which allows the creation of non sinusoidal motion profiles. As we have seen earlier in the chapter, this is an important aspect if the engine operates with small regenerator and hot-end dead volumes. Figure 6.17 shows the part balanced arrangement with a cam type eccentric.

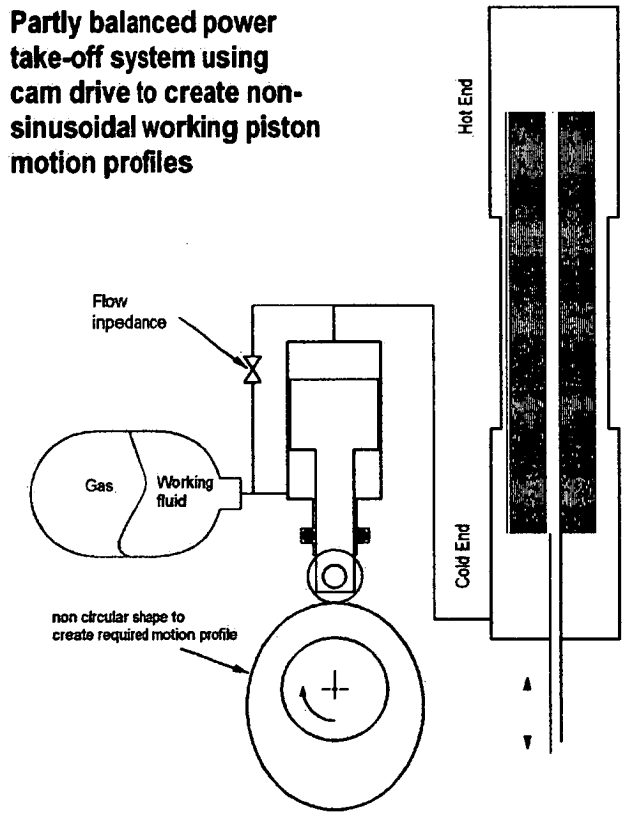


Figure 6.17. Maintaining a positive force on the working piston during the cycle allows the use of cam type eccentrics to create non-sinusoidal piston motion profiles.

To guarantee a positive force on the working piston during the cycle, the area ratio between the offsetting piston and the working piston must not exceed the pressure ratio between mean cycle pressure and minimum cycle pressure.

$$\frac{A_{offset}}{A_{working}} \leq \frac{P_{minimum}}{P_{accumulator}} \qquad 6.5$$

If we presume a symmetrical PV-Diagram in the proposed Artemis Malone engine, it is possible to estimate the mean cycle and, therefore, the mean accumulator pressure. With a maximum cycle pressure of 400 bar and a minimum cycle pressure of 220 bar the mean cycle pressure becomes 310 bar. This results in an area ratio between the offsetting and the working piston of 1:1.4 . In other words the area of the working piston must be at least 1.4 times that of the offsetting piston, if a positive force is to be maintained during the cycle.

6.1.7 Fully-balanced piston system

The fully balanced piston system uses the same basic principle as the partially balanced system. Again, an accumulator is connected through an impedance to the working fluid so that the pressure in the accumulator levels around the mean cycle pressure. In contrast to the part balanced system where a positive force on the main working piston is maintained at all times, the fully balanced system creates alternating positive and negative forces on the working piston. The working piston is then working in push and pull mode. Practically, this can be done through the use of the crankcase and the far side of the working piston allowing the working piston and the balancing piston to have the same area. It is then possible to connect the crankcase to the working pressure and the far side of the piston to the mean pressure from the accumulator, or the reverse of this. As in the partially balanced system, it is not important to achieve a perfect seal between the working piston and the cylinder. The sealing problem in this arrangement is reduced to a single seal on the main shaft. When the TD-Pile is connected to the crankcase, the shaft seal for the regenerator drive and the main shaft can become one.

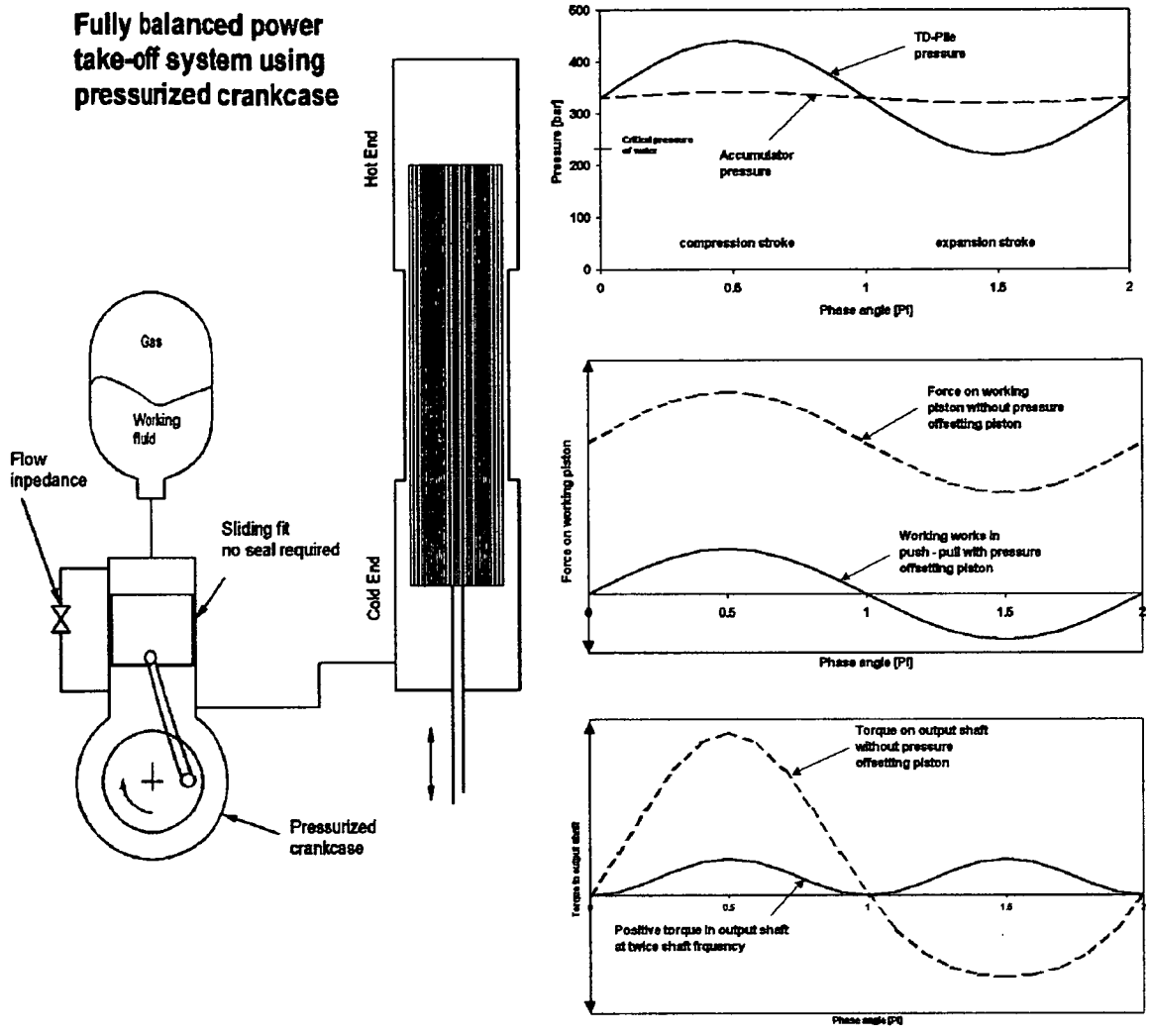


Figure 6.18: The fully-balanced piston arrangement can be seen to the left of the figure. The force on the working piston and torque on the output shaft during the cycle are shown to the right of the figure.

It can be seen that the force on the working piston becomes negative as a result of the accumulator pressure being higher than the minimum cycle pressure and the working and offsetting piston having the same area. This results in two positive output torque ripples within one cycle, and the complete elimination of any reverse torque during the compression stroke.

The disadvantage of this arrangement compared to the part balanced system is that it is not possible to use a simple cam arrangement to create non-sinusoidal working piston profiles.

6.5 Summary and conclusion

The results from the different power take-off systems presented in chapter 6 show that the high bottoming pressure and low compressibility of the working fluid in the cold-end requires a different power take off system from that used for the Stirling engine.

It was found that the efficiency of the power take-off system can be drastically reduced when working with a low ratio between the maximum and minimum cycle pressures. This is particularly a problem in engines using fluids with a high critical pressure as the working fluid.

It was further found that the use of sinusoidal regenerator and piston motion profiles resulted in unacceptably high pressures towards the end of the compression stroke where most of the working fluid is in the liquid state and, therefore, incompressible.

It was possible to show that an increase in hot-end dead-volume and a reduction in phase angle between the regenerator and the working piston can be used to reduce the maximum cycle pressure.

Crank arrangements and the Artemis digital displacement^{TM} power take-off system were analysed. The results from the different digital displacement pump/motors made during the study suggests that it is possible to create the required power take-off piston motion profiles. The efficiency of the power take-off system in the example of the proposed engine was found to be around 50%. An increase to around 70% could be achieved by supercharging the pump/motor to 200 bar.

The conceptual study on a number of different conventional crank type power take-off systems suggests that a significant reduction in reverse torque and seal friction can be achieved by partially or fully balancing the force on the working piston.

To which extent the increased control over the motion profile with the digital displacement solution justifies the increased complexity over the partially or fully balanced piston arrangement has still to be analysed.

It might further be possible to combine the two solutions, whereby the fully balanced piston arrangement produces a sinusoidal motion profile covering most of the required displacement. A smaller digital displacement pump/motor is then applied to correcte the sinusoidal motion profile to the required optimum motion profile. This system would have the advantages of a simple and efficient crank drive with the ability to create the optimum motion profile.

7 Conclusion and further recommendations

7.1 Summary

The design of the Artemis Malone engine has been studied and a preliminary analysis of the main components in the engine has been made. The different novel ideas that have been proposed for the engine are investigated and their operating characteristics analysed. It was possible to gain fundamental understanding of both the advantages and limitations of the Malone engine technology.

7.2 Conclusion

Separate, detailed conclusions can be found in the relevant sections of each chapter. At this point, a short summary of the main findings will be made. Following this, recommendations for further work are made.

Combustion system

A combustion system using propane gas as fuel has been built and experiments have been conducted using a water-cooled dummy hot-end heat exchanger. Results suggest that it is possible to achieve the required high heat transfer rate into the hot-end of the Malone engine, while keeping the production of NO_x and the gas flow losses to a minimum. It has be shown that the combination of combustion gas recirculation (**CGR**) and exhaust gas recirculation (**EGR**) offers a way of increasing the heat transfer into the hot-end, while creating an uniform temperature profile in the combustion chamber. With the prototype combustion system, it was possible to demonstrate this and to quantify the heat transfer into the hot-end.

Hot-end heat exchanger

A number of different hot-end heat exchangers have been made and analysed with regard to their corrosion, fatigue and heat transfer properties. The results from tests of the initial design, made from copper and inconel, suggest that it is not possible to provide sufficient corrosion protection for the copper and to guarantee a reliable seal

between the different materials. It was further found that the low creep strength of Copper at temperatures over 600°C requires designs where the copper is not used under the slightest stress.

Results from further development work on hot-end heat exchangers made from Monel K500 and Molybdenum TZM showed that it is possible to transfer the required heat flow into the engine with an acceptable temperature drop from the combustion gas to the supercritical water. It was further possible to find ways to protect these hot-end heat exchangers against corrosion. Substantial difficulties were experienced in maintaining a seal between the different hot-end heat exchanger parts and the TD-Pile structure. Initial tests, using friction welding, to join the relevant parts showed good results both in sealing and in structural behaviour.

Regenerator

The study of the TD-Pile identifies the regenerator as the most problematic component in the Malone engine. It can be shown that it is not possible to use designs such as those typically found in Stirling engines.

In the Malone engine, a high ratio of regenerator matrix volume to the swept volume is required. This is due to the high heat capacity of the working fluid. For regenerator designs of low packing ratios, for example made from wire mesh, this results in large regenerator dead volumes, which reduces the amplitude of the fluid motion in the regenerator. This then causes a decreased temperature swing in the working fluid resulting in hugely increased irreversible regenerator losses.

Very high regenerator packing ratios of over 90% are required to achieve the necessary small dead volumes to minimize this effect. This results in the need for small hydraulic diameters in the flow channels, requiring more sophisticated designs to avoid increased pumping losses.

An investigation analysing Malone`s original regenerator was undertaken. It was found that the valves used in Malone`s original regenerator were necessary to

overcome the limitation of reduced temperature swing of the fluid. This allowed the efficient operation of a regenerator with significantly larger dead volumes.

A theoretical optimisation on the regenerator system for the proposed engine was carried out. This optimization was primarily concerned with regenerators constructed from coiled shim metal. The optimum regenerator parameters using water, as the working fluid, a hot-end temperature of 600°C and cold end temperature of 200°C were found to be as follows:

- The optimum regenerator matrix mass was found to be 50 to 100 times larger than the swept working fluid mass. A further increase in matrix mass from this point onwards showed little further gains in the reduction of irreversible losses due to reduced temperature swing of the matrix material. These gains were then outweighed by the increased thermal conductivity losses.

- The optimum regenerator length to diameter ratio was found in the region of 1 to 1.5. The gains in reduced flow losses for a shorter regenerator length are outweighed by the increase in thermal conductivity losses.

- The optimum for the hydraulic diameter of the flow channels was found in the region of 0.01 - 0.02 mm. At this point a high heat transfer coefficient, together with acceptable regenerator dead volumes and pumping flow losses was achieved.

- A matrix shim thickness in the region of 0.2 mm was found as the optimum for stainless steel as the matrix material. At this thickness a Biot number of less than 0.2 is maintained and an adequate surface area provided.

Hydraulic power take-off system

Two aspects, specific to the power take-off system for the Artemis Malone engine, were analysed.

(i) With a theoretical model it can be shown that, in the Malone engine, it is not possible to use the same sinusoidal regenerator and working piston profiles as typically used in the Stirling engine. The working fluid, present in the compression space during the compression stroke, is liquid and, therefore, cannot be compressed. To overcome the problem of the resulting large pressure peaks the system has either to be operated with non-sinusoidal working piston motion profiles or to have extra compressibility in the system.

(ii) It was found that, for efficient operation of the regenerator, evaporation and condensation of the working fluid must be prevented. To avoid this, the working pressure has to be maintained above the critical pressure throughout the cycle. 220 bar, the critical pressure of water, sets the minimum cycle pressure. With the maximum cycle pressure limited by the hot strength of the materials used in the engine, this can result in a limited ratio of mean expansion stroke pressure to mean compression stroke pressure. It was found that, the extra losses encountered from the relatively high pressure in the compression stroke, can cause a significant reduction in the power take-off system efficiency. It was possible to show that biasing of the working piston, to the pressure level of the compression stroke, offers a way to reduce these losses.

With the different Artemis digital displacement machines, made during the study, it was possible to show that the required motion can be achieved using this technology. It was further possible to demonstrate that the digital displacement technology can be operated with an elevated reservoir pressure. Significant efficiency improvements could be achieved by offsetting the pump/motor reservoir to the compression stroke pressure and to pump and motor in reference to this pressure.

7.3 Recommendation for further work

i. The regenerator is the element with the most influence on the efficient operation of the engine. Further work in this area is crucial in the development process of the Artemis Malone engine. An experimental investigation to validate the theoretical model would be of importance. It is recommended that these experiments are carried out in a test rig, which allows the independent measurement of the thermal regenerator efficiency and pumping losses. This for example could be done in a test rig with an electrically heated hot-end, allowing the accurate measurement of the heat input. Further a force or differential pressure transducer could be used to measure the flow losses in the regenerator.

ii. While it was possible to demonstrate that the digital displacement power take-off system can produce the required working-piston motion profiles, it was found that the efficiency of the system was insufficient to be used in a practical engine. It is suggested that an investigation into the different loss sources should be made, thereby the maximum efficiency of future systems may be determined.

iii. The low overall efficiency of the combustion system of 72% was found to be a result of the high exhaust gas temperature. A significant increase in the combustion system efficiency might be achieved with the installation of a further exhaust-gas heat exchanger. An investigation, which determines the extent to which this is practically feasible and cost effective, is recommended.

iv. Due to the problems experienced with the regenerator is was not possible to analyze the heat transfer in the hot-end heat exchanger under the same flows, temperatures and pressures as expected in the final engine. The construction of a test setup, which allows the simulation of these conditions, independent from the functioning of the regenerator, is recommended. This test setup could use the same combustion system as the proposed engine uses, but would use external pumps and heat exchanger to reproduce the required conditions inside the heat exchanger.

v. In mobile applications there might be the requirement to protect the engine against damage from freezing of the working fluid. An examination into possible areas were damage would occur and an investigation into ways to overcome these should be undertaken.

References

Allen P.C., Knight W.R., Paulson D.N. and Wheatley J.C. (1980), "Principals of liquids working in heat engines" *Proceedings of the National Academy of Sciences,* Vol 39, 1980

AMESim® 4.0.1 (2002), "Modeling and simulation environment for systems engineering" Imagine SA, 42300 Roanne, France, 2002

Asselman G.A.A. and Green D.B. (1973), Philips Tech. Rev., P. 138-148, 1973

Brey H.de (1942), Netherlands Patent. No. 51975, 20 April 1939

Carlqvist S.G. (1977), " Developing the Stirling engine for fuel economy" 12th Int. Cong. Combustion Eng., Tokyo

Commanday M. (1963) US Patent No.: US 3 090 702 A (21 May 1963)

Copper Development Association (1994), "CD-Rom: Megabytes on Copper" Copper Development Association, Herfordshire, UK

Dunn P.D, Rice G. and Thring R.H (1975), "Hydraulic and Rotary Drive Stirling Engines with Fluidxised Bed Combustion/Heat Pipe System",*10th Inter-society Energy Conversion Engineering Conference*, Paper No. 759141, pp. 942-947, Newark NJ USA, 1975.

Eguchi K., Fujii S. and Gomi M. (1984) "A design approach to Stirling burners with intese combustion" Proc. 2nd international conference on Stirling engines, Shanghai, China

Ehsan Md, Rampen W.H.S. and Taylor J.R.M (1995), "Simulation and Dynamic Response of Computer Controlled Digital Hydraulic Pump/Motor System Used in Wave Energy Power Conversion", *2nd European Wave Power Conference*, pp. 305-311, Lisbon, 8-10 Nov 1995.

Ehsan Md, Rampen W.H.S. and Salter S.H. (1996), "Computer Simulation of the Performance of Digital-Displacement Pump-Motors" *ASME International Mechanical Engineering Congress and Exposition*, FPST Volume-3, pp.19-24, Atlanta Nov. 1996.

Ehsan Md, (1997), "A new type of Malone Engine with Digital-Displacement Hydraulic Drive" Ph.D. thesis, University of Edinburgh, Scotland, 1997

Finkelstein T (1960), "Generalized Thermodynamic Analysis of Stirling Engines", SAE winter annual meeting, paper No. 118B, 1960.

Finkelstein T. (1975), " Computer analysis of the Stirling Engine" Proc. 10th I.E.C.E.C., pp.933-941, Newark, N.J., Aug. 20 - 25

Finkelstein T. (2001), Finkelstein T, Organ A. J. "Air Engines", Professional Engineering Publishing, UK 2001, ISBN 1-86058-338-5.

Ford R.A. (1983), "Secrets of the Malone Engine" Simplified Technology Services, Colombia MO

Gaugler R.S. (1944), United States Patent, no. 2350348, 1944

Greene G.A. and Finfrock C.C. (2000) "Total hemispherical Emissivity of oxidised Inconel 718", Brookhaven National Laboratory, Upton, New York, April 2000

Ghajar A. J. (1980), "Physical properties for some fluids in the supercritical region" Oklahoma University, 1980

Gianfranco A. (2000), "Real gas effects in Stirling engines" Dipartimento di Energetica, AIAA-2000-2811, Milano, Italy

Hall W. B. (1958), "Reactor heat transfer" Temple press Ltd, Bowling green lane, London, 1958

Hargreaves C.M. (1991), "The Philips Stirling Engine", Elsevier Science Publishers B.V, Amsterdam, 1991.

Hausen H. (1983), "Heat transfer in counterflow, parallel flow and cross flow" McGraw-Hill Book Company, New York

Haywood R.W. (1990), "Thermodynamic Tables in SI Units", Cambridge University Press, Cambridge, UK, 2000, ISBN 0-521-38693-4

Hidenori K., Fujiwara M. and Sigimoto T. (1992), "Study on Stirling engine combustor" 27 Intersociety energy conversion, San Diego, USA

Howard E. B. and Timothy L.G. (1984), "Metals Handbook" L.G. Asm Intl, Ohio, USA

Inco Alloy Intl, (1985a), : "INCONEL alloy 625", Inco Alloys International 1985, product catalogue, England.

Inco Alloy Intl, (1985b), "INCONEL alloy 718", Inco Alloys International 1985, product catalogue, England.

Inco Alloy Intl, (1984), "Monel alloys 400, 401, 404, R-405, K-500", Inco Alloys International 1984, product catalogue, England.

Incropera P.F. and Dewitt P.D (1990), "Introduction to Heat Transfer", 2nd Edition, John Wiley & Sons, Singapore 1990. ISBN 0-471-51728-3.

Kays W. M. and London A. L. (1964), "Compact Heat Exchangers", McGraw-Hill Book Company, 2nd Edition

Kolin I. (1972), "The Evolution of the Heat Engine" , Moriya Press, P. O. 384, River Falls, WI 54022, 1998

Malone J. F. J. (1924), "Heat engine" United States Patent No. 1,487,664, Patented Mar. 18, 1924

Malone J. F. J. (1929), "Heat engine operated by the expansion of liquids" United States Patent No. 1,717,161 Patented June 11, 1920

Malone J.F.J (1931), "A New Prime Mover", *Journal of Royal society of Arts*, Volume 79, pp. 679-709, London 1931.

Mattavi J.N, Heffner F.E. and Miklos A.A (1969), "The Stirling Engine for Underwater Vehicle Applications", SAE paper no. 690731, pp. 2376-2400, 1969.

Meijer R.J (1959), "The Philips Hot-Gas Engine with Rhombic Drive", Philips Technical Review, vol. 20, pp. 245-276, 1959.

Michel A.P.J. (1971), "NO formation" Proc. 6th I.E.C.E.C. Paper 719134, Nov. 1971

The National Institute for Standards and Technology, Gaithersburg, internet link: http://www.nist.gov , accessed Mai 2003

Neelen G.T.M., Ortegren L. G. H. and Kuhlmann P. (1971), "Stirling engines in traction applications" 9th Int. Congress on Combustion Eng., Paper A26, Stockholm, Sweden

Organ A.J (1991), "Stirling Engine Thermodynamic Design", Cambridge: MRT publications 1991. ISBN 0-951-80870-2.

Organ A.J (1992), "Thermodynamic Analysis of the Stirling Cycle Machine - A Review of the Literature", *Proceedings of Institution of Mechanical Engineers (IMechE)*, vol. 201, No.C6, pp. 381-402, 1987.

Organ A. J. (1992), "Thermodynamics and Gas Dynamics of the Stirling Cycle Machine", Cambridge University Press 1992, ISBN 0 521 41363.

Organ A. J. (1997), "The Regenerator and the Stirling engine", Mechanical Engineering Publication Ltd, UK, 1997, ISBN 1-86058-010-6

Palsson M. (1997a), "Design and testing of Stirling engine premix CGR combuster for ultra low emission" 8th International Stirling engine conference, Ancona

Palsson M. (1997b), "Design and testing of Stirling engine premix CGR combuster for ultra low emission" 8th International Stirling engine conference, Ancona

Parker M.D. and Malik M.J. (1962), "Investigation of a 3 kW Stirling cycle solar power system" Vol. 1-10, W.A.D.D. TR-61-122, US 1962

Plansee (1992), "Product catalogue: Molybdenum and Tungsten" Plansee AG, Tirol, Austria

Rampen W.H.S. and Salter S.H, (1990), "The Digital Displacement Hydraulic Piston Pump", *Proc. 9th International Symposium on Fluid Power*, BHR Group, Cambridge, STI, pp. 33-46, April 1990.

Rampen W.H.S. (1992), "The Digital Displacement Hydraulic Piston Pump", Ph.D thesis, University of Edinburgh, Scotland, 1992.

Rampen W.H.S, Almond J.P, and Salter S.H. (1994), "The Digital Displacement Pump/Motor Operating Cycle: Experimental Results Demonstrating the Fundamental Characteristics". *International Fluid Power Workshop*, Bath 1994.

Rampen W.H.S, Almond J.P, Taylor J.R.M, Ehsan Md. and Salter S.H (1995), "Progress on the Development of the Wedding-cake Digital Hydraulic Pump/Motor", *2nd European Wave Power Conference*, pp.289-296, Lisbon, 8-10 Nov 1995.

Rampen W.H.S, Ehsan Md. and Stein U.B.P. (1997), "A Digital Power Take-Off for Stirling Engines", *8th International Stirling Engine Conference and Exhibition*, pp.601 - 611, Ancona, 1997.

Rathenau G.W. and Maijer R.J. (1973) "Presentation on Stirling engine to subcommittee" Automotive Research and Development Act, 4 may 1973, S. 1055

Reader G.T. and Barnes C. (1988), "The Effect of Bottom End Temperature on the Performance of a Stirling Engine", *Proceedings of the 23rd Inter-society Energy Conversion Engineering Conference* (by ASME), Paper no. 889350, Denver USA, 1988.

Reader G.T. and Hooper C. (1983), "Stirling Engines"E & F N Spon, London and New York 1983, ISBN 0-419-12400-4.

Reatz K. (1984) "Malone thermal engine" Deutsches patent, No: DE3305253

Richard A. (1983), "Secrets of the Malone Engine", Simplified Technology Service, Lindsay Publications, Bradley, Columbia, MO

Ross M.A (1979), "Balanced Crankshaft Mechanism for the Two-piston Stirling Engine", US Patent no. - 4,138,897.

Salter S.H. and Rampen W. H. S. (1993), "The Wedding Cake Multi-Eccentric Radial Piston Hydraulic Machine with Direct Computer Control of Displacement", *Proc. 10th International Conference on Fluid Power*, BHR Group, Brugge, MEP, pp. 47-64, April 1993.

Schimdt G. (1861), "Theory der Geschlossen Calorischen Maschine" Laubroy und Schwatskopff in Berlin. Z. ver Oster Ing. p.79, 1861.

Schmidt F.W. and Willmott A.J. (1981), "Thermal Energy Storage & Regeneration" Hemisphere Publishing Corporation, London, 1981, ISBN 0-07-055346-7.

Senft R.J. (1993), "Ringbom Stirling Engines" Oxford University Press, New York, ISBN 0-19-507798-9

Senft R.J., (1996) : "Low Temperature Differential Stirling Engines" Moriya Press, River Falls, USA, ISBN 0-9652455-1-9

Senft R.J. (1997), "Brake power maxima of engines with limited heat transfer" 32nd I. E. C.E. C., Honolulu, USA, July 1997

Siegel R. and Howell J.R. (1992), "Thermal radiation heat transfer" Taylor & Francis, USA, 1992, ISBN 0-89116-271-2

Srinivasan V., Walker G., Fauvel R., Senft J.R. (1985), "Ringbom-Stirling Engine Simulation and Parametric Study", ASME 85-DGP-21, 1985.

Stirling R. (1817), "Improvements for diminishing the consumption of fuel and in particular, an engine capable of being applied to the moving machinery on a principle entirely new" British patent 4081

Swift G.W. (1989a), "Simple Theory of a Malone Engine", 24th *Inter-society Energy Conversion Engineering Conference*, paper no. 899055, pp2355-2361, 1989.

Swift G.W (1989b), "Experiments with a Malone Engine", 24th *Inter-society Energy Conversion Engineering Conference*, paper no. 899054, pp. 2385-2393, 1989.

Swift G.W. (1989c), "Free displacer and Ringbom displacer for a Malone refrigerator", 29th IECEC, Montery,1994

Swift G.W. (1990), "Swift G.W, "Malone refrigeration", Ashrae Journal, , pp.28 – 34, Atlanta, USA, November 1990

Swift G.W. (1992), "John Malone and Liquid Engines", Scientific American Inc., New York, USA, September 1992

Swift G.W. (1993), "Malone Refrigeration an Old Solution to a New Problem", Los Alamos Since, Number 21, Los Alamos USA, 1993

Swift G. W. and Brown A. O. (1993), "Free Displacer and Ringbom Displacer for a Malone Refrigerator" 29th Proc. I.E.C.E.C., pp.1394 – 1415, Montery, USA, Aug 1994

Urieli I. and D.M. Berchowitz (1984), "Stirling Cycle Engine Analysis" London, UK

Visser J.A. and Du Plessis J. (1992), *"Swirling flow in a Closed Combustion Chamber"*, Proc. 2nd Int. Conf. for Advanced Computational Methods in Heat Transfer, Milan, Vol 2, pp 665-676

Walker G. (1980), "Stirling Engines", Clarendon press, Oxford, 1980. ISBN 0-19-856209-8.

Walker G. and Khan M. (1965), "The Theoretical Performance of Stirling Cycle Engines", SAE paper no. 949A, *International Automotive Engine Conference*, Detroit, Jan 1965.

Walker G, Weiss M, Reader G, Fauvel O.R (1990), "Adventures with MARWEISS : A Summary of Experience with Stirling Simulation", *Proceedings of the 25th Inter-society Energy Conversion Engineering Conference,* pp. 342-345, Reno NV, USA 1990.

Walker G., Weiss M., Reader G., Fauvel R. and Bingham E.R. (1992), "The Stirling Alternative", *Proceedings of the 27th Inter-society Energy Conversion Engineering Conference*, vol.5, pp.97-100, Aug 3-7, San Diego CA, 1992.

Walker G, Reader G, Fauvel O.R. and Bingham E.R (1994), "The Stirling Alternative", Gordon & Breach Science Publishers, Switzerland, 1994. ISBN 2-88124-600-1.

Weldon M. (2001), "High efficiency Malone compressor" United States Patent, No 6,282,908

West C.D (1982),"Liquid Piston Stirling Engines", Van Nostrand Reinhold Co. New York, 1982.

West C.D (1986), "Principles and Applications of Stirling Engines", Van Nostrand Reinhold Co, New York, 1986.

Willmott A. J. (2001), "Dynamics of Regenerative Heat Transfer", Taylor & Francis, New York, USA, 2002, ISBN 1-56032-369-8

Wolgemouth, C.H. (1969), "Dynamic Preformance of a thermodynamic cycle using a chemically reactive gas" Proc. 4th I.E.C.E.C., pp. 599 - 605

Wuenning J. (1997), "Flameless oxidation as a combustion method for Stirling engines" 8th International Stirling engine Conference and Exhibition, pp 309-317,University of Ancona, Italy,1997

Webb R.L. (1994), "Principals of enhanced heat transfer" Jon Wiley & Sons, ISBN 0-471-57778-2, USA 1994

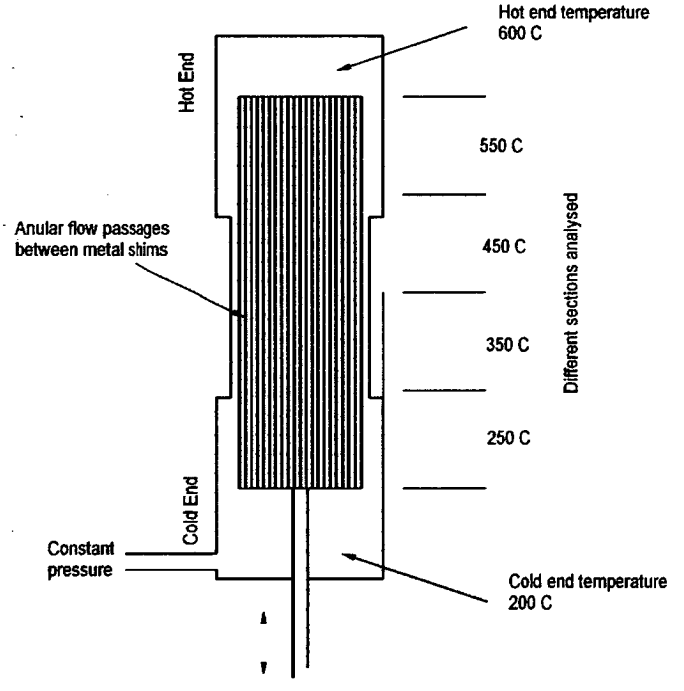
Zarinchang J. (1972), "The Stirling Engine" Intermediate Technology Development Group, London 1972

Zhaolin G., Haruki S., Xiao F. (2001), "Using supercritical heat recovery process in Stirling engines for high thermal efficiency" Applied Thermal Engineering, Pergamon, 2001.

Appendix A.

Regenerator optimiztion

The following calculations analyze the different losses occurring in the regenerator system of the proposed Artemis Malone engine. The losses from imperfect regeneration, internal pressure drop and thermal conductivity through the regenerator matrix have been considered.
The analysis is restricted to the case of flow between parallel plates at constant pressure of 350 bar. The mass flow rate along the regenerator is set as constant.
The regenerator has been divided into 4 different temperature regions, which have been analysed individually. The fluid properties in each section have been presumed constant. Figure 1 shows the schematic of the regenerator system analysed.
The input parameters are divided into variable and fixed parameter. The number of variable parameters has been restricted to four essential parameters that define the regenerator geometry. A number of different values have been analysed for each of these parameters to determine the optimum operating point. Due to the large number of solutions it was not practical to plot the results with the equtions. The resulte can be found in section 5.4.3.



1 Fixed regenerator pameters

Initially a number of parameters have been set to a fixed value. These parameters are not considerate in the regenerator optimisation (see also section 5.4 in main text).

1.1 Matrix material parameters

Matrix material:	stainless steel	
$ks := 20$	$\frac{W}{m \cdot K}$	Thermal conductivity of matrix material at mean matrix temperature
$\rho s := 8000$	$\frac{kg}{m3}$	Density of matrix material
$cps := 490$	$\frac{J}{kg \cdot K}$	Heat capacity matrix material at mean matrix temperature

1.2 Fluid properties

The fluid properties have been treated as constant inside each of the four temperature section. The mean value has been used for the calculations.

Density [kg/m3]	Viscosity [m2/s]	Thermal conductivity [W/mK]	Prandtl	Thermal capaciy cp [W/kg*K]
$\rho 550 := 98.4$	$\nu 550 := 0.32 \cdot 10^{-6}$	$k550 := 0.11$	$Pr550 := 0.13$	$cp550 := 3600$
$\rho 450 := 148$	$\nu 450 := 0.18 \cdot 10^{-6}$	$k450 := 0.12$	$Pr450 := 0.15$	$cp450 := 6700$
$\rho 350 := 644$	$\nu 350 := 0.12 \cdot 10^{-6}$	$k350 := 0.26$	$Pr350 := 0.4$	$cp350 := 6400$
$\rho 250 := 826$	$\nu 250 := 0.14 \cdot 10^{-6}$	$k250 := 0.58$	$Pr250 := 0.6$	$cp250 := 4600$

1.3 Cycle parameters

$mswept := 0.0250$	kg	Mass of swept working fluid
$F := 4$	Hz	Frequency
$bt := \frac{1}{2 \cdot F}$		
$bt = 0.125$	s	Time for each blow
$Thot := 600$	C	Temperature of fluid inhot end
$Tcold := 200$	C	Temperature of fluid in cold end
$\Delta T := Thot - Tcold$		
$\Delta T = 400$	C	Temperature difference between hot and cold end of engine
$\eta c := \frac{Thot - Tcold}{Thot + 273}$		
$\eta c = 0.458$		Carnot efficiency

2. Variable parameters used in optimization

The following four parameters have been analysed over a range of values to determine the optimum regenerator geometry.

$tf := 0.00001, 0.00002 .. 0.00003$	m	range of values for flow channel width (gap between shims)
$tf \cdot 1000 = \begin{pmatrix} 0.01 \\ 0.02 \\ 0.03 \end{pmatrix}$	mm	width of flow channels
$ts := 0.0001, 0.00015 .. 0.0002$	m	range of values for matris shim thickness
$ts \cdot 1000 = \begin{pmatrix} 0.1 \\ 0.15 \\ 0.2 \end{pmatrix}$	mm	Shim thickness
$ms := 0.75, 1.75 .. 2.75$	kg	range of values for matrix shim thickness
$ms = \begin{pmatrix} 0.750 \\ 1.750 \\ 2.750 \end{pmatrix}$	kg	Ratio of matrix mass to swept fluid mass.
$rl := 0.05, 0.1 .. 0.15$	m	range of values for regenerator length
$rl \cdot 1000 = \begin{pmatrix} 50 \\ 100 \\ 150 \end{pmatrix}$	mm	Regenerator length

3. Main equations defining the regenerator geometry

3.1 Martix volume

The Matrix volume is calculated from the matrix mass **ms** and the matrix density **ρss**

$$vs(ms) := \frac{ms}{\rho s} \qquad kg$$

3.2 Surface area

The Matrix surface area is calculated from the matrix mass **ms**, density **ρss** and matrix shim thickness **ts**.

$$As(ts, ms) := 2 \cdot \frac{ms}{\rho s \cdot ts} \qquad m2$$

3.3 Shim length

The unrolled length of the shim is calculated from the surface area **As** and the regenerator length **rl**.

$$ls(ts, ms, rl) := \frac{As(ts, ms)}{2 \cdot rl} \qquad m$$

3.4 Regenerator dead volume

The dead volume is calculated from the flow passage between the shims **tf** and the matrix surface area **As**

$$vds(tf, ts, ms) := tf \cdot \frac{As(ts, ms)}{2} \qquad m3$$

3.5 Total regenerator volume

The total volume of the regenerator can be calculated from the matrix volume **vs** and the regenerator dead volume **vs**.

$$vr(tf, ts, ms) := vs(ms) + vds(tf, ts, ms) \qquad m3$$

3.6 Regenerator packing ratio

The packing ratio rp can be calculated from the regeneator matrix volume **vs** and the total regenerator volume **vr**.

$$pr(tf, ts, ms) := \left(\frac{vs(ms)}{vr(tf, ts, ms)} \right)$$

3.7 Regenerator diameter

The diameter can be calculated from the regenerator length **lr** and the regnerator volume **vr.**

$$rd(tf, ts, ms, rl) := 2 \cdot \sqrt{\frac{vr(tf, ts, ms)}{\pi \cdot rl}} \qquad m$$

3.8 Regenerator length to diamter ratio

Regenerator length to diameter ratio can be calculated from the regenerator length **rl** and the rgenerator diameter **rd**

$$rld(rl, tf, ts, ms) := \frac{rl}{rd(tf, ts, ms, rl)}$$

3.9 Front area of regenerator

The frontal area of the regenerator can be calculated from the regenerator diameter **rd**

$$ra(tf, ts, ms, rl) := \left(\frac{rd(tf, ts, ms, rl)}{2}\right)^2 \cdot \pi \qquad m2$$

3.10 Open flow area

The open flow area can be calculated from the packing ratio **pr** and the regenerator diameter **rd**.

$$aflow(tf, ts, ms, rl) := \left(\frac{rd(tf, ts, ms, rl)}{2}\right)^2 \cdot \pi \cdot (1 - pr(tf, ts, ms)) \qquad m2$$

Main equation describing the flow in the regenerator matrix

The mass flow rate **mflow** in the regenerator can be calculated from the swept mass **mswept** and the time for each stroke **bt**.

$$mflow := \frac{mswept}{bt}$$

$mflow = 0.2$ $\frac{kg}{s}$ Mass flow in regenerator rate

4.1 Volume flow rate

The volume flow in regenerator can be calculated at each point along the regenerator from the mass flow rate **mflow** and the fluid density **ρf** . This has been done for the 4 different temperature regions in the regenerator.

$$vflow550 := \frac{mflow}{\rho 550}$$

$vflow550 \cdot 1000 \cdot 1000 = 2033$ $\frac{cc}{s}$

$$vflow450 := \frac{mflow}{\rho 450}$$

$vflow450 \cdot 1000 \cdot 1000 = 1351$ $\frac{cc}{s}$

$$vflow350 := \frac{mflow}{\rho 350}$$

$vflow350 \cdot 1000 \cdot 1000 = 311$ $\frac{cc}{s}$

$$vflow250 := \frac{mflow}{\rho 250}$$

$vflow250 \cdot 1000 \cdot 1000 = 242$ $\frac{cc}{s}$

4.2 Fluid velocity

With the density ρ, the open flow area **aflow** and the volume flow rate **vflow** it is possible to calculate the fluid velocity.

$$velf550(tf,ts,ms,rl) := \frac{mflow}{\rho550 \cdot aflow(tf,ts,ms,rl)}\ \frac{m}{s} \qquad velf450(tf,ts,ms,rl) := \frac{mflow}{\rho450 \cdot aflow(tf,ts,ms,rl)}\ \frac{m}{s}$$

$$velf350(tf,ts,ms,rl) := \frac{mflow}{\rho350 \cdot aflow(tf,ts,ms,rl)}\ \frac{m}{s} \qquad velf250(tf,ts,ms,rl) := \frac{mflow}{\rho250 \cdot aflow(tf,ts,ms,rl)}\ \frac{m}{s}$$

4.3 Reynolds number

To define the calculation for the heat transfer and the pressure drop it is important to anlyze the Reynolds number to determine between laminar and turbulent flow in the regenerator.

$$Re550(tf,ts,ms,rl) := \frac{velf550(tf,ts,ms,rl) \cdot 2tf}{v550} \qquad Re450(tf,ts,ms,rl) := \frac{velf450(tf,ts,ms,rl) \cdot 2tf}{v450}$$

$$Re350(tf,ts,ms,rl) := \frac{velf350(tf,ts,ms,rl) \cdot 2tf}{v350} \qquad Re250(tf,ts,ms,rl) := \frac{velf250(tf,ts,ms,rl) \cdot 2tf}{v250}$$

5. Main equations describing the heat transfer

5.1 Flush ratio

The flush ratio can be calculated from the ratio between the regenerator dead volume **vds**, the volume flow rate **vflow** and the blow time **bt**.

$$rflush550(tf,ts,ms) := \frac{4vflow550 \cdot bt}{vds(tf,ts,ms)} \qquad rflush450(tf,ts,ms) := \frac{4vflow450 \cdot bt}{vds(tf,ts,ms)}$$

$$rflush350(tf,ts,ms) := \frac{4vflow350 \cdot bt}{vds(tf,ts,ms)} \qquad rflush250(tf,ts,ms) := \frac{4vflow250 \cdot bt}{vds(tf,ts,ms)}$$

5.2 Nusselt Number for laminar flow in regenerator

The Nussel for laminar flow is independant of the Reynolds number

$$Nul550 := 8.23 \qquad Nul450 := 8.23$$

$$Nul350 := 8.23 \qquad Nul250 := 8.23$$

5.2 Heat transfer coefficient

The heat transfer coefficient can be calculated from the Nusselt number **Nu** and the thermal conductivity **k** of the fluid .

$$h550(tf) := Nul550 \cdot \frac{k550}{tf} \qquad h450(tf) := Nul450 \cdot \frac{k450}{tf}$$

$$h350(tf) := Nul350 \cdot \frac{k350}{tf} \qquad h250(tf) := Nul250 \cdot \frac{k250}{tf}$$

5.3 Biot number

The Biot number can be calculated with the heat transfer coefficient **h** the thermal conductivity **ks** of the solid and the shim thickness.

$$Bi550(tf,ts) := \frac{h550(tf)\cdot\frac{ts}{2}}{ks} \quad \frac{W}{mK} \qquad Bi450(tf,ts) := \frac{h450(tf)\cdot\frac{ts}{2}}{ks} \quad \frac{W}{mK}$$

$$Bi350(tf,ts) := \frac{h350(tf)\cdot\frac{ts}{2}}{ks} \quad \frac{W}{mK} \qquad Bi250(tf,ts) := \frac{h250(tf)\cdot\frac{ts}{2}}{ks} \quad \frac{W}{mK}$$

5.4 Reduced length

The reduced length for each section can be calculated with the heat tranfer coeffcient **h**, the matrix surface area **As**, the mass flow rate **mflow**, and the heat capacity of the fluid **cp**. For Biot numbers of less than 0.1 it is possible to negect the error from the temperature drop in the matrix material.

$$\Lambda550(tf,ts,ms) := \frac{h550(tf)\cdot As(ts,ms)}{mflow\cdot cp550} \qquad \Lambda450(tf,ts,ms) := \frac{h450(tf)\cdot As(ts,ms)}{mflow\cdot cp450}$$

$$\Lambda350(tf,ts,ms) := \frac{h350(tf)\cdot As(ts,ms)}{mflow\cdot cp350} \qquad \Lambda250(tf,ts,ms) := \frac{h250(tf)\cdot As(ts,ms)}{mflow\cdot cp250}$$

5.5 Reduced period

The reduced period for each section can be calculated from the matrix surface area **As**, the heat transfer coefficient **h**, the matrix mass **ms** and the matrix heat capacity **cps**.

$$\Pi550(tf,ts,ms) := \frac{h550(tf)\cdot As(ts,ms)}{ms\cdot cps}\cdot\left(bt - \frac{vds(tf,ts,ms)}{4vflow550}\right) \qquad \Pi450(tf,ts,ms) := \frac{h450(tf)\cdot As(ts,ms)}{ms\cdot cps}\cdot\left(bt - \frac{vds(tf,ts,ms)}{4vflow450}\right)$$

$$\Pi350(tf,ts,ms) := \frac{h350(tf)\cdot As(ts,ms)}{ms\cdot cps}\cdot\left(bt - \frac{vds(tf,ts,ms)}{4vflow350}\right) \qquad \Pi250(tf,ts,ms) := \frac{h250(tf)\cdot As(ts,ms)}{ms\cdot cps}\cdot\left(bt - \frac{vds(tf,ts,ms)}{4vflow250}\right)$$

5.6 Regenerator efficiency

The temperature deficit after a return sroke and the regenerator efficiency can be calculated from the reduced length and the reduced period.

$$Tswing550(tf,ts,ms) := \frac{(Thot - Tcold)}{4}\cdot\left[1 - \left(\frac{1}{rflush550(tf,ts,ms) + 1}\right)\right] \quad C$$

$$\Delta Th550(tf,ts,ms) := \frac{2}{\Lambda550(tf,ts,ms) + 2 - \left(\Pi550(tf,ts,ms) + 2 - 2.35\cdot\sqrt{\Pi550(tf,ts,ms)}\right)}\cdot Tswing550(tf,ts,ms) \quad C$$

$$\eta r550(tf,ts,ms) := \frac{\Delta T - 4\,\Delta Th550(tf,ts,ms)}{Thot - Tcold} \quad \%$$

$$Tswing450(tf,ts,ms) := \frac{(Thot - Tcold)}{4}\cdot\left[1 - \left(\frac{1}{rflush450(tf,ts,ms) + 1}\right)\right] \quad C$$

$$\Delta Th450(tf,ts,ms) := \frac{2}{\Lambda450(tf,ts,ms) + 2 - \left(\Pi450(tf,ts,ms) + 2 - 2.35\cdot\sqrt{\Pi450(tf,ts,ms)}\right)}\cdot Tswing550(tf,ts,ms) \quad C$$

$$\eta r450(tf,ts,ms) := \frac{\Delta T - 4\,\Delta Th450(tf,ts,ms)}{Thot - Tcold} \quad \%$$

$$Tswing350(tf,ts,ms) := \frac{(Thot - Tcold)}{4}\cdot\left[1 - \left(\frac{1}{rflush350(tf,ts,ms) + 1}\right)\right] \quad C$$

$$\Delta Th350(tf,ts,ms) := \frac{2}{\Lambda 350(tf,ts,ms) + 2 - \left(\Pi 350(tf,ts,ms) + 2 - 2.35\sqrt{\Pi 350(tf,ts,ms)}\right)}\cdot Tswing350(tf,ts,ms) \quad C$$

$$\eta r350(tf,ts,ms) := \frac{\Delta T - 4\Delta Th350(tf,ts,ms)}{Thot - Tcold} \quad \%$$

$$Tswing250(tf,ts,ms) := \frac{(Thot - Tcold)}{4}\cdot\left[1 - \left(\frac{1}{rflush250(tf,ts,ms) + 1}\right)\right] \quad C$$

$$\Delta Th250(tf,ts,ms) := \frac{2}{\Lambda 250(tf,ts,ms) + 2 - \left(\Pi 250(tf,ts,ms) + 2 - 2.35\sqrt{\Pi 250(tf,ts,ms)}\right)}\cdot Tswing250(tf,ts,ms) \quad C$$

$$\eta r250(tf,ts,ms) := \frac{\Delta T - 4\Delta Th250(tf,ts,ms)}{Thot - Tcold} \quad \%$$

$$\Delta TAll(tf,ts,ms) := \Delta Th550(tf,ts,ms) + \Delta Th450(tf,ts,ms) + \Delta Th350(tf,ts,ms) + \Delta Th250(tf,ts,ms)$$

The energy lost can be calculated from the temperature deficit and the heat capacity of the fluid.

$$Qrloss550(tf,ts,ms) := \Delta Th550(tf,ts,ms)\cdot cp550\cdot mswept\cdot F_* \quad W$$

$$Qrloss450(tf,ts,ms) := \Delta Th450(tf,ts,ms)\cdot cp450\cdot mswept\cdot F_* \quad W$$

$$Qrloss350(tf,ts,ms) := \Delta Th450(tf,ts,ms)\cdot cp350\cdot mswept\cdot F_* \quad W$$

$$Qrloss250(tf,ts,ms) := \Delta Th450(tf,ts,ms)\cdot cp250\cdot mswept\cdot F_* \quad W$$

$$Qrloss(tf,ts,ms) := (\Delta Th550(tf,ts,ms)\cdot cp550 + \Delta Th450(tf,ts,ms)\cdot cp450 + \Delta Th350(tf,ts,ms)\cdot cp350 + \Delta Th250(tf,ts,ms)\cdot cp250)\cdot mswept\cdot F$$

W

6. Pumping losses

Laminar flow is expected around the optimum operating point. The pressure drop for flow between parallel plates can then be calculated from the mass flow rate mflow, the kinematic viscosity v, the flow channel width tf and the flow channel length (shim length) ls.

$$\Delta Pressl550(tf,ts,ms,rl) := \frac{12\cdot mflow\cdot\frac{rl}{4}\cdot v550}{tf^3\cdot ls(ts,ms,rl)} \quad Pa \qquad Qpumpl550(tf,ts,ms,rl) := \Delta Pressl550(tf,ts,ms,rl)\cdot vflow550 \quad W$$

$$\Delta Pressl450(tf,ts,ms,rl) := \frac{12\cdot mflow\cdot\frac{rl}{4}\cdot v450}{tf^3\cdot ls(ts,ms,rl)} \quad Pa \qquad Qpumpl450(tf,ts,ms,rl) := \Delta Pressl450(tf,ts,ms,rl)\cdot vflow450 \quad W$$

$$\Delta Pressl350(tf,ts,ms,rl) := \frac{12\cdot mflow\cdot\frac{rl}{4}\cdot v350}{tf^3\cdot ls(ts,ms,rl)} \quad Pa \qquad Qpumpl350(tf,ts,ms,rl) := \Delta Pressl350(tf,ts,ms,rl)\cdot vflow350 \quad W$$

$$\Delta Pressl250(tf,ts,ms,rl) := \frac{12\cdot mflow\cdot\frac{rl}{4}\cdot v250}{tf^3\cdot ls(ts,ms,rl)} \quad Pa \qquad Qpumpl250(tf,ts,ms,rl) := \Delta Pressl250(tf,ts,ms,rl)\cdot vflow250 \quad W$$

Total pumping power

$$QpumpAll(tf, ts, ms, rl) := Qpumpl550(tf, ts, ms, rl) + Qpumpl450(tf, ts, ms, rl) + Qpumpl350(tf, ts, ms, rl) + Qpumpl250(tf, ts, ms, rl) \quad W$$

7. Thermal losses through regenerator matrix

The thermal losses through the regenerator can be calculated from the thermal conductivity of the matrix material ks, the regenerator length and the frontal area of the shim material. The thermal losses in axial direction through the fluid are small enough to be neglected. An increased thermal resistance is achieve through a number of thin fluid layers along the length of the regenerator

$fl := 0.0003$ m — Thickness of fluid layer

$fl \cdot 1000 = 0.3$ mm

$no := 3$ — Number of fluid layers along the regenerator

$kfm := 0.3$ $\frac{W}{m \cdot K}$ — Mean thermal resistance of working fluid

$$Qtl(tf, ts, ms, rl) := \frac{ra(tf, ts, ms, rl) \cdot (Thot - Tcold)}{\left(\frac{rl}{ks} + \frac{no \cdot fl}{kfm}\right)} \quad W$$

8. Total regenerator system losses

The following section analyzes the total losses in each section of the regenerator matrix. The losses arising from the reduced regenerator efficiency, pumping losses and thermal conductivity losses through the regenerator are considerate. To determine the effect of the different parameters their effect on the input power has been calculated. The pumping losses have been multiplied by the Carnot efficiency. The effect from the regenerator efficiency has been calculated from the temperature deficit after each cycle and the thermal conductivity of the fluid in each section. The effect from the thermal conductivity losses has been directly added to the losses.

$$Qtotal550(tf, ts, ms, rl) := Qpumpl550(tf, ts, ms, rl) \cdot \frac{1}{\eta c} + \frac{Qtl(tf, ts, ms, rl)}{4} + Qrloss550(tf, ts, ms) \quad W$$

$$Qtotal450(tf, ts, ms, rl) := Qpumpl450(tf, ts, ms, rl) \cdot \frac{1}{\eta c} + \frac{Qtl(tf, ts, ms, rl)}{4} + Qrloss450(tf, ts, ms) \quad W$$

$$Qtotal350(tf, ts, ms, rl) := Qpumpl350(tf, ts, ms, rl) \cdot \frac{1}{\eta c} + \frac{Qtl(tf, ts, ms, rl)}{4} + Qrloss350(tf, ts, ms) \quad W$$

$$Qtotal250(tf, ts, ms, rl) := Qpumpl250(tf, ts, ms, rl) \cdot \frac{1}{\eta c} + \frac{Qtl(tf, ts, ms, rl)}{4} + Qrloss250(tf, ts, ms) \quad W$$

The total energy loss in the regenerator system can now calculated from the losses in the indivudual sections.

$$Qtotal(tf, ts, ms, rl) := Qtotal550(tf, ts, ms, rl) + Qtotal450(tf, ts, ms, rl) + Qtotal350(tf, ts, ms, rl) + Qtotal250(tf, ts, ms, rl) \quad W$$

Appendix B.

System pressure change for power take-off system with sinusoidal motion profile

The following calculations analyze the pressure in the TD-Pile of the proposed Artemis Malone engine. The calculations are done under the assumption of perfect heat transfer and for a sinusoidal motion profile of the working piston and regenerator.

1 Key input parameters

1.1 Regenerator

The calculations are based on a tubular regenerator of given length and diameter. The packing ratio defines the matrix to fluid volume ratio inside the regenerator. The motion profile of the regenerator is sinusoidal and defined as the distance from TDC. The temperature inside the regenerator is assumed linear between the hot end and the cold end temperature.

$TH := 550$ C — Hot-End temperature

$TC := 150$ C — Cold-End temperature

$Rdia := 0.039$ m — Regenerator outer dia.

$Rs := 0.02$ m — Stroke of Regenerator

$Rl := 0.2$ m — Length of Regenerator

$$Rarea := \left(\frac{Rdia}{2}\right)^2 \cdot \pi$$

$Rarea = 1.19459 \times 10^{-3}$ m2 — Regenerator top area

$Rp := 0.1$ — Fluid to matrix ratio in regenerator

$C550 := 3000$ $\frac{kJ}{kg}$ — Internal energy of water at 550 bar

$C120 := 500$ $\frac{kJ}{kg}$ — Internal energy of water at 120 C

$Rv := Rarea \cdot Rl \cdot Rp$

$Rv = 2.389 \times 10^{-5}$ m3 — Volume in Regenerator

$mHEmax := 0.024$ kg — Maximum mass of fluid in hot end

$$cpmean := \frac{(C550 - C120)}{(550 - 120)}$$

$cpmean = 5.814$ $\frac{kJ}{kg \cdot K}$ — Mean heat capacity of water betweenT-hot and T-cold

$\rho ss := 7800$ $\frac{kg}{m3}$ Density stainless steel

$mRmatrix := Rl \cdot Rarea \cdot \rho ss \cdot 0.9$ kg

$cpss := 0.51$ $\frac{kJ}{kg \cdot K}$ Heat capacity stainless steel

$\Gamma := \frac{cpss \cdot mRmatrix}{mHEmax \cdot cpmean}$

$\Gamma = 6.13$ Heat capacity ratio between matrix and fluid that passing during a half stroke.

1.2 Hot End

The volume in the hot end can be calculated from the regenerator diameter and position.

$Hdia := Rdia$ Diameter hot end

$HEdspace := 3Rs \cdot Rarea$

$HEdspace = 7.168 \times 10^{-5}$ m3 Volume in hot end at times the regenerator is at TDC

1.3 Working piston

The working piston motion profile is sinusoidal and described as the distance from TDC. The diameter is set to be the same as the regenerator diameter and the stroke is used to define the differential displacement.

$Pdia := Rdia$ m Piston outer diameter

$Ps := 0.015$ m Stroke of piston

$Parea := Rarea$ m2 Piston area

The following calculations are done for one full cycle of the Regenerator in steps of 5 ms

$F := 2.5$ $\frac{1}{s}$ Cycle frequency

$P := \frac{1}{F}$ $P = 0.4$ s Period

$\omega := 2 \cdot \pi \cdot F$

$\omega = 15.708$

$t := 0.00, 0.010 .. 0.40$ s Time analysed

2. Regenerator / Piston velocity and Position

It is possible to calculate the position, mass and volumes for the different places in the engine.

$$Pvel(t) := \frac{Ps}{2} \cdot \omega \cdot \sin\left[\left(t - \frac{P}{4}\right) \cdot \omega\right] \quad \frac{m}{s}$$ Velocity of the piston as a function of (t)

$$Ppos(t) := \left[\frac{Ps}{2} \cdot \cos\left[\left(t - \frac{P}{4}\right) \cdot \omega\right]\right] - \frac{Ps}{2} \quad m$$ Position of piston from regenerator base as a function of (t)

$$Rvel(t) := \frac{Rs}{2} \cdot \omega \cdot \sin(t \cdot \omega) \quad \frac{m}{s}$$ Velocity of the regenerator as a function of (t)

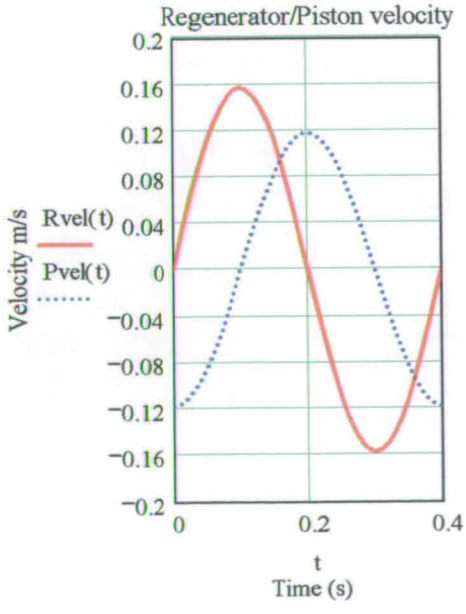
$$Rpos(t) := \frac{Rs}{2} \cdot \cos(\omega \cdot t) - \frac{Rs}{2} \quad m$$ Position of regenerator from hot end top as a function of (t)

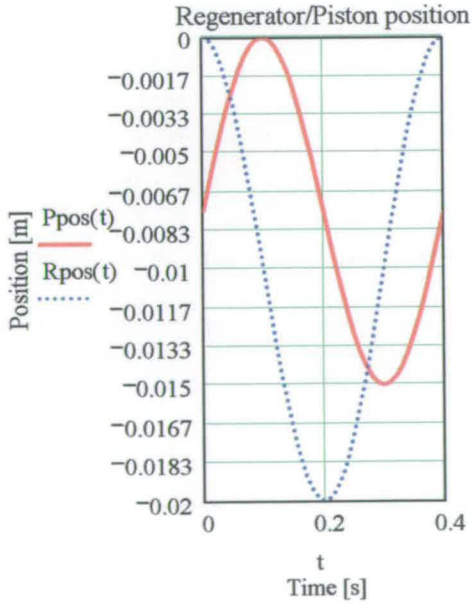
The volume in the hot end and cold end space of the engine can be calculated from the position of the regenerator and working piston.

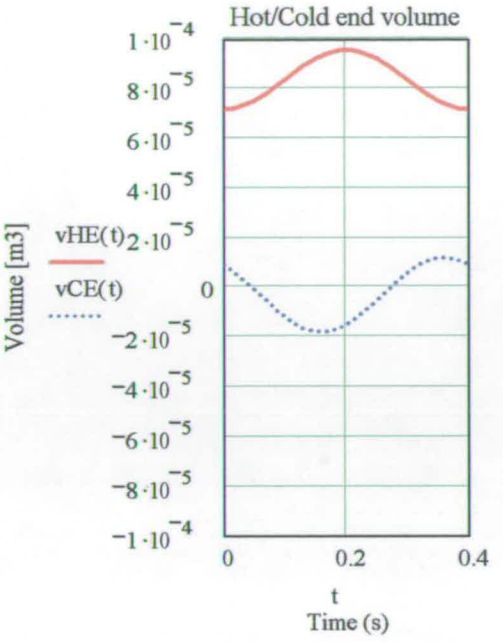
$vHE(t) := Rpos(t) \cdot Rarea \cdot (-1) + HEdspace$ m3 Hot end volume

$vCE(t) := (Rpos(t) - Ppos(t)) \cdot Rarea$ m3 Cold end volume

The positon and velocity of the regenerator and working piston and the hot and cold space volume has been analysed within one cycle.







3. Mass and volume in different engine spaces

The total mass of working fluid remains constant throughout the cycle. The water in the cold end is incompressible and its mass is, therefore, a direct function of the cold end volume. The mass in the hot end and the regenerator is a function of the total mass minus the cold end mass. From the mass, temperature, density and volume in the hot end space and regenerator it is possible to determine the system pressure as a function of the crank angle. The pressure in the system during one cycle has been analyzed.

$\rho water := 980$	$\frac{kg}{m3}$	Density of liquid water in cold end space
$mS := 0.025$	m3	Total mass of working fluid in system (chosen to create minimum cycle pressure of >220 bar)
$mCE(t) := vCE(t) \cdot \rho water$	kg	Mass of working fluid in cold end space
$mHER(t) := mS - mCE(t)$	kg	Mass in hot end space plus regenerator dead space

$\rho water550 := 0.001 \cdot P^2 + 0.4679 \cdot P + 5.7282 \frac{kg}{m3}$ Density of water

From the regenerator motion it is possible to calculate the volumes in the hot end, cold end and regenerator during a cycle. The mass of working fluid will level out so that the pressure is the same at each point in the engine. For a known temperature it is then possible to calculate the resulting pressure from the relation of pressure and density.

$mHE + mR + mCE = mS$

The mass in all three spaces of the engine equals the system mass.

$oHE * vHE + oR * vR + oCE + vCE = mS$

The mass can be defined over the density and the volume.

$mHER = mS - vCE * oCE$

The mass in the hot end and the regenerator can be calculated by subtracting of the cold end mass from the total mass.

$vHER(t) := (Rv + vHE(t))$

From the density at the relevant temperature it is possible to calculate the ratio of mass in the hot end and the regenrator.

$\rho F := 2.35$

Factor of mean regenerator fluid density to density in hot end space

$$\rho R(t) := \frac{mHER(t)}{\left(\frac{vHE(t)}{\rho F}\right) + Rv}$$

Density in regenerator

$$\rho HE(t) := \frac{mHER(t)}{vHE(t) + (\rho F \cdot Rv)}$$

Density in hot end space

$mHE(t) := \rho HE(t) \cdot vHE(t)$

$vSys(t) := vHE(t) + Rv + vCE(t)$

Volume of complete system

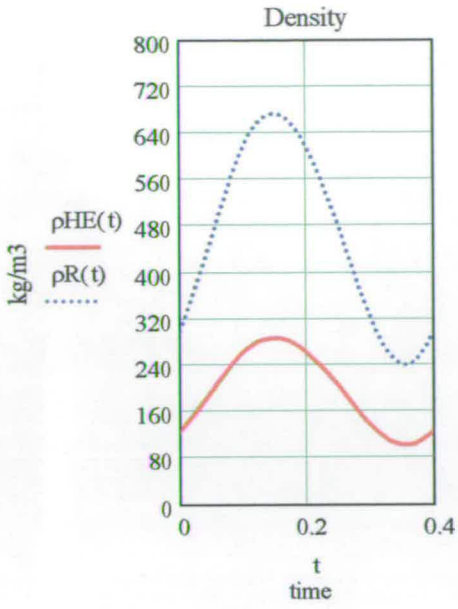
The calculated pressure from the temperature and volumes in the hot end space and the regenerator must result in the same pressure.

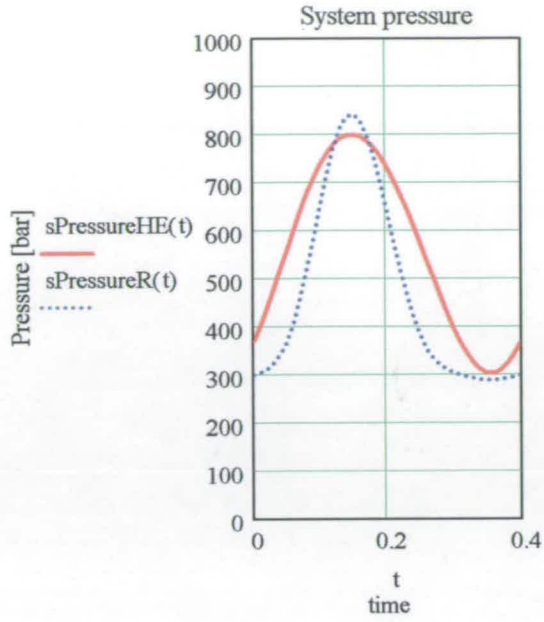
$$sPressureR(t) := 9 \cdot 10^{-6} \cdot \rho R(t)^3 - 0.008 \cdot \rho R(t)^2 + 2.54 \cdot \rho R(t) + 13.8$$

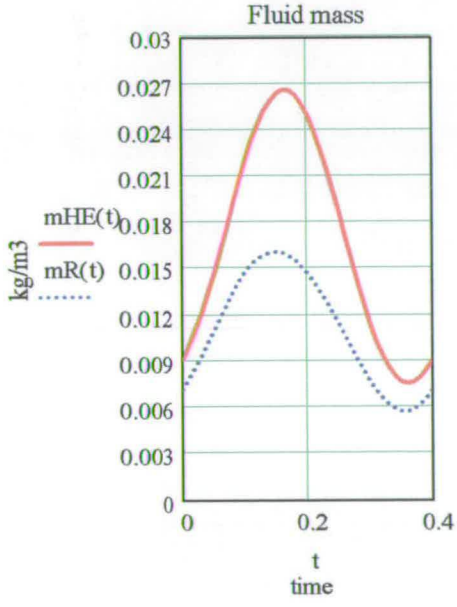
System pressure from regererator density

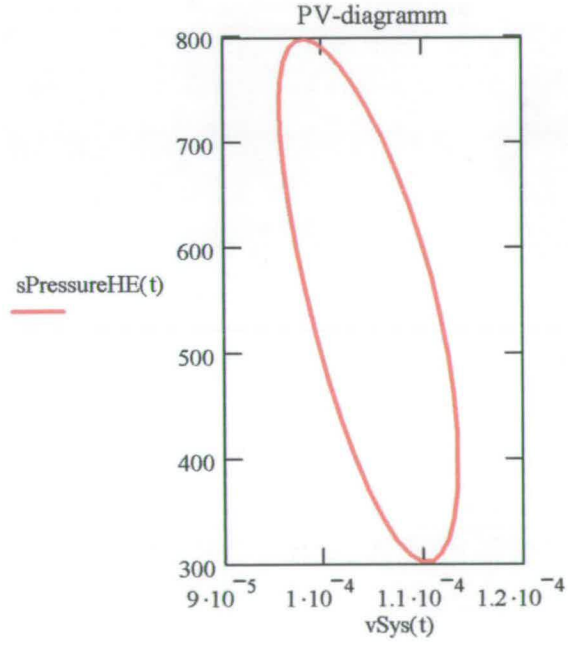
$sPressureHE(t) := 2.7 \cdot \rho HE(t) + 26$

System pressure from hot end density


Density
800
720
640
560
480
400
320
240
160
80
0
kg/m3
ρHE(t)
ρR(t)
0
0.2
0.4
t
time


System pressure
1000
900
800
700
600
500
400
300
200
100
0
Pressure [bar]
sPressureHE(t)
sPressureR(t)
0
0.2
0.4
t
time


Fluid mass
0.03
0.027
0.024
0.021
0.018
0.015
0.012
0.009
0.006
0.003
0
kg/m3
mHE(t)
mR(t)
0
0.2
0.4
t
time


PV-diagramm
800
700
600
500
400
300
sPressureHE(t)
9·10⁻⁵
1·10⁻⁴
1.1·10⁻⁴
1.2·10⁻⁴
vSys(t)

Appendix C.

Combustion chamber calculations

The energy, volume and mass flow, inside the combustion chamber of the proposed engine has been analysed.

Input parameters of proposed combustion system

$Qout := 5000$ W — Proposed engine output power

$TH := 600$ C — Hot end temperature

$TC := 200$ C — Cold end temperature

$$\eta c := \frac{TH - TC}{TH + 273}$$

$\eta c = 0.458$ — Carnot efficiency

$\eta b := 0.9$ — Burner efficiency (supplied by manufacture)

For a given engine output power, it is possible to calculate the heat flow into the hot end of the engine.

$$Qin := \frac{Qout}{\eta c}$$

$Qin = 10913$ W — Theoretical input power to hot end of engine

To calculate the required input power to the burner an initial guess of energy loss from the exhaust gas is made. The process is begun by initially setting a value for the exhaust gas losses (***Qex)*** and later correcting the value to solve the loop.

$Qex := 4000$ W — Energy loss from exhaust gas

With the input power to the burner and the losses from the exhaust gas it is possible to calculate the required input power from the burner.

$$Qb := \frac{Qin}{\eta b} + Qex$$

$Qb = 16125$ W — Required input power from burner

The required mass flow of propane and combustion air can be calculated from the calumetric value.

$$Mm := \frac{\frac{Qin}{\eta b} + Qex}{47 \cdot 10^6}$$

$Mm = 3.4 \times 10^{-4}$ $\frac{kg}{s}$ Mass flow rate Propane

For the combustion equation of propane it is possible to calculate the required amound of combustion air.

$$C_3H_8 + 5O_2 + 20N_2 = 3CO_2 + 4H_2O + N$$

$$Mma := Mm \cdot \frac{44 + (5 \cdot 32 + 20 \cdot 28)}{44}$$

$Mma = 6.0 \times 10^{-3}$ $\frac{kg}{s}$ Mass flow Propane + Air

A lambda ratio of 1.3 was chosen to garantee complete combustion.

$AR := 1.3$ Lambda number

$Mb := AR \cdot Mma$

$Mb = 7.74 \times 10^{-3}$ $\frac{kg}{s}$ Total mass flow through Burner

$Tr := 293$ K Incoming air temperature

$Tex := \frac{Qex}{Mb \cdot 1220} + Tr$ Exhaust gas temperature is calculated from the exhaust mass flow and exhaust energy.

$Tex = 716$ K

$Tia := (Toh - Tex) + Tr$

$Tia = 776.636$ K Combustion air temperature after preheating

The energy flow towards the burner can be calculated from the air mass flow and the air preheat temperature.

$Qib := Mb \cdot 1220 \cdot (Tia - Tr)$

$Qib = 4569$ W Energy flow to burner

The flame temperature is calculated from the preheated combustion air flow and the energy supplied from combustion of propane.

$$TF := Tia + \frac{Mm \cdot 47 \cdot 10^6}{Mb \cdot 1220}$$

$TF = 2483$ K — Flame temperature

The number of recirculations that the combustion gas undergoes is known from the experiments conducted in the combustion flow test rig.

$RF := 2$ — Recalculations factor (number of times the combustion gas swirls inside the combustion chamber).

$Mh := RF \cdot Mb$

$Mh = 0.0155$ $\frac{kg}{s}$ — Mass flow through the combustion chamber

It is now possible to calculate the temperature drop in the combustion gas when it passes the hot end heat exchanger.

$\frac{Qin}{Mh \cdot 1220} = 577$ — Temperature drop in combustion chamber

$$Tih := \frac{TF \cdot Mb + Toh \cdot \frac{Mh}{RF}}{Mh}$$

$Tih = 1842$ K — Mean gas temperature in combustion chamber

$$Toh := Tih - \frac{Qin}{Mh \cdot 1220}$$

$Toh = 1264$ K — Temperature of gas leaving combustion chamber

$$TF := \frac{TF + Toh}{2}$$

$TF = 1874$ K — Average temperature of combustion gas passing hot end heat exchanger fins.

Appendix D.

Heat transfer by radiation

The heat transfer from the combustion chamber wall onto the hot end has been calculated using the equation for radiant heat transfer between two concentric cylinders. Incropera, (1990)

$$Q_R = \frac{\sigma\left[(T_1)^4 - (T_2)^4\right]}{\left[\left(\frac{1-\varepsilon_1}{\varepsilon_1 * A_1}\right) + \left(\frac{1}{A_1 * F_1}\right) + \left(\frac{1-\varepsilon_2}{\varepsilon_2 * A_2}\right)\right]}$$

Input data

Tw := 1500	K	Combustion chamber wall temperature
The := 900	K	Hot end wall temperature
εhe := 0.6		Emissivity of hot end wall (Inconel 718 @ 900 K)
εw := 0.9		Emissivity of combustion chamber wall (Inconel 718 @ 1500 K)
h := 0.12	m	Hight of hot end and combustion chamber
$\sigma := 5.67 \cdot 10^{-8}$		Stephan-Bolzmann Constand
dhe := 0.06	m	Mean hot end diameter
Ahe := dhe·π·h	m2	Hot end wall area
F1 := 1		View factor from hot end to combustion space wall

Radiant heat transfer for 155 mm combustion diameter

dw155 := 0.155	m	combustion space diameter
Aw155 := dw155·π·h	m2	combustion wall area

$$F2_155 := \frac{F1 \cdot Ahe}{Aw155}$$

F2_155 = 0.387 — view factor from combustion space wall to hot end wall

$$Qr155 := \frac{\sigma \cdot \left(Tw^4 - The^4\right)}{\left[\left(\frac{1-\varepsilon w}{\varepsilon w \cdot Aw155}\right) + \left(\frac{1}{Aw155 \cdot F2_155}\right) + \left(\frac{1-\varepsilon he}{\varepsilon he \cdot Ahe}\right)\right]}$$

Qr155 = 3305 W

Radiant heat transfer for 210 mm combustion diameter

$dw210 := 0.21$ m combustion space diameter

$Aw210 := dw210 \cdot \pi \cdot h$ m2 combustion wall area

$$F2_210 := \frac{F1 \cdot Ahe}{Aw210}$$

$F2_210 = 0.29$ view factor from combustion space wall to hot end wall

$$Qr210 := \frac{\sigma \cdot \left(Tw^4 - The^4\right)}{\left[\left(\frac{1 - \varepsilon w}{\varepsilon w \cdot Aw210}\right) + \left(\frac{1}{Aw210 \cdot F2_210}\right) + \left(\frac{1 - \varepsilon he}{\varepsilon he \cdot Ahe}\right)\right]}$$

$Qr210 = 3327$ W

Radiant heat transfer for 310 mm combustion diameter

$dw310 := 0.31$ m combustion space diameter

$Aw310 := dw310 \cdot \pi \cdot h$ m2 combustion space wall area

$$F2_310 := \frac{F1 \cdot Ahe}{Aw310}$$

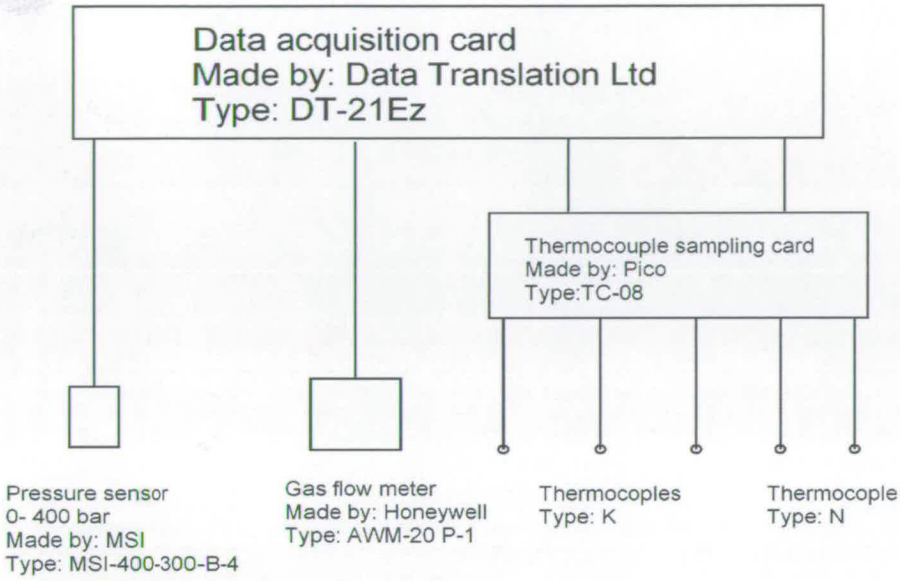
$F2_310 = 0.194$ view factor from combustion space wall to hot end wall

$$Qr310 := \frac{\sigma \cdot \left(Tw^4 - The^4\right)}{\left[\left(\frac{1 - \varepsilon w}{\varepsilon w \cdot Aw310}\right) + \left(\frac{1}{Aw310 \cdot F2_310}\right) + \left(\frac{1 - \varepsilon he}{\varepsilon he \cdot Ahe}\right)\right]}$$

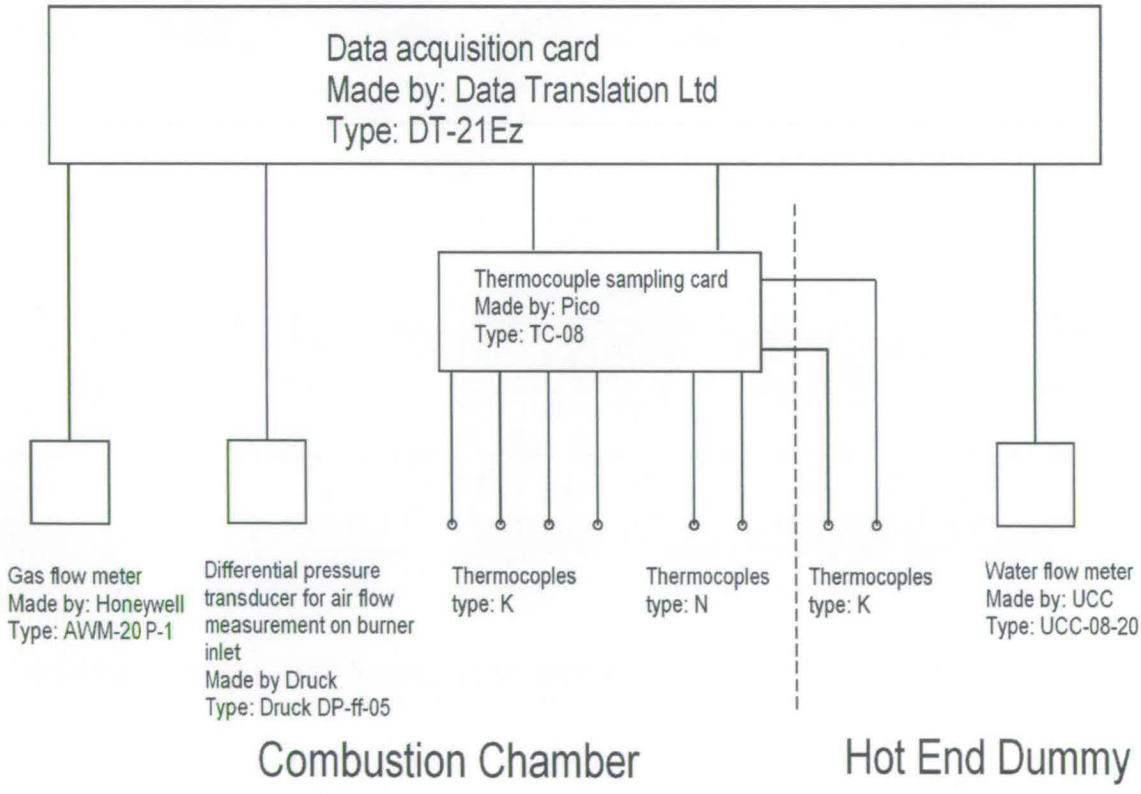
$Qr310 = 3348$ W

Appendix E

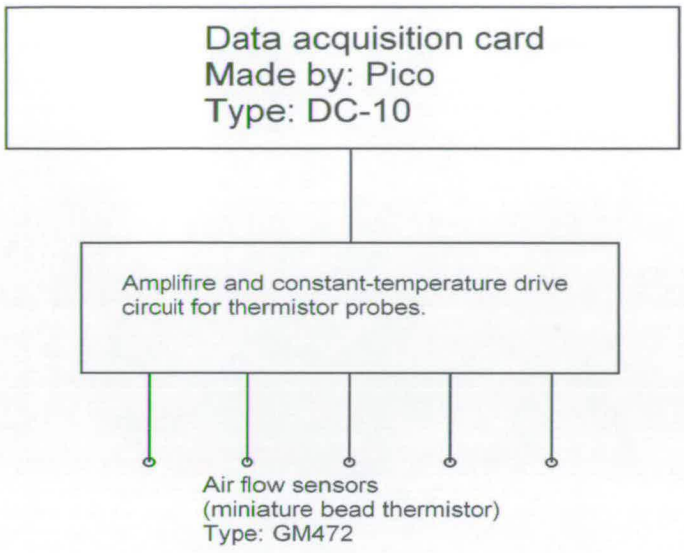
The following schematics detail the different data sampling systems used during the study.



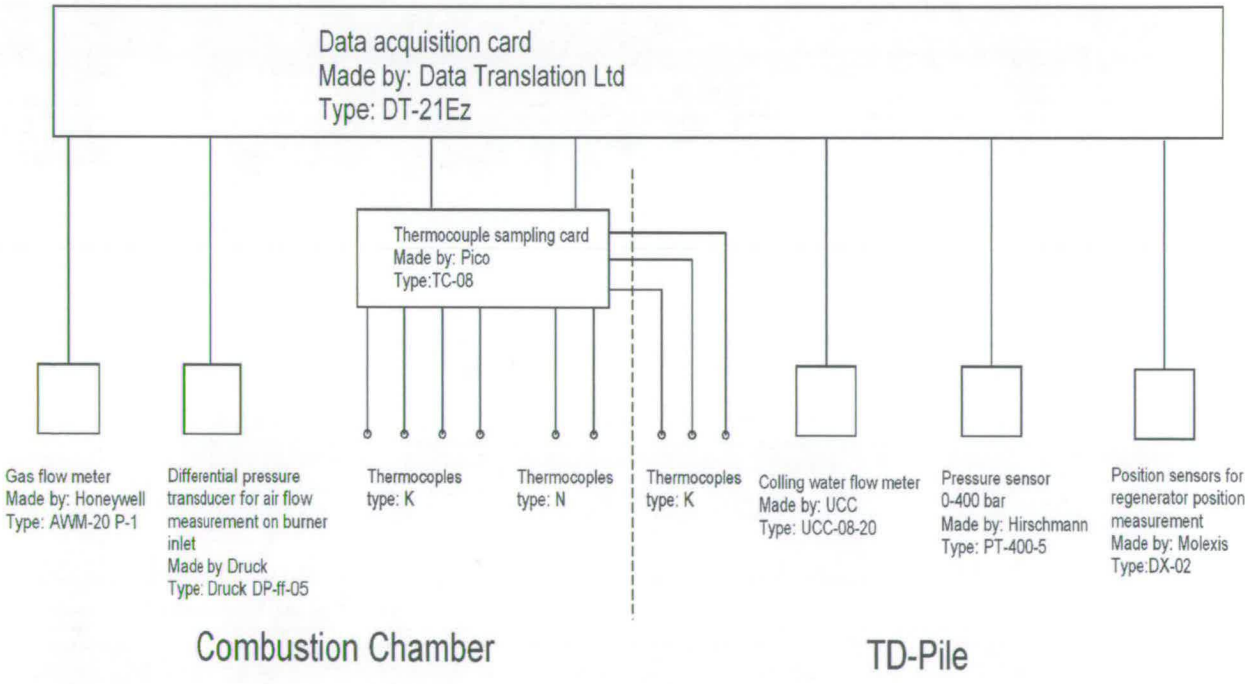
First combustion system (chapter 3.2.1)



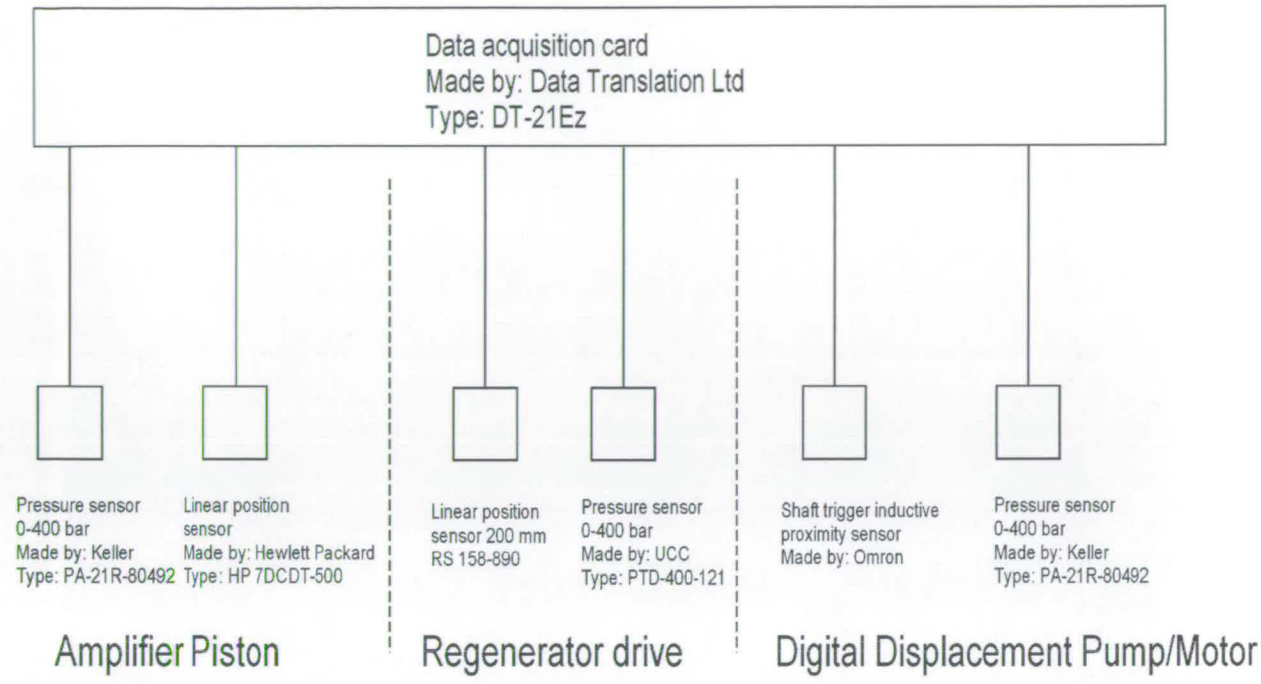
Second combustion system (chapter 3.2.2)



Combustion chamber flow test rig (chapter 3.4)



TD-Pile test rig (chapter 4.3 and 5.2)



Digital Displacement Pump/Motor test rig (chapter 6.4)

Appendix F.

The following calculations determine the temperature drop on the internal hot end fin structure of the proposed Artemis Malone engine. The fin structure is made from flow passages (holes) along the length of the hot end heat exchanger. A number of these holes are connected in series and wires are placed into the holes to increase the flow velocity and enhance the heat transfer.
The analysis is restricted to the case of flow at constant pressure of 350 bar and a temperature of 550C.

1. Input parameters

$Qout := 5000$	W	Proposed engine shaft power
$TH := 550$	C	Hot end fluid temperature
$TC := 150$	C	Cold end temperature
$PH := 350 \cdot 10^5$	Pa	System pressure
$\rho 550 := 124$	$\frac{kg}{m3}$	Density at 550 deg C
$F := 4$	$\frac{1}{s}$	Frequency
$hl := 0.1$	m	Hot end heat exchanger length
$s := 0.08$	m	Stroke of Regenerator
$ro := 0.039$	m	Outer regenerator diameter

$$Areg := \left(\frac{ro}{2}\right)^2 \cdot \pi$$

$Areg = 1.1946 \times 10^{-3}$ m2 Regenerator top area

Estimated input power to hot end heat exchanger

$$\eta c := \frac{TH - TC}{TH + 273}$$

$\eta c = 0.486$	Carnot efficiency
$\eta s := 0.75$	System efficiency

$$Qin := \frac{Qout}{\eta s \cdot \eta c}$$

$Qin = 13717$ W Input power

2. Flow conditions in hot end heat exchanger

All the following calculations are done for one full regenerator cycle in steps of 5 ms

$P := \frac{1}{F}$

$P = 0.25$ s Period

$\omega := 2 \cdot \pi \cdot F$

$\omega = 25.133$

$t := 0.005, 0.010 .. 0.25$ s Time analysed

Initially it is required to anlyse the internal flow in the hot end heat exchanger.

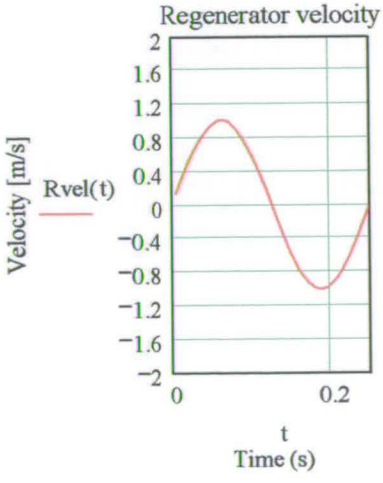
$Rvel(t) := \frac{s}{2} \cdot \omega \cdot \sin(t \cdot \omega)$ $\frac{m}{s}$ Regenerator velocity as a Function of (t)

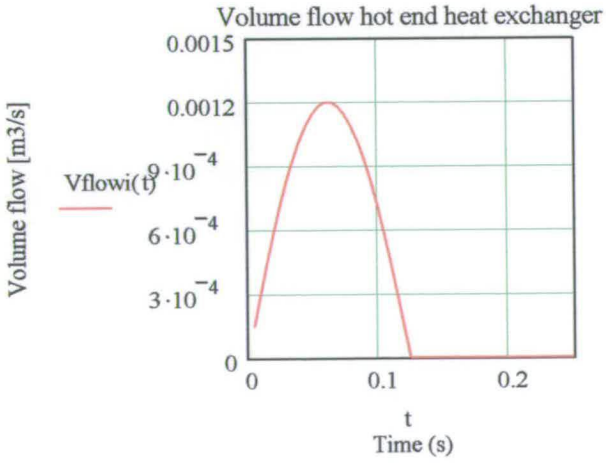
The mass flow through the hot end heat exchanger can be calculated from the regenerator motion and the regenerator frontal area.

$Vflow(t) := Rvel(t) \cdot Areg$ $\frac{m3}{s}$ Volume flow

The one-way valve on the top of the regenerator bypasses the flow in the compression stroke. During this time there is no flow in the hot end heat exchanger.

$Vflowi(t) := if(Vflow(t) > 0, Vflow(t), 10^{-10})$ $\frac{m3}{s}$ Actual flow in hot end heat exchanger





The velocity in the heat exchanger holes can be calculated from the volume flow rate and the open flow area in the heat exchanger holes.

$Nh := 48$ Number of holes

$hdia := 0.003$ m Diameter of hole

$wdia := 0.002$ m Diameter of wire

To increase the velocity in the holes and guarantee a constant temperature in the hot end heat exchanger a number (NS) of holes have been connected in series.

$NS := 3$ Number of holes connected in series

$$Fa := \frac{Nh}{NS}\cdot\left[\left(\frac{hdia}{2}\right)^2\cdot\pi - \left(\frac{wdia}{2}\right)^2\cdot\pi\right]$$

$Fa = 6.283 \times 10^{-5}$ m^2 Flow area in holes

$As := hdia\cdot\pi\cdot hl\cdot Nh$

$As = 0.045$ m^2 Total pipe outer surface area

$$velp(t) := \frac{Vflowi(t)}{Fa}$$ $\frac{m}{s}$ Steam velocity in the hot end heat exchanger holes.

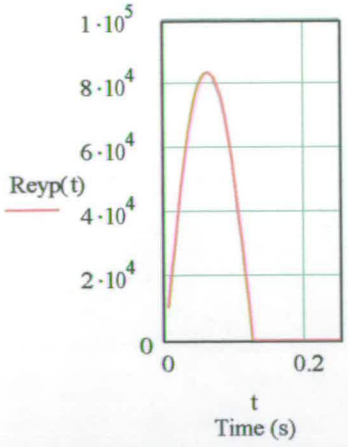
$$hmdia := \frac{4\cdot\left[\left(\frac{hdia}{2}\right)^2\cdot\pi - \left(\frac{wdia}{2}\right)^2\cdot\pi\right]}{hdia\cdot\pi + wdia\cdot\pi}$$

$hmdia = 0.001$ m Hydraulic mean diameter

$$\mu s550 := 27.86\cdot10^{-6}\cdot\sqrt{\frac{TH + 273}{800}}$$

$\mu s550 = 2.826 \times 10^{-5}$ Pa·s Viscosity of steam in Hot-End (Incropea, 199O)

$$Reyp(t) := \frac{velp(t)\cdot hmdia\cdot\rho 550}{\mu s550}$$ Reynolds number in pipe



2. Temperture drop on internal fins of hot end heat exchanger

With the reynolds number indicatin turbulent flow it is now possible to calculate the heat transfer coefficient.

$$ks := 0.0592 + (TH + 273 - 800)\cdot\frac{0.0637 - 0.0592}{50}$$

$ks = 0.061$ $\frac{w}{m\cdot K}$

Thermal conductivity supercritical water at hot end temperature

$Pr := 1.02$

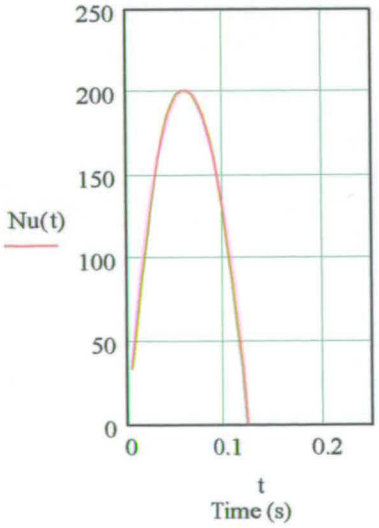
Prandtl number

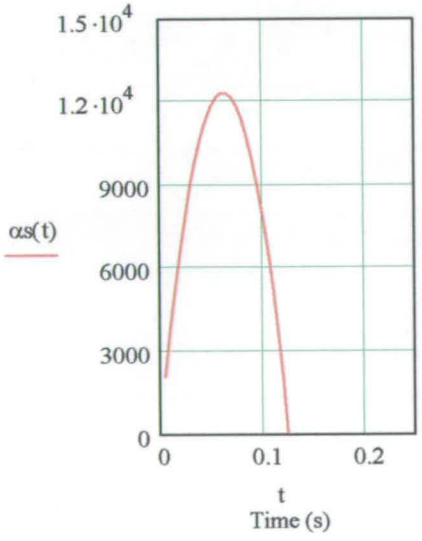
$$Nu(t) := \frac{0.0235\cdot\left(Reyp(t)^{0.8} - 230\right)\cdot Pr}{1 + \frac{1.947}{Reyp(t)^{0.1}}\cdot\left(Pr^{\frac{2}{3}} - 1\right)}$$

Nussel Number for fully turbulent flow. (Incropera and Witt 199O)

$$\alpha s(t) := Nu(t)\cdot\frac{ks}{hmdia}$$

Heat transfer coefficient





With the heat transfer coefficient, the surface areas and the energy flow it is now possible to calcualte the temperature drop from the internal structure of the hot end heat exchanger to the working fluid.

$\alpha smean := 4100$ Mean heat transfer coefficient steam to hot end heat exchanger.

$$\Delta T := \frac{Qin}{\alpha smean \cdot As}$$

$\Delta T = 74$ C Temperature drop steam fin to steam

The temperature drop from the internal fin structure to the fluid without wires in the holes was found as 173 deg C.
For the case of no wires and individal holes (not connected in series) it was was found to be 374 deg C.
For the case of no wires and a hole diameter of 1.5 mm a temperature drop af 192 deg C was found.